

The Effects of Kaolinite-Clay on the Undrained
Strength Characteristics and Static Liquefaction
Behavior of East Coast Sand

Ademola Bolarinwa

PhD

2022

The Effects of Kaolinite-Clay on the Undrained
Strength Characteristics and Static Liquefaction
Behavior of East Coast Sand

Ademola Bolarinwa

17972252

A thesis submitted to the Auckland University of
Technology in fulfilment of the requirements for the
degree of Doctor of Philosophy (Ph.D.)

2022

School of Future Environments

Attestation of Authorship

“I Ademola Bolarinwa, hereby declare that this submission is my own work and that, to the best of my knowledge and belief, it contains no material previously published or written by another person (except where explicitly defined in the acknowledgments), nor material which to a substantial extent has been submitted for an award of any other degree or diploma of a university or other institution of higher learning”.

Name: Ademola Bolarinwa

Signature:

Date: 15/07/2022

Acknowledgments

First and foremost, to God be the glory, the giver of knowledge, the Engineer General, the Omnipotent, Omniscient, and Omnipresent Almighty God. My sincere appreciation goes to the Auckland University of Technology (AUT) for the award of the Doctoral Scholarship given to me to fund my studies for three years. A special thanks to *Itasca Consulting Group*, Minneapolis, Minnesota, the USA, for the award and admittance into the Itasca Education Partnership program, *IEP-scholarship* to utilize the relevant geomechanical software for the numerical simulation aspect of the work. Many thanks to *Beca Ltd.*, Auckland, New Zealand, for the support given me to complete this work.

Most importantly, I thank my primary Supervisor, Dr. Roohollah Kalatehjari, for bringing me to AUT and allowing me to work under his unalloyed support and guidance; I cannot ask for a better supervisor. My gratitude goes to the rest of my supervisory team, Prof. John Tookey, My secondary supervisor, Dr. Mani Poshdar, Prof. Ahmad Safuan A. Rashid (Universiti Teknologi Malaysia), and the entire academic staff of the Faculty of Design & Creative Technologies for their loving support at all times. My sincere appreciation also goes to the Laboratory Management of the School of Engineering, Computer, and Mathematical Sciences for supporting me throughout the challenging times in the laboratory. Specifically, I would like to thank Simon Hartley, Stephen Hartley, Dave Croft, Andrew Virtue, Allan Dixon, and several others for the assistance rendered during the research study.

A special thanks goes to Dr. Michael Jefferies (*Lincoln*, U.K.) for his assistance/advice during the experienced challenges associated with the several complex concepts of advanced numerical modeling of soils and Dr. Zhao Cheng (*Itasca Consulting Group*) for his unrelenting support as my mentor for the FLAC and FLAC3D numerical geotechnical software.

Lastly, I appreciate the support given to me by my loved ones, my family (My Mum and siblings), my wife (Oluwatoyin), and my sons (David and Emmanuel). Unfortunately, my loving Dad (*A Physicist*), who mentored me from a kid to become the engineer that I am today, passed on, and not able to witness this great achievement, May his gentle soul rest in perfect peace, Amen!

Table of Contents

Abstract.....	viii
CHAPTER 1: INTRODUCTION.....	1
1.1 General Background	1
1.2 Rationale and Significance of Study.....	7
1.3 Statement of Research Problem	9
1.4 Research Aim and Objectives	10
1.5 Research Questions.....	11
1.6 A Summary of Research Methodology.....	12
1.6.1 Scope of laboratory and experimental work	13
1.6.2 Monotonic triaxial compression tests	14
1.6.3 Physical modeling of dynamic soil liquefaction mechanisms	14
1.6.4 Numerical modeling and calibration.....	15
1.7 Outline of the Thesis.....	16
CHAPTER 2: LITERATURE REVIEW.....	17
2.1 Introduction and General Background.....	17
2.1.1 Factors affecting soil liquefaction.....	19
2.1.2 Recent records of earthquake-triggered soil liquefaction and resulting damages.....	21
2.2 Relevant and fundamental theoretical concepts relating to soil liquefaction physics/math	22
2.2.1 The steady-state framework.....	23
2.2.2 The critical state theory.....	26
2.2.3 Basics of ground motions and ground motion intensity quantification	28
2.3 An overview of liquefaction assessment methods routinely applied in practice	29
2.3.1 In-situ based liquefaction assessment methods.....	30
2.3.1.1 Standard penetration test (SPT) assessment of cyclic resistance ratio.....	32
2.3.1.2 Assessment of CRR by the application of the CPT technique.....	33
2.3.1.3 Assessment of CRR by vane shear test.....	34
2.3.1.4 Liquefaction assessment by other in-situ based methods.....	35
2.3.2 Existing laboratory-based assessment techniques for soil liquefaction	35
2.3.2.1 Liquefaction evaluation through triaxial testing of soils.....	36
2.3.2.2 Shaking table experiment in liquefaction studies (physical Model)	53
2.3.3 Plasticity-based liquefaction analysis	55
2.3.3.1 Impacts of silts and non-plastic fines on the liquidization mechanisms of sands.....	56
2.3.3.2 Impacts of plastic fine on liquefaction resistance	57
2.3.4 Numerical modeling in soil liquefaction assessment	71
2.4 An overview of existing soil liquefaction mitigation methods	74
2.5 Summary	77
CHAPTER 3: RESEARCH METHODS AND SOIL TESTING PROGRAM	78
3.1 Introduction.....	78
3.2 Materials	79
3.3 Soil classification tests.....	80

3.3.1 Particle size and hydrometer analysis	80
3.3.2 The Consistency/Atterberg Limits	83
3.3.3 The soil classification as per the unified soil classification system (USCS).....	85
3.4 Other practical soil index tests	87
3.4.1 Scanning Electron Microscopic (SEM) imaging of samples	87
3.4.2 Specific gravity	88
3.4.3 The maximum and minimum void ratios	89
3.4.4 The soil permeability test.....	92
3.5 The soil geomechanical strength characteristic tests	96
3.5.1 Soil sample preparation for monotonic triaxial compression tests	99
3.5.2 The saturation stage	104
3.5.3 The consolidation stage.....	105
3.5.4 The monotonic compression shearing stage	107
3.5.5 The triaxial experimental result calculations and plotting formula.....	109
3.5.6 One-dimensional consolidation (oedometer) experiment	112
3.6 The application of the Norsand advanced constitutive model for numerical soil modeling	114
3.6.1 Summary of Norsand model	115
3.6.2 Breakdown of the calibration for the Norsand numerical model soil properties	118
3.6.2.1 The critical state (CSL) parameters.....	119
3.6.2.2 The soil elasticity-based parameters	120
3.6.2.3 The soil plasticity-based parameters	121
3.6.2.4 The initial soil state-based parameters	125
3.6.3 Numerical modeling in the VBA and FLAC codes	125
3.7 The physical model testing (shake table experiments)	128
3.7.1 The 600N rated-capacity shaking table setup	128
3.7.2 The model setup, instrumentation, and data acquisition (DAQ) system.....	132
3.7.3 The model sample preparation.....	133
3.7.4 The scaling/similitude laws.....	135
3.7.5 The shaking test information.....	137
3.8 Summary	137
CHAPTER 4: SHAKING TABLE DYNAMIC POREWATER CHARACTERISTIC TESTS	139
4.1 Introduction.....	139
4.2 The base input ground motions.....	140
4.3 The excess porewater pressures characteristics	141
4.3.1 Analyses and discussions of the low-shake case (F10A2).....	142
4.3.2 Analyses and discussions of the intermediate-shake case (F10A3).....	143
4.3.3 Analyses and discussions of the high-shake case (F10A4).....	144
4.3.4 Other observed key manifestations of liquefaction.....	145
4.4 The seismically-induced immediate settlements.....	146
4.5 The soil amplification characteristics	146
4.6 Summary	147
CHAPTER 5: THE STEADY/CRITICAL STATE UNDRAINED STRENGTH CHARACTERISTICS OF ECS AND CLAYEY-ECS.....	149
5.1 Introduction.....	149

5.1.1 The state characterization.....	153
5.1.2 The state concept as a basis of soil behavior type classification.....	154
5.1.3 Reference to the critical state line (CSL)	154
5.2 Discussions of the experimental static liquefaction behavior of the reconstituted soil specimens.....	157
5.2.1 Analyses of the deviatoric stress-strain, effective stress paths (ESPs), and excess PWP.....	158
5.3 Discussions of the numerically validated soil properties of ECS00 and ECS30	167
5.4 Summary	184
CHAPTER 6: CONCLUSIONS AND RECOMMENDATIONS	186
6.1 The critical state characterization	186
6.2 The dynamic excess pore water characteristics	187
6.3 The intrinsic advanced soil geomechanical characteristics.....	188
6.4 The steady/critical state failure modes.....	190
6.5 Recommendations.....	192
6.6 The practical applicability of the research and notable limitations.....	193
CHAPTER 7: References	195
APPENDICES	211
APPENDIX A – Particle size analysis (PSD) of ECS00	I
A1: Test 1.....	I
A2: Test 2.....	II
A3: Test 3.....	III
APPENDIX B – Atterberg's' Limits	IV
Atterberg limits for Kaolinite (Casagrande's method).....	IV
B1: Test 1 for Kaolinite (100% by weight).....	IV
B2: Test 2 for Kaolinite	V
B3: Test 3 for Kaolinite	VI
The fall-cone liquid limit method and plastic limit of kaolinite	VII
B4: Consistency limits of Kaolinite (Clay).....	VII
B5: Consistency limits of ECS05.....	VIII
B6: Consistency limits of ECS10.....	IX
B7: Consistency limits of ECS15.....	X
B8: Consistency limits of ECS20.....	XI
B9: Consistency limits of ECS30.....	XII
APPENDIX C - The scanning electron micrograph (SEM) of sand matrix soils	XIII
APPENDIX D - Specific gravity test datasheets	XIV
D1: Specific gravity of kaolinite (clay).....	XIV
D2: Specific gravity of east coast sand (ECS00)	XV
D3: Specific gravity of sand matrix sample (ECS05).....	XVI
D4: Specific gravity of sand matrix sample (ECS10).....	XVII
D5: Specific gravity of sand matrix sample (ECS15).....	XVIII
D6: Specific gravity of sand matrix sample (ECS20).....	XIX
D7: Specific gravity of sand matrix sample (ECS30).....	XX
APPENDIX E - Test datasheets for maximum index density parameters	XXI

E1: Maximum index density of ECS00	XXI
E2: Maximum index density of ECS05	XXII
E3: Maximum index density of ECS10	XXIII
E4: Maximum index density of ECS15	XXIV
APPENDIX F - Tests datasheets for standard compaction tests.....	XXV
F1: Maximum index density of ECS20.....	XXV
F2: Maximum index density of ECS30.....	XXVI
APPENDIX G - Tests datasheets for minimum index density	XXVII
G1: Minimum index density of ECS00.....	XXVII
G2: Minimum index density of ECS05.....	XXVIII
G3: Minimum index density of ECS10.....	XXIX
G4: Minimum index density of ECS15.....	XXX
G5: Minimum index density of ECS20.....	XXXI
G6: Minimum index density of ECS30.....	XXXII
APPENDIX H - Tests datasheets for soil permeability tests	XXXIII
H1: The permeability result of ECS00.....	XXXIII
H2: The permeability test of ECS05	XXXIV
H3: The permeability test of ECS10	XXXV
H4: The permeability test of ECS15	XXXVI
H5: The permeability test of ECS20	XXXVII
H6: The permeability test of ECS30	XXXVIII
APPENDIX I - Tests results for one-dimensional consolidation oedometer tests.....	XXXIX
I1: The load-unload loop for ECS00.....	XXXIX
I3: The load-unload loop for ECS15.....	XL
I4: The load-unload loop for ECS20.....	XL
I5: The load-unload loop for ECS30.....	XLI
APPENDIX J – The stress – dilatancy relationship measured in sand matrix samples.....	XLII
J1: The stress-dilatancy of ECS10	XLII
J2: The stress-dilatancy of ECS15	XLII
J3: The stress-dilatancy of ECS20	XLIII
APPENDIX K – Typical undrained FLAC simulation code formatted in notepad	XLIV
APPENDIX L – Deviatoric stress-strains.....	XLV
APPENDIX M – Effective stress paths (ESP).....	XLVII
APPENDIX N – Evolution of excess pore water pressures (PWP).....	L

List of Figures

Figure 1.1 Typical scenarios of the consequences of CES 2010-2011 earthquake-induced soil liquefaction in Christchurch adapted after Cubrinovski <i>et al.</i> (2012); Rosser and Dellow (2017).	3
Figure 1.2 Geological map of the studied area as per Edbrooke and Brook (2009).	6
Figure 1.3 Location map of the source studied ECS sand as per GoogleEarthPro (2022)	6
Figure 1.4 A summary of study path and scope.....	12
Figure 2.1 Representation of various state indices and CSL/SSL	23
Figure 2.2 State parameter (ψ^*) for equivalent granular condition (EG-SSL) adapted after Rahman et al. (2014b).....	26

Figure 2.3 SPT-liquefaction triggering curves for estimating CRR based on case histories after Boulanger and Idriss (2014).....	33
Figure 2.4 CPT-liquefaction triggering plots for determining CRR based on case histories after Boulanger and Idriss (2014).....	34
Figure 2.5 A summary of soil liquefaction mitigation techniques.....	76
Figure 3.1 The source primary soil specimens as stored in the geotechnical engineering laboratory	79
Figure 3.2 The utilized mechanical sieve shaker	80
Figure 3.3 Particle size distribution (PSD) analyses plot.....	81
Figure 3.4 The hydrometer analysis, sedimentation test in progress	82
Figure 3.5 The PSD of kaolinite in sedimentation test	83
Figure 3.6 (a) The Casagrande's and (b) the fall-cone devices for Atterberg limits determination	84
Figure 3.7 Determination of plastic limits of kaolinite-clay	84
Figure 3.8. Devices used in determining moisture content in the Geotechnical laboratory.....	85
Figure 3.9 SEM micrographs of kaolinite and east coast sand (ECS00)	87
Figure 3.10 Maintaining a constant temperature during the specific gravity test.....	88
Figure 3.11. Laboratory mechanical mixer.....	90
Figure 3.12 Compaction processes to determine maximum index density parameters	90
Figure 3.13 Compaction curves of ECS20.....	91
Figure 3.14. Compaction curve of ECS30	91
Figure 3.15. Flow chart of the utilized permeability device after Kalatehjari (2020).....	94
Figure 3.16 The permeability test set up.....	95
Figure 3.17 The permeability behavior of tested samples	96
Figure 3.18 The Alfa triaxial machine	98
Figure 3.19 A typical triaxial soil specimen after preparation.....	102
Figure 3.20 Schematics of soil behavior during compression and unloading in consolidation	106
Figure 3.21 Examples of experienced physical failures of soil specimens after shearing	108
Figure 3.22 The automated manual oedometer test setup.....	113
Figure 3.23 Evaluation of the soil critical state parameters from the stress invariants.....	120
Figure 3.24 Derived critical state lines (CSL)	120
Figure 3.25 Elastic modulus used during simulation.....	121
Figure 3.26 Stress dilatancy relationship measured in east coast sand (ECS00) with trendlines for CS selection of M_{tc} value.....	122
Figure 3.27 Stress dilatancy relationship measured in east coast sand (ECS30) with trendlines for the CS selection of M_{tc} value.....	123
Figure 3.28 Calibration of stress dilatancy parameters of ECS00 and ECS30	123
Figure 3.29 State-dilatancy plot of ECS00 and ECS30	124
Figure 3.30 The specified boundary conditions in the FLAC software.....	126
Figure 3.31 Specification of initial stress in FLAC using FISH	126
Figure 3.32 Mechanics of typical SDOF motion for earthquake ground motion modified after Chopra (1995)	129
Figure 3.33 The shaking table setup and main components	130
Figure 3.34 Details of the designed and fabricated soil model rigid box.....	131
Figure 3.35 Calibration of soil model container volume by calculation and water-measuring method	132
Figure 3.36 Schematics of the hardware setup	133
Figure 3.37 Layouts of the test instrumentation	133
Figure 3.38 Sample preparations of shake table experiment specimens.....	134
Figure 4.1 Base input motion for the low-shake (F10A2) case	140
Figure 4.2 Base input motion for the intermediate-shake (F10A3) case	141
Figure 4.3 Base input motion for the high-shake (F10A4).....	141

Figure 4.4 Excess porewater pressures (Δu) for the low-shake (F10A4) event @ PP1 and PP2	142
Figure 4.5 Liquefaction coefficient (r_u) for the low-shake (F10A4) events @ PP1 and PP2.	143
Figure 4.6 Excess porewater pressures (Δu) for the intermediate-shake (F10A3) event.....	143
Figure 4.7 Liquefaction coefficient (r_u) for the intermediate-shake (F10A3) events	144
Figure 4.8 Excess porewater pressures (Δu) for the high-shake (F10A4) event.....	144
Figure 4.9 Liquefaction coefficient (ru) for the high-shake (F10A4) events.....	144
Figure 4.10 Observed surface manifestation of liquefaction in all the studied soil specimens	145
Figure 4.11 The immediate settlements for all samples.....	146
Figure 4.12 The computed amplification factors (AF) for all samples and shaking cases	147
Figure 5.1 The schematics of locating the IL in q-p' stress space as per Yang (2002)	152
Figure 5.2 The schematics of locating the IL in q-p' stress space as per Yang (2002)	152
Figure 5.3 Typical undrained monotonic responses classification types for sands	154
Figure 5.4 Illustration of the CSL in stress spaces.....	156
Figure 5.5 Deviatoric stress-strain of ECS00.....	158
Figure 5.6 ESP of ECS00.....	159
Figure 5.7 Generated excess PWP of ECS00 during monotonic shearing.....	159
Figure 5.8 The deviatoric shear stresses of the soil specimens at 50kPa testing stress level....	162
Figure 5.9 The deviatoric shear stresses of the soil specimens at 100kPa testing stress level..	162
Figure 5.10 The deviatoric shear stresses of the soil specimens at 200kPa testing stress level	163
Figure 5.11 ESPs of all soil specimens at a mean effective stress level of 50kPa	164
Figure 5.12 ESPs of all soil specimens at a mean effective stress level of 100kPa	164
Figure 5.13 ESPs of all soil specimens at a mean effective stress level of 200kPa	165
Figure 5.14 The evolution of excess PWP of all soil specimens at 50kPa mean effective stress	166
Figure 5.15 The evolution of excess PWP of all soil specimens at 100kPa mean effective stress	166
Figure 5.16 The evolution of excess PWP of all soil specimens at 200kPa mean effective stress	167
Figure 5.17 Simulation results of ECS00 at 50kPa mean confining stress level	169
Figure 5.18 Simulation results of ECS00 at 100kPa mean confining stress level	170
Figure 5.19 Simulation results of ECS00 at 200kPa mean confining stress level	171
Figure 5.20 Simulation results of ECS00 at 300kPa mean confining stress level	172
Figure 5.21 Simulation results of ECS30 at 50kPa mean confining stress level	173
Figure 5.22 Simulation results of ECS30 at 100kPa mean confining stress level	174
Figure 5.23 Simulation results of ECS30 at 200kPa mean confining stress level	175
Figure 5.24 Simulation results of ECS30 at 500kPa mean confining stress.....	176
Figure 5.25 FLAC simulated versus experimental measured excess PWP for ECS00 @ 50kPa	177
Figure 5.26 FLAC simulated versus experimental measured excess PWP for ECS00 @ 100kPa	177
Figure 5.27 FLAC simulated versus experimental measured excess PWP for ECS00 @ 200kPa	178
Figure 5.28 FLAC simulated versus experimental measured excess PWP for ECS00 @ 300kPa	178
Figure 5.29 FLAC simulated versus experimental measured excess PWP for ECS30 @ 50kPa	179
Figure 5.30 FLAC simulated versus experimental measured excess PWP for ECS30 @ 100kPa	179
Figure 5.31 FLAC simulated versus experimental measured excess PWP for ECS30 @ 200kPa	180
Figure 5.32 FLAC simulated versus experimental measured excess PWP for ECS30 @ 500kPa	180

Figure 5.33 Cross-comparisons of VBA and FLAC simulated stress strains with Experimental data of ECS30 @ 100kPa.....	182
Figure 5.34 Cross-comparisons of VBA and FLAC simulated ESP with experimental data of ECS30 @ 100kPa confining stress	184

List of Tables

Table 1.1 Comparison between the research objectives and research questions	12
Table 1.2 Naming nomenclature and composition of kaolinite in the studied ECS sand samples	13
Table 2.1 Effects of sample reconstitution methods on cyclic responses of soils: A systematic review.....	39
Table 2.2 Systematic review of liquefaction resistance of sand mixed with plastic fines	59
Table 2.3 A modified critical review of UBCSAND, PM4SAND, DM04, P2P, NORSAND liquefaction models modified after Cheng (2018)	73
Table 3.1 Hydrometer analysis tests data.....	82
Table 3.2 Comparison between Casagrande and Fall-Cone method of Atterberg's Limits for kaolinite	84
Table 3.3 USCS classification of all soil samples.....	86
Table 3.4 Specific gravity (G_s) of all soil samples at a glance.....	88
Table 3.5. Summary of test results for maximum and minimum index density parameters.....	89
Table 3.6 Types of soil sample reconstitution techniques in triaxial testing	100
Table 3.7 Computation factors for failure time estimates.....	107
Table 3.8 The applicable strain rates in the executed ICU and ICD tests.....	107
Table 3.9 Summary of some initial soil parameters in the undrained monotonic tests (ICU) – Experimental evidence.....	111
Table 3.10 Summary of some initial soil parameters in the drained monotonic tests (ICD) – Experimental evidence.....	111
Table 3.11 Summary of some initial soil parameters in the undrained monotonic tests (ICU) – Numerical model calibration purpose	112
Table 3.12 Summary soil parameters in the drained monotonic tests (ICU) – Numerical model calibration purpose.....	112
Table 3.13 Consolidation test loading schedule for each soil sample.....	113
Table 3.14 Estimated compression and swelling indices of the studied soil samples	114
Table 3.15 Summary of the relevant material properties for the Norsand model as per Itasca (2021).....	127
Table 3.16 Summary of experimental shaking table-physical model properties	135
Table 3.17 Some applicable similitude laws as per (Iai, 1989; Towhata, 2008)	136
Table 5.1 Result summary of undrained monotonic characteristics of tested soils	160
Table 5.2 The calibrated Norsand model soil properties	183

Abstract

In recent decades, the geotechnical research community has studied well the soil liquefaction problem, considered a significant threat to the entire built environment. Most investigations in the past were concentrated on homogenous soils (i.e., either clean sands or clays otherwise referred to as textbook soils), while studies executed on mixed soils for the evaluation of liquefaction susceptibility are still few. A literature review of past works on mixed soils (e.g., silty sands, clayey sands) indicated the existence of some elements of controversies regarding the trends of liquefaction susceptibility of the bracketed especially clayey sands. In reality, in-situ soils often exist as mixed soil composites and some case histories have indicated the occurrence of liquefaction of mixed soils in the past. Hence, the justification of the requirement of additional investigations on mixed soils is considered to comprehend their strength characteristic and resistance to natural disasters such as static and earthquake-induced soil liquefaction. In the current study, the static liquefaction mechanisms of east coast sand (ECS) and other derived mixed soil specimens by mixing ECS with 10%, 15%, 20%, and 30% by weight of an industrial kaolinite-clay are presented. ECS is a commercially available mined sand from the shores of Pakiri beach, Pakiri, and is mostly utilized in geotechnical earthworks construction works around Auckland and the Northlands of New Zealand. The statically-induced liquefaction cases were examined under the undrained triaxial compression conditions to provide experimental evidence as well as the numerical models for the observed extreme cases. In addition, the generation of excess porewater pressure (PWP) as a result of the application of synthetic dynamic/earthquake loads was studied with the aid of a 600N-capacity shaking table for the remolded soil specimens. The engineering characteristics of soils are well-known to exhibit nonlinear stress-strain relationships and overall complex behavior. The Norsand model framework was tested to numerically validate five aspects of the soil's undrained behavior under triaxial compression conditions. The studied aspects include the complex stress-strain relationships, effective stress paths, excess porewater pressures, stress-state dilatancies, and the critical state characterized by the state parameter. It is particularly useful to understand the soil liquefaction behavior of varieties of soils in practice as this would assist in the selection of soils that are suitable for soil replacement mitigation measures applicable in hydraulically placed fills, earth dams, tailing dams, and other earthwork applications in geotechnical engineering that are susceptible to any type of liquefaction-related failures. The obtained basic soil index properties of the control study sample (ECS) were predominantly of a poorly graded sand (SP) according to the unified soil classification system (USCS). The USCS classification of the utilized kaolinite clay indicated a lean or low plasticity clay (CL). The other created sand matrix soils indicated the soil classification of clayey sand (SC). Scanning electron microscopy of the ECS indicated that its grain shape is angular to subangular and fine in texture. The ECS has a specific gravity of 2.60, minimum and maximum density in the range of 1.43g/cm^3 to 1.67g/cm^3 , corresponding minimum and maximum void ratios of 0.561 to 0.820, respectively, permeability in the range of 4.76×10^{-4} to $6.66 \times 10^{-4}\text{cm/s}$,

compression index C_c of 0.000232 and swelling index C_s of 0.0000597. The obtained liquid limit of the applied kaolinite was 45%, and the plastic limit of 35%, with a plasticity index of 10.

The monotonic triaxial compression test results were conducted for the initial testing mean effective stress levels of 50kPa, 100kPa, and 200kPa for all the studied remolded soil specimens. These stress levels are considered realistic for soils that may be susceptible to static liquefaction failure. The undrained shear strength of the ECS decreased with the initial introduction of the kaolinite in its fabric and then increased at some marginal optimal percentage by weight content of the kaolinite. The resulting experimental evidence as per the executed triaxial monotonic compression tests suggests that an optimal static liquefaction resistance is achievable for the ECS mixed with 15% to 20% by weight of the kaolinite clay with a reduced excess porewater pressure. The analyses of the static liquefaction cases were interpreted based on the steady-state/critical state frameworks. Numerical modeling and data validation of the soil's advanced geomechanical properties was carried out for observed extreme cases of the studied samples; specifically, the clean sand (ECS00) and clayey sand with 30% kaolinite (ECS30), which experienced typical flow failures at all testing stress levels. The applied software for numerical modeling is the *Itasca* geomechanics software (*numerical modeling tools*), Fast Lagrangian Analysis of Continua (*FLAC*). The executed shaking table further showed that the generated excess PWP decreased as the kaolinite content increased within the fabrics of the ECS. Overall, the outcome of the current study contributes to the benefits of alternative soil additives as sustainable replacements of some conventional soil improvements. Inclusions are those that apply cement, lime, and other poisonous chemicals that may impair the sustainability of the built environment and impede the achievement of the global goal of zero-emission of greenhouse gases, notably (carbon dioxide, i.e., CO_2). In addition, insights are provided on suitable soil parameter calibration and numerical modeling processes for mixed soils which have received little attention to date. The significance of the current thesis further highlights the need to reconsider either the application of finite element or finite difference methods to inform better design decisions of mixed soils' global stability issues rather than the current applied conventional limit equilibrium method coupled with the well-known Mohr-Coulomb model in practice which are not capable of capturing important soil properties like plastic flow, hardening, softening, and excess porewater pressures.

Keywords: Critical state, Steady-state, Static liquefaction, Norsand model, Flow Failure, Model calibration, East coast sand, Kaolinite, Dynamic excess pore water pressures.

CHAPTER 1: INTRODUCTION

1.1 General Background

During the process of soil liquefaction phenomenon, the effective stress (σ') in granular soil structure is decreased or completely lost (i.e., reduced to zero) due to the proliferation in excess pore water pressure (u), which eventually equates to the intergranular effective confining stress of the soil medium. Sudden loss of friction (i.e., the sole shear strength parameter) in cohesionless soils is the natural consequence of the above scenario due to the vanishing effective stresses in the soil fabrics during liquefaction interplay mechanisms and physics. In other words, soil liquefaction occurs when the shear strength of saturated loose to medium dense sand decreases or either vanishes overall when subjected to either monotonic, cyclic or dynamic loads, and time is not usually available for the expulsion of the generated excess pore water pressure (PWP) (e.g., Castro & Poulos, 1977; Dixit et al., 2012; Poulos et al., 1985; Taylor et al., 2015).

Monotonic loads (i.e., unidirectional loads) act mostly through tension or compression until the soil skeleton fails. Cyclic loads, as the name implies, operate in the way of alternating loads harmonically by the application of either cyclical tension, compression, or a combination of both. PWP build-up rate rises as the frequency of loads increases during liquefaction mechanisms (Martin et al., 1975). Dynamic loads are typically moving/transient motion loads such as oscillatory and seismic/earthquake loads.

The two primary typical liquefaction mechanisms encountered in granular geomaterials during earthquakes are often referred to as ‘flow (static) liquefaction’ and ‘cyclic mobility.’ The contractive action of loose granular soils (e.g., sand) is referred to as flow liquefaction. In contrast, the dilative behavior of both dense and loose granular geomaterials at low confining pressures is known as cyclic mobility (Li & Ming, 2000). In addition, the term ‘cyclic softening’ is often associated with and applicable to clayey soils. The soil may tend to exhibit a liquidized behavior at the onset of the flow liquefaction interplay. Flow liquefaction entails the most devastating soil deformation and failure mode associated with its notable sudden occurrence. Casagrande (1969) explained the cyclic mobility phenomenon as “the progressive softening of a saturated sand specimen when subjected to cyclic loading at constant water content.” Cyclic mobility behaves in a ratcheting effect mode. The theoretical concept which incorporates both mechanisms in numerical analyses of liquefaction assessment is known as the ‘stress dilatancy,’ e.g. (Dafalias & Manzari, 2004; Dafalias et al., 2004).

It is well known that earthquake-triggered failures such as soil liquefaction pose significant damaging threats to the entire built environment, most notably in seismically prone regions of the world (i.e., places located within the proximity of the ring of fire). New Zealand is one such location situated along the seismically active faults (i.e., the pacific ring of fire) and hence highly susceptible to seismic activities. A significant amount of damage due to earthquake-induced soil

liquefaction has been recorded and reported in past earthquake events in New Zealand, such as the Kaikoura earthquake (M_w 7.8) on 14 November 2016; Canterbury Earthquake Sequence (CES) 2010-2011 (M_w 5.5 to 7.1), which happened between 4 September 2010 and 23 December 2011 (Cubrinovski et al., 2012). Maurer, Green, Cubrinovski, et al. (2015), for instance, reported primary induced manifestation of liquefaction in Christchurch as (i) lateral spreading and settlement-induced failure of bridges; (ii) failures of roads as a result of induced fissures and cracks on pavements; (iii) several observed liquefaction ejecta (sand boils); (iv) massive collapse of lifelines due to differential settlements and floatation; (v) impairment of port facilities due to ground deformations and (vi) widespread differential settlements and tilting of infrastructures which summarily resulted in high collateral damage (huge economic loss), loss of lifeline (i.e., utilities), and in some cases loss of lives.

Typical scenarios of the effects mentioned above from Christchurch's liquefaction are shown in Figure 1.1. Collateral damage and economic loss worth approximately \$15-billion were the consequential effects of the 2010-2011 CES (Cubrinovski et al., 2017; Potter et al., 2015). Several other liquefaction-induced infrastructural damages recorded due to the 2016 Kaikoura earthquake event are well-detailed (Dizhur et al., 2017; Stringer et al., 2017); Also documented are about 27,000 houses reportedly damaged in the eastern Japan earthquake-induced liquefaction (Towhata et al., 2016).



(a) Observed lateral spreading and fissures parallel to the Avonside drive, Christchurch after M 6.3 Christchurch earthquake of 22 February 2011 (Rosser & Dellow, 2017).



(b) Massive liquefaction ejecta (sand boils) in Kaiapoi about 45km away from the epicenter of the M 7.1 Darfield earthquake (Rosser & Dellow, 2017).



(c) Loss of lifelines (buried pipes) due to the M 7.1 Darfield earthquake (Rosser & Dellow, 2017)



(d) The visible submerged area due to liquefaction in residential areas, Christchurch (Cubrinovski et al., 2012)

Figure 1.1 Typical scenarios of the consequences of CES 2010-2011 earthquake-induced soil liquefaction in Christchurch adapted after Cubrinovski et al. (2012); Rosser and Dellow (2017).

Most existing, conventional liquefaction-mitigation methods operate under the principles of densification, solidification, improvement of soil engineering properties, soil reinforcements, soil replacement, and drainage improvement-based techniques (Bao et al., 2019; Huang & Wen, 2015). Conventional and emerging soil liquefaction-mitigation methods are useful but are mostly associated with one or more limitations. Such limitations include poor cost feasibility, sustainability issues such as production of greenhouse gases (mainly CO_2), negative environmental impacts (due to introducing chemical agents, polluting the groundwater), and disturbance to ancillary structures that are sensitive to deformation and vibrations due to waves and disruptive installation effects (Conlee et al., 2012; Huang & Wang, 2016; Huang & Wen, 2015; O'Donnell, 2016; Xiao et al., 2018). More recently, Bao et al. (2019) presented a review of existing liquefaction mitigation methods and highlighted some limitations associated with them, indicating their effectiveness, applicability, sustainability, duration time, durability, cost, and long-term observation. The quest for economic, sustainable (environmental-friendly), and effective means of mitigating seismically-induced liquefaction justifies the need to carry out more research/studies on composite or mixed soils such as sand matrix soil.

Sand matrix soils are sandy soils with some percentage of fines (which can be either plastic or non-plastic) and, or gravels. Currently, published literature indicates that the impacts of plastic fines on sands' liquefaction resistance are still controversial. For instance, Polito (1999) and El-Mohtar et al. (2014) reported that sands' liquefaction resistance is directly proportional to their corresponding plasticity indices. Other research workers, Law and Ling (1992); Bouferra and Shahrour (2004); Cubrinovski and Ishihara (2002), have stated that liquefaction resistance of sands is inversely proportional to their respective plasticity indices at some predetermined threshold fine's content (f_c) after which the proportionality signs changes to the direct-proportionality. Subsection 2.3.2.3 of the current work provides further explanations of the

observed controversies found in the literature. One key aim of the present study is to investigate the reliability of such findings in the above works and numerically validate same.

The systematic literature review executed in chapter 2 of this work indicated that material characterization, in-situ state characterization, and system response studies are required to produce a clearer assessment of soil liquefaction-induced failures. The most significant features of the evaluation procedures mentioned above should include controlled validated laboratory experiments with a practical advanced soil liquefaction constitutive and critical state-compatible numerical model, mathematical modeling of equations governing the conservation of mass, inertia, momentum, and infiltration mechanisms of the pore water pressure in the soil matrix, and accurate description of the boundary conditions to mimic the impacts of earthquake energy in the form of surface and body waves, when assessing earthquake-induced liquefaction related problems (Vytiniotis, 2011). Overall, it is also important to consider three critical aspects while evaluating soil liquefaction, namely the susceptibility, initiation, and effects of liquefaction. Loose sands and silty sands often are listed as the types of soil which are highly/mostly prone to both statically and cyclically/earthquake-triggered liquefaction failures (Yamamuro & Lade, 1998). Poulos et al. (1985) reported that liquefaction could also occur in quick clays (i.e., remolded or disturbed clays).

A detailed review of case histories in earthquake-induced liquefaction carried out by Yamamuro and Lade (1999, p. 547) indicated that silty sand is the most liquefaction-prone type of soil, with over 95% liquefaction cases recorded from the same. Similarly, Vytiniotis (2011) stated that the soil materials most likely prone to liquefactions are saturated, loose, granular materials, such as those deposited in hydraulic sand filling operations, earth or tailing dams. Most experimental soil liquefaction studies in the literature focused more on pure (i.e., clean) sands, silts, and silty sands. The reason for the choice of these studied materials is because these are the soils that are most likely prone to liquefaction failures. A thorough understanding of the mechanical and pore water pressure generation/dissipation behavior and characteristics of other mixed/transitional soils such as clayey sand/sandy clay soils may help prescribe suitable soil replacement options for clean or silty sands in most earthwork-related applications during routine practice. Furthermore, mixed soils with improved strength properties could serve as a soil replacement option in other geotechnical earthwork applications such as soil replacement operations (overhauling), hydraulic fills, engineered fills, tailing dams, and other ground engineering applications. As used above, the term ‘replacement’ is often substituted for ‘cut and fill’ or ‘soil borrowing’ or ‘soil replacement’ or ‘alternative materials’ in earthworks. Replacement operations are frequent in earthwork applications such as embankments or dams, retaining walls, slope stability, port facilities, etc.

Typical in-situ soils that exist in the mixed state are mostly composed of fractions of clays, silts, and sands, which makes it equally significant to understand the diverse performance characteristics of mixed soils, especially under both static and dynamic loading conditions. The

static and cyclic strength characteristics of soils are most routinely studied from laboratory monotonic and cyclic triaxial tests respectively by simply consolidating saturated soil samples under an all-round isotropic, constant effective confining pressure; subsequently subjected to deviator stress increase under undrained soil conditions (Martin et al., 1975). The cyclic simple shear device invented by Peacock (1968) also provides a more accurate simulation of in-situ field conditions which was reportedly deficient in conventional triaxial tests. In recent times, physical model tests such as the centrifuge and shaking table are routinely used to study the soil dynamic responses, excess pore-pressure generation, and the physics of cohesionless granular material behavior under dynamic loads. These tests' obtained results usually are correlated with some numerical simulations for analytical discussions and risk evaluations.

The current study focuses on evaluating the undrained static flow failure behavior of East Coast Sand (ECS) as the control primary sample in comparison with other resulting soil sample variants when ECS is admixed with some varying percentage composition by weight of typical lean, industrial kaolinite clay. The selected case study's primary/control sample (ECS) from Auckland is available in large commercial quantities and routinely utilized for local earthworks applications around the Auckland region. The source of the studied primary sand sample, ECS is from near the shore of Pakiri Beach, Mangawhai, about a 2-hour drive from Auckland. ECS has been continuously mined for decades to date for construction purposes, yet it has no published detailed information on its geotechnical properties. The main geological origin of ECS is from the Pakiri Group as observed from the local geological map of the Whangarei area, authored by Edbrooke and Brook (2009) and classified in geological terms as Fixed Younger Parabolic Dunes, Late Pleistocene, and Holocene age and named 1Qd and Q1d from the Auckland Geological map. The sand has been described by the former author as either weakly cemented or non-cemented in-situ. The geological map of the studied source sand is shown in Figure 1.2, and Figure 1.3 shows its location map.

The current study consists of experimental parametric monotonic triaxial compression and shaking table tests under soil undrained conditions. The aim of the executed physical model tests (shaking table experiments) was to study only the dynamically generated excess PWP of the examined soil samples. The soil-rigid-container applied in the shaking table experiment was designed and fabricated to significantly reduce the well-known effects of body shear waves (P-waves) on rigid containers' transient boundaries. The impact of this type of boundary condition may be investigated and compared with the well-known quiet and free-field boundaries in numerical models. The purpose of the monotonic triaxial compression tests (both drained and undrained) are to provide the experimental evidence and results of the soil samples investigated for discussion and calibrate numerical models as a means of validating the studied advanced soil parameters for both the clean sand (ECS00) and a typical clayey sand (ECS30) containing about 30% by weight of kaolinite clay. The computational data validation was carried out according to

the numerical framework of the Norsand advanced soil liquefaction constitutive model in the FLAC software.

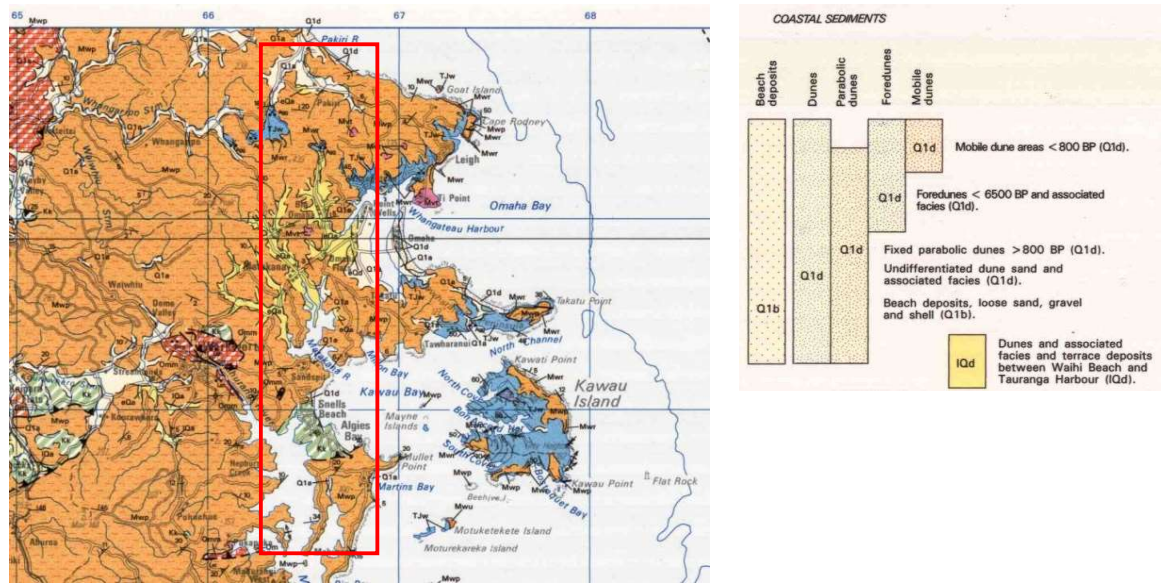


Figure 1.2 Geological map of the studied area as per Edbrooke and Brook (2009).

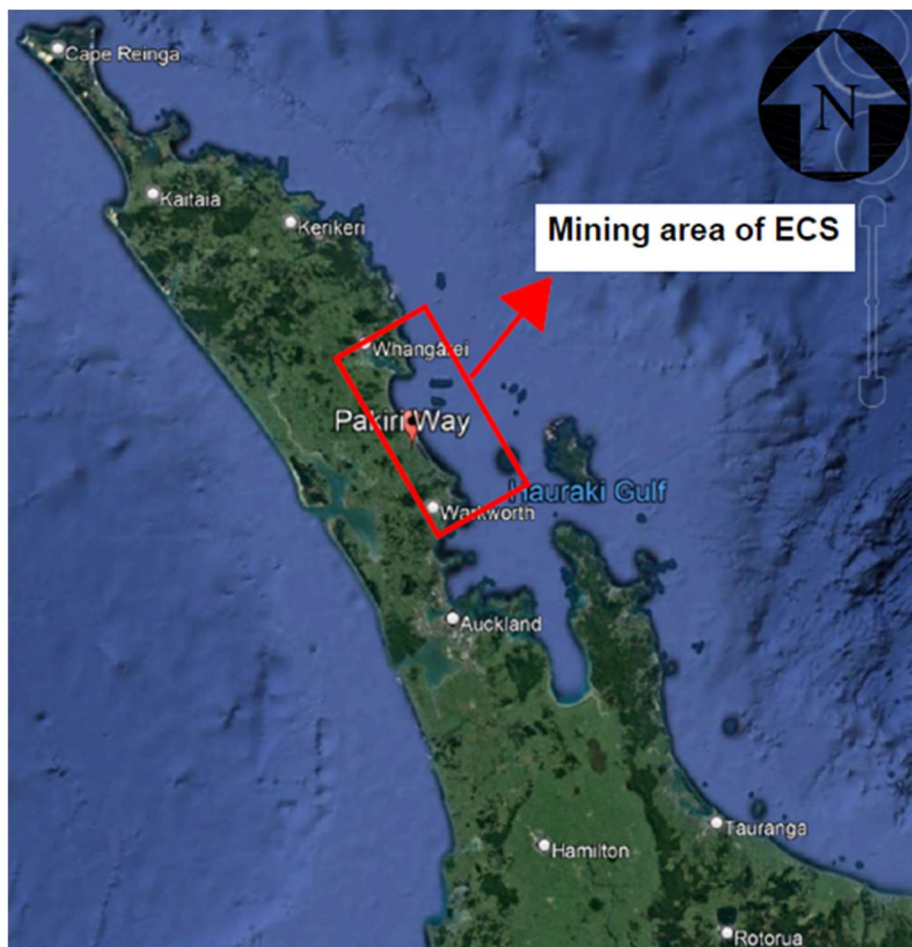


Figure 1.3 Location map of the source studied ECS sand as per GoogleEarthPro (2022)

1.2 Rationale and Significance of Study

The existing literature on the subject has shown that limited studies were focused on studying mixed soils for improved mechanical, PWP, and yield properties evaluation as a substitute for clean sands or silty sands. It is a well-established fact that clean sands or silty sands are the most liquefaction-prone type of soil. Several studies have been executed in the past to understand the cyclic and shear strength responses of these soils under varying conditions. However, more research/studies are required on the liquefaction resistance of mixed soils, which may provide insights into the design of practical, cheap, and safe liquefaction mitigation techniques. Mixed soils may offer improved liquefaction performance/resistance and may serve as a replacement for sands used in earthworks applications. In addition, alternative soil additives are required in place of some conventional soil additives like cement, lime, and other chemical binders which may pollute the groundwater with leachates and/or contribute to the emissions of greenhouse gases notably, Carbon Dioxide (CO₂).

Been and Jefferies (1985, p. 99) noted that there are several deficiencies associated with the art of using undensified sands in earthworks operations, and research on suitable material substitutes for such activities has received little attention up to date. Similarly, Gutierrez (2005), in his work, reported that a unified framework of transitional soils for marginal soil implementation and improved ground is lacking. The genesis of a framework based on the critical state for the analysis of mechanical behavior of saturated remolded soils was first carried out by Schofield and Wroth (1968). Currently, there are existing divergent and controversial views on the impacts of plastic fines on the liquefaction mechanisms of soils in the literature. Gutierrez (2005) has attributed the controversial ideas in the current research trend of soil mixtures as a result of the lack of a unified theoretical framework for modeling and characterizing soils. The concept of critical state is relevant in addressing the above scenario because it is a framework incorporating both the strength and consolidation characteristics of soils.

The concepts of the steady-state, critical state, elasticity, plasticity, yield surface, stress dilatancy, state dilatancy, flow rule, hardening rule, and softening rule are all fundamental to understanding the non-linear physics of liquefaction and failure mechanisms in soils. A systematic literature review revealed that information on the control studied sand sample (i.e., ECS) is either limited or scarce, most notably on their pore water pressure characteristics, yield behavior, and critical state failure mechanisms. More so, this material is utilized continuously for local construction purposes around the Auckland region and its environs. Hence, this study creates an avenue to use the ECS as a case study and control for establishing a robust information database on its shear strength and static liquefaction properties. A comparative discussion of ECS with other derived/remolded samples containing typical low plastic fines was made to decipher and discuss their strength characteristics. The strength and deformation properties were derived by the application of critical state soil mechanics (CSSM). The critical state parameters are particularly

useful in understanding soil behavior under static monotonic loads. Also, liquefiable soils have been characterized by the well-known state parameter (Ψ) by previous workers.

While keeping in mind that the overall strength characteristics of in-situ soils are influenced by their particular initial conditions known as ‘state’ and geological histories, the present study intends to produce a publishable database on the flow failure behavior of ECS and sand-clay matrix soils/mixtures. The obtained results are expected to be useful as reference criteria to the local and entire geotechnical community by providing insights into the static/flow failure of the studied sand in comparison with other standardized sand such as Toyoura sand in the literature (e.g., Verdugo & Ishihara, 1996; Yoshimine & Ishihara, 1998). Furthermore, the correct selection of a suitable advanced liquefaction constitutive numerical model to capture the related liquefaction mechanisms in mixed soils (e.g., clayey sand) is still lacking in the literature. The researchwork also supports achieving the global goal of zero-emission of greenhouse gases to slow down the processes of global warming and climate change.

Generally, the bearing capacity of soils depends on their shear strength variables, which typically include the effective angle of internal friction (ϕ'), effective cohesion (c'), and the overburden pressure (a function of soil unit weight (γ) and soil depth. Improvements in soil shear strength can be achieved either by soil densification (improved relative density), improving soil drainage properties, changing the soil composition to impede rapid PWP-generation properties, etc. The soil remediation option related to the PWP criteria was considered in the current study for research exploration.

The liquefaction resistance of granular geomaterial such as sand may decrease as its plasticity increases up until an attained optimum point after which the rapid strain-softening phenomenon sets in. However, it turns out that further increase of plasticity may result in improved soil undrained shear strength when several required factors for the evaluation of flow liquefaction are considered. A preliminary liquefaction physical test in the laboratory using a 600N-capacity shaking table indicated an observed decreased subsidence rate of model buildings placed on soil samples with increasing plasticity, an optimum decrease rate of building subsidence, and submergence was achieved between 15% to 20% kaoline mixed with ECS. An example of the factor responsible for the decreased rate of building subsidence is the decreased void ratio of sand and permeability, which subsequently impeded the rapid extent of pore pressure development in the particulate sand structure (or fabric). Previous works on the aging effects of mixed soils (Ltifi et al., 2014; Schmertmann, 1991, 1993; Yusa, 2015) have also indicated significantly improved liquefaction resistance of in-situ ground that are composed of mixed soils; besides, the presence of plasticity may accelerate aging in soils. Observations from the studies mentioned above showed that aging soil effects on its shear strength/resistance grew remarkably by observed modification in the soil state, its physical and geomechanical properties.

A significant criterion considered as motivation in the present study is that the universal abundance of clay is well known. Furthermore, it is relatively cheap compared to other chemical soil stabilization methods. Besides, clay has unique properties expected to alter pore water pressure redistribution in silty or loose sand during liquefaction-occurring scenarios. Typically, clays have good pozzolanic and cohesion features that could effectively balance liquefaction-prone-sands' weak cohesive properties. Clays may act as a partial replacement for other conventional soil additives used in soil stabilization like cement, lime, etc. The re-engineering of the in-situ grounds' clay mineralogy may also be implemented through different ground improvement methods such as grouting, injection, passive site remediation techniques, and several other advanced deep soil mixings (DSM) techniques. The concept of soil mixing is also promising in this regard.

1.3 Statement of Research Problem

It may be safer to use soil mixing techniques than some emerging low-cost liquefaction mitigation techniques such as the utilization of shredded tire chips, which further pollute and intoxicate the groundwater and environments with heavy metals such as Lead leachates. Similarly, other soil desaturation methods' time sustainability was doubted in the literature since such methods may deteriorate over time, thereby leaving the soil in its initial liquefaction risk state/condition. Furthermore, it is worthy of note that, the use of high plastic clays such as bentonite and laponite may improve liquefaction resistance, but they can further constitute instability to structures due to their high and unstable swelling index. Would the preferable alternative avoid the above scenarios be mixing sand with a low/lean plasticity clay such as kaolinite?

Generally, soil liquefaction is considered a threat to the entire built environment, especially in countries like New Zealand, located within the proximity of the ring of fire (i.e., seismically active regions), where the Pacific plate continuously meets with the Australian tectonic plate. The liquefaction-prone soils of the Southern Island and Canterbury region in New Zealand often experience earthquake-induced soil liquefaction whenever a seismic shake occurs in this region. Overall, earthquake-triggered soil liquefaction is considered a significant issue for the New Zealand geotechnical community at large.

However, issues related to sample disturbance effects often are attributed to laboratory assessment of soils for accurate liquefaction analyses in the direct simulation of the relative characteristic behavior of soils in in-situ field conditions (Cetin et al., 2004). In the current study, a hybrid of various approaches was applied for evaluating the strength, deformation (in terms of the stress-strain behavior), consolidation, and excess PWP generation characteristics (induced by static and dynamic loads) of ECS sands and other derived variants of sand-clay matrix soils. The study methods include both drained and undrained monotonic triaxial soil tests, physical model tests, and numerical simulations/data validation. Useful insights to engineers during the assessment of similar grounds and choice of replacement design in practice are one key overall goal of the

current study. The sudden transitioning of a stable ground from a drained condition to unstable undrained conditions needs to be properly understood before any ground improvement technique to mitigate the same may be provided. Moreso, suitable sustainable ground improvement methods which reduce the carbon dioxide emissions into the atmosphere are still to be developed and adopted for practice. The majority of the conventional ground improvement techniques using cement, lime, and other poisonous chemicals are contributing factors to the production of greenhouse gases. For instance, the production of cement itself is a major contributor to the emissions of carbon dioxide (CO_2), Smitha et al. (2021).

Lastly, a correct selection of an applicable advanced liquefaction constitutive numerical model to capture the related liquefaction behavior and mechanisms in transitional soils (e.g., clayey sand) is still lacking in the literature. The current study summarized some limitations and advantages of some selected critical state-compatible liquefaction constitutive models and the Norsand was adopted for simulating the behavior of typical clayey sand (ECS30). The match of the resulting outputs of simulations and experimental data is identical and in agreement for all the studied five aspects of the soil undrained response under static triaxial compression conditions. The studied soil undrained aspects include the stress-strain relationships, the effective stress paths (ESP), the volumetric strain-shear strain plots, the void ratio-mean effective stress space ($e - \log p_0'$), and the evolution of excess pore water pressure with shear strains.

1.4 Research Aim and Objectives

The study aims to assess certain aspects of the impacts of low plastic fines (typically kaolinite) on the undrained behavior and mechanism of ECS when subjected to both static and dynamic loads for numerical data validation purposes. The formulated research objectives to help achieve the overall aim of the study are:

1. to determine the advanced critical state characteristics of the soil samples with extreme flow failure behaviors.
2. to analyze the evolution of the dynamic pore water pressure behavior/mechanisms of all the studied remolded soil samples due to the inclusions of clay fines in the fabrics of east coast sand.
3. to evaluate the relevant advanced soil geomechanical properties of the reconstituted studied samples and analytically compare the obtained experimental evidence with the resulting characteristics outputs from a critical state-computable advanced liquefaction constitutive numerical model.
4. to critically assess the steady-state/critical state failure modes of the soil samples with the extreme flow failure trends.

1.5 Research Questions

The following are the research questions designed to achieve the overall research objectives as described above. Table 1.1 shows the relation of these research questions with the respective research goals. The questions are addressed at different stages of the research work.

1. What are the relevant advanced critical state characteristics of typical clean sand (e.g., ECS00) and clayey sand (e.g., ECS30)?
2. What are the effects of low plasticity fines (kaolinite) on the generated dynamic pore water pressure mechanisms of the ECS sand?
3. What are the relevant advanced soil geomechanical properties of the studied remolded specimens that are required for providing experimental evidence and advanced numerical model/soil data validation of the respective undrained soil properties?
4. What are the deciphered critical state failure modes of all the studied remolded soil samples?

Table 1.1 Comparison between the research objectives and research questions

Research Questions	Research Questions	Research Objectives
RQ1	What are the critical state soil characteristics caused by the addition of plastic fines to sands?	Determine the critical state characteristics of the studied remolded specimens.
RQ2	What are the effects of plastic fines on the dynamically generated excess PWP characteristics of sands?	Assess the evolution of the dynamic PWP characteristics of the studied soil samples.
RQ3	What are the required soil properties to produce efficient critical state computational models of the studied soil specimens?	Evaluate the relevant soil geomechanical parameters required for the analyses of the soil's undrained behavior.
RQ4	What are the critical state flow failure modes for the studied extreme cases?	Analytically compare the steady-state/critical state behavior of the soil specimens.

1.6 A Summary of Research Methodology

A summary of the research methods and paths designed to accomplish the current study's aim and objectives is summarized below. The path followed in this research is illustrated in the path shown in Figure 1.4.

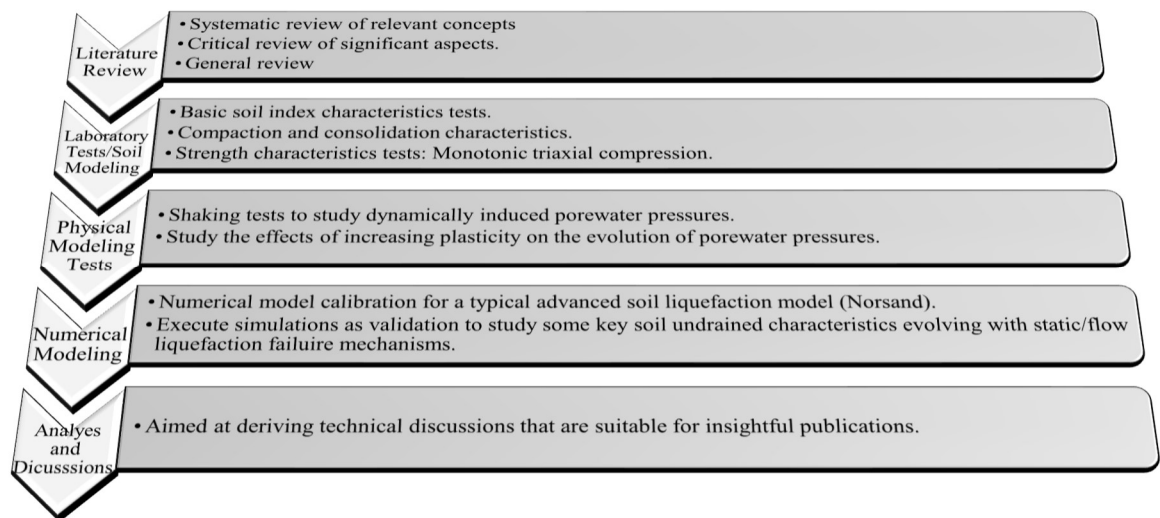


Figure 1.4 A summary of study path and scope

1.6.1 Scope of laboratory and experimental work

One of the most regularly used kinds of sand for ground construction development purposes in Auckland, the east coast sand (ECS) and commercial kaolinite (clay) were acquired for laboratory soil sample preparations and relevant soil testings. A retail marketer, “Central Landscape Supplies Ltd” from Auckland, New Zealand (Centrallandscape supplies, 2020), provided the ECS utilized in this study. The kaoline clay was supplied by “Imerys Minerals Australia Pty, Ltd,” Auckland, New Zealand (Imerys, 2020).

The unified soil classification system (USCS), as per ASTM D2487-17 (2017), was applied in classifying all studied soil samples. The primary soil index and classification tests carried out include sieve analysis (soil gradation) for the sands (ECS); hydrometer analysis for the plastic fines (kaolinite); Atterbergs’ limits or consistency tests which include the liquid limit (w_L or LL), plastic limit (w_P or PL) and plasticity index (I_P or PI); minimum and maximum relative densities or void ratios and specific gravity tests. All the fundamental soil classification experiments were executed according to the recommendations stated in Table 4.1 of MBIE (2016a) concerning relevant standards. The recommended standards in MBIE (2016a) include BS EN ISO 17892 1-12, and ASTM D420-D5876 (ASTM, 2019) standards for soil testing.

Before each test execution, the reconstituted sand matrix soil was prepared by either dry or wet mixing techniques depending on the required state of samples, the nature of tests required, and test requirements. The reconstituted mixed soil samples were achieved by mixing 0%, 5%, 10%, 15%, 20%, and 30% by weight of kaolinite with ECS. The adopted numbering nomenclature for the studied soil samples is described in Table 1.2. For instance, a sand sample labeled ECS00 indicates the alphabets as the east coast sand type, while the numbers indicate the percentage composition by weight of kaolin.

Table 1.2 Naming nomenclature and composition of kaolinite in the studied ECS sand samples

Sample Name	% composition by weight of kaolinite
ECS00	0
ECS05	5
ECS10	10
ECS15	15
ECS20	20
ECS30	30

Testing soil samples with various combinations of initial mean effective stresses and void ratios or relative densities (D_r) is fundamentally crucial for the determination of the steady-state line (*SSL*), critical-state lines (*CSL*), and also distinguish between their stress-dilatancy, and state-dilatancy behavior.

1.6.2 Monotonic triaxial compression tests

The consolidation, static undrained shear strength, and PWP characteristics of all soil samples were studied with a newly acquired, fully automatic triaxial testing machine (T-5001/A) manufactured by “Alfa Instruments” and designed according to ASTM D2850 D4767 and D7181. Monotonic tests under both isotropic consolidation drained (ICD) and undrained (ICU) conditions were carried out on all the reconstituted soil samples. The purpose of executing the monotonic compression tests is to provide experimental data for the overall technical discussions of the obtained experimental evidence of static flow liquefaction behavior of all the studied soil samples and provide some data for numerical validation of the studied soil properties for typical clean sand (with no plastic fines, i.e., ECS00) and clayey sand matrix soil (i.e., ECS30). The utilized triaxial machine, equipped with two pressure-volume-actuator (PVAs) controls and measures pressure and volume change in the cell and soil sample. The device can perform triaxial, uniaxial UCS tests, and permeability tests. The device setup is equipped with tools for all sample preparation methods that are mostly applied in similar studies. All experiments were performed remotely from a computer with state-of-the-art triaxial control software installed. The software encompasses an automatic data capturing (DAQ)/acquisition system. All tested samples were approximately 70mm in diameter and 140mm in height (based on the slenderness ratio, i.e., diameter to height ratio of 1:2). Similar to the classification and soil index tests listed earlier, all monotonic tests were carried out based on recommended standards as found in MBIE (2016a).

1.6.3 Physical modeling of dynamic soil liquefaction mechanisms

The boundary effects and similitude/scaling laws on physical models executed in the laboratory are well-known issues in the geotechnical engineering research community. Consequently, previous researchers tend to study the dynamic characteristics of soils by utilizing large-scale models. A literature review on the subject shows that large-scale physical model tests with the shaking table have associated advantages and limitations. Large-scale soil models' benefits may include experimenting with a substantial amount of materials to provide near in-situ (i.e., field) response of the prototype soils. Possible minimal boundary effects are achievable, and the volume located around the central area of the soil model container usually is considered an adequate representation of free-field dynamics. The control is possible for a large shaking table's input motion (i.e., 1-D, 2-D, 3-D, and multiples axis), and precise measurement of data is possible (Dihoru et al., 2010). Furthermore, shaking table tests is justifiable for validating numerical models to understand soil liquefaction-related problem failure mechanisms.

On the other hand, limitations of large-sized, shaking table models may include associated increased high cost of procurement and maintenance of actuators as the number of required actuators and payload increases (Prasad et al., 2004). Besides, a large-size model often requires outsized space to fit (or accommodate) test setup, especially in small-spaced laboratories; the unavoidable long durations, laborious, and fatiguing requirements for sample preparations are notable associated limitations.

It is well-known in principle that the similitude laws in terms of stress and strain cannot be satisfied in reduced-scale physical model experiments such as shaking tables (Douglas, 2003; Mizuno et al., 2000; Prasad et al., 2004). However, when a large-scale shaking table system is absent, and the required liquefaction characteristic assessment is desired for water and ground-retaining structures (such as embankments, dams, retaining walls, sheet piles, quay walls for shoreline protection work), a horizontal, single degree of freedom (SDOF) shaking table is assumed adequate. A novel 600N rated-capacity, 1-dimensional (1-D), small-scaled automated shaking table made available at the Auckland University of Technology (AUT) Geomechanics Laboratory was used to assess the studied soil sample's dynamically-induced liquefaction-related excess PWP mechanisms. The utilized shaking table can overcome the existing limitations observed with the conventional large-scale shaking tables as mentioned previously. The goal of the shaking table experiment is to experimentally observe the evolution of excess pore water pressures in all the studied reconstituted soil specimens. A more detailed explanation of the shaking table system is presented in section 3.6 of Chapter 3.

1.6.4 Numerical modeling and calibration

The computational data validation of the studied clean sand (ECS00) and a clayey sand matrix sample with 30% kaolinite content (ECS30) was carried out according to the numerical framework of the Norsand advanced soil liquefaction constitutive model. Simulations were carried out in both NorTx12 and FLAC. NorTx12 is an open-source excel program with embedded VBA code containing the Norsand formulas and it is an open-source program attached to the critical state textbook authored by Jefferies and Been (2015). FLAC – Fast Lagrangian Analysis of Continua is a two-dimensional finite difference software that is applied for solving complex geotechnical problems. Academic licenses to utilize the programs (i.e., both FLAC and FLAC3D) were issued to the author in support of the Itasca Education Partnership (IEP) scholarship program in which the author was a beneficiary. The FLAC software was applied for the numerical modeling and data validation aspects of the study. The Norsand numerical framework captured about five aspects of the soil behavior accurately and was confirmed to work for soils ranging from varieties of properties such as non-plastic to highly plastic, a wide range of confining stresses (typically 50kPa to 500kPa in the current study) in combination with a wide range of void ratios (0.500 – 1.000), quantified through the state parameter. The executed FLAC simulations also showed very good agreements with the VBA simulations and experimental data for a one-zone

soil element behavior response in cross-comparisons. The numerical framework, calibration, and simulations methodology are comprehensively explained in section 3.6 of Chapter 3. The required advanced soil geomechanical model parameters and the subsequent numerical simulation results are further discussed in Chapter 5.

1.7 Outline of the Thesis

Chapter 1 provides a general background of the study, significance/rationale of the study, research problems, aim, objectives, research questions, a summary of research methods, and work scope.

Chapter 2 describes a comprehensive literature review of soil liquefaction-related mechanisms, theories, and associated phenomena. The literature survey was structured to cover a general overview of soil liquefaction mechanisms, relevant theoretical and fundamental concepts including equations, and charts related to soil liquefaction studies, a systematic review of sample reconstitution methods, a review of related current research (effects of plastic fines on liquefaction resistance of sands) and previous studies on physical modeling (shaking table experiments for liquefaction analysis), a brief review of the fundamentals of numerical modeling in soil liquefaction analyses (static and cyclic), and a critical review of some existing liquefaction mitigation methods in the literature.

Chapter 3 describes the comprehensive quantitative research methods that were adopted in the work for the numerical, experimental, and physical modeling/validating studies.

Chapter 4 analyzed and discussed the obtained results of the executed physical model (i.e., shaking table tests).

Chapter 5 analyses and discusses the results of the soil's undrained behavior under compressive triaxial compression conditions (TC) with a strong reference to the steady/critical state for interpreting flow failures.

Chapter 6 provides a summarized discussion, conclusions, and recommendations for further research.

The textbook soils (mostly known as clean sand and pure clay) are well studied, but in the real world, most of the field soils that exist in the field situation are mixtures of both coarse and fine particles. In-situ field soils would mostly exist as a mixed soil and hence, the key relevance of the current research study.

CHAPTER 2: LITERATURE REVIEW

2.1 Introduction and General Background

In most cases, the accumulated excess pore water pressure (PWP), observed in loose, water-saturated cohesionless sands during earthquake events or seismic vibrations, leads to the eventual loss/reduction in their effective confining stress and the contact forces holding the soil particle grains together. The above mechanisms often cause an abrupt loss in the effective angle of frictional resistance, which is the sole shear strength factor of cohesionless soils, and consequently, the phenomenon of liquefaction, otherwise known as soil-liquidization, occurs. As per some early investigations regarding the topic, “sands with low densities (loose) mostly contract while sands of higher densities tend to dilate during cyclic loading” (Castro & Poulos, 1977; Martin et al., 1975; Poulos et al., 1985). An overview of the most routinely applied liquefaction assessment framework in practice is summarized herein in this chapter. Also, the parameter ‘pore pressure ratio’ (r_u) expressed in Equation (2.1) has been widely used in the research world as a proxy to quantify liquefaction. The coefficient r_u , “defined as the ratio of ‘residual or excess pore water pressure’ (Δu) to ‘initial confining effective stress’ (σ'_0 , or σ'_c , or σ'_3) of the soil,” (Boulanger & Idriss, 2006; Ganainy et al., 2012; Mohammadi & Qadimi, 2015; Polito et al., 2008; J. Wang et al., 2020; Yamamuro & Lade, 1999; Yegian et al., 2007). Liquefaction resistance explained, “as the required frequencies or the number of cycles for double amplitude strain to achieve the specific value of 5% strain” (Mohammadi & Qadimi, 2015, p. 153).

$$r_u = \frac{\Delta u}{\sigma'_0} \quad 2.1$$

The path to soil liquefaction based on the parameter r_u is summarized as when $r_u \geq 1$, full liquefaction is said to occur; when $r_u = 0.25$ to 0.70 , it implies that partial occurrence of liquefaction (cyclic mobility) has occurred and where $r_u = 0$, a condition of no liquefaction applies. Boulanger and Idriss (2006) explained the term “cyclic mobility” as the condition when temporarily ($r_u = 100\%$) as a result of reversed s-shaped stress-strain loops otherwise known as pseudo-steady static state with the development of limited strains.

Boulanger and Idriss (2006) further suggested the term liquefaction for “largely developed strains in fine-grained soils manifesting sand-like characteristics while cyclic softening, be applied in describing the same mechanisms in fine-grained soils manifesting clay-like behavior.” However, the dynamics of the soil liquefaction process are analyzed with the principles and theories of effective stresses. The idea of effective stress as established by the father of soil mechanics “Karl Terzaghi” (Terzaghi, 1943), critical state parameters (Schofield & Wroth, 1968), bounding and dilatancy surfaces (Cheng, 2013; Dafalias & Manzari, 2004; Dafalias et al., 2004), yield criterion, flow rule, elastic law, elastoplasticity, hypoplasticity (Z. L. Wang et al., 1990), equivalent linear and nonlinear analyses (Itasca, 2021) are all relevant for comprehensive soil liquefaction analyses.

Hence, the routine liquefaction analysis typically is executed regarding the soil's undrained condition in the effective stress state since the mechanical properties of the ground (compressibility and strength) are directly determined by effective stress, Head (2014). The effective stress principle is expressed in Equations (2.2), as stated by Terzaghi (1943) in 1924. The effective stress sometimes is indicated as the 'intergranular stress' in routine practice (i.e., the existing stress binding the solid particle grains of the soil and holding them together).

$$\sigma' = \sigma - u_w \quad 2.2$$

And σ' is the existing soil's vertical effective stress or overburden, σ is the total geostatic stress in a given soil element, given by Equation (2.3), and u is the pore water pressure in the soil voids given by Equation (2.4)

$$\sigma = \gamma h \quad 2.3$$

The total specific unit weight of soil is γ , and h the depth of soil element under consideration.

$$u_w = \gamma_w h = h \rho_w g \quad 2.4$$

The unit weight of water is γ_w , and h is the reference depth [i.e., groundwater level (GWL) or groundwater table (GWT)].

Hence, expanding Equation (2.2) gives Equation (2.5) from (2.3) and (2.4) thus:

$$\sigma' = \gamma h - \gamma_w h = (\gamma - \gamma_w) h = \gamma' h \quad 2.5$$

“where $(\gamma - \gamma_w)$ Or γ' is the submerged or buoyant unit weight of soil,” Fang (2013).

Several forms of stresses exist in the soil element, and most of them are mentioned here in the literature. For instance, in the triaxial condition, the effective stresses acting on the major planes are known as principal effective stresses (major and minor). The major principal effective stress (σ'_1) also known as the axial stress (σ'_a) and the minor principal effective stress (σ'_3) similarly referred to as the confining stress (σ'_c) or effective radial stress (σ'_r). The effective intermediate stress (σ'_2) usually is equivalent to the minor effective stress, i.e., ($\sigma'_3 = \sigma'_2$). The stress invariants, the deviatoric stress (q) and mean effective stress (p') expressed in Equations (2.6), usually are defined with respect to the axial stress and radial stress (Hird & Hassona, 1990). According to the Cambridge stress fields, the two stresses expressed in Equation 2.6 usually are known as stress invariants (Been & Jefferies, 2004). A good summary of both the MIT and Cambridge stress fields frameworks is available in Head (2014, p. 73).

$$q = \sigma'_1 - \sigma'_3 \text{ or } \sigma'_a - \sigma'_r ; \quad p' = \frac{\sigma'_1 + \sigma'_2 + \sigma'_3}{3} = \frac{\sigma'_1 + 2\sigma'_3}{3} \text{ or } \frac{\sigma'_a + 2\sigma'_r}{3} \quad 2.6$$

The ratio of q to p' which represents the characteristic soil behavior is known as stress ratio (η) (Jefferies & Been, 2015).

Similarly, the relative strain invariants to the above-mentioned stress invariants are expressed in Equation 2.7, where the dot notation signifies small increments.

$$\dot{\epsilon}_v = \dot{\epsilon}_1 + 2\dot{\epsilon}_3 ; \dot{\epsilon}_q = 2/3(\dot{\epsilon}_1 - \dot{\epsilon}_3) \quad 2.7$$

The ratio of $\dot{\epsilon}_v$ to $\dot{\epsilon}_q$ corresponding to the maximum stress ratio η is known as the stress dilatancy or measure of dilation, where the dot notation on the strains implies increment on the same. The comprehensive, detailed information and explanation of the stress-dilatancy framework are well-explained in Been and Jefferies (2004). The dilatancy denoted by D , is defined as the likelihood of soils to increased change volume and it is routinely computed with respect to the strain increments, and not the original strains.

The shear stress (τ), also equivalent to the undrained strength (S_u) of soils is expressed in Equations (2.8) and (2.9) as the average difference between the major principal and minor principal stresses, thus:

$$\sigma'_1 - \sigma'_3 = 2S_u \quad 2.8$$

In the conventional stress analysis of soils, the analysis of effective stresses, the soil's shear strength is often approximated by the Mohr-Coulomb (MC) equation as stated by Terzaghi in (2.9).

$$\tau = \sigma' \tan(\phi') + c' = (\sigma - u_w) \tan \phi' + c' \quad 2.9$$

where ϕ' is the soil's effective angle of internal friction, otherwise known as angle of shear resistance, which has some invariants such as critical state friction angle (ϕ'_{cv}), peak friction angle (ϕ'_p), and residual friction angle (ϕ'_r); c' is the effective or apparent cohesion (intercept on the shear stress axis of the Mohr circle), which largely depends on the considered stresses and do not necessarily imply the soil property. The effective stress cannot be measured directly but rather it is estimated from the applied stresses and pore water pressures obtained from triaxial tests and other well-known instrumented tests.

2.1.1 Factors affecting soil liquefaction

Stability analyses in soil liquefaction problems often depends on the soils' initial state, known as the ground's in-situ soil conditions, typically factored through the void ratios or densities as the state parameter (ψ) coupled with existing mean effective stresses in the fabrics of soil element. The undrained steady-state strength of the soil is the numerator, and the driving shear stress is the denominator in the factor of safety analysis (Poulos et al., 1985). Generally, for soil liquefaction to occur, the soils must be loose with granular sediments (loose sand/silty sand), water-saturated, and there must be a strong seismic load (in the form of dynamic shakings/excitations or oscillatory or harmonic loads from earthquakes). The soils' mechanical properties are primarily dictated by the material granularity (i.e., particle size gradation), material elastoplastic parameters (e.g., shear, bulk modulus), geometric properties of soil grains (particle-shapes such as degree of roundness, elongation, and flakiness), the mineralogy of soils, and the soil state parameters (typically a combination of void ratios and existing mean effective stresses), etc. In the context of laboratory studies for soil liquefaction, Hird and Hassona (1990) attributed some of these factors

to testing techniques (strain rate, specimen preparation, and stress history) and some material properties (compressibility and particle shape), while Castro and Poulos (1977) stated that, “amount of PWP generated during a cyclic test depends on the extent of cyclic loads, the total number of cycles (N), nature of test and soil properties. Dixit et al. (2012); Figueroa et al. (1994); Youd and Idriss (2001) have all stated clearly some factors affecting soil liquefaction susceptibility, and they are summarized as follows:

- (a) soil gradation (particle size distribution) and fine contents
- (b) soil relative density
- (c) applied load/stress types
- (d) soil drainage characteristics, the saturation degree, permeability and porosity properties
- (e) acting effective confining stress on soil and respective void ratio combinations
- (f) soil structure and bond-types existing between the soil inter-particle contacts
- (g) intensity and duration of cyclic/vibratory/dynamic/earthquake loads
- (h) deposits strain histories
- (i) quantities of entrapped air in deposits
- (j) deposit's thickness
- (k) distance from the earthquake source
- (l) ground acceleration amplitude and frequency of shaking

All the factors mentioned above were all observed to play significant roles in liquefaction development than others. In their study, Riemer and Seed (1997) examined “the impacts of consolidation stress, drainage, and effective stress-path on the location of the SSL through triaxial and simple shear tests” to highlight the significance of deformation mode on strength characteristics of soils at large strains. Conclusions drawn from the above study indicated that the initial mean effective consolidation stress (σ'_c , or σ'_3) has significant effects on the minimum undrained strength (“i.e., quasi-steady-state”), while higher mean consolidation stress has produced higher strength over a good range of strains. The merits of drainage conditions appear to have negligible effects on the steady-state relationship in compression than extension tests during triaxial conditions. The measured minimum undrained strength in triaxial extension was reduced as compared to compression tests. A little alteration of laboratory tests can produce huge effects on obtained results for sands' properties at large strains, especially with the experimentally determined void ratios if not done by the application of the widely advocated freezing method after tests.

It is also well-known that saturated loose sand within the steady-state or critical state envelope may exhibit some unstable behavior under drained stress-controlled conditions, otherwise known as “static liquefaction” (i.e., “drained collapse”). The above scenario is well-reviewed and studied by Gajo et al. (2000).

2.1.2 Recent records of earthquake-triggered soil liquefaction and resulting damages

Soil liquefaction related studies have developed and advanced over time since the occurrence of the two significant earthquakes in Niigata, Japan ($M_w 7.5$) and Alaska, USA ($M_w 8+$) both in 1964 (Castro & Poulos, 1977; Cornejo, 2015; Jafarian, Vakili, et al., 2013; Jefferies & Been, 2015; R. B. Seed et al., 2003). A significant estimate of economic loss, loss of lives, and lifelines are usually the consequences of the most recent earthquake-induced soil liquefaction events.

More instances of earthquake-induced soil liquefaction histories in New Zealand include the Kaikoura earthquake of magnitude ($M_w 7.8$) happening on 14 November 2016 (Cubrinovski et al., 2018; Cubrinovski et al., 2017; Duputel & Rivera, 2017; Hollingsworth et al., 2017; Stringer et al., 2017; Woods et al., 2017). One of the most debilitating events occurring about a decade ago is the Canterbury Earthquake Sequence (CES), beginning on 4 September 2010 with the Darfield seismic shakes $M_w 7.1$ earthquake (Morikawa & Cho, 2020; J. Wang et al., 2020). Other series of shocks in the CES event include the Christchurch earthquake series of 22 February 2011 with $M_w 6.2$, 13 June 2011 with $M_w 6.0$, and 23 December 2011 with $M_w 5.8$ to $M_w 5.9$ (Bradley & Hughes, 2012; Khoshnevisan et al., 2015; Maurer et al., 2014; Maurer, Green, Cubrinovski, et al., 2015; Taylor et al., 2015; vanBallegooy et al., 2015; Wotherspoon, Orense, Bradley, et al., 2015; Wotherspoon, Orense, Green, et al., 2015). A useful reference on the older historical earthquake-induced soil liquefaction case histories in New Zealand is Fairless and Berrill (1984).

The usually experienced civil failures with seismically triggered soil liquefaction include observed differential settlements and tilting of buildings, lateral spreading and settlement-induced failures of bridges, failure of lifelines (buried pipes, dilapidated electric poles, communication lines), failed road functionality, impaired port structures, sand boils and submerged environment. Castro and Poulos (1977), Jefferies and Been (2015) highlighted and summarized most conventional high-profile damage caused by flow liquefaction and cyclic mobility. Examples of such failures occur in hydraulic-fill applications such as flow slides that happened in Zealand, Holland, and along the Mississippi river; failures of dams such as Fort Peck dam in Montana in 1938, Calaveras dam in California in 1920, and Lower Lan Norman dam in California in 1971.

Other recent examples of earthquake-induced soil liquefaction, which resulted in severe collateral damage, include the Nepal Gorkha earthquake with $M_w 7.8$ on 25 April 2015 (Gautam et al., 2017). The 26 January and 3 February 2014 Cephalonia, Greece earthquakes with magnitude $M_w 6.1$ and $M_w 6.0$ respectively (Papathanassiou et al., 2016); 20 and 29 May 2012 Emilia-Romagna region, Italy earthquakes with magnitude $M_w 6.1$ and $M_w 6.0$, respectively (Gautam et al., 2017; Papathanassiou et al., 2015). The 11 March 2011 Tohoku earthquake in Japan, known as one of the greatest in the history of Japan earthquakes with $M_w 9.0$ (Sana & Nath, 2016; J. Wang et al., 2020) recorded devastating damage to infrastructures; 12 January 2010 Haiti earthquake with $M_w 7.0$ (Olson et al., 2011) and 17 August 1999 Turkey earthquake with $M_w 7.4$ (Kanibir et al., 2006).

2.2 Relevant and fundamental theoretical concepts relating to soil liquefaction

physics/math

The underlying conceptual framework of static liquefaction analyses revolves around the theories of “steady-state” (SS), mostly regarded as equivalent to the “critical-state” (CS) soil mechanics in the literature. Castro and Poulos (1977), in their work, distinguished between the term “cyclic mobility” and “liquefaction” while utilizing the steady-state line (SSL) for some laboratory data. Other names synonymously developed in the literature for cyclic mobility include cyclic liquefaction, cyclic softening, and initial liquefaction, while the actual liquefaction or ‘flow liquefaction’ usually is used for the static liquefaction cases (Jefferies & Been, 2015, p. 14).

The reviewed ‘critical state line’ (CSL), as found in Mohammadi and Qadimi (2015, p. 152), was illustrated as “the equivalent orientation of the soil material in $v: \ln p'$ space (where $v = 1 + e_{cs}$ or $1 + G_s w$ is the specific volume) while considering the reaction of density and stress intensity on the soil behavior”. “Where e_{cs} is the critical void ratio at the critical state, G_s is the soil's specific gravity, and w is the soil weight” Mohammadi and Qadimi (2015). SS and CS concepts are well-established concepts for static liquefaction analyses and the technical implications/discussion of the undrained behavior of soils.

Most studies in recent times (Mohammadi & Qadimi, 2015; Phan et al., 2016) have integrated either the SSL/CSL frameworks. Figures 2.1 (a) and (b) showed some explicit representations of such integrations. The sands' contractive response at the critical state often is used to describe their liquefaction interplay mechanisms in both the (SSL) and CSL frameworks. Though the SSL and CSL have been assumed as the same in the literature, the key difference is that the CSL is a computable one while the SSL is not. Therefore, when the state point (SSL) of soil is above the CSL, with a positive state parameter (ψ), the sand may contract when sheared. In other words, when the state point falls below the CSL with a negative (ψ), the sand may likely dilate during shearing. The mean effective stress (determined from Equation 2.6), e_0 the post-consolidation void ratio, v_i is initial specific volume, and v_{cs} is the specific volume at critical state are all the required parameters for deriving the state parameter (ψ) or modified state parameter (ψ_m). In addition, dense sands tend to exhibit positive dilatancy while loose sand experiences negative dilatancy, Towhata (2008).

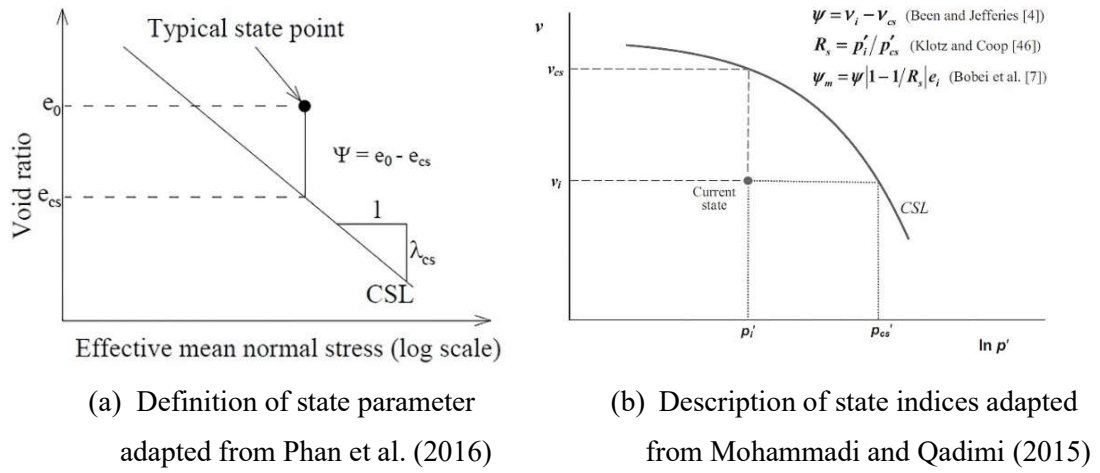


Figure 2.1 Representation of various state indices and CSL/SSL

2.2.1 The steady-state framework

The “steady-state” (SS) framework, initially proposed by Poulos (1981) is still relevant and currently applied in 21st-century soil mechanics to define the state of soils under static loads. The SS case of soil is explicitly explained by Poulos (1981, p. 553) as “that condition where the soil continuum is perpetually deforming at constant shear stress, constant volume, constant normal effective stress, and constant velocity.” In other words, “the reference state (locus of all points) from which the stretch of sand from the so-called reference state describes “SS” or “steady-state line” (SSL) of sand in the void ratio-stress space,” (Been & Jefferies, 1985, p. 104). The determination of SSL is well-described in (Castro & Poulos, 1977; Castro et al., 1992; Poulos, 1981; Poulos et al., 1985; Vaid & Sivathayalan, 2000), and it is spectacular in the shearing process, not in the steady static state. Instances of the occurrence of SS deformation mechanisms were reported by (Bobei et al., 2009; Poulos, 1981). For instance, the undrained tests of fully saturated loose sand, drained tests on sand at large strains, and undrained or drained tests on clays. According to Castro and Poulos (1977), “cyclic mobility is easily differentiated from liquefaction with the aid of the SSL.”

Summarily, the locus of the steady-state in the void ratio, mean effective stress, and deviatoric stress - space can be used to establish the proneness of sand to flow liquefaction. The resulting soil strength from the SS is called “steady-state, residual or post-peak strength” (Jafarian, Ghorbani, et al., 2013, p. 739). Several studies have utilized the SS concept to analyze the strength of sands in the past, for instance: (Been & Jefferies, 1985; Bobei et al., 2009; Castro & Poulos, 1977; Jafarian, Ghorbani, et al., 2013; Poulos, 1981). Three different forms of undrained soil responses include flow, limited flow, and non-flow (Bobei et al., 2009). The flow and limited flow is associated with ‘static liquefaction’ while the non-flow is related to the ‘cyclic liquefaction’ (Bobei et al., 2009, p. 3). The concept of “state parameter” introduced by Been and Jefferies (1985) is one of the most detailed works describing “state” (referred to as the initial physical condition of a soil material), which in turn is applied in determining the advanced geomechanical properties of such soils (i.e., the soils’ initial state, critical state void ratio, and

plasticity, and elasticity-based parameters). The latter work above postulated that the material behavior of sands could be characterized in terms of two variables, namely:

- (a) The state parameter (ψ) which combined the effects of stress and void ratio/relative density and expressed in Equation (2.10) as:

$$\psi = e_0 - e_{ss} \quad 2.10$$

" ψ known as the state parameter is the difference between the present void ratio and the SS void ratio, e_0 is the current void ratio, and e_{ss} the SS void ratio" (Bobei et al., 2009, p. 4). Intuitively, a negative ψ indicates dense or dilatant soils analogous to non-flow characteristics, while a positive ψ corresponds to loose or contractive soils which relates to static liquefaction scenarios (Been & Jefferies, 2004; Bobei et al., 2009).

The state parameter differentiates between void ratio at SSL and the present void ratio at the constant effective mean stress. It also indicates the initial 'stress-density' condition of the soil sample. Equation (2.11) defined the relative density of soils and regarded as one of the essential parameters for sample preparation in determining the SSL.

$$D_r = \frac{(e_{max} - e)}{(e_{max} - e_{min})} \quad 2.11$$

Here, e is the initial void ratio at in-situ state, e_{max} and e_{min} the maximum void ratio (in the loosest condition) and minimum void ratio (densest state) of the soil, respectively.

- (b) The fabric parameter accounts for sand grains/matrix structure at the microscopic or macroscopic level.

The state parameter ψ routinely is obtained from the void ratio (e) and effective mean stress (p') for the CSL, as shown in Figure 2-1(a) by Phan et al. (2016).

However, recent studies have revealed that (e) is not precisely a suitable parameter for representing the state of sand density containing fines because small deviation in fines' content reportedly changed the location of the SSL on the $e - \log(p')$ space (Rahman et al., 2014a; Rahman & Lo, 2008b; Thevanayagam et al., 2002). Therefore, a sand matrix soil containing a low percentage of fines content (f_c) may consider the f_c inactive in-between the intergranular force skeleton of the sand because of the possibilities fines trapped in between the voids space of sand particles (Rahman & Lo, 2008a). The concept of equivalent granular void ratio (e^*) was therefore introduced by Thevanayagam et al. (2002) to consider fines as partially active in the transmission of particle to particle contact forces between the matrix structure of the sand. All the relevant equations applicable to the concept of equivalent granular void ratio (e^*) and equivalent granular steady-state line (EG-SSL) are summarized in Equations 2.12 to (2.17).

Hence:

$$e_g = \frac{e + f_c}{1 - f_c} \quad 2.12$$

$$e^* = \frac{e + (1 - b)f_c}{1 - (1 - b)f_c} \quad 2.13$$

Where e_g is the inter-granular void ratio; (f_c) is fines content; f_{thre} is the threshold fine content defined as the point of transitional behavior of sand-fines, which changes from “fines in the sand” to “sand in fines”; (b) is active fines fraction transferring forces between sand grains where the inactive fine content regarded as voids. Comprehensive estimation procedures for b -values and f_{thre} are detailed in Rahman and Lo (2008b); Rahman et al. (2014a, p. 265); Rahman and Lo (2008a).

$$b = \left[1 - \exp \left(-0.3 \frac{\left(\frac{f_c}{f_{thre}} \right)}{k} \right) \right] \times \left(r \frac{f_c}{f_{thre}} \right)^r \quad 2.14$$

Or

$$\left(1 - e^{\left(\frac{m[f_c]^n}{k} \right)} \right) \left(\frac{r f_c}{f_{thre}} \right)^r \quad 2.15$$

Where m and n are empirical constant; $(1 - r^{0.25})$ and $r = \frac{1}{\chi} = \left(\frac{D_{10}}{d_{50}} \right)^{-1}$, k and r are obtainable from gradation curves while a value of 0.3 can be assumed for f_{thre} (the threshold fines content) otherwise, be calculated from Equation (2.16) where χ ranges from 2 to 42:

$$f_{thre} = 0.40 \left(\frac{1}{1 + e^{0.5 - 0.13\chi}} + \frac{1}{\chi} \right) \quad 2.16$$

Hence, recent researchers suggested that the SSL substituted with the equivalent granular steady-state line (EG-SSL), the state parameter (ψ) substituted with ψ^* and replace e with e^* with Equation (2.10) becoming Equation 2.17:

$$\psi^* = e^* - e_{ss}^* \quad 2.17$$

Where e^* and e_{ss}^* are equivalent granular void ratio at the present state and void ratio at steady state for the corresponding effective mean stress respectively as shown in Figure 2.2.

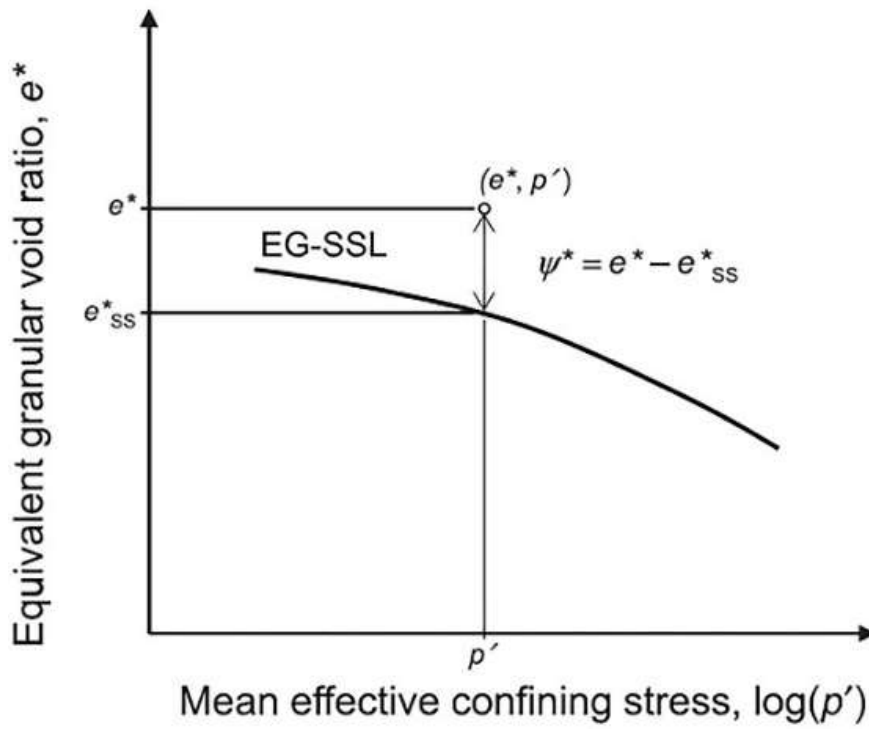


Figure 2.2 State parameter (ψ^*) for equivalent granular condition (EG-SSL) adapted after Rahman et al. (2014b)

In general, it is a well-established fact that the stress-strain behaviors of soils are usually nonlinear as soil stiffness (tangential modulus) often reduces as the shear stress and strains increase up to the peak failure stress.

2.2.2 The critical state theory

The critical state (CS) of a soil continuum explained by Poulos (1981, p. 557) “is positioned between its peak and residual strength, i.e., at a point at which steady-state of deformation is not occurring” or the point at which the metastable soil structure is destroyed. In other words, Jefferies and Been (2015) simply defined the CS as the endpoint of the shearing resistance of soils where the soil does not deform further even with additional shearing loads, and knowledge of this is required to produce suitable liquefaction mitigation designs. Another noted difference in the definition of CSL from SSL is the absence of the word “constant velocity”, otherwise all the other mentioned constants are reflected in the definition of both theories. The concept of CS, first established by Roscoe et al. (1958), is well-established, considered in the current world of several advanced soil constitutive numerical models. The framework explains the interrelationships between the consolidation and strength characteristic soil behavior as a correlated interpretation, a proper understanding of the CS framework would show that the former mentioned two aspects are related.

The critical void ratio state was applied explicitly based on the (p', e, q) space for three-dimensional stress-invariant analyses. The critical void ratio line (C.V.R. line) was defined as “a

unique line that exists to which all loading paths in the (p', e, q) space converge according to the obtained data of drained and undrained tests” (Roscoe et al., 1958, p. 28). “The critical state line (CSL) is known as loci of critical state points in the $v: \ln p'$ or (p', e, q) space,” (Mohammadi & Qadimi, 2015; D. M. Wood, 1990). At a CS, the pore water pressures and effective stress do not change even with continuous shearing and deformation. This state may be inferred as a reference state to illustrate other effects on soil strength failure characteristics such as relative density, stress paths, and overconsolidation ratio (Poulos et al., 1985). The CS emerged from the well-known plasticity theory and is comprehensively explained in Jefferies and Been (2015).

The location of the CSL does not depend on the following factors: initial state stress history, shearing rate, relative density, stress path, and drainage conditions but mainly depends on the fines content, as indicated in section 2.2.1 with the concept of intergranular void ratio. Summarily, the fundamental concept behind the CS is based on conditions of uniform shearing. A unique relationship exists between deviator stress at critical state (q_{cs}), mean effective stress at CS (p'_{cs}) and void ratio or specific volume at CS ($v_{cs} = 1 + e_{cs}$). CSLs may be evaluated for any type of soil in the triaxial compression condition based on Equation (2.18) to (2.20) while Equation (2.19), (2.20), and (2.21) works for sand thus:

$$q_{cs} = Mp'_{cs} \quad 2.18$$

$$v_{cs} = 1 + e_{cs} = \Gamma - \chi_{cs} \ln p'_{cs} \quad 2.19$$

$$M = \frac{6 \sin \phi_{crit}}{3 - \sin \phi_{crit}} \quad 2.20$$

where M is the CS stress ratio, χ_{cs} the CS compression index, Γ is specific volume or void ratio intercept at $p' = 1$).

For sand, the relative density parameter is most predominantly applicable, thus:

$$D_{R,cs} = \frac{(e_{max} - e_{cs})}{(e_{max} - e_{min})} = \frac{1}{\ln \left(\frac{\sigma_c}{p'} \right)} \quad 2.21$$

Alternatively, Li et al. (1999) proposed Equation (2.20) to produce the CSL (e_{cs} vs p'):

$$e_{cs} = e_0 - \chi_s \left(\frac{p'}{p_a} \right)^\xi \quad 2.22$$

where e_0 is void ratio when $p' = 0$, p_a is reference atmospheric pressure (usually 100kpa), χ_s and ξ are material constants.

Both concepts of SS and CS are mostly inferred to be governed by the same physics in the literature as both are attached to the state parameter defined in Equation 2.10, but a significant difference is that the steady-state do not have a computable model or theory while the CS has (Jefferies & Been, 2015).

2.2.3 Basics of ground motions and ground motion intensity quantification

The knowledge of ground motions and ground motion intensity measurements are fundamentally significant in the case of earthquake-induced liquefaction assessment. The cause of earthquakes originates from the Earth's crust with the unexpected dissipation of stored elastic strain energy along the fault planes (Vytiniotis, 2011). The dissipated elastic strain energy is noticed on the Earth's surface by the generated seismic body waves, including the primary waves (i.e., P-waves), shear, or secondary waves (i.e., S-waves), and surface waves. The wave types mentioned above typically are Rayleigh and Love waves (Kramer, 1996). Most well-known ground motion intensity quantifications are well-summarized in Vytiniotis (2011). The moment magnitude is the most well-known earthquake intensity measure and is stated in Equation 2.23

$$M = \frac{2}{3} \log_{10} M_0 - 10.7 \quad 2.23$$

In Equation 2.23, M_0 = seismic moment magnitude in dyne centimeters (10^{-7} Nm).

Other essential ground motion intensity/quantification include the peak ground acceleration (*PGA*), Arias intensity (I_a), peak ground velocity (*PGV*), predominant frequency f_p) which is the frequency corresponding to the highest value in the Fourier spectrum, the bracketed duration (T_d), the root mean square acceleration (a_{rms}), the characteristic intensity (I_c), and the equivalent number of cycles (*CSR*) causing liquefaction described in Equation 2.25 of section 2.3.1. The attenuation relationships for the majority of the ground motion intensity mentioned above are well-researched and summarized by Kayen and Mitchell (1997); (Sadigh et al., 1997).

The required input ground motion (GM) to investigate seismic characteristics of soils can either be synthetic or recorded, Vytiniotis (2011). The synthetic input ground motions are from models or simulated sinusoidal motion. In contrast, recorded motions, as the name implies, are time history records obtained from past seismic events with GM-recording instruments (Kwong, 2015). Examples of synthetic GM are those obtained from the shaking table and centrifuge model tests. Several recorded GM databases exist on the internet, for instance, Pacific Earthquake Engineering Research Center (PEER) (2020), COSMOS Virtual Data Center (n.d.), Luzi et al. (2017), Zealand (n.d.), Orfeus (n.d.). In routine practice, GM (either synthetic or recorded) contains standard and non-standard noise. These noises must be filtered out or removed by baseline adjustments within a specific frequency range. Boore and Bommer (2005) provided the reasons for processing GM records, methods for executing processing, and the consequential effects of each technique used. GM records' required principal parameters for engineering applications are the ordinates of response spectra for both acceleration and displacement Vytiniotis (2011). The parameters PGV and peak ground displacement (PGD) are generally obtainable from the acceleration's first and second integrals, respectively. Several computer program tools are available for processing either analog or digitally recorded GM time histories

for baseline correction/filtering, scaling, and response spectra analysis; Papazafeiropoulos and Plevris (2018) have provided a comprehensive review of most GM processing software tools.

2.3 An overview of liquefaction assessment methods routinely applied in practice

Approximate or nearly accurate liquefaction triggering assessment is the first and the most significant step customarily required in any analysis and design for a proposed soil liquefaction-mitigation design scheme (Bolarinwa et al., 2019). The extensive amount of study carried out in the current literature work is a bid to summarize the prediction of liquefaction triggering mechanisms or liquefaction susceptibility of soils. However, all previous studies' outcomes were found to be scattered and not well collated to form a unified framework for the world geotechnical community's reference in one place. More importantly, there currently exist some contradictions between methods proposed by Idriss and Boulanger (2010); Youd and Idriss (2001); Cetin et al. (2004). In practice, the Idriss and Boulanger (2010), Boulanger and Idriss (2014) approach is most routinely utilized.

NASEM (2016), in their report, carried out an extensive review of current liquefaction assessment methods and classified them as “stress approach, cyclic strain-based, energy approach-based, laboratory tests, physical model-based, numerical modeling-based, performance evaluation, and design-based techniques.” A review presented here is to primarily provide an overview in addition to a conference paper presented by the author at the “Pacific Conference of Earthquake Engineering” (Bolarinwa et al., 2019). The current trends for accurate liquefaction assessment require material characterization, in-situ state characterization, and system response studies. Therefore, the present literature work presents an overview of some standard liquefaction assessment techniques. These methods are categorized as in-situ-based, laboratory-based (e.g., triaxial and shaking table), and numerical simulations/modeling in subsequent subsections to reflect the commonly adopted routine assessment techniques in practice.

2.3.1 In-situ based liquefaction assessment methods

Most of the field routine in-situ testing techniques are applied to obtain some key proxies for liquefaction quantification of cyclic resistance ratio (*CRR*). Such in-situ tests include the standard penetration test (*SPT*), cone penetrometer test (*CPT*), shear vane (V_s), becker penetration test (*BPT*), screw driving test (*SDT*), and large penetration test (*LPT*). The primary objective of such field tests mentioned above is to obtain some field index parameters and subsequent correlations with previous case histories (Idriss & Boulanger, 2006). The focus is to empirically estimate a factor of safety (*FOS*) for soil liquefaction (Boulanger & Idriss, 2014, 2015; Idriss & Boulanger, 2006, 2010; MBIE, 2016b; Poulos et al., 1985). The in-situ field tests often are applied as a proxy to quantify the existing shear strength of the investigated soil (i.e., *CRR*). The *CPT* and *SPT* are the mostly and routinely utilized in-situ testing techniques for liquefaction assessment, while others are only adopted in exceptional circumstances or requirements (Boulanger & Idriss, 2014).

H. B. Seed and Idriss (1971), firstly proposed the simplified stress method (otherwise known as “Seed-Idriss simplified method”). The simplified approach is about the most widely applicable technique for liquefaction triggering assessments in routine practice for in-situ based liquefaction evaluation techniques, where the *FOS* is estimated as the ratio of the cyclic resistance ratio (*CRR*) to cyclic stress ratio (*CSR*) (Kongar et al., 2017; MBIE, 2016b; NASEM, 2016). In this regard, the *CRR* method is a measurement of the soil’s capacity to resist liquefaction (i.e., *CSR* that will cause liquefaction occurrence) and stated for some in-situ methods in subsequent subsections. The *CSR* empirically quantifies the earthquake loading (cyclic shear stress) and is generally estimated as 65% of the maximum cyclic shear stress ratio, i.e., $0.65 \frac{\tau_{max}}{\sigma'_{v0}}$ (Boulanger et al., 2011) and *FOS* is estimated from Equation (2.24) as

$$FOS = \frac{CRR}{CSR} \quad 2.24$$

In an alternative to conducting an explicit site response investigation, the *CSR* is estimated from Equation (2.25) based on Newton’s second law as:

$$CSR = 0.65 \times \frac{PGA}{g} \times \frac{\sigma_v}{\sigma'_{v0}} \times r_d \quad 2.25$$

where g is gravity acceleration, PGA is peak ground acceleration (horizontal component), σ_v is overall stress overburden at depth z , σ'_{v0} is effective overburden stress at depth at z . The *CSR* is corrected by a magnitude scaling factor (*MSF*) to estimate effects of earthquake duration of shaking for a magnitude moment of an earthquake ($M_w 7.5$) given in Equation (2.26), Equation (2.25) has been modified into Equation (2.27) by Boulanger et al. (2011).

$$MSF = \left(\frac{M_w}{7.5} \right)^{-2.56} \quad 2.26$$

$$CSR_{M=7.5, \sigma'_v=1atm} = 0.65 \times \frac{\sigma_v}{\sigma'_{v0}} \times \frac{a_{max}}{g} \times r_d \times \frac{1}{MSF} \times \frac{1}{K_\sigma} \quad 2.27$$

where K_σ is a factor accounting for overburden stress, Computations for previous records are such that the CSR induced by the earthquake is modified to a reference $M_w 7.5$ and $\sigma'_v = 1atm$ (101kPa). The CRR and CSR are both normalized by the effective vertical stress during the analysis.

r_d is a reduction factor for shear stress accounting for dynamic reactions of the considered soil profile and summarized in Equation (2.28) and (2.29) for depths specified (Boulanger & Idriss, 2014; Youd & Idriss, 2001)

$$r_d = 1.0 - 0.00765z \text{ (with } z \leq 9.15m) \quad 2.28$$

$$r_d = 1.174 - 0.0267z \text{ (with } 9.15m < z \leq 23m) \quad 2.29$$

Idriss and Boulanger (2006) suggested some values for r_d (Equations 2.30 to 2.33) and recommended them be related for depths less than 20m as the uncertainty of these values keeps increasing with depth,

$$\ln(r_d) = \alpha(z) + \beta(z)M \quad 2.30$$

$$\alpha(z) = -1.012 - 1.126 \sin\left(\frac{z}{11.73} + 5.133\right) \quad 2.31$$

$$\beta(z) = 0.106 + 0.118 \sin\left(\frac{z}{11.28} + 5.142\right) \quad 2.32$$

$$r_d = 0.12 \exp(0.22M) \quad 2.33$$

where M is earthquake magnitude.

However, in the original proposed simplified approach by H. B. Seed and Idriss (1971), CRR was estimated from SPT number (i.e., blow counts) of soils, while ensuing modifications of this technique applied to other soil indices obtained from the CPT, V_s , BPT and SDT etc. A detailed review of above methods are well-outlined and explained by Youd and Idriss (2001). Summarily, liquefaction occurs for computed factors of safety whenever $FOS \leq 1$ and non-liquefaction when $FOS > 1$.

Additionally, Iwasaki et al. (1984) presented a relationship called the liquefaction potential index (LPI) to assess liquefaction severity at ground level based on extension of the FOS method. LPI evaluates the chance of liquefaction at ground level by harmonizing the function of FOS for soil layers inside the top 20m of soil. LPI is calculated from Equation (2.34), where $F^* = 1 - FOS^*$. In one soil layer, liquefaction possibility presumed is very minimal when $LPI = 0$; low if $0 < LPI \leq 5$, high if $5 < LPI \leq 15$ and highly certain if $15 < LPI \leq 20$. Where F^* is a corrected factor of safety multiplied by 1.4 (i.e. Equation (2.24) is multiplied by 1.4).

$$LPI = \int_0^{20} F^*(10 - 0.5z)dz \quad 2.34$$

Maurer, Green, and Taylor (2015) later modified Equation 2.34 as " LPI_{ISH} " and derived in Equation (2.35)

$$LPI_{ISH} = \int_0^{20} F(FS) \frac{25.56}{z} dz \quad 2.35$$

Similarly, following the CES of 2010-2011, vanBallegooy et al. (2014) suggested the term "liquefaction severity number" (LSN) to estimate severity of liquefaction occurrence expressed in Equation (2.36) thus:

$$LSN = 1000 \int \frac{\varepsilon_v}{z} dz \quad 2.36$$

where the volumetric strain the term ' ε_v '. Summarily, from Equation (2.34), the extent of liquefaction was interpreted as $0 < LSN \leq 20$ for minor, $20 < LSN \leq 50$ for moderate, and $LSN > 50$ for major. There exist some relative merits and demerits of all in-situ-based liquefaction assessment techniques, which are well-explained in Youd (1999, p. 84), Youd and Idriss (2001); Youd et al. (2003).

2.3.1.1 Standard penetration test (SPT) assessment of cyclic resistance ratio

The firstly proposed "simplified stress approach" of liquefaction triggering assessment was built around the SPT technique. However, several modifications had been made to this approach over the previous years to provide a more precise, consistent, and unified framework. A typical example of such modifications/revision was carried out by R. B. Seed et al. (2003). Current state-of-the-art utilizes the $(N_1)_{60}$ explained as the corrected blow count to overburden stress state of about 100kPa with hammer efficiency of 60%, R. B. Seed et al. (2003). The correlations assumed a MSF to earthquake of magnitude ($M_{7.5}$) and effective stress of 100kPa. Case histories data points of some sites were plotted, and best fit lines were drawn to indicate boundary for liquefaction and non-liquefaction occurrence. Figure 2.3 shows example of an updated version of such SPT-correlation plot adopted after Boulanger and Idriss (2014) for estimating CRR . Typical equations for corrected blow counts (normalization) as found in R. B. Seed et al. (2003) are expressed in Equation 2.37 to 2.39.

$$N_1 = N \cdot C_N \quad 2.37$$

$$C_N = \left[\frac{1}{\sigma'_{v0}} \right]^{0.5} \quad 2.38$$

$$(N_1)_{60} = N_1 \times C_R \times C_S \times C_B \times C_E \quad 2.39$$

where N is N-value of SPT, C_N is a correction factor, C_R is a factor for correction of the length of the rod, C_S is factor accounting for a non-calibrated sampler, C_B is a correction factor for borehole diameter and C_E is a factor accounting for the efficiency of the hammer. The complete SPT procedures are well-explained and revised in (Idriss & Boulanger, 2006; R. B. Seed et al., 2003).

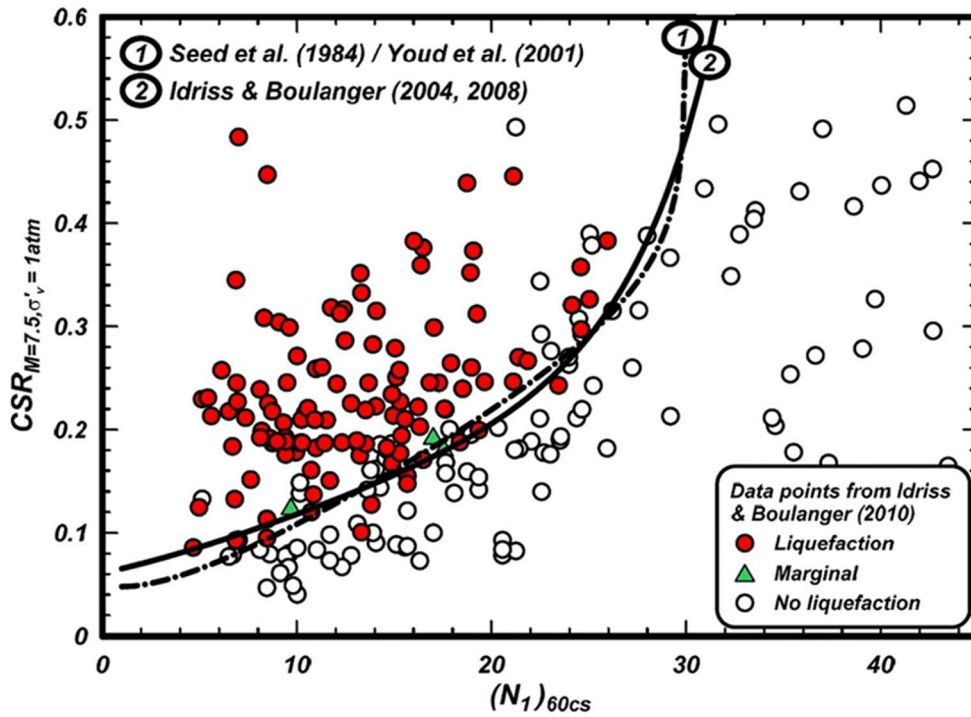


Figure 2.3 SPT-liquefaction triggering curves for estimating CRR based on case histories after Boulanger and Idriss (2014)

2.3.1.2 Assessment of CRR by the application of the CPT technique

Robertson and Wride (1998) firstly introduced the CPT-based method for quantifying the ground soil parameters. Like the SPT-based technique, the CPT has gone through several revisions/modifications over the years since its first inception, and current state-of-the-art utilizes the corrected cone tip resistance (q_{c1N}) for *CRR* estimation. Recent advancement in technology and test repeatability has further made the CPT-based technique more popular than others. For instance, CPT invariants such as piezocone (CPTu) can measure three significant ground parameters, namely the cone end resistance (q_c), the sleeve friction resistance (f_s), and pore pressure (u). Similarly, the seismic CPT device (seismocone), in addition to the parameters measured by CPTu, can accurately determine shear wave velocity (V_s) and low strain in-situ compression. The q_{c1N} is typically corrected for overburden stress effects based on Equation (2.40), as obtained from Boulanger and Idriss (2014).

$$q_{c1N} = C_N q_{cN} = C_N \frac{q_c}{P_a} \quad 2.40$$

In Equation 2.40, the C_N is an overburden correction factor, P_a is atmospheric pressure, $q_{cN} = q_c/P_a$ and q_{c1N} is obtained penetration resistance at overburden stress of 1atm when other soil state remains constant. The *CRR* depends on shaking duration of earthquakes usually factored through the *MSF* and effective geostatic stress obtained by a factor K_σ , Boulanger and Idriss (2014). Also, *CRR* is influenced by the static shear and obtained through a factor K_α (usually minimal/negligible) and the soil fines content (*FC*). Details of the full CPT procedural

methodology is well explained in Boulanger and Idriss (2014). An illustration of a typical CPT case history chart for estimating *CRR* in liquefaction triggering is shown in Figure 2.4.

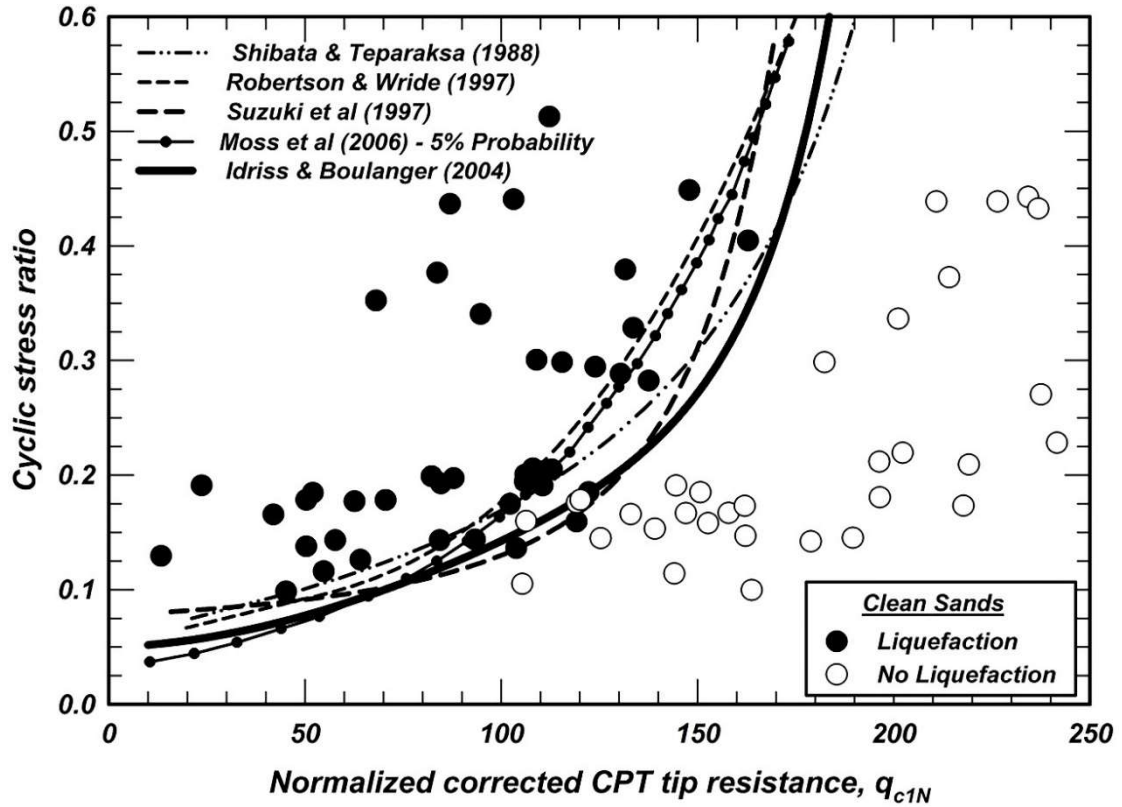


Figure 2.4 CPT-liquefaction triggering plots for determining CRR based on case histories after Boulanger and Idriss (2014)

2.3.1.3 Assessment of CRR by vane shear test

The shear wave velocity (V_s), usually derived from the vane shear test, is another handy soil index method developed to assess the liquefaction strength of soils. The procedural applicability of the technique is well detailed in Andrus and Stokoe (2000) with the modern-day physics/math of the approach being explicitly explained by Kayen et al. (2013). Notable merits of utilizing the V_s include the possibilities of quantifying soils whose samples are hard to get, and it is also useful where SPTs and CPTs provide inaccurate penetration such as the case of pumiceous sand deposits (e.g., Orense et al., 2020). Laboratory measurements are possible, allowing comparison with field measurement. The V_s is an important mechanical property directly related to maximum shear modulus G_{max} expressed in Equation 2.41. The V_s is a significant parameter in seismic-soil interaction analyses and a relatively fast approach for liquefaction assessment/evaluation (Andrus & Stokoe, 2000).

$$G_{max} = \rho V_s^2 \quad 2.41$$

In Equation 2.41, ρ is the unit density of the soil and V_s is the estimated average shear wave velocity.

Other soil elastic/stiffness parameters and empirical relationships also exist for computing the soils' bulk modulus (K) by adopting a reasonable/suitable value of Poisson's ratio (ν); For instance, the maximum bulk modulus (K) may be computed from Equation 2.42:

$$K = \frac{2G_{max}(1 + \nu)}{3(1 - 2\nu)} \quad 2.42$$

Several works have applied the shear wave velocity for liquefaction assessment in the past, the notable advantages and limitations of the vane shear test are well-detailed in (e.g., Andrus & Stokoe, 1999; Andrus et al., 2004; Juang et al., 2005; Kayen et al., 2013; Youd et al., 2003). Similar charts for estimating the CRR using the V_s are found in the above works. The estimated CSR in V_s method is approximately similar with those of the conventional simplified SPT and CPT approach.

2.3.1.4 Liquefaction assessment by other in-situ based methods

Other in-situ-based assessment methods of liquefaction potentials such as Becker penetration test (BPT) and screw driving test (SDT) usually are applied in some special situations where other methods are not adequate. The procedures for BPT are available in (Harder, 1997; R. B. Seed et al., 2003; Sy & Campanella, 1994); and for SDT (Maeda et al., 2015; Mirjafari et al., 2016). The description of such methods is considered out of scope in the current study.

2.3.2 Existing laboratory-based assessment techniques for soil liquefaction

The required laboratory testing of soils for subsequent liquefaction assessment is one of the most widely adopted approaches for liquefaction evaluation among researchers in recent times. The adoption of this approach primarily by researchers is perhaps due to its relatively incurred low cost than the other procedures such as in-situ testing and system response studies. Another primary reason for the vast applicability of laboratory procedures is the difficulty encountered in obtaining completely undisturbed sand samples. Laboratory-based liquefaction assessment techniques are capable of evaluating most soil characteristics and behaviors, such as shear strength characteristics (Ueng, 2010), generated excess pore water pressure (PWP) (Alainachi & Mamadou, 2019; Fad et al., 2015; Moretti et al., 1999; Ye et al., 2007; Yegian et al., 2007), critical state behavior derived from the critical state lines (CSL) (Taiebat & Dafalias, 2008; Taiebat et al., 2010; Taiebat et al., 2007), and strain/deformational properties (Rollins & Seed, 1990; Yasuda et al., 1992).

The generated excess pore water pressure (PWP) is considered one of the most significant liquefaction indicators (Alainachi & Mamadou, 2019). Currently, several laboratory test methods exist for the liquefaction evaluation (both statically and dynamically triggered cases), including monotonic compression triaxial tests, cyclic triaxial, cyclic torsional, simple cyclic shear, resonant column test, centrifuge, and shaking table test. However, the subsequent subsections only reviewed the relevant types of selected experiments utilized in the current study; therefore,

others were considered out of scope. The soil index tests may also be used as parameters to evaluate soils' liquefaction proneness (Youd & Idriss, 2001).

2.3.2.1 Liquefaction evaluation through triaxial testing of soils

The static/monotonic and dynamic triaxial testing of soils is the most common routine method for the laboratory-based liquefaction assessment/evaluation of sands for both flow and cyclic liquefaction assessment. The procedures for the triaxial testing of saturated soils are well-established elsewhere (e.g., Alyousif, 2015; Donaghe et al., 1988; Head, 2011). Several soil liquefaction indicators and factors usually are investigated in the laboratory to simulate the soil's likely in-situ undrained behavior under static loads. The likely experimental testing criteria may include the imposed loading conditions on the soil specimen (e.g., static or dynamic), drainage conditions (drained and undrained), boundary conditions (isotropic and anisotropic), consolidation (consolidated or unconsolidated) Donaghe et al. (1988); Head (2014). The typical kinds of tests required for liquefaction assessment include mostly the monotonic and cyclic, isotropically consolidation drained (ICD or CD), and isotropically consolidated undrained tests (ICU or CU) tests. However, the third type of experiment, referred to as an unconsolidated undrained (UU) test, is rarely used for liquefaction evaluation since the obtained Mohr circles are the same in diameter sizes, and the failure envelope is not obtainable from the test. The ICD and ICU tests required for the SSL and CSL-based evaluation of soil's strength are crucial for liquefaction analysis and obtaining calibrated numerical soil model parameters.

In the past, the conventional triaxial device has been modified to give numerous versions, such as Danish triaxial (Ibsen, 1994), true triaxial (Reddy et al., 1992), and axisymmetric device. Improvement of the axisymmetric triaxial testing devices has evolved in recent years by implementing simplifications for usually involved complexities in previous versions. Success was achieved by incorporating automation (software) for the measurement of displacements, deviatoric stress, volumetric strains, permeabilities, pore pressures, and other essential soil parameters with improvised instrumentation using transducers/sensors. The multistage testing (i.e., loading and unloading) techniques (Alyousif, 2015; Ho & Fredlund, 1982) was implemented to avoid the usually required test repeatability of three or more samples in monotonic tests but this technique is not capable of determining critical state parameters. Three or more experiments are often needed in monotonic loading/testing to enable the Mohr failure plane's derivation. The Mohr failure plane is the tangent drawn on the obtained Mohr circles. The problems of membrane penetration have also been fixed by including its correction effect in the software's automated calculation.

Typically, the stages involved in triaxial tests would include sample preparation, saturation, consolidation, and shearing. The several types of soil sample preparation methods had reportedly produced different soil strength (stress-strain) characteristic behavior (e.g., Amini & Qi, 2000; Kuerbis & Vaid, 1988; Vaid & Sivathayalan, 2000). Some studies claimed that the moist tamping

(MT) method gave higher cyclic resistance than pluviation methods (i.e., AP, WP) even when prepared to the same density coupled with the same void ratios, relative densities, mean effective stresses (Ladd, 1978). Other studies equally showed that specimens derived by the MT overestimated the liquefaction potentials of samples. Wet pluviated (WP) samples may produce dilative soil specimens in the same vein, which can underestimate liquefaction if sheared monotonically (Askari et al., 2011). Askari et al. (2011) also reported that the WP method might not be suitable for sand samples containing fines (e.g., clay) due to possible segregation problems inherent therein. The slurry deposition method (SD) method introduced by Kuerbis and Vaid (1988) addressed some of the issues mentioned above, especially concerning the issues of particle segregation. Apart from producing homogeneous and saturated mixture, which further facilitates back pressure saturation, the SD method proved to create samples with fabric similar to natural soil deposits (Carraro & Prezzi, 2007). The various soil sample reconstitution methods in the laboratory have been well-reviewed by previous researchers (Carraro & Prezzi, 2007; Papadimitriou et al., 2005). However, the systematic review summarized in Table 2.1 highlighted some critical findings concerning the effects of sample reconstitution methods on the soils' static and cyclic shear strength properties.

Brandon et al. (1990) suggested applying effective stress below 35kPa while utilizing back pressures to a maximum of 700kPa during the saturation stage. The prescribed saturation method above would ensure that samples are not overconsolidated. In most cases, the soil sample is isotropically consolidated by applying an all-round equal effective stress/pressure (σ'_3); anisotropically consolidated (i.e., the major principal stresses (σ'_1) is usually higher than the minor principal (σ'_3)) and K_0 or any customized stress path conditions depending on test requirements and capability of the device (Head, 2011). The obtained results from consolidation usually are subsequently used in deriving the shearing rate specified in Equation 2.43 and 2.44 (ASTM, 2019)

$$\mathcal{E} = \frac{4\%}{16 \times t_{90}} \quad (\text{for cases with side drain}) \quad 2.43$$

$$\mathcal{E} = \frac{4\%}{10 \times t_{90}} \quad (\text{for cases with no side drain}) \quad 2.44$$

where \mathcal{E} is strain rate, t_{90} is a time the value obtainable from the consolidation stage. However, the desired strain rate other than 4% in the above equations can be substituted for the former accordingly.

The last step in triaxial tests is the shearing process (or systematic loading of soil samples to failure), which typically is achieved by monotonically or cyclically shearing the soil sample. The stress path/invariants usually are used to obtain the stress-strain relation depending on either drained or undrained conditions.

Table 2.1, which contains the executed systematic review on the effects of sample remolding methods for liquefaction-related tests, experimental evidence suggests that some significant

controversies exist between the types of sample remolding methods which would simulate or mimic the naturally deposited soils. Considering factors such as void ratio/density, soil mineralogical classification, soil gradation, plasticity indices, and percentage of fines content may be relevant in future works.

Table 2.1 Effects of sample reconstitution methods on cyclic responses of soils: A systematic review

S/N.	References	Method	Key Findings
1.	Kuerbis and Vaid (1988)	A review of sample reconstitution methods and a recommendation of the depositional slurry technique (SD)	The slurry deposition method was developed to overcome particle segregation's inherent problems regardless of fine contents, gradation, or saturation state of soils.
2.	Carraro and Prezzi (2007)	A critical review of MT, AP, WP, and SD reconstitution method. Experimental investigations of reconstitution methods for sands with fines	The modifications of Kuerbis & Vaid (1988) SD-methods by describing how the maximum void ratio of the sample without oven could be determined. They concluded that water-depositional methods best simulate in-situ soil strength characteristics.
3.	Raghunandan et al. (2012)	An experimental program to compare the void ratios obtained in samples prepared by DT, AP & WP methods. Drop height was varied during the preparation of tamping samples.	<ul style="list-style-type: none"> -Microscopic images showed that packing was more compact in the MT-method. -AP samples showed that funnel opening has a more significant effect on void ratio than drop height of soil sample. -Medium dense sand dilated more in AP-samples than WP-samples, and dilation was observed maximum in DT-samples.
4.	Been and Jefferies (1985)	Laboratory testing program of sands with 0%, 2%, 5% & 10% FC. Tests include isotropic CD and undrained (stress & strain-controlled, cyclic) and anisotropic CU-test with a stress-controlled, cyclic direct shear test using MT & pluviation methods	<ul style="list-style-type: none"> -Derivation of the state parameter (ψ) -Correlation between state parameter and friction angle -Literature review shows that tamping procedures produce contractive samples, and pluviation methods always result in dilatant samples

Table 2.1 Effects of sample reconstitution methods on cyclic responses of soils: A systematic review (continued)

S/N.	References	Method	Key Findings
5.	Yimsiri and Soga (2010)	Experimental and distinct element method (DEM) to investigate soil samples (loosest & densest state), ICD, ICU-triaxial; shearing modes (compression & extension); different shearing directions (vertical & horizontal); soil fabric quantified by contact normal. PFC^{3D} , Itasca software used for numerical analysis.	<ul style="list-style-type: none"> -Results showed that the initial fabric of a particle assembly has immediate effects on its mechanical behavior. -The anisotropic fabric changes more often during the change from compression to dilation in drained situations.
6.	Jiang et al. (2007)	A discrete element model proposed to develop a bond contact model called NS2D.	<ul style="list-style-type: none"> -A simple contact model proposed -Development of a 2D discrete element code to simulate compression tests.
7.	Khari et al. (2014)	Application of mobile pluviator to compute relative density (R_D) of sands.	<ul style="list-style-type: none"> -Use of pluviator to obtain different densities of sands -Acquired stress-strain responses of specimens at different densities. -Acquired different friction angles for different samples.

Table 2.1 Effects of sample reconstitution methods on cyclic responses of soils: A systematic review (continued)

S/N.	References	Method	Key Findings
8.	Been et al. (1991)	<ul style="list-style-type: none"> -Determination of difference between CSL & SSL for sands. -Variation of sample preparation methods for MT and WP cases. -Testing conditions included drained undrained, stress-controlled, strain-controlled, and stress path tests. 	<ul style="list-style-type: none"> -Concluded that CSL & SSL are the same (although, criticized in the discussion section of this paper). -No practical and straightforward method exists to quantify the fabric effects of soils.
9.	Dave and Dasaka (2012)	Experimental evaluation of portable traveling pluviator to study effects of sand deposition intensity and rained height on R_D of samples.	<ul style="list-style-type: none"> -Predominant effects were observed at lower altitudes to increase the R_D of sands. -Uniformity achieved at higher R_D-tests by using cone penetrometer tests for checking.
10.	Chaudhary et al. (2002)	<ul style="list-style-type: none"> -Investigation of effects of initial fabric and shearing direction on the cyclic response of sands for the inherent stress-strain response, shear modulus, damping ratio using hollow cylinder torsional apparatus. -AP, WP & DT were considered sample reconstitution methods. 	<ul style="list-style-type: none"> -The effects of the initial fabric were not too significant. -Recorded highest sand anisotropy in AP-method. -It was reported that the same hysteretic damping ratio exists for all three remolding methods.

Table 2.1 Effects of sample reconstitution methods on cyclic responses of soils: A systematic review (continued)

S/N.	References	Method	Key Findings
11.	Papadimitriou et al. (2005)	Comparative study analysis by experimental and model simulation for stress-strain responses of Toyoura sands based on DD, DT, MT & AP-methods.	<ul style="list-style-type: none"> -Most observed effects included dilatancy and plastic modulus characteristics. -MT samples had higher cyclic resistance and were most dilative with stiff response than the dry samples (DD, AP & DT). -Differences were due to water content. -Different preparation methods affect the quasi-static state of sands.
12.	Bradshaw and Baxter (2007)	A comparative experimental study of silty material for the investigation of modified tamping method (MT), SD, and in-situ block samples.	<ul style="list-style-type: none"> -SD samples had a more uniform density along their length, while MT samples had variability of densities. -The water content of sample preparation had a significant impact on the cyclic strengths of MT samples. -Stress-strain behavior of MT-samples likened to block of (in-situ) samples for silts.
13.	Wan and Guo (2001)	A stress-dilatancy-based constitutive model with microstructural dependencies was developed and presented with formulated equations.	<ul style="list-style-type: none"> -Impacts were visible by volume change under drained conditions and amassed excess pore pressure noted under undrained conditions. -The stronger the fabric in the vertical principal stress direction, the higher the tendencies for flow failure in undrained conditions. -Structure alters the $e - \log P'$ curve.

Table 2.1 Effects of sample reconstitution methods on cyclic responses of soils: A systematic review (continued)

S/N.	References	Method	Key Findings
14.	Miura and Toki (1984)	Undrained monotonic, cyclic triaxial compression and extension experiments were executed on undisturbed samples to assess anisotropic characteristics.	<ul style="list-style-type: none"> -Anisotropy was noticeable in naturally deposited sands. -Concluded that the pluviation of sands through the air mimicked the behavior of sand in in-situ state conditions closely. -In-situ sand displayed anisotropic time histories.
15.	Tatsuoka et al. (1986)	Torsional shear and triaxial tests on 2-kinds of sands, carried out using the AP, MT, and water-vibrated reconstituted samples.	<ul style="list-style-type: none"> -Cyclic undrained stress-strain responses decreased with increased strain for different methods at the same density. -Wet-vibrated samples produced the highest cyclic strength, while AP samples had the lowest resistance. -Suggested that the critical number of loading cycles was a better strength index than the conventional stress ratio index.
16.	Yoshimine et al. (1998)	Triaxial compression and torsional tests carried out on DD-samples.	<ul style="list-style-type: none"> -Shear behavior is more contractive and softer in extension than compression mode. -Directions and amplitude of principal stress do induce consequential influence on the undrained strength characteristic behavior of sands.

Table 2.1 Effects of sample reconstitution methods on cyclic responses of soils: A systematic review (continued)

S/N.	References	Method	Key Findings
17.	Tatsuoka et al. (1979)	Resonant-column apparatus & static torsional device used to investigate the shear moduli and hysteric damping ratios for DT, AP, MT, and vibration-specimen remolding methods.	<ul style="list-style-type: none"> -Shear modulus ranging from 10^{-6} to 10^{-4} by drained resonant-column test decreases slightly with an increase in saturation degree. -Shear modulus and hysteric damping ratio at 2nd cyclic loading or more are not affected by the change in saturation degree. -Shear modulus and hysteric damping ratio are not sensitive to different methods of sample remolding.
18.	Tatsuoka et al. (1982)	Cyclic torsion undrained experiments on 2-types of sands were studied using the MT and AP methods of sample reconstitution.	<ul style="list-style-type: none"> -MT & AP specimens had similar strengths for R_D up to 65%. -For $R_D > 65\%$, MT-samples have greater cyclic strength than AP-samples.
19.	Miura and Toki (1982)	A multiple sieving pluviation apparatus (MSP) developed and used to investigate static and cyclic strength response of Toyoura sand.	<ul style="list-style-type: none"> -Dilatancy variations were prominent in triaxial extension tests than compression. -MSP specimens showed the lowest cyclic response from all the methods investigated -MSP can produce samples with uniform properties.
20.	Okochi and Tatsuoka (1984)	K_0 -consolidation tests on AP & MT reconstituted sand specimens executed	<ul style="list-style-type: none"> -K_0 values were observed higher for AP than MT samples -Effective angles of internal friction (ϕ') were reported independent on the 2-methods.

Table 2.1 Effects of sample reconstitution methods on cyclic responses of soils: A systematic review (continued)

S/N.	References	Method	Key Findings
21.	Ibraim et al. (2012)	Triaxial testing & numerical modelling of fiber-reinforced sands using MT & MV sample reconstitution methods.	<ul style="list-style-type: none"> -MT methods have limited effects on fiber orientation distribution. -Mechanical responses of MT & MV samples were similar.
22.	Yamamuro and Wood (2004)	<ul style="list-style-type: none"> -Undrained triaxial compression tests of silty sands prepared by DD, WP, SD, AP, and MDD reconstitution methods. -Microscopic studies using a scanning electron microscope (SEM) to decipher the microstructure of WP and DD samples 	<ul style="list-style-type: none"> -For identical densities and stress conditions, the undrained behaviour was different for all samples. -Using the SEM, the authors developed a method to evaluate the microstructure of silty sands. -Relative quantities of silts in samples under SEM analysis correlate with their corresponding undrained behaviours.
23.	Silver et al. (1980)	Applied both cyclic triaxial and cyclic simple shear to evaluate cyclic strengths of sands by MT and AP preparation methods.	<ul style="list-style-type: none"> -In triaxial tests, specimens of MT showed higher resistance to cyclic undrained shear than AP-specimens. -In simple shear tests, negligible strength differences observed. -Suggested that cyclic undrained triaxial strength of sand by MT may give overestimate of liquefaction strength, but simple cyclic shear may provide a fair estimate.

Table 2.1 Effects of sample reconstitution methods on cyclic responses of soils: A systematic review (continued)

S/N.	References	Method	Key Findings
24.	Silver and Park (1976)	Stress and strain-controlled triaxial tests were carried out for loose to medium dense sand using MT & vibration sample reconstitution methods.	<p>-At the same initial conditions of density, values of modulus, and liquefaction potential were higher for MT-specimens than dry vibrated samples.</p> <p>-No significant difference observed for the obtained damping ratios of both methods.</p>
25.	Ghionna and Porcino (2006)	Cyclic undrained triaxial tests were executed on disturbed (AP & WP) and undisturbed (frozen) sand samples. Initial effective overburden stress and densities were maintained for all experiments.	<p>-Results indicated that cyclic liquefaction resistance obtained for WP-reconstitution samples closely approximates to the one exhibited by undisturbed samples.</p> <p>-Obtained results for AP-prepared samples showed a marked underestimation of liquefaction resistance.</p>
26.	Duku et al. (2008) et al	Experimental investigation and model calibration of some factors affecting volumetric strains of sand subjected to cyclic loads.	<p>-Results indicated that fabric effects do not affect seismic compression.</p> <p>-Other factors which do not affect seismic compression are particle angularity, mineralogy, void ratio and 'breath' ($e - e_{min}$).</p> <p>-Factors affecting compression susceptibility were confining stress and R_D.</p>

Table 2.1 Effects of sample reconstitution methods on cyclic responses of soils: A systematic review (continued)

S/N.	References	Method	Key Findings
27.	Yu et al. (2012)	Physical modeling with a centrifuge to investigate the inherent anisotropy of sand based on deposition history and pattern.	<ul style="list-style-type: none"> -Fabric anisotropy of sand influenced by the ground response in displacement, acceleration and excess pore pressure -Models with higher deposition angles had higher liquefaction potential.
28.	Sze and Yang (2013)	A systematic experimental investigation of impacts of specimen preparation methods on the dynamic response of sands.	<ul style="list-style-type: none"> -A classified undrained cyclic failure into flow-type failure, cyclic mobility, accumulation of plastic strain, minor flow accompanied by cyclic mobility, and some flow accompanied by a collection of strains. -Three failure modes were noticed for MT and DD samples. -The last 2-failure patterns were observed for DD-samples. -From a microscopic perspective, sands remoulded by DD were highly anisotropic while, MT specimens are isotropic.
29.	Hird and Hassona (1990)	Experimental investigation of some factors affecting liquefaction which includes sample preparation methods of MT & WP methods of reconstitution	<ul style="list-style-type: none"> -Position of the SSL in the $e - \log P'$ space depends on strain rate -Round-shaped sands are at higher risk to liquefaction than angular ones. -MT samples are more prone to liquefaction than water sedimented ones.

Table 2.1 Effects of sample reconstitution methods on cyclic responses of soils: A systematic review (continued)

S/N.	References	Method	Key Findings
30.	DeGregorio (1990)	Laboratory investigation of Ottawa sands' stress-strain behavior prepared by AP, MT & MV methods using dead load apparatus.	<p>-The relative position of the SSL curve is influenced by preparation methods.</p> <p>-Samples prepared by AP, MT & MV in that order showed higher peak and steady-state strengths when sheared with the dead load device.</p> <p>-AP samples showed a more significant peak pore-water pressure response than others.</p>
31.	Lee et al. (1999)	In-situ tests and triaxial tests to study the undrained behavior of 2-types of sands using AP and MT-reconstitution methods.	<p>-Summarized that some soils with relatively the same initial condition (density/void) and prepared with different ways exhibited different/varying behavior.</p> <p>-MT samples have the highest liquefaction resistance, followed by AP samples.</p> <p>-The cyclic and static triaxial test results indicated a strong correlation for soil fabric structure between the fill placement techniques and laboratory preparation structure.</p>

Table 2.1 Effects of sample reconstitution methods on cyclic responses of soils: A systematic review (continued)

S/N.	References	Method	Key Findings
32.	Amini and Qi (2000)	150-stressed controlled undrained cyclic triaxial tests using MT & WP reconstitution methods	<p>-Liquefaction resistance of uniform and soils in layers was similar despite different preparation methods.</p> <p>As confining stress increased, sands' liquefaction resistance containing silts was reduced for both MT & WP samples.</p>
33.	Vaid et al. (1999)	An investigative study to compare the undrained behavior of sands prepared by MT, AP & WP-samples	<p>-At identical initial states, the MT-sand has lower liquefaction resistance, and the WP-samples were more dilative.</p> <p>-A comparison of the undisturbed frozen sample's undrained behavior closely matches the WP-samples.</p> <p>-WP samples found to simulate typical in-situ fluvial and hydraulic fill sand.</p> <p>-The frictional angles vary with the methods of specimen preparation.</p>
34.	Ibrahim and Kagawa (1991)	Experimental investigation for specimen preparation effects on the fabric of sand and change in the structure due to cyclic loading using cylindrical hollow apparatus. AP, MT, and MV methods were considered.	<p>-Microscopic observation showed that AP-samples tend to have more "uniform" particle orientations and higher variation of local void ratios than MT samples.</p> <p>-Dry vibrated specimens produced an intermediate result between AP & MT samples.</p> <p>Conclusions drawn by the author indicated soil remolding method has a notable effect on soils' cyclic properties.</p>

Table 2.1 Effects of sample reconstitution methods on cyclic responses of soils: A systematic review (continued)

S/N.	References	Method	Key Findings
35.	F. M. Wood et al. (2008)	Experimental investigation of the undrained behavior of Nevada sand plus silt with zero plasticity while utilizing DD, WP, SD, and AP methods of sample preparation.	-As density increased, the depositional method effects decreased. -Depositional method effects increased as silts content increased primarily at lower densities.
36.	Wijewickreme et al. (2005)	Experimental investigation using constant-volume direct, simple shear tests to calibrate the numerical simulation for the centrifuge tests. Ap and WP reconstituted specimens were considered in the study.	-AP samples are more susceptible to liquefaction under cyclic loading than WP samples. -Increased confining stress (densification) increased cyclic resistance of AP-samples, and this effect was not prominent in WP-samples.
37.	Rad and Tumay (1987)	Experimental investigation on the impacts of 'sand rainer' on R_D of specimens. Studied variables include shuttle porosity, deposition intensity, shutter hole pattern, vertical stress on the shutter, falling distance, distance between diffuser sieves, falling height, diffuser opening, and number of diffuser sieves.	- R_D of specimen formed by pluviation is dictated by the sand particle velocity immediately before deposition. -The initial velocity of the sand particle depends on the sand height. The shutter porosity or deposition intensity has the most significant effects on R_D . -The diffuser sieve diameter, falling height, shutter-hole nature are more or less negligible by impacting the results. Negligible effects of falling heights between diffuser sieves and the number of used sieves. - Different R_D obtained by changing the shutter porosity.

Table 2.1. Effects of sample reconstitution methods on cyclic responses of soils: A systematic review (continued)

S/N.	References	Method	Key Findings
38.	Mulilis et al. (1977)	Triaxial testing carried out using an undrained, stress-controlled, cyclic loads on 11-different remolded samples. The methods, broadly categorized as pluviation, vibration, and tamping techniques were considered.	<ul style="list-style-type: none"> -Differences were evident in the cyclic behavior of the sands prepared by the various methods. -The difference in cyclic behavior can be dependent on the function of sand type. -The difference in fabric structure formed by the various techniques is a significant reason for the different cyclic responses. -The varied orientation of contacts between the grains and packing are critical reasons for the distinct behavior of sands.
39.	Ladd (1978)	A method for achieving uniform compaction all through the height of samples was proposed and introduced as ‘undercompaction.’	<ul style="list-style-type: none"> -The undercompaction (UC) technique minimizes particle segregation commonly experienced in pluviation methods. -The method makes the determination of optimum cyclic strength of sands possible over a given dry unit weight.

More specifically, it is well-established that the sample remolding method's choice ultimately determines the liquefaction behaviors of soils from laboratory-based soil assessment/testing. For instance, pluviation through water (WP) for sands containing fines reportedly results in the segregation of fines from the coarser sand grains due to the different settling velocities experienced by the soil particles' grain sizes. Stokes Law is about the best justification for the segregation behavior of fines mixed with sands. Another associated limitation of the WP method is the challenge posed by determining the various range of relative densities or void ratios. As reported by some authors, summarized in Table 2.1 showed that routine tamping techniques such as MT or dry tamping (DT) often result in either under-estimation or over-estimation of sands' liquefaction resistance. The above is true if field tests such as CPT and SPT were not executed on representative soil samples to establish the actual soil relative density. A notable advantage of the tamping techniques is their capability to produce soil samples of known densities and the test repeatability is consistent. Hence, the justification for the adoption of this method by several previous researchers and the utilized MT method in the current work.

The air pluviation (AP) method replicate soils deposited by air or wind agents such as silts, aeolian soils, and dunes. The slurry deposition method (SD), initially introduced by Kuerbis and Vaid (1988), simulates closely the fabric structure of naturally deposited soils (e.g., coastal lands, hydraulic fill operations, fluvial soils, and engineered fills). The SD method may prevent the segregation of fines from larger soil particles. The SD method was observed as rarely used in most studies summarized in Table 2.1, and this may be due to the long-time factor required for the practical implementation of this method in the laboratory, hence a notable limitation of the technique. Other in-situ soil conditions like the degree of compaction and consolidation can be closely simulated in triaxial tests, shaking table experiments, and centrifuge experiments with most of the earlier mentioned remolding methods. Mulilis et al. (1977) showed some significant insights into the impacts of the sample remolding technique on the shear strength behavior of soils.

2.3.2.2 Shaking table experiment in liquefaction studies (physical Model)

The 1-g shaking table experiment or physical model study is well-established for liquefaction investigation and soil-structure interaction analysis/studies. Typically, in soil liquefaction research studies, the saturated soil sample placed in a container, usually prepared by one or more of the sample reconstitution methods is subjected to ground motions from shakings. The input ground motions are mostly sinusoidal or harmonic. Soil samples placed into a water-tight/proof box/container are stationed and fixed with bracings on the shaking table to prevent it from sliding or prevent any parallel or relative movement to the shaking table. The transducers used for measuring the dynamic soil properties are typically installed at desired locations of the test set-up. Commonly utilized instrumentation for the complete test setup includes accelerometers for measuring accelerations or velocities of both the base input shaking intensities and that of the ground response, pore pressure transducers/piezometers for measuring excess generated pore pressures, linear variable differential transformers (LVDTs) for measuring soil displacements/deformations, bender elements for measuring shear wave velocities, and data acquisition system usually a software to record/capture all data from the sensors in a systematic and digitized manner.

Several kinds of soil boxes have been used in the past to study earthquake-induced liquefaction of soils by utilizing the shaking table. Bhattacharya et al. (2012) listed and described some commonly applied soil container types for liquefaction evaluation as rigid soil box, rigid box with flexible boundaries, rigid box consisting of hinged end-walls, equivalent shear beam (ESB), laterally flexible and active boundary box. However, some notable limitations are associated with all container types. For instance, the mimicking of infinite lateral boundary conditions by using a rigid soil box is not logical and challenging (Fishman et al., 1995; Ueng et al., 2005). The non-similarities of vertical stresses for the soil box frictionless boundaries and prototype in-situ soil; shear/P-waves reflection problems (Bhattacharya et al., 2012). To overcome the challenges mentioned above, some researchers have devised some ways to minimize some of the issues. For instance, the ESB and laminar containers are used to minimize lateral stiffness (Anastasopoulos et al., 2010; Guoxing et al., 2015). The above is achieved by modeling lateral free-field conditions similar to the infinite lateral extent of in-situ soil and reinforcement of end walls which are perpendicular to the direction of shaking with absorbing materials like sponge or foam to minimize the problem of p-waves reflection (Bhattacharya et al., 2012; Lombardi et al., 2015).

Furthermore, Fishman et al. (1995) noted that a free-field is not achievable in rigid boxes having distances between $1.5H$ to $2.0H$; where H is soil depth. Lombardi et al. (2015) in their study evaluated the dynamic characteristics of damping material (foams) used in lining end walls of a rigid container, and they estimated the amount of energy dissipated by it. They found that minimized reflections from container boundaries by applying some absorbing medium at the transient boundaries, and their obtained results showed a significant reduction of energy

dissipated between 41% to 92%. Hence, rigid boxes with absorbing boundaries presented some advantages regarding minimizing the body reflected waves on containers since all model containers must have a finite boundary condition. The above scenario may be assumed as replicating the “quiet boundary conditions” in numerical models (Ecemis, 2013; Tabatabaiefar et al., 2014). The requirements of a perfect model container are well-reviewed by Bhattacharya et al. (2012). A conclusion drawn was that none of the model boxes were accurate enough to replicate the right field or in-situ conditions. Summarily, the authors provided valuable recommendations on a model box's choice depending on the required application for study/assessment.

A good number of studies done in the past using shaking table testing exist to understand further, for instance, soil-structure interaction mechanisms (S. Chen et al., 2020; Mizuno et al., 2000; Ueng, 2010; Ueng et al., 2005), possible liquefaction mitigation techniques (Alainachi & Mamadou, 2019; Chouw et al., 2017; Dinh et al., 2020; Towhata et al., 2015; Uchimura et al., 2007), slope stability and ground displacement mechanisms (Murao et al., 2018; Yasuda et al., 1992). Özener et al. (2020) recently proposed a method for discovering the time of liquefaction triggering based on some time-frequency analyses. The mimicking of a prototype earthquake may require a shaking table with a six-degree of freedom (Prasad et al., 2004). This type of system may be very complicated and can be associated with high procurement, maintenance, and operations costs. When such a system is absent, and the required behavior assessment are those of earth structures such as an embankment, dam, retaining walls, quay walls for shoreline protection works, then a horizontal, single degree of freedom (SDOF) shaking table is considered adequate. For the achievement of a relatively accurate numerical assessment, original ground motion records are recommended as an applied input earthquake. The NGA-West2 currently houses a database of thousands of earthquake ground motion records/case histories and available to the world earthquake engineering community Ancheta et al. (2014).

Sasaki and Taniguchi (1982) have identified some purposes of performing the shaking table test. They include assessing the dissipation and generation of pore water pressure characteristics in the soil due to shakings such as earthquake loads, investigating the effectiveness of some liquefaction mitigation measures, and evaluating some effects of soil liquefaction mechanisms structures built on them (soil-structure interaction studies). Fishman et al. (1995) listed other shake table applications as inelastic response studies, reinforced backwalls with cohesionless backfills, shallow and deep foundations (e.g., pile-soil structure analysis) while offering some improvements on end wall effects. The shaking table test is also useful for validating studies executed on numerical models and laboratory testing such as triaxial tests (Anastasopoulos et al., 2010; G. Chen et al., 2008; Ye et al., 2007). The simulation of soil undrained behavior under shaking table conditions appears to be more realistic when compared with other laboratory testing methods. The above assertion is because the stress conditions and deformations in soil samples

tested under triaxial, and other laboratory tests are greatly affected by boundary conditions. The applied loads do not mimic actual field situations such as infinite lateral extents (Ueng et al., 2005).

2.3.3 Plasticity-based liquefaction analysis

The Chinese criteria, otherwise known as the plasticity-based liquefaction criteria recommended by Youd and Idriss (2001), is a well-known empirical technique to assess soil's likelihood to trigger liquefaction. The Chinese criteria, first introduced by W. Wang (1979), have undergone several amendments/reviews by several other authors (Andrews & Martin, 2000; Koester, 1994; H. B. Seed et al., 1983; R. B. Seed et al., 2003). Most of the modifications are because soil index properties obtained from Casagrande's device are varied from those obtained from the fall cone device. The original Chinese criteria were formulated with the aid of Casagrande's liquid limit device. The metamorphosis of the modified Chinese criteria is well summarized in Polito (2001) and Tan et al. (2013). H. B. Seed (1982) gave a summary of Wang's discovery as "clayey soils with lower than 15% finer than $5\mu\text{m}$, liquid limit (w_L or LL) lower than 35%, and moisture content (w_c) higher than $0.9LL$ may be prone to loss of significant effective confining strength during earthquake vibrations".

Andrews and Martin (2000) reported 1) soils could liquefy if containing lower than 10% finer than $2\mu\text{m}$ & $LL < 32$, 2) soils will liquefy if they have $\geq 10\%$ finer than $2\mu\text{m}$ & $LL \geq 32$, and 3) further suggested more detailed studies for materials meeting one of above conditions. Similarly, Bray et al. (2004) reported 1) fine-grained materials are prone to liquefaction if plasticity index (I_p or PI) ≤ 12 and $w_c > 0.85LL$, 2) fine grained soils may not be liquefaction prone and prone to cyclic mobility if $12 < PI < 20$ and $w_c > 0.8LL$. The basis of classification according to R. B. Seed et al. (2003) correlates with those of Bray et al. (2004); the exception is that the ratio of w_c to LL are slightly different than later authors and also includes some limitations on LL . The criteria according to R. B. Seed et al. (2003) was based on 3-zones (A, B, & C) classification and was summarized as follows: 1) Zone-A soils having $PI \leq 12$, $LL \leq 37$ are likely prone to "classic triggered cyclic liquefaction if $w_c > 80\%$ of LL ; 2) Zone-B having $PI \leq 20$ and $LL \leq 47$ are potentially vulnerable to liquefaction with more laboratory testing recommended if $w_c > 85\%$ of LL ; and 3) Zone-C soils having $PI > 20$ or $LL > 47$ not subject to cyclic triggered liquefaction and recommendations are made for investigations.

Boulanger and Idriss (2006) noted that it is uncertain and overly conservative in utilizing the mere index criteria to derive the liquefaction likelihood of soils and suggested that more detailed monotonic and cyclic tests will provide more insights on the liquidization behaviors of such materials. The impacts of fine contents (f_c) on liquefaction behaviour of sands as extracted from the elaborate literature database is reported to be made up of divergent/incoherent views. This indicates the necessity for further detailed research to draw a clear distinction between effects of

(f_c) for both plastic and non-plastic fines. Bray and Sam (2006) made a beneficial suggestion of utilizing the plasticity index parameter instead of the commonly used clay fraction in studying the f_c effects on liquefaction susceptibility of sands. Fines content may exist in sand matrix soils as “clay-like” which can experience cyclic softening or “sand-like” which is susceptible to cyclic liquefaction. Hence, the recommendation of the former author is strongly supported to replace the fines percentage which at present seems to be routinely applied in the Modified Chinese criteria to plasticity index-based assessment. This would generally distinguish clearly between impacts of plastic and non-plastic fines on liquefaction characteristics of cohesionless soils.

2.3.3.1 Impacts of silts and non-plastic fines on the liquidization mechanisms of sands

Many executed investigations in the past to understand the impact of silts or non-plastic fines on the cyclically triggered liquefaction mechanisms of sands (Lade et al., 1998; Lade & Yamamuro, 1997; Papadopoulou & Tika, 2008; Polito, 1999; Polito et al., 2008; Polito & Martin, 2001; Xenaki & Athanasopoulos, 2003) abound in the literature. The previous works identified contradictory interpretations of the impacts of non-plastic fines on cohesionless soils' liquefaction properties. Polito (1999), in his investigation, reported similar observations in his literature. Some studies concluded that adding more silt content to the sand would escalate its liquefaction strength (Amini & Qi, 2000; Ishihara, 1996; Papadopoulou & Tika, 2008). On the contrary, others reported an increase in silt content would decrease its liquefaction resistance ratio (Belkhatir et al., 2010; Lade & Yamamuro, 1997; Miura et al., 1995; Papadopoulou & Tika, 2008; Troncoso, 1985; Vaid, 1994).

Few studies also described that an increase in silt percentage of sand would lower their liquefaction resistance ratio up to when a certain threshold silt percentage is reached, and the resistance surges up after that (Koester, 1994; Papadopoulou & Tika, 2008). Some studies also indicated that an increase in non-plastic fines percentage would increase the liquefaction resistance ratio up to a limiting estimate and then decreases subsequently with increased non-plastic fines (Polito & Martin, 2001; Thevanayagam & Mohan, 2000; Xenaki & Athanasopoulos, 2003; S. L. Yang et al., 2006). The threshold fine transitional contents usually are referred to as the point in which the effects of fines alternate from positive to negative or vice versa (Papadopoulou & Tika, 2008). Similarly, other studies reported that sands' liquefaction behavior of those containing silts is nearly associated with its void ratio, soil structure, and relative density than silts contained thereof (Kuerbis & Vaid, 1988; Vaid, 1994). Therefore, it is evident that the summarized works based on the literature are somewhat contradictory and made up of non-consistent findings.

2.3.3.2 Impacts of plastic fine on liquefaction resistance

In-situ soils, in most cases, usually contain varying amounts of fines, which can be either plastic (clay) or non-plastic fines (silt) or both rather than clean sands. Previous authors like Polito (1999), El-Mohtar et al. (2014), and H. B. Seed et al. (1983) noted that the liquefaction resistance, i.e., the stress ratio (τ'/σ'_v) of sands generally rises with the inclusions of plastic or clayey fines. On the contrary, other studies e.g., Law and Ling (1992), indicated that the normalized liquefaction resistance decreased for sand-clay mixture up to 10%, after which it increases with increased f_c . Similarly, Bouferra and Shahrour (2004) indicated a similar trend of results obtained by Law and Ling (1992), except that a threshold value of 15% f_c was specified in their case study. In addition, Yamamuro and Lade (1998) reported that sands containing plastic fines are more prone to liquefaction during undrained shearing at low effective stress than at higher effective stress. Boivin et al. (2004) stated that the clay content and clay type (based on mineralogical composition) could significantly influence the physical properties of soils, most notably, the soil shrinkage characteristics that are widely used in characterizing soil structure.

Cubrinovski and Ishihara (2002), in their work, concluded that f_c controls the deformational behavior of soils from $f_c > 30\%$ while sands are the dominant material properties when $f_c < 20\%$. Guo and Prakash (2000) indicated that within the range of lower plasticity, liquefaction resistance is not directly proportional to PI while in the case of high plasticity, the proportionality is a direct type between liquefaction resistance and PI . Also reported was that the CSR was highly sensitive to the plasticity index parameter in their formulated best-fit equation for the same. Tan et al. (2013), however, noted that the addition of plastic clay to sands might produce two conflicting behavior of the sand matrix soil, namely: 1) decrease the hydraulic conductivity and surge the rate at which pore water pressure generates, 2) improve the cohesive property of the sand matrix soil and consequently increase its liquefaction resistance. A systematic literature review is presented herein in Table 2.2 to highlight the summary of previous researchers' findings based on the impacts of plastic fines on sand matrix soils' liquefaction mechanisms.

The threshold f_c or transition zones for clayey sands are still unclear because several studies have indicated this in the range between 10% to 20%. Therefore, a reasonable hypothesis proposal may suggest that the critical transition zone of clay contents in a sand matrix varies according to soil gradation, particle shapes, sizes, soil types, mineralogical composition of the clays, and other factors such as aging effects. In their study, El-Mohtar et al. (2014) established the significant impacts of aging on sands' liquefaction behavior when admixed with some fraction of bentonite (3% & 5%). The application of high-swelling, clay minerals such as montmorillonite and bentonite for liquefaction mitigation measures must be carefully reconsidered. Although the nature of clays may offer a high plasticity index to the soil, thereby increasing its liquefaction resistance. The critical points observed are the possibility of constituting severe instability to

structures built on them because of their high expansive nature. It is already well-known that high-expansive clay minerals usually are considered problematic to foundations of infrastructures because they swell when wet and shrink when dry (very unstable). Based on the above, more reasonable recommendations may include investigating the effects of low expansive/swelling clays such as kaolinite for liquefaction mitigation assessment and research purposes. The conclusion at this point is that no consistent framework is established yet for the threshold f_c based on both non-plastic (silt) and plastic (clay) impacts on soils' liquefaction mechanisms.

Table 2.2 Systematic review of liquefaction resistance of sand mixed with plastic fines

S/N.	References	Method	Key Findings
1.	Derakhshandi et al. (2008)	-strain-controlled triaxial tests executed to study the effects of kaolinite clay on pore pressure generation in saturated sands	<ul style="list-style-type: none"> -specimens reaching 20% plastic fines produced higher pore pressures than clean sands -specimens at 30% f_c generate decreased pore pressures than clean sands -threshold strain ($\gamma_t \sim 0.006 - 0.008\%$) was observed for 0 to 20% f_c but increased to 0.025% for 30% f_c -similar volumetric compressibility observed for all tested specimens after pore pressure build-ups -f_{thre} were typically between 20% and 30% and this was ascribed to variation in soil fabric controlled by the sand to fine-grained
2.	Bobei et al. (2009)	-drained and undrained triaxial executed to investigate the impacts of plasticity on the CSL/SSL of sands by both isotropic and anisotropic consolidated specimens	<ul style="list-style-type: none"> -results indicate that a small amount of f_c can change the position of SSL/CSL -a modified state parameter suggested -the shape of isotropic consolidation line (ICL) observed to change with the addition of fines -original state parameter found to have limitations in predicting the behavior of sands with fines

Table 2.2 Systematic review of liquefaction resistance of sand mixed with plastic fines (continued)

S/N.	References	Method	Key Findings
3.	Boivin et al. (2004)	<ul style="list-style-type: none"> - experimental investigations of shrinkage properties of the mixture of kaolinite, natural sand, and vertisol - kaolinites varied effects were studied 	<ul style="list-style-type: none"> -the tested soil samples exhibited different shrinkage characteristics based on type and amount of clay contents -the micro-pore volume experienced a decreased swelling capacity with increased clay contents -recommended further studies on clay-matrix swelling properties on the fabric and structure of soils.
4.	Sivapullaiah et al. (2000)	<ul style="list-style-type: none"> -experimental studies on hydraulic conductivities of sand-bentonite mixtures -studied variables include the size of coarser fractions in sands and clay contents 	<ul style="list-style-type: none"> -the coefficient of permeability (k) $\log_{10} k$ reportedly varied linearly with void ratio over the full range of loading pressures -$\log_{10} k$ decreases with the rise in the percentage content of bentonite -the effects of coarser fractions of sands observed at lower percentage content of bentonite - proposed four methods for predicting the coefficient of permeability (k) -method-2 recommended for a more accurate estimation
5.	Arnedo et al. (2008)	<ul style="list-style-type: none"> -experimental and numerical modeling investigation on gas flow through sand-bentonite mixtures 	<ul style="list-style-type: none"> -compaction characteristics of the mixtures play some significant role during gas flow through specimen -porosity is considered a considerable variable of material behavior under gas injection pressure -numerical model and experiment agree closely with results

Table 2.2 A systematic review of liquefaction resistance of sand mixed with plastic fines (continued)

S/N.	References	Method	Key Findings
6.	Blatz et al. (2002)	-triaxial testing by quick undrained type to investigate the consequence of suction on strength mechanisms of compacted sand-bentonite mixtures	-results indicate that stiffness and strength increased non-linearly with increasing suction -suggested the grains in strength and stiffness may be attributed to an increase in density -recommended further testing on unsaturated materials
7.	Le-Hir et al. (2011)	-calibration of a numerical model for sediment transport of sand in mud mixtures based on conducted laboratory settling test	-signifies a model's capacity to simulate layering processes and variation of time in the way sediment erodes
8.	Othman and Marto (2018)	-laboratory experiments to determine e_{min} and e_{max} of sand-kaolinite mixtures -three different sizes of sands (fine, medium, & coarse) were mixed with 0 to 40% kaolinite by weight	-results showed that e_{min} and e_{max} decreased with increased f_c to a minimum range of 0 - 30% and vice versa for coarse sands mixed with kaolinites Similar properties were observed for medium and fine-grained sands but at a different percentage by weight of fines (10% to 30%)
9.	Law and Ling (1992)	-cyclic triaxial tests conducted on cohesionless silts and cohesive clay mixed with sands.	-problems relating liquefaction resistance to individual physical parameters of grain size, Atterberg limits, and void ratios were evident in the study and previous literature -soil strength variables (cohesion and angle of friction) may be directly related to the liquefaction resistance of soils.

Table 2.2 A systematic review of liquefaction resistance of sand mixed with plastic fines (continued)

S/N.	References	Method	Key Findings
9	Law and Ling (1992)		<p>-observed is decreased normalized liquefaction resistance (τ/σ'_{v0}) for sand-clay matrix soils up till 10% after which it increases with increased cohesive fines</p> <p>-a useful relationship deduced between liquefaction resistance (τ/σ'_{v0}) and shear strength parameters (ϕ_d & c_d) as $\frac{\tau}{\sigma'_{v0}} = f$ where f is a function of N and $\tan\phi_d/c_d$</p>
10.	Bouferra and Shahrour (2004)	-investigating liquefaction resistance by experimental undrained compression and cyclic triaxial tests on remolded sands with varying amounts of kaolinite	<p>-increased f_c reaching 15% decreased liquefaction resistance of sand-clay mixtures;</p> <p>-the decreased liquefaction resistance phenomenon suggested that the function of fines was to lower the dilatancy tendencies of the resulting soil mixture</p>
11.	Marto and Tan (2012)	A literature review on the role of fines in liquefaction mechanisms of sands	<p>-the composition of fines and plasticity are primary factors contributing to alteration of liquefaction behavior of sands</p> <p>-reported that previous works are without a clear distinction between non-plastic fines (silts) and plastic (clays) and this have reportedly caused misleading/misinterpretation of fines effects on sand liquefaction within the geotechnical community</p> <p>-gave evidence of soils containing a significant amount of clay content that has liquefied in past earthquakes case histories</p>

Table 2.2 A systematic review of liquefaction resistance of sand mixed with plastic fines (continued)

S/N.	References	Method	Key Findings
12.	Guo and Prakash (2000)	-data from published literature were collected and analyzed for undisturbed and remolded samples	<p>-increase in PI lowers the liquefaction resistance of silty-clay matrix soils in low plasticity range. For high plasticity range, strength observed increased with increase in PI</p> <p>-pore pressure generation behavior of silty clay may be different from sands</p> <p>-elevated pore pressures developed in the soil mixture due to reduced hydraulic conductivity caused by the clay particles within the low plastic range</p> <p>-the higher the plasticity, the higher the liquefaction resistance observed</p>
13.	Polito (2001)	-a review of plasticity-based liquefaction executed	<p>-the soil's plasticity used to separate clayey sands from "cyclic mobility" and "flow liquefaction"</p> <p>-the plasticity chart can identify zones with cyclic mobility, and degree of liquefaction susceptibility (i.e., susceptible, potentially susceptible, or not susceptible)</p>
14.	Park and Kim (2012)	<p>-undrained cyclic triaxial tests executed a sand matrix soil with clay (10% by weight) with varying PI</p> <p>-the liquefaction resistance was studied to study the impact of plasticity on resulting soil matrix soils</p>	<p>-liquefaction resistance decreases with increased PI of 10% fines in the specimen</p> <p>-loose specimen influenced slightly by plasticity</p> <p>-liquefaction resistance lowered until 40% as PI of 10% fines rises.</p>

Table 2.2 A systematic review of liquefaction resistance of sand mixed with plastic fines (continued)

S/N.	References	Method	Key Findings
15.	Rahman et al. (2014b)	-numerical modeling of static liquefaction with low plastic fines	-recommended/suggested that the equivalent granular void ratio (e^*) and equivalent state parameter (ψ^*) should replace the existing corresponding state parameters (e) and (ψ) to enable capture of f_c effects on liquefaction behavior of soils -some significant derivations observed in the model for non-flow behavior -suggested that the model may not be valid for high plastic fines
16.	Rahman and Lo (2011)	-A hypothesis suggesting that when $f_c < f_{thre}$, the instability ratio (η_{IS}) and ψ^* can be represented by a single relationship regardless of the f_c at the start of shearing	-the instability ratio (η_{IS}) describes the beginning of fluctuations in undrained shearing - ψ^* explains in terms of e^* and EG-SSL used in obtaining the effects of fines -reported that ψ^* from the onset of undrained shearing, η_{IS} showcased a correlation irrespective of f_c -The influence of sample preparation in the investigation was not analyzed
17.	Rahman et al. (2014a)	-a total of 56 tests which includes strain-controlled monotonic tests and stress-controlled cyclic tests executed for describing the EG-SSL by single relationship - f_c ranges between 0 to 30%, with initial void ratio (in a wide range) and initial effective confining stresses	-a single EG-SSL, irrespective of f_c applied in defining the EG-state parameter (ψ^*); -the undrained monotonic behavior classified as flow, non-flow, and limited flow. When $\psi^*(0) > 0.042$, it is termed flow or transition provided the value remains positive; for $\psi^*(0) < -0.030$, it is termed non-flow; and for $0.009 < \psi^*(0) < 0.042$, it is termed limited flow. Cyclic liquefaction classified into cyclic instability, cyclic mobility, and hybrid -if $\psi^*(0) > 0.042$ (+ve), it is termed cyclic instability; for $\psi^*(0) < 0.049$ (-ve), it is termed cyclic mobility; and if $0.020 < \psi^*(0) < -0.049$, it is hybrid

Table 2.2 A systematic review of liquefaction resistance of sand mixed with plastic fines (continued)

S/N.	References	Method	Key Findings
			-cyclic liquefaction described as identical to flow-type behavior in monotonic loading
18.	El-Mohtar et al. (2014); El-Mohtar et al. (2012)	-study of effects of bentonite on pore pressure generation in loose sands by resonant column, static triaxial and cyclic triaxial tests -3% and 5% by mass of bentonite investigated for aging effects on liquefaction resistance for 1 to 10-days	-increase in the amount of bentonite and time (aging) increased the liquefaction resistance of sands -an increased bentonite content and extended aging time reduces the measure of rise in pore pressure during loading -the resulting frequency required for liquefaction occurrence increased with increased f_c and extended aging time
19.	Talamkhani and Naeini (2018)	-investigation of clay effects on liquefaction strength of sands -0, 5, 10, 15, 20 and 30% by weight of clay fines investigated	-raising the clay content until 10% reduced the liquefaction strength and increased subsequently with higher f_c -the presence of clay changed the dilative characteristics of clean sands to contractive behavior -the SSL moved downwards by increasing the f_c
20.	Tsai et al. (2010)	-a comparative experimental study executed on effects of non-plastic (silts) and plastic (clay) on liquefaction resistance of sands	-increased silt percentage in the sand matrix reduces its liquefaction strength and caused increased volumetric strains Increased clay content in the sand matrix soils caused subsequently increased liquefaction resistance and reduced volumetric strain in the sand matrix

Table 2.2 A systematic review of liquefaction resistance of sand mixed with plastic fines (continued)

S/N.	References	Method	Key Findings
21.	Boulanger and Idriss (2006)	-analysis of case history data and recommendations on evaluation of cyclic characteristics of silts plus clays	-recommendations were that fine-grained soils that behaved more of “clay-like” materials should be further evaluated for undrained cyclic and monotonic behaviors -as per fine-grained soils showing “sand-like” properties, the SPT and CPT framework was suggested for evaluation of their cyclic resistance -claylike behavior exhibited with $5 \geq PI \geq 7$ for practical purposes -recommended the discontinuation of the Chinese criteria
22.	Carraro (2004); Carraro et al. (2009)	-an extensive investigation on the role of plastic and non-plastic fines on the characteristics of quartz sand were however limited to 15% f_c (Carraro, 2004) -testing methods include environmental scanning electron microscope (ESEM), monotonic (ICD), cyclic undrained triaxial tests for assessing the role of f_c on liquefaction mechanisms of sands	-recommendations were that the mechanical behavior of sands was intrinsically affected by the amount and plasticity of f_c -a systematic drop of liquefaction strength of sands reported with a less dilative soil response for the range (0, 2, 5, and 10%) percentage content of kaolinite -the shear modulus reduced by the plasticity of fines -plastic fines decreased the peak and critical-state friction angles

Table 2.2 A systematic review of liquefaction resistance of sand mixed with plastic fines (continued)

S/N.	References	Method	Key Findings
23.	Beroya et al. (2009)	<ul style="list-style-type: none"> - systematic experimental testing of the effects of clay minerals on silt using montmorillonite, illite, and kaolinite -same amounts of clay minerals were applicable in verifying the mineralogical impacts on the silt behavior 	<ul style="list-style-type: none"> -montmorillonitic mixtures exhibited the highest cyclic strength, followed by illitic soils and then kaolinitic mixes -the bond offered by the different minerals suggested that individual minerals were responsible for the varying cyclic strength contrary to the percentage content of clays or PI
24.	Upreti (2016)	<ul style="list-style-type: none"> -24 stress-controlled cyclic triaxial tests to evaluate the impacts of plasticity on silt -The range of plasticity (<i>PI</i>) tested was from 0 to 14.53 -objectives were to study the impact of <i>PI</i> on pore pressures generation and liquefaction resistance 	<ul style="list-style-type: none"> -CSR found reduced progressively for the range of plasticity tested -the minimum void ratio decreased as f_c increased to 15% and then heightens afterward -the cyclic resistance of silt-clay matrix soils initially decreased up till a <i>PI</i> of 3.46 and then amplified with subsequent increase in <i>PI</i> -the generated pore pressure was highest at a <i>PI</i> of 3.46 -increased plasticity observed to delay the pore pressure development

Table 2.2 A systematic review of liquefaction resistance of sand mixed with plastic fines (continued)

S/N.	References	Method	Key Findings
25.	Bayat et al. (2014)	-effects of plastic fine (kaolinite & bentonite) investigated on shear strength responses of sand -0, 5, 10, 15, 20, and 30% of plastic fines investigated and samples reconstituted by wet compaction method	-specimen with 5% bentonite has the f_{thre} value and lowest post-peak strength -specimen with 20% bentonite observed with highest peak strength -specimen with kaolinite experienced decreased peak strength between 0 to 20% with f_{thre} at 20% content - the generated excess PWP decreased with the inclusion of the plastic fines
26.	Rugg et al. (2011)	-rheological tests and CU triaxial tests executed on sand permeated with bentonite suspension	-undrained shear properties indicated no change in cohesion and friction angle showing that the pressure used in permeation did not affect the sand fabric -recommended that permeating sand fabrics with some plastic fines could mitigate liquefaction of sands
27.	Benghalia et al. (2015)	-investigated effects of fines on 3-types of Algerian sands	-summarily suggested that obtained results agreed with published literature while noting that liquefaction strength drops until f_{thre} and then increases with additional fines
28.	Sadek and Saleh (2007)	-investigated impacts of silts and carbonaceous fines on liquefaction strength of sands -utilized moist tamping sample reconstitution method	-the limiting or threshold fine content (f_c) further confirmed with the plasticity index threshold -cyclic strength decreased with increased plasticity index from 0-13% while further increase in PI at 25 induces an increase in cyclic strength which was reportedly lower than cyclic strength of clean sand

Table 2.2 A systematic review of liquefaction resistance of sand mixed with plastic fines (continued)

S/N.	References	Method	Key Findings
29.	Ghahremani and Ghalandarzadeh (2006)	-cyclic triaxial tests applied in investigating the liquefaction resistance of sand mixed with kaoline	-conclusions are, for increased clay content between 10 to 30%, a decreased liquefaction resistance was notable while the reverse was the case when clay content increased beyond 30%
30.	Moretti et al. (1999)	A digital shaking table was used to study the soft-sediment deformation of some soil mixtures called seismites	Their results observed and recorded two-stage deformation mechanisms, (1) the decreased shear strength of sediments due to liquefaction, (2) sedimentation induced increase in shear strength after the occurrence of liquefaction
31.	Cornejo (2015)	-investigated effects of a low percentage (1-5%) by dry mass of laponite on the cyclic mechanisms of cohesionless-sands	-cyclic mobility of sands was considerably lowered during cyclic loading -the very high plastic laponite significantly increased the cyclic resistance of sands and improved the pore pressure generation characteristics due to the high bonding effect -recommended that laponite may be beneficial for mitigation of liquefaction

While summarizing the obtained facts from the systematic literature review executed in Table 2.2, inferences made are that a small change in percentage fines inclusion can relocate the position of the SSL/CSL. Therefore, the equivalent state parameters EG-SSL, ψ^* , and e^* were recommended as a substitute to the original state parameter SSL, ψ , and e . The reason for the above assertion by some schools of thought is because the equivalent state parameters offer a more accurate and predictive capability than the conventional state parameters (SSL, ψ , and e) for sands inclusions with fines, Rahman et al. (2014b). The idea of equivalent granular void ratio reportedly captures more accurately the liquefaction strength of sandy soils containing f_c and enhanced prediction of the threshold fines content f_{thre} (i.e., transitional to sand-like or clay-like behavior) better than the global void ratio. A reported wide range of obtained results for f_{thre} (0-30%) in current literature is controversial and suggests the need for further detailed studies. The shear strength of mixed soils is more dependent on the mineralogical composition of plastic fines, aging effects, fines plasticity-index, gradation (size and shape) of both sand and fines. Further studies by utilizing a micro-geomechanical approach may help understand more facts on the gradation of mixed soils (or matrix soils). The generated pore water pressures in sand matrix soils were affected by the plasticity index of fines.

A clear distinction between the function of plastic and non-plastic fines on liquefaction resistance of sands is recommended in practice to avoid further misleading recommendations under the generalized subject of “fine contents (f_c)”. The distinction is possible by using the PI as a criterion and not percentage fines content (f_c). The “sand-like” or clay-like behavior of sand matrix soils (or sands containing fines) are distinguished by PI and f_{thre} . Researchers should reconsider the application of plastic fines with a high plasticity index such as laponite and bentonite as a mitigation or stabilization agent for liquefaction-prone soils. The high-swelling clays are problematic on the foundations of structures due to the severe instability they may pose (swelling/dilation and shrinkage/contraction). It is already well-known that when wet, swelling, or dilation may be significantly high, and when they are in a dry state, significant shrinkage and contraction may also be recorded/experienced. The above scenario can cause failures like differential settlement and cracks on superstructures built on them due to experienced high instability that is constituted by soils with extremely high PI due to high moisture fluctuations.

The choice of the utilized soil sample reconstitution method is a significant factor in the derived soil fabric during laboratory tests. It is considered necessary to build up a framework in pertinent geotechnical engineering norms/standards to develop unified criteria that specify the soil sample remolding method in laboratories for mimicking specific types of in-situ soils based on the soil classification, mode of formation, and mineralogical composition. Aging in sands containing fines can significantly alter their strength properties since aging will consequently imply a stronger bond and inter-particle force development between the sands and fines fabric structure.

2.3.4 Numerical modeling in soil liquefaction assessment

The mimicking of the drained/undrained, monotonic, and cyclic characteristics of a 2-phase medium consisting typically of soil and water usually are executed using either a coupled or uncoupled approach. The uncoupled analyses typically involve numerical modeling of the undrained response of saturated soils separately without considering interactions between the soil-water phases and pore water pressure. The above is usually carried out independently by another model, while fully-coupled analyses involve more unified methods where all variables (i.e., stresses, strains, and pore pressures) are calculated concurrently during every time step effects (Cheng & Detournay, 2021; Puebla, 1999; Taiebat et al., 2007). The fully coupled analysis is idealized as a more logical constitutive model and simulation of the problematic physical domain than the uncoupled approach. In a fully coupled solution of a hydro-mechanical problem such as soil liquefaction, the unknowns are usually displacements experienced in the whole system and generated excess PWP by either monotonic load or cyclic loads. In either approach mentioned above, the dynamics equations of motion are solved chiefly by coded computer codes, calibrated with experimental data that are typically obtained from laboratory and in-situ field tests. The significant reasons for calibrating numerical models for soil characteristic undrained behavior against laboratory or in-situ test data are due to a) the peculiarities of physical instabilities (i.e., path-dependencies) usually associated with soil as a geomaterial, b) the non-linear stress-strain behaviors/laws, c) the issue of localization (shear bands) mainly relating to strain-softening materials.

Several material constitutive models are available in numerical codes and are well-documented in Itasca (2021). For instance, the basic material constitutive models embedded/implemented in the Itasca (2021) software (FLAC, FLAC3D) include the null model, plastic model category (e.g., Drucker-Prager, Mohr-Coulomb, ubiquitous-joint, strain-hardening/softening, bilinear strain-hardening/softening ubiquitous joint, double-yield, modified cam-clay, Hoek-Brown, and Cysoil model), elastic model category (e.g., elastic-isotropic and elastic-transversely isotropic models). The elastic and Mohr-Coulomb models are mostly used to compute the soil's initial stress state before applying further modifications/alterations with other advanced models. Some of the several existing constitutive, advanced liquefaction models found in the literature database include Wang2D (Z. L. Wang et al., 1990); DM04 or SANISAND (Dafalias & Manzari, 2004; Dafalias et al., 2004); PM4SAND (Boulanger & Ziotopoulou, 2015); NTUA-SAND (Andrianopoulos et al., 2010a, 2010b); DAMES & MOORE (Dawson & Mejia, 2012); UBCHYST (Naesgaard, 2011); UBCSAND (Byrne et al., 2003; Byrne et al., 2004; Byrne & Seid-Karbasi, 2003); P2P (Cheng, 2018; Cheng & Detournay, 2021); Norsand (Been et al., 1991) etc.

Each constitutive model has its peculiar advantages and limitations. It is vital to choose suitable material and constitutive liquefaction models to simulate the required soil liquefaction mechanism reasonably. In general, geomechanics problems are typically analyzed based on either continuum

or discontinuum mechanics approach. Continuum problems such as liquefaction are usually analyzed, solved, or simulated by the application of either discrete element method (DEM), finite element method (FEM), finite volume method (FVM), or finite difference method (FDM). One of the latter, as mentioned above, is implemented in almost all available commercial and open-source numerical codes. Examples of FEM model codes include Plaxis (Plaxis, 2019); Diana; OpenSees, while FLAC and FLAC3D are FVM-based numerical codes.

Similarly, some discrete element method (DEM) codes for simulating properties such as bonding and interparticle force between grain-to-grain contacts in a soil medium have been developed in recent years. Examples of DEM codes include PFC, Edem, UDEC, and 3DEC. All the liquefaction models mentioned above are incorporated in most cases as user-defined models (UDM) in commercial codes such as FLAC, FLAC3D, and Plaxis codes. The comprehensive review of all the constitutive liquefaction models is considered out of scope in the current study. The selection criteria of the appropriate liquefaction constitutive model utilized in this study were based on their capability to predict the typical undrained behavior of soils specified in each case under specific mean effective stress. According to the literature survey, sands' drained and undrained physics containing fines less than 30% could be modeled as a soil fabric dominated by sand-like properties. Therefore, it is assumed that material properties of a sand-matrix material containing less than 30% fines would intrinsically be represented in their elastoplasticity, shear strength/deformation parameters, critical state properties, relative density/void ratios, permeability, porosity components of the material properties.

Cheng (2013) executed a critical review of the fundamental mechanisms of existing bounding surface theory, critical state, and soil state fabric-dilatancy theory. The original related fabric-dilatancy and sand plasticity model (DM04), initiated by Dafalias and Manzari (2004) and Dafalias et al. (2004) were improved by Cheng (2018). The P2P model implemented by Cheng and Detournay (2021) modified the original DM04 by substituting all void-ratio-associated formulas with relative density data and incorporating plastic hardening modulus, elastic modulus, critical state, and other associated theories/hypotheses. The aim was to provide more straightforward model calibration when using in-situ soil data such as those from *CPT*, *SPT*, and V_s , which engineers purportedly favor for simple model calibration. A modified critical review of some merits and limitations of some selected critical state-compatible numerical models such as UBCSAND, PM4SAND, DM04, P2P, and NORSAND liquefaction constitutive models after Cheng (2018) is best summarized in Table 2.3. The merits are in green, while limitations are in red text and italic fonts. From the table, it could be inferred that the P2P and NORSAND model may be assumed suitably ok for relatively easy model calibration and subsequent analyses. Additionally, the models have been calibrated to match the recommended CRR-curves by Youd and Idriss (2001) for clean sands. The K_α effect is mostly neglected in practice due to varying discrepancies of its formulations in numerical models.

Table 2.3 A modified critical review of UBCSAND, PM4SAND, DM04, P2P, NORSAND liquefaction models modified after Cheng (2018)

Properties	UBCSAND	PM4SAND	DM04 or SANISAND	P2P	NORSAND
simplicity (or user-friendly)	Yes	Yes	No	Yes	Yes
CRR $(N_1)_{60}$ curve	Matched semi-empirical	Match semi-empirical	Do not match semi-empirical	Match semi-empirical	Match semi-empirical
CSR (N-curves)	Ok	Ok	Highly steep	Ok	Ok
Damping at large strain	High damping	Ok	High damping	Ok	Ok
Loop overlapping issues	Yes	No	Yes	No	No
Lode angle effect	Equivalent to the conventional MC model	No	Yes, but convex	Yes	Yes
Compatibility for static or monotonic and dynamic loads (softening & hardening laws)	Ok	Not suitable for static Needs different calibration	Ok	Ok	Ok
Varying densities	Need different calibration	Need different calibration	One set of parameters	One set of parameters	One set of parameters
K_σ effect	Empirical match	Empirical match	Not matching	Empirical match	Empirical match
K_α effect	Empirical match	Empirical match	Not matching	Not satisfying for dense sands	Empirical match
Complexities of formula Formula documentation	Relatively simple Poor documentation	Overly complex and lengthy Well documented	Relatively simple Well documented	Relatively simple Well documented	Relatively simple Well documented
Good quality of 3D Model	No, only for plain strain	No, only for plain strain	Yes	Yes	Yes

2.4 An overview of existing soil liquefaction mitigation methods

Most executed studies in the past to develop liquefaction mitigation techniques that are economical, environmentally friendly, foster the implementation of the global goal of the zero-emission target, and produce little or no disturbance effects to existing ancillary structures are still lacking. The aforementioned criteria are necessary for sustainable liquefaction mitigation in the 21st century if the environmental sustainability issues need to be factored into real-life projects. The summarized liquefaction mitigation techniques that are widely employed in practice include densification techniques, improvement of soil drainage properties, and enhancement of soil engineering properties by solidification, reinforcements, and other various grouting/soil improvement techniques.

The recently published literature survey by Bao et al. (2019) summarized the existing liquefaction mitigation techniques. According to Bao and co-workers, such mitigation methods include soil densification procedures using gravel columns, vibro-compaction, compaction grouting, dynamic compaction, compaction piles. The grouting technique is a well-known method of improving soil engineering properties. The grouting of in-situ soils with stabilization agents such as cement, lime, sodium silicate, acrylate, and epoxy is common in routine practice. Other types of soil improvement include soil replacement, and drainage improvement techniques. The recently developed methods include passive site remediation techniques with nanomaterials like colloidal silica, laponite, bentonite, short synthetic fibers. Furthermore, recycled materials (e.g., tire chips/shreds, glass fibers, construction wastes) are gaining more recent practice popularity.

Recent several research works have showcased the effectiveness of the application of biological processes, chemical grouting, partial saturation methods, grouting with micro-fine cement, and other pozzolanic materials (e.g., fly-ash (FA), slay-bentonite, zeolite, and cement additives). The review carried out by Bao et al. (2019) is considered comprehensive as it summarizes the important details involved with the practicability of liquefaction mitigation methods. A tree diagram summarizing most of the existing liquefaction mitigation methods with suitable ground stabilization additives is presented herein in Figure 2.5 for an easy visual at a glance.

In general, each of the liquefaction mitigation methods outlined in Figure 2.5 has one or more limitations associated with either limited cost or economy of applicability, environmental issues, and disturbance to existing/ancillary structures. Also, the well-researched use of scrap tires may seem economical and practical for liquefaction mitigation. Still, they are often associated with environmental issues such as the risk of groundwater pollution through the leaching of poisonous/hazardous chemicals such as lead (Pb). Similarly, some emerging techniques, such as partial saturation methods, may deteriorate over time, leaving the soil in the initial liquefaction risk status. The cost-effectiveness sustainability of the application of colloidal silica in passive site treatments requires further investigations. The main challenge for geotechnical engineers in

the 21st century remains the invention of sustainable liquefaction mitigation methods that could meet all criteria mentioned above.

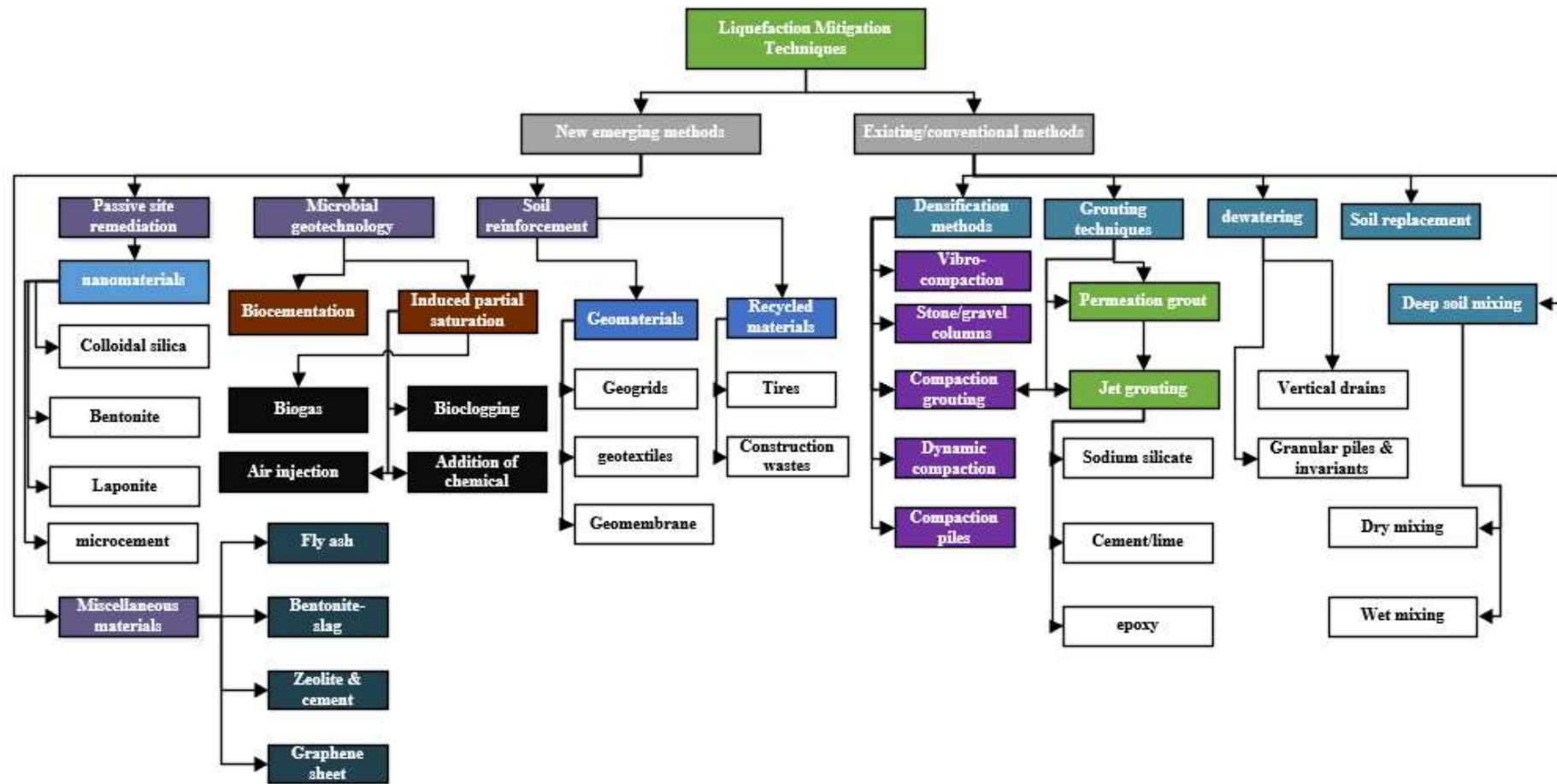


Figure 2.5 A summary of soil liquefaction mitigation techniques

2.5 Summary

There is a need for further research on how low plasticity and clay minerals interact with sand particles since its expansive nature is minimal when considering the soil mass's overall stability in terms of the swelling index. The electric charges on the clay surfaces may be balanced up when admixed with sands, thereby reducing its expansive nature (Kolay & Ramesh, 2016; Nagaraj, 2016). The balanced strength characteristic derived from sand matrix soils could provide a more promising liquefaction mitigation approach through deep soil mixing, grouting, and passive site remediation techniques. Christie et al. (2000) have identified the available clay minerals in New Zealand, reported in commercial quantities. Commercially available clay minerals in New Zealand include bentonite, halloysite, brick, kaolinite, and pottery clays. Experimental investigations of the role of some of these clay types on sands' liquefaction behavior may be worthwhile in future research studies.

Granular soils' porous and highly permeable structure makes them extremely prone to both static and earthquake-triggered soil liquefaction; therefore, the clay minerals may be suitable to make up for the aforementioned deficiencies and act as either full or partial replacements for other conventional soil improvement additives (e.g., cement, lime, and other chemicals). Typically, a clean sand soil's main shear strength parameter is its shearing resistance angle; its internal cohesion is approximately zero. Further studies are needed to include comprehensive investigations of mixed soils, i.e., granular soils (e.g., sand) mixed with varying percentage content of different clay mineral types. The effects of utilizing clay as a partial replacement for soil stabilizing agents such as cement are promising. The two effective shear strength variables (i.e., the *effective angle of shearing resistance* ' ϕ ' and *apparent cohesion* ' C ') are essential for the optimal performance of engineered soils or grounds in terms of stability, rigidity, resistance to pore water pressure accumulation. To the author's knowledge, studies on sand matrix soils (i.e., clayey sands) with numerical modeling and complete data validation using numerical modeling are still rare from the literature as the majority of the previous studies focused more on either clean sands or silty sands. For instance, more studies are required to generate adequate data of soil model properties for varieties of mixed soils and appropriate comparisons with the highly liquefaction-prone sands, this would inform proper design decisions to be made during soil replacement-related engineering works during designs and constructions.

A review of previous studies on mixed soils indicated that numerical modeling is still relatively scarce for sand matrix soils as a data validation for experimentally obtained evidence. Some advanced critical state compatible models were selected and cross-critically reviewed and it was concluded that the Norsand model may be suitable to capture most essential features of soil undrained behavior during flow failure mechanisms. It is already well-known that the mean effective stress and critical void ratio are the key factors determining the flow failure undrained behavior of loosely deposited sandy soils.

CHAPTER 3: RESEARCH METHODS AND SOIL TESTING PROGRAM

3.1 Introduction

This chapter described the applicable soil testing programs and other research methods in the current study. All the studied soil samples were remolded/reconstituted in the AUT Geotechnical Engineering Laboratory. The studied soil samples, already presented in Chapter 1, include a typical type of clean sand called east coast sand (ECS) and their corresponding derived sand matrix variants obtained by mixing/varying (5-30%) kaolinite percentage by weights of ECS. The utilized soil-sample preparation methods depend on the nature of the required individual corresponding tests and are explained accordingly in relevant sections and subsections of this chapter. The adopted research methodology elaborates on the implemented quantitative and parametric/comparative research techniques, including laboratory experiments, physical model experiments (i.e., the shaking table), and soil geomechanical properties. The initial laboratory tests aim to obtain the basic soil index properties of the studied soil samples and subsequently classify them (soil characterization) according to the unified soil classification soil system (USCS). The juxtaposition of all studied soil sample results is necessary for analytical and comparative technical discussions. The executed soil classification characteristics/index tests include particle size analysis (PSD) of ECS, hydrometer analysis of kaolinite-clay, scanning electron microscope (SEM) imaging for all the studied remolded soil samples, Atterberg's limits (i.e., liquid limits (LL), plastic limits (PL), plasticity index (PI)), specific gravity (G_s), permeability tests, minimum, maximum dry densities (ρ_{min}, ρ_{max}), minimum, maximum void ratios (e_{min} & e_{max}) respectively.

The shear strength properties of all soil studied samples were derived from undrained and drained monotonic compression tests while the consolidation properties were derived from both 1-dimensional and triaxial testing itself. The executed monotonic tests typically are isotropically consolidated undrained (ICU) based on the conventional triaxial testing techniques. The soils' undrained behavior is most relevant to liquefaction physics and mechanics since soil samples that liquefy usually are in a saturated state, hence, all stresses are effective unless otherwise stated. In practice, the soils' drained behavior under the triaxial condition usually is applicable for simulating its long-term strength and consolidation characteristic behavior under static loads. The goal of executing the monotonic triaxial test in this study includes: (1) extraction of the deformational and strength (i.e., geomechanical) properties of all soil samples (primarily, the critical state, state dilatancy, and stress dilatancy parameters); (2) Discuss the obtained critical state mechanism (CSL) and static liquefaction behavior. The deformational and strength properties of soils would help interpret the statically triggered liquefaction cases under the triaxial conditions. On the other hand, the executed shaking table provides insight into the evolution of the dynamic pore water pressure (PWP) behaviors of the studied soil samples.

The executed physical model tests involve mainly the shaking table experiments. The physical model tests usually are required to simulate the soil behavior under dynamic loads in laboratory conditions. More facts about the utilized, designed, and fabricated shake table device and experiments are well-explained in this Chapter's relevant subsection and published in Bolarinwa et al. (2021). The basic technical specifications of the shake table are summarized in section 3.7.1 of the current Chapter.

3.2 Materials

The description of the studied soil materials, already discussed in section 1.6.1 of Chapter 1, provided information on the source of studied soil samples, soil sample preparations, and sample numbering nomenclature. The acquired ECS, packaged in plastic bags of 20kg and kaolinite clay, wrapped in paper bags of 25kg, were stored in the laboratory for use (Figure 3.1). Except where explicitly stated, distilled or completely de-aired water was utilized in all sample preparations and soil testing.



(a) East coast sand (ECS) in plastic bags of 20kg



(b) Kaolinite (clay) in paper bags of 25kg

Figure 3.1 The source primary soil specimens as stored in the geotechnical engineering laboratory

The results of other derived/remolded soil samples by varying the percentage content mixtures of kaolinite (clay) with ECS were analyzed, discussed, and compared with the ECS00, which acts as the primary/control soil sample. The ECS, classified as poorly graded sand (SP) is greyish in color and has an average specific gravity of 2.60, its grains are sub-angular to sub-rounded in shape. The clay (kaolinite), classified as per USCS as a lean clay (CL), is whitish, has a specific gravity of 2.42, LL is 47%, PL is 32%, and PI is 15%.

To investigate the lean kaolinites' role in the dynamically generated excess PWP and related liquefaction mechanisms of ECS, studying the characteristics of the various sand matrix of ECS variants are essential research work scope herein. The percentage by weight content of kaolinite in the sand matrix samples ranged from 0% to 30%. The list of all tested soil samples already presented in Table 1.2 of section 1.6.1 in chapter one summarizes the mixed ratio and sample numbering/naming nomenclature.

3.3 Soil classification tests

3.3.1 Particle size and hydrometer analysis

The quantitative determination of the particle size granulometric composition (PSD) of sand grains that made up ECS00 was executed according to D6913/D6913M-17 ASTM (2017), is summarized in this section. On the other hand, the hydrometer analysis was carried out on the kaolinite-clay sample as per ASTM D7928-16 (2017). The two tests subsequently provided insights that helped estimate the other derived remolded mixed soil samples' classification characteristics, including the sand matrix soil samples. The selected test technique for the particle size analysis of ECS is the test method-B of D6913/D6913M-17 ASTM (2017) based on the inherent maximum particle size criteria of ECS less than 4.75mm sieve size. In this test, the sample processing of ECS00 is by the oven drying method. The mechanical sieve shaker with sieves configuration is shown in Figure 3.2 and utilized for the sieve analysis of ECS00; three sets of tests were executed to ensure accuracy and confirmation of test repeatability. The detailed test results sheets are annexed in Appendix A1 to A3, while a combined plot of the three sets of test results is shown in Figure 3.3. The plot's key observation in Figure 3.3 indicated the achieved PSD curve's consistency. Hence, the tests' repeatability of the result is reasonably/relatively consistent.



Figure 3.2 The utilized mechanical sieve shaker

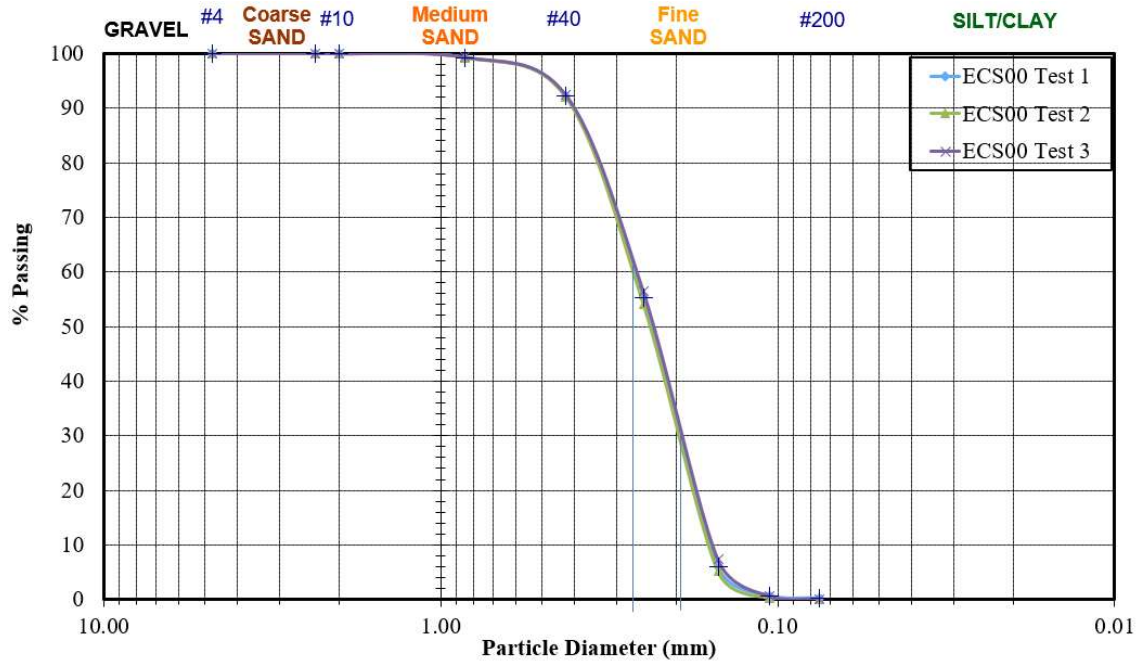


Figure 3.3 Particle size distribution (PSD) analyses plot

The averaged grain size gradation of ECS00 indicates its composition of 99.81% sand particles and 0.19% fines, which appear as silt (i.e., non-plastic fines). The 99.81% content of sand grains suggests that the ECS00 sand sample is relatively or may be approximately referred to as clean sand with a negligible quantity of fines content (i.e., 0.19%). The mean grain size of ECS, i.e., D_{50} is about 0.25mm; the effective particle size, D_{10} is 0.16mm; the particle size at which 30% are finer, D_{30} is 0.20mm; and the particle size at which 60% are finer, D_{60} is 0.26mm. The derived coefficient of uniformity, C_u of ECS00 is 1.63, and the compression coefficient, C_c is 0.96. Hence, based on the obtained PSD of ECS, one can infer that the sand is a typical poorly graded sand (SP) as per the USCS soil classification system.

The hydrometer analysis of the utilized kaolinite clay executed was carried out as per specifications set out in D7928-16 (2017) - Standard test method for particle-size distribution (gradation) of fine-grained soils using the sedimentation (hydrometer) analysis. The hydrometer analyses utilized the 152H Hydrometer, 1000mL-sedimentation cylinders, thermometer, soil mixer, and a timing device. It is well-known that hydrometer analysis applies Stoke's law and its assumptions to determine the particle quantity in a sedimentation suspension at a particular position in time.

The test procedure first determined the required mass of the test kaolinite sample by determining its moisture content (w). The obtained moisture content of the kaolinite-clay is 0.91%. The required test sample mass was determined according to Equation 3.1 as per D7928-16 (2017).

$$M_{mest} = H_c \left(\frac{100}{\%est} \right) \left(1 \times \left(\frac{w_{cest}}{100} \right) \right) \quad 3.1$$

In the above equation, M_{mest} is estimated moist mass, H_c is hydrometer capacity (in this case 55g for the 152H), $\%est$ is the estimated percentage of soil passing the No. 200 (75 μ m) sieve, and w_{cest} the estimated moisture content.

It follows that, $M_{mest} = 55 \times \left(\frac{100}{100}\right) \times \left(1 \times \left(\frac{0.91}{100}\right)\right) = 55.5g$

Therefore, the utilized mass of kaolinite in the hydrometer analysis was 55.5g. The dispersing agent used was sodium hexametaphosphate; 5g of the former was measured and mixed with the prepared slurry sedimentation specimen and reference test solution. Other test procedures as specified in the test standard were followed. The test process is shown in Figure 3.4 and the obtained particle size gradation curve is shown in Figure 3.5. The hydrometer test data as observed/reported are detailed in Table 3.1

Table 3.1 Hydrometer analysis tests data

Time, T	Hydrometer, Ra	Temperature	Hyd Corr Rcp	Effective Depth, L	Diameter	Percent Finer
min	gm/L	deg C	gm/L	cm	mm	%
1.0	60.0	17.8	52.4	6.52	0.03679	97.37%
2.0	59.8	17.8	52.2	6.56	0.02610	96.91%
4.0	58.3	17.8	50.7	6.81	0.01880	94.12%
15.0	57.5	17.8	49.9	6.93	0.00979	92.73%
30.0	56.3	18.0	48.7	7.13	0.00701	90.50%
60.0	54.8	18.0	47.2	7.38	0.00504	87.72%
240.0	47.8	17.9	40.2	8.52	0.00271	74.67%
1440.0	29.0	17.1	21.3	11.57	0.00130	39.49%



Figure 3.4 The hydrometer analysis, sedimentation test in progress

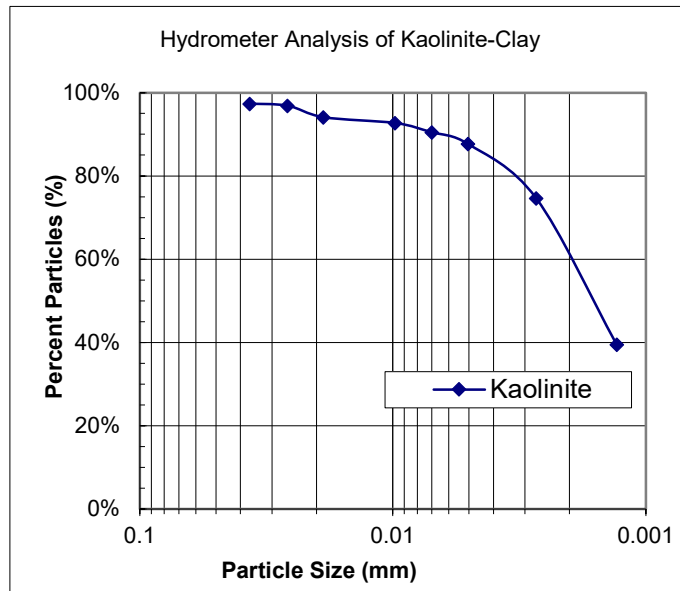


Figure 3.5 The PSD of kaolinite in sedimentation test

3.3.2 The Consistency/Atterberg Limits

The consistency limits are helpful for the classification of clayey sand samples with cohesive/plastic soil properties. First, the liquid limits (*LL*) and plastic limits (*PL*) determination for the kaolinite clay used in deriving other sand matrix soils was executed according to BS/EN/ISO-17892-12 (2018). The obtained *LL* and *PL* were then used in deriving plasticity index (*PI*) of the soil samples. For comparisons purposes, both the Casagrande's device (Figure 3.6 a) and the fall-cone methods, shown in Figure 3.6 (b), were applied in determining the *LL* properties of the utilized kaolinite. A minimum of three (3) tests were executed each for both methods to establish suitable consistency and repeatability of the obtained results.

The Casagrande method result sheet for the kaolinite clay is shown in Appendix B1 to B3, while the fall-cone test result sheet is shown in Appendix B4. Although the summary of obtained experimental data from both methods shown in Table 3.2 indicated some minor variations, in summary, both techniques yielded approximately the same classification on the plasticity chart since all the *PI* plots of *PI* against *LL* all fall above the A-line of the plasticity chart. Figure 3.7 illustrates the plastic limit testing procedures. The obtained results of Atterberg limits for other remolded soil samples with clayey/cohesive properties, including ECS05, ECS10, ECS15, ECS20, and ECS30, are annexed as Appendix B5 to B9. The obtained consistency limits of the kaolinite data fall within the suggested range of values indicated by Head (2006, p. 59) for same. Head (2006) presented the typical range of experimental values of Atterberg characteristics for kaolinite as $LL = 40 - 60$; $PL = 10 - 25$ and these values are in good proximity with the obtained data in Table 3.2.

The soils' moisture content is crucial in the determination process of Atterberg limits and several other important soil engineering properties. Hence, all moisture content determination in the

current work was executed according to BS/EN/ISO-17892-1 (2014). A two (2)-degree decimal precision digital weighing balance (Figure 3.7a), a digitally and thermostatically controlled oven (Figure 3.8b), a desiccator (Figure 3.8c), and a digital thermometer (Figure 3.8d) were utilized in the testing process.



(a) Casagrande's Liquid limit device during testing



(b) The fall-cone device in operation

Figure 3.6 (a) The Casagrande's and (b) the fall-cone devices for Atterberg limits determination



(a) Mixing of kaolinite (clay) sample



(b) The rolling of the soil sample in threads until breakage determination of *PL*

Figure 3.7 Determination of plastic limits of kaolinite-clay

Table 3.2 Comparison between Casagrande and Fall-Cone method of Atterberg's Limits for kaolinite

Atterberg properties	Casagrande's method	Fall-cone method
Liquid limits (%)	45	47
Plastic limits (%)	35	32
Plasticity index	10	15
USCS classification	CL	CL



(a) Digital weighing balance (2-decimal degree precision)



(b) Thermostatically and digitally controlled drying oven



(c) Desiccator



(d) Digital thermometer

Figure 3.8. Devices used in determining moisture content in the Geotechnical laboratory

3.3.3 The soil classification as per the unified soil classification system (USCS)

Based on the USCS as detailed in ASTM D2487-17 (2017) – Standard Practice for Classification of Soils for Engineering Purposes, clayey sands are soils which (a) consist > 50% grains held on the No. 200 sieve (75 μm); (b) consist 50% or > of coarse particles passing through the No. 4 sieve (4.47 mm); (c) consists > 12% grains smaller than 75 μm of the weight fraction. The USCS utilizes dual symbols for classifying sands with fines greater than 5% and less than 12%. Usually, the obtained test data from the sieve analysis and Atterberg limits are sufficient to classify all soil samples. As specified in the standard, equations for determining the coefficient of curvature, C_c and coefficient of uniformity, C_u indicated in Equation 3.2 and 3.3 are respectively applicable.

$$C_c = (D_{30})^2 / (D_{10} \times D_{60}) \quad 3.2$$

$$C_u = D_{60} / D_{10} \quad 3.3$$

Where, D_{60} , D_{30} , and D_{10} are grain sizes correlating with 60%, 30%, and 10% finer on the cumulative granulometric curve. The obtained USCS soil classification for all the soil samples shown in Table 3.3 also indicated the classification criteria applied in the process. The C_u and C_c for all sand matrix samples can not exceed the obtained range of values for the clean sand (i.e., ECS00). Hence, the collected PI data and percentage fines content were used as supplementary information to decipher their respective classification since sieve analysis was not repeated for the mixed samples. From Table 3.3, it can be inferred that the activity ratio of the studied soil specimens, which is the ratio PI to percentage clay (i.e., fines) content, can be considered inactive. Soils with an activity ratio less than 0.75 can be regarded as inactive, while soils with an activity ratio greater than 1.25 are considered active and considered fatal for geotechnical works (Knappett & Craig, 2012, p. 10).

Table 3.3 USCS classification of all soil samples

S/N.	Sample No./Name	C_u	C_c	PI	% Fines content (%)	Classification based on ASTM D2487-17 (2017) criteria	USCS classification and symbol
1.	ECS00	1.63	0.96	NA	NA	$C_u < 6.0$ and $C_c < 1.0$	Poorly graded sand (SP)
2.	ECS05	NA	NA	NA	5	$C_u < 6.0$ and $C_c < 1.0$	Poorly graded sand (SP)
3.	ECS10	NA	NA	2	10	5-12% fines	Poorly graded sand with clay (SP-SC)
4.	ECS15	NA	NA	5	15	>12% fines	Clayey sand (SC)
5.	ECS20	NA	NA	7	20	>12% fines	Clayey sand (SC)
6.	ECS30	NA	NA	9	30	>12% fines	Clayey sand (SC)
7.	KK00	NA	NA	15	100	$PI > 7$ and plots above the "A" line	Lean/inorganic clay (CL)

*Note: NA = Not available in the table

3.4 Other practical soil index tests

3.4.1 Scanning Electron Microscopic (SEM) imaging of samples

The significance of executing the scanning electron microscope (SEM) is to provide visual information on the observed individual physical particle grain shapes and interlocking/inter-particle structural arrangement of the soil samples. Although a comprehensive image analysis was considered out of scope in the current study, the executed SEM provided a magnified, 3-dimensional view of the soil particles with a high depth of focus. The micrographs were captured at X50, X200, and X5000 magnifications for all remolded samples. The SEM micrographs of the clean sands (ECS00) and kaolinite (clay) shown in Figure 3.9 indicate that the shape of ECS is sub-angular to sub-rounded e.g., (Zheng & Hryciw, 2018), while kaolin possesses flaky platelike forms/shapes e.g., (Xu & VanDeventer, 2002). The interlocking properties of the kaolinite particles in between the sand grains were further revealed in the other sand matrix soil samples and are available in Appendix C.

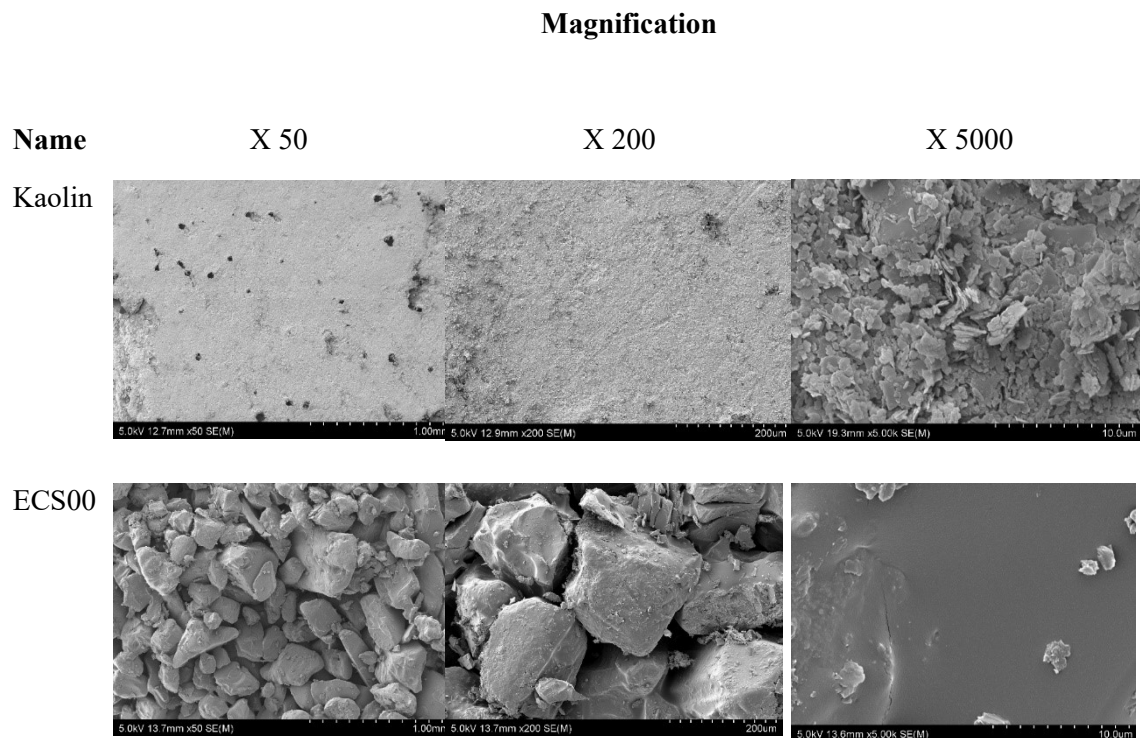


Figure 3.9 SEM micrographs of kaolinite and east coast sand (ECS00)

The SEM micrograph of ECS at X50 magnification presented a precise visual observation of the individual particle grains. At a higher viewing magnification of X5000, the presence of non-plastic fines suggests the presence of fractions of silts. In contrast, a precise inspection of kaolinite particles was impossible at X50 and X200 magnification, but the visual inspection was accessible at X5000 viewing magnification. The reason for the above result is that kaolinite clay is composed of too tiny particles.

3.4.2 Specific gravity

The details of the specific gravity (G_s) tests for all the studied soil samples as executed as per ASTM-D854-14 (2014) are summarized here. The specific gravity of solids is required in subsequent other test types, varieties of calculations, and is regarded as one of the most significant soil engineering parameters. The specific gravity of soils is applicable for estimating the void ratio, the degree of saturation, the density of soils' solids, needed in hydrometer analysis of soils, calculation of zero-air voids curves in compaction tests, in triaxial compression tests, etc. The oven-dried sample method B is more comfortable to use and thus adopted herein. All experiments were executed based on a programmed constant temperature of 27.2°C, achieved with a constant-temperature water bath (Figure 3.10), equipped with a thermometric device to regulate temperature as desired.



(a) Constant temperature water bath



(b) Specific gravity tests in progress

Figure 3.10 Maintaining a constant temperature during the specific gravity test

A summary of the specific gravity (G_s) obtained for all samples is shown in Table 3.4, and the detailed results test sheets for each soil sample are attached as Appendix D1 to D7

Table 3.4 Specific gravity (G_s) of all soil samples at a glance

Sample Number	Sample Name	Specific gravity (G_s)
ECS00	Clean East Coast Sand	2.60
ECS05	Sand matrix with 5% clay	2.54
ECS10	Sand matrix with 10% clay	2.61
ECS15	Sand matrix with 15% clay	2.53
ECS20	Sand matrix with 20% clay	2.59
ECS30	Sand matrix with 30% clay	2.56
KC00	Pure Kaolinite – clay	2.42

3.4.3 The maximum and minimum void ratios

First, a consistent, uniform, and homogenous soil sample mixture was achieved with the mechanical mixer as shown in Figure 3.11. As per the ASTM-D4253-16 (2016) – Standard Test Method for Maximum Index Density and Unit Weight of Soils Using a Vibrating Table, the maximum index density test is restricted to soils consisting of 15% maximum fines content. Therefore, the determination of the soil samples' maximum index density parameters (i.e., maximum dry densities (ρ_{max}), minimum – index void ratio (e_{min}) were executed for ECS00, ECS05, ECS10, and ECS15 according to ASTM-D4253-16 (2016). While ASTM-D698-12 (2012) – Standard Test Methods for Laboratory Compaction Characteristics of Soil Using Standard Effort (12 400 ft-lb/ft³ (600 kN-m/m³)) was adopted for the determination of maximum index density parameters for ECS 20 and ECS30 soil samples.

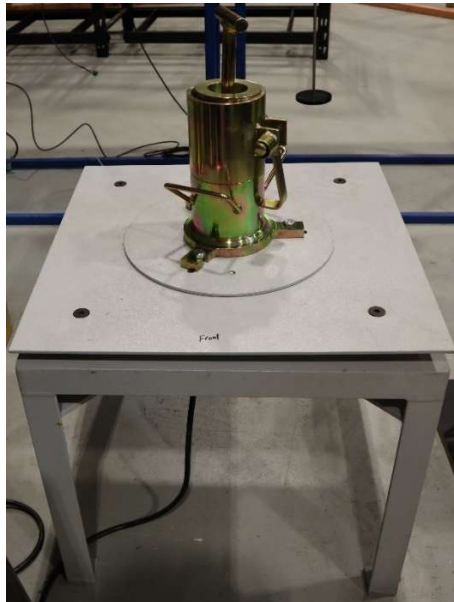
The above choice of experimental methods is consistent with previous works such as Polito (1999); Carraro (2004). The effects of the fines content in a granular material such as sand relating to the intrinsic index density parameters are well detailed and explained in Carraro et al. (2009). The obtained test datasheets of the executed maximum index density parameters in this study are detailed in Appendix E1 to E4. The result of the index soil density parameters test is summarized in Table 3.5. Figure 3.12 (a) shows the maximum compaction test using the vibratory table, while Figure 3.12 (b) shows the compaction process by using the rammer.

Table 3.5. Summary of test results for maximum and minimum index density parameters

Sample No./Name	Maximum dry density ρ_{max} (g/cm³)	Minimum void ratio e_{min}	Minimum dry density ρ_{min} (g/cm³)	Maximum void ratio e_{max}
ECS00	1.67	0.56	1.43	0.82
ECS05	1.64	0.55	1.32	0.93
ECS10	1.57	0.66	1.22	1.14
ECS15	1.43	0.76	1.18	1.15
ECS20	1.95	0.33	1.10	1.35
ECS30	1.94	0.32	0.900	1.84



Figure 3.11. Laboratory mechanical mixer



(a) Compaction by the vibrating table



(b) Compaction by using a rammer

Figure 3.12 Compaction processes to determine maximum index density parameters

The compaction curves shown in Figures 3.13 and 3.14 indicate a maximum dry density of 1.95g/cm^3 and 1.94g/cm^3 for ECS20 and ECS30, respectively. The optimum moisture content (*OMC*) was 11.5% and 10.8%, respectively. The test datasheet of the standard proctor compaction tests attached as Appendix F1 and F2 produced the compaction curves shown in Figure 3.13 and 3.14, respectively.

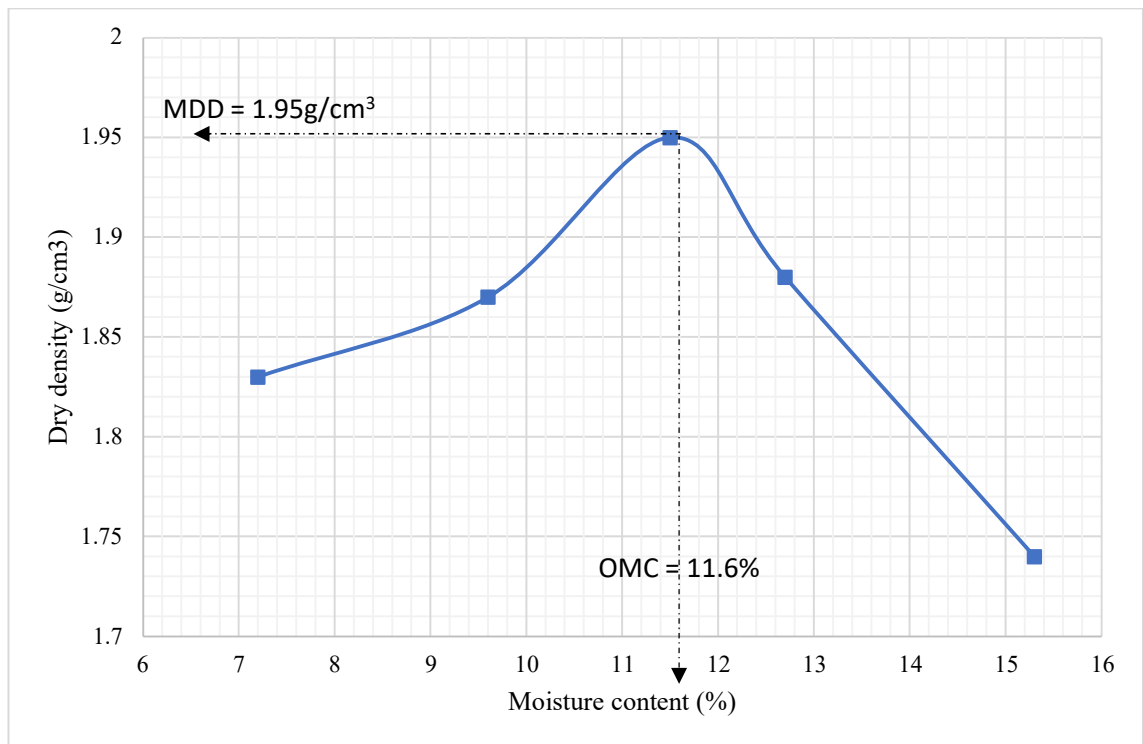


Figure 3.13 Compaction curves of ECS20

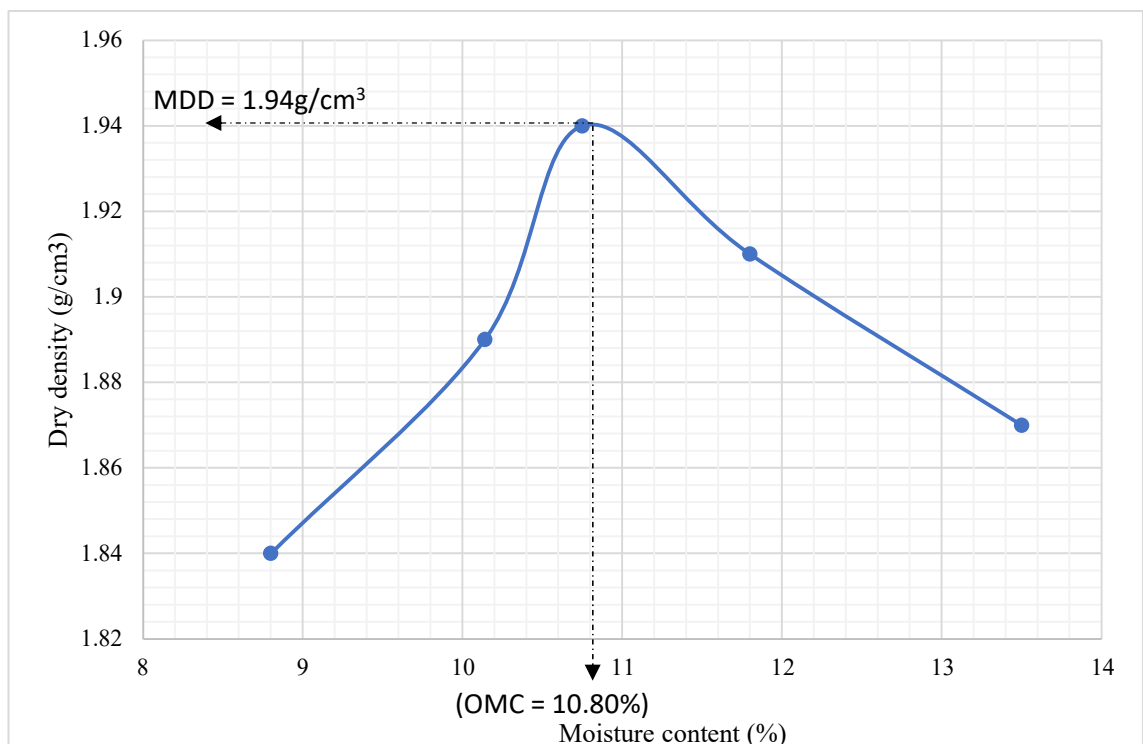


Figure 3.14. Compaction curve of ECS30

Correspondingly, the ASTM-D4254-16 (2016) – Standard Test Method for Minimum Index Density of Soils and Calculation of Relative Density is restricted to soils having maximum fines content of 15%. Since there is no prescribed alternative standard for evaluating the minimum density-related parameters, the same standard was utilized. Method B in which the minimum density is obtained by slowly pouring the soil samples into a standard mold of a known volume was the applicable test procedure. The test data for the minimum index density parameters are well-detailed in Appendix G1 to G6.

Recalling from the literature, the selection of density quantification parameters is crucial for sands containing fines because they influence the overall shear strength and cyclic resistance Carraro et al. (2009). The estimated e_{min} and e_{max} of ECS20 and ECS30 were derived based on the concept of the global void ratio (e). The intergranular void ratio (e_g), stated in Equation 2.12 and equivalent granular void ratio (e^*) (Equation 2.13) detailed in the literature have also been utilized by several other researchers in the past to quantify relative density parameters.

3.4.4 The soil permeability test

The soil permeability is explained as the tendency or capability of a porous media such as soil to permit fluid flow (typically water in most cases) Head (2011). The soil permeability coefficient (k_θ) is defined as the water flow rate (Q) at 20°C under laminar flow conditions, through a unit cross-sectional area (A) of the soil medium, under a unit hydraulic gradient (H), AS 1289.6.7.1 (2001). The coefficient of permeability (k_θ) are mostly in the order of 0.001 to 0.1m/s for granular soils such as sand and less than 10^{-8} m/s for soils containing clay, Towhata (2008). Mostly, in the soil laboratory, there are two common techniques for determining the coefficient of permeability (k_θ) of soils; namely the constant head permeability test (CHPT) and the falling head permeability test (FHPT) Head (2011). The k_θ of soils may be coupled as part of numerical soil model parameters to simulate the undrained soil behavior during flow liquefaction failures. The k_θ is considered part of the important soil parameters and it helps to further understand the physics of the generation of excess pore water pressure (EPWP) and water dissipation characteristics of soils. In general, the permeability coefficient is applicable for solving problems related to:

- (a) Soil yield behavior when in a saturated state
- (b) The stability analysis of earth dams and other forms of embankments such as slopes, water canals, etc.
- (c) Seepage problems in earth dams
- (d) Coupling a realistic numerical model for soil liquefaction scenarios
- (e) Settlement issues

The soil permeability coefficient k_θ depicts the drainage characteristics of the soil. Also, the k_θ is considered an essential soil property for describing the dilation, contraction, rate of soil consolidation, and compaction characteristics.

Firstly, the soil permeability testing process involves achieving a complete homogenous mix for all studied sand matrix soil specimens using an efficient mechanical mixer in the laboratory, shown previously in Figure 3.11. Based on the literature of permeability tests, the recommended and suitable testing technique for granular materials such as clean sands with no fines and gravel is the CHPT. The Australian Standards, AS 1289.6.7.1 (2001), applies to the CHPT regarding the clean sand (ECS00), ECS05, and ECS10, while the AS 1289.6.7.2 (2001) followed for the FHPT for some range of mixed clayey samples. Precisely, the FHPT worked out well during testing for sand matrix samples ranging between 15% to 30% percent by weight of the kaolinite clay (i.e., ECS15, ECS20, and ECS30). Identifying the type of test applicable to a specific soil sample was based on observations made during the laboratory work. In the CHPT, compacted air-dried ECS00, ECS05, and ECS10 specimens were achieved by the vibration table using standard test procedures while the method of compaction applies to ECS15, ECS20, and ECS30 during the FHPT. The typical permeability setup flow chart indicating the operation mechanisms is shown in Figure 3.15, while Figure 3.16 shows the pictorial test setup of the permeability device.

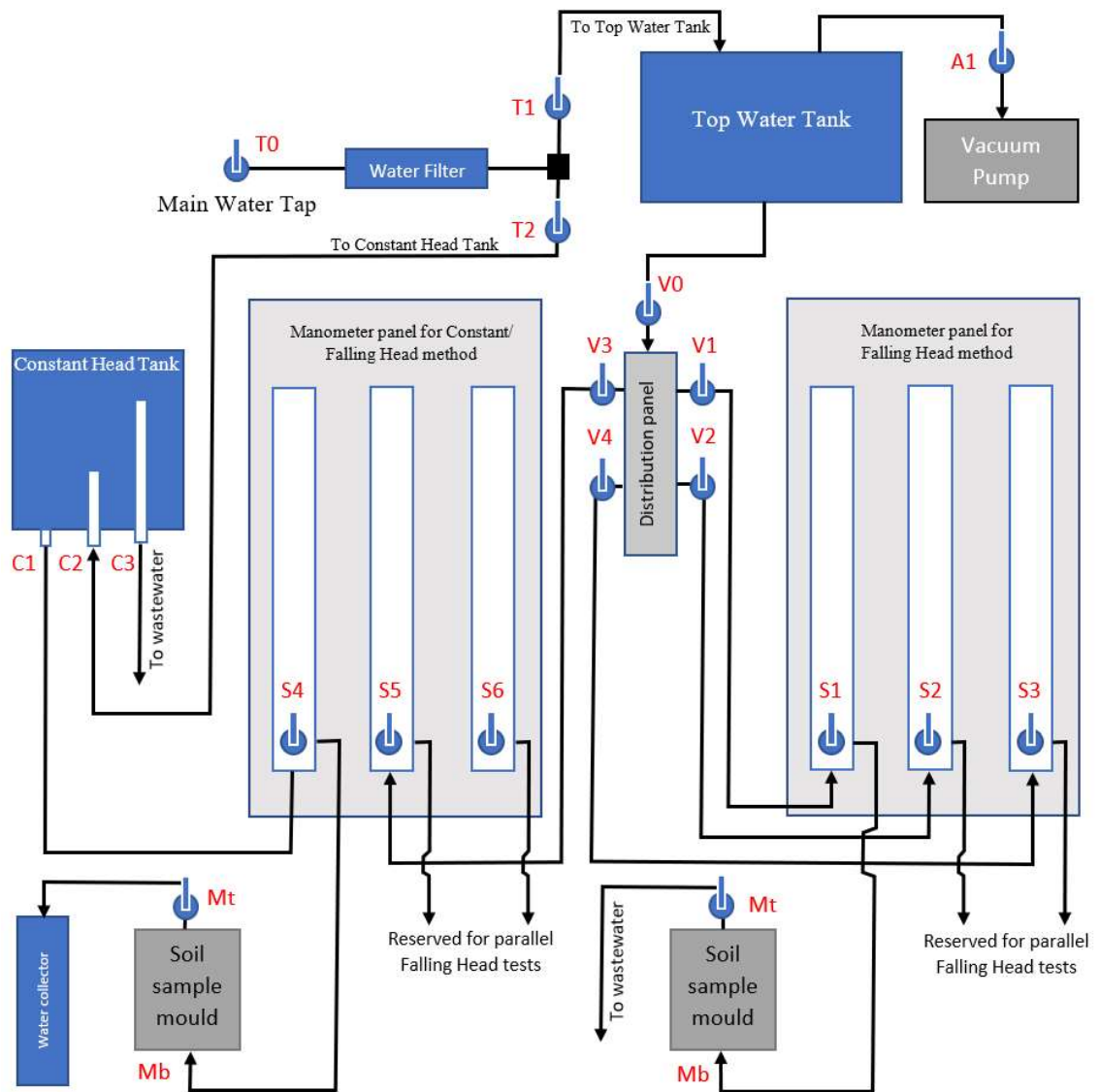
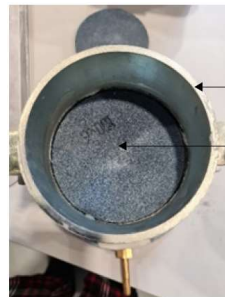


Figure 3.15. Flow chart of the utilized permeability device after Kalatehjari (2020)

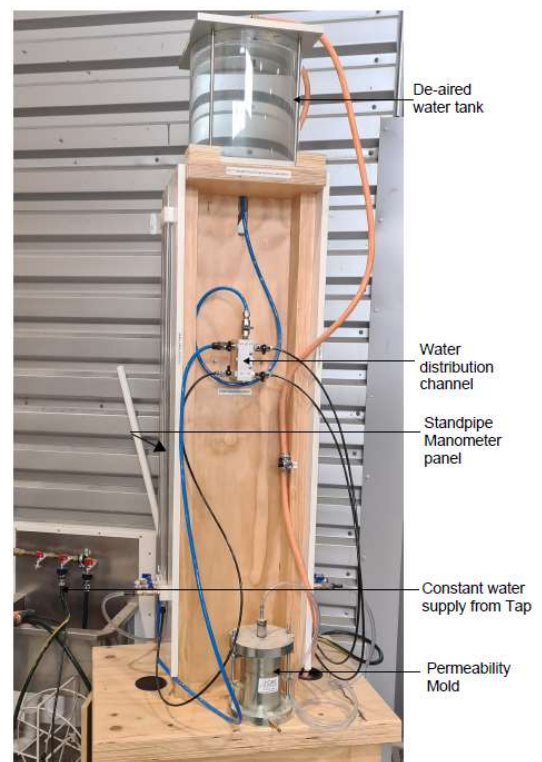


Digital Vernier Calipers for accurate measurements of dimensions



100mm diameter mold
Porous stone (paired top and bottom)

(a) The mold calibration process



(b) The pictorial test setup

Figure 3.16 The permeability test set up

Completely de-aired water produced with the aid of a vacuum pump was utilized throughout the permeability testing. The combined plot of the coefficients of permeability (k_T) m/s tested at 60, 120, 180, and 240 seconds for all samples is presented in Figure 3.17. The soil permeability test results datasheets are attached as Appendix H1 to H6. As expected from Figure 3.17, the ECS's permeability coefficient decreased as the percentage content by weight of the kaolinite increased within the sand voids.

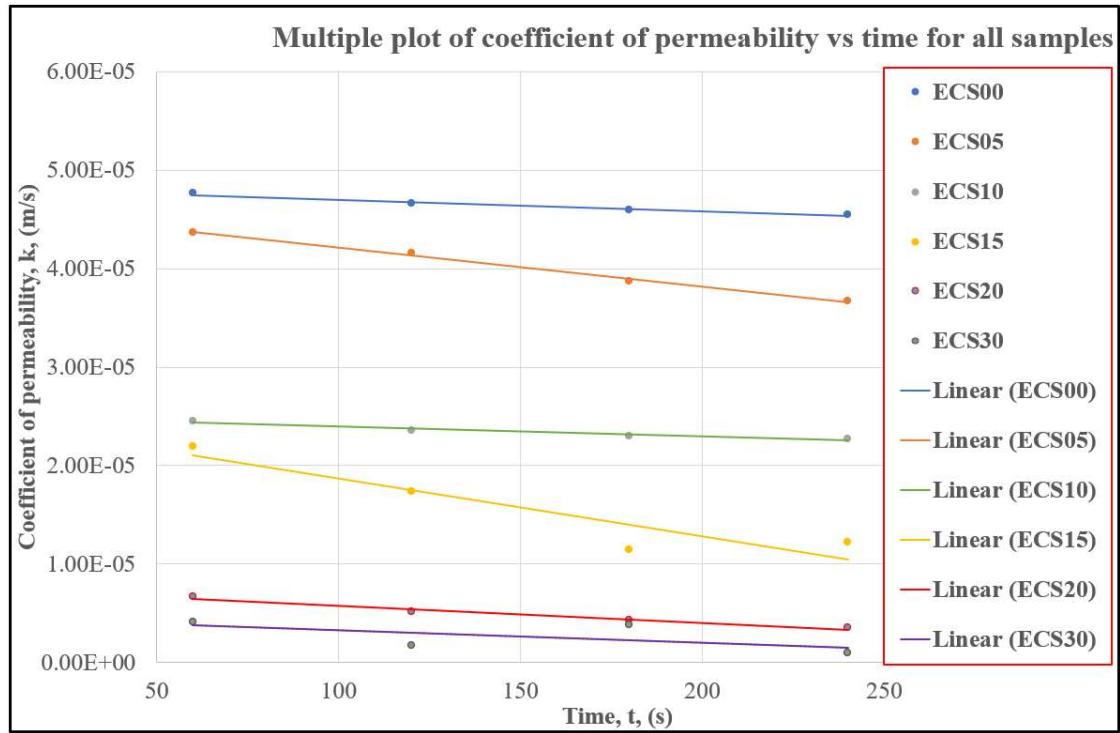


Figure 3.17 The permeability behavior of tested samples

The soil samples were tested at the laboratory density ratio (LDR) ranging from 0.80 to 0.97, and the void ratio ranging from 0.45 to 1.09. A minimum of three (3) No. tests were executed for each soil sample, while the average value of the coefficient of permeability was adopted as the final value.

3.5 The soil geomechanical strength characteristic tests

Brief details of the employed testing technique in evaluating the studied soil samples' geomechanical behavior (i.e., strength and deformation properties) and their corresponding PWP characteristics under the isotropic consolidation, drained (ICD), and undrained (ICU) triaxial compression (TC) loading conditions are presented herein. According to Jefferies and Been (2015), the TC is referred to as the standard reference test for the critical state determination of soils in geotechnical engineering practice. The free drainage of water from the soil pore volume during compression loading/shearing causes the rearrangement of the soil grains, and this mechanism is referred to as *drained*. On the contrary, when drainage is not permitted during shearing, the soils' response is referred to as *undrained* (Puebla, 1999).

Several low strain-controlled, undrained, and drained static compression tests were carried out to evaluate the soil's effective stresses and advanced geomechanical properties. In order to technically discuss the validated soil specimens within the critical state framework, their geomechanical properties, change in void ratios, stress-dilatancy (i.e., the occurring change in volume due to shearing), state dilatancy, and their critical state characteristics are all required. The above-required parameters are readily obtainable from high-quality monotonic compression triaxial tests. Tests were executed under the conventional monotonic compression static loading.

A breakdown of the testing schedule is divided into two categories: 1), Execute both drained and undrained tests on all the soil specimens to generate data for their experimental behavior and subsequent parametric discussions of trends as observed; 2), Execute numerical model calibration tests for subsequent data validation as necessary. The numerical modeling calibration tests are typical of three categories, namely undrained tests on loose samples, drained tests on loose samples, and drained tests on dense samples. The numerical model calibration set of tests requires certain technical specifications/details and as such, they are very expensive and complex. Hence due to the limited research budget/fund for this project, and the initially obtained results from the shake table physical modeling, only two from the total 5 soil samples were numerically validated. The validated soil specimens are the clean ECS00 with no plastic fines and a typical clayey sand matrix soil with 30% by weight of kaolinite content (ECS30). The validated samples will enable comparative discussions to be made on the effects of the kaolinite on the flow liquefaction behavior of the ECS.

The considered testing mean effective consolidation stress level ranged from 50 kPa to 500kPa with a combination of a range of targeted void ratios for accurate estimation of the soils' critical state parameters. Generally, all soils will experience their corresponding unique critical state at a certain range of critical void ratios and combinations of corresponding mean effective stresses, they would likely dilate when prepared slightly above the critical void ratios and when looser than the critical, they may exceed the critical state and consequent flow failure may be inevitable. Therefore, an equilibrium point or a balance has to be made to be able to achieve a reasonable critical state locus. The above can only be achieved under laboratory conditions by performing several trial tests to determine the best estimate of the CSL since the void ratios are highly sensitive to any slight change in corresponding densities. In reality, the earlier specified testing stress levels above are more practical for soils in routine geotechnical practices globally even though it is nearly impossible to replicate complete field conditions in the lab.

In the foregoing, the purpose of the undrained tests on loosely prepared soil specimens is to determine the critical state parameters, the goal of the drained shear tests on loosely prepared specimens is to determine some soil plasticity parameters, and support engineering judgment for the determination of the critical state locus (CSL), this is key to the accurate determination of the soil critical state parameters. Lastly, the significance of the executed drained tests on densely prepared specimens is to discern both the state and stress-dilatancy soil parameter which is usually difficult to decide based on executed tests on loose specimens alone. There are other numerous required key details for the numerical modeling calibration tests, some of them would be explained in later subsections of this chapter. For instance, the majority of these requirements are well explained in the critical state approach to soil liquefaction book by Jefferies and Been (2015), Jefferies and Shuttle (2020), Viana da Fonseca et al. (2021).

The utilized soil triaxial testing device in this study is the Alfa automated triaxial tester (T-333/A), manufactured by Alfa testing equipment, Turkey, and supplied by CMT, Australia. The device's available features include an incorporated state-of-the-art automated data capturing mechanism (sensors) and computer software for easy post-data processing. A schematic picture showing the major components of the device is shown in Figure 3.18. The description of the studied soil materials, already discussed in section 1.6.1 of Chapter 1, provided information on the source of studied soil samples, soil sample preparations, and sample naming/numbering nomenclature.

An overview of the test stages' breakdown, the soil sample preparation, saturation, consolidation, and the shearing stage, are summarized in the subsequent subsections. Mostly applicable triaxial testing standards are those of the American Society for Testing and Materials (ASTM) and British Standards (BS). Most of the procedural details specified in ASTM, such as D2850, D4767, and D7181-11, are very relevant and applicable to all test stages herein. Further comprehensive test procedures for the specifics of critical state testing of soils and the conventional procedures are available in typical references such as Viana da Fonseca et al. (2021), Jefferies and Shuttle (2020), Jefferies and Been (2015), Head (2014), Head (2011), Donaghe et al. (1988); Ehrgott (1971) etc.

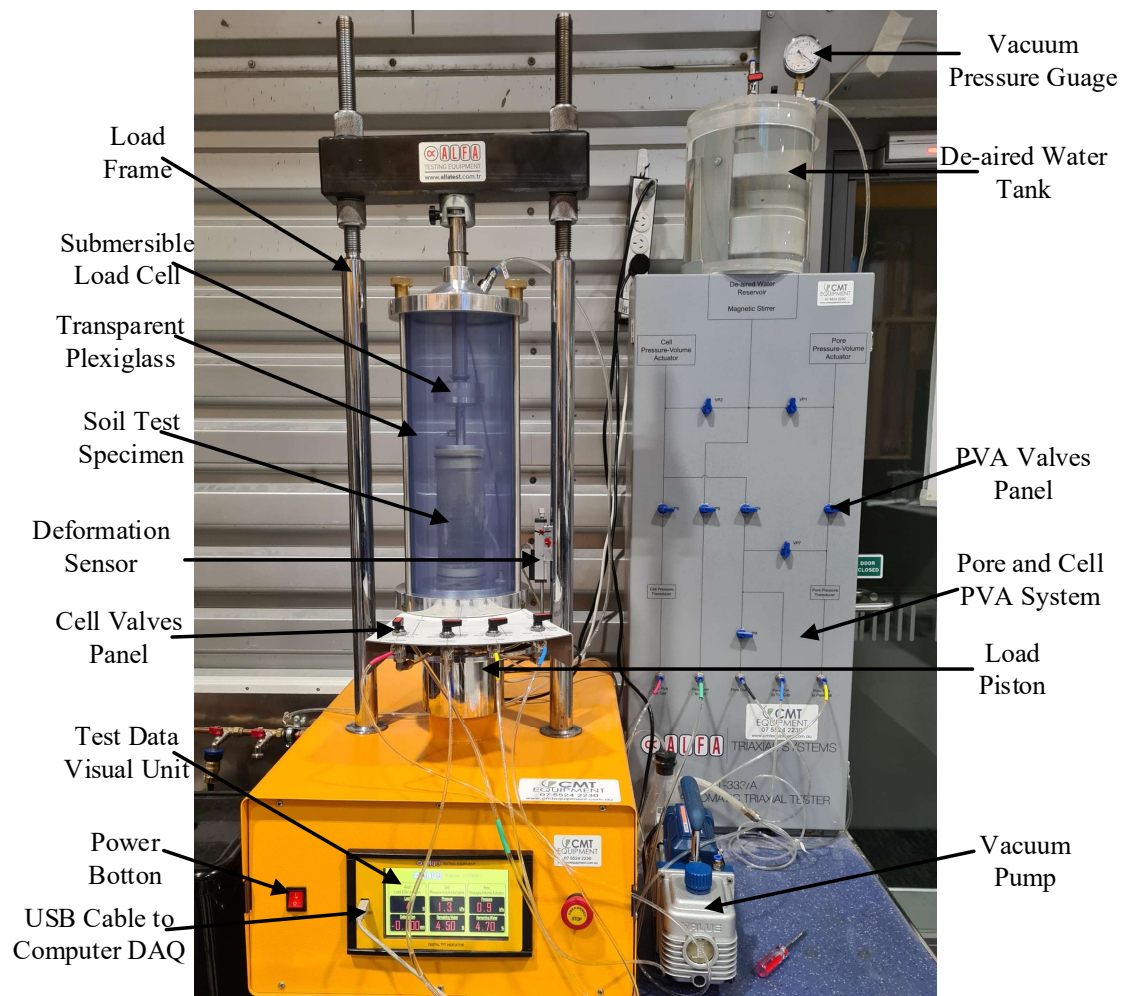


Figure 3.18 The Alfa triaxial machine

3.5.1 Soil sample preparation for monotonic triaxial compression tests

Previously executed systematic literature review of the effects of sample preparations on the effective shear strengths of soils showed the significance of taking some considerations before selecting a sample remolding method during triaxial testing. In this study, the moist tamping (MT) technique was the adopted sample reconstitution method for the triaxial specimens on the basis that several previous researchers e.g., (Jefferies & Been, 2015; Viana da Fonseca et al., 2021) recommended it for preparing predetermined/known sample void ratios, the segregation of fines from the sand particles are effectively circumvented, and overall, the MT method has been recommended for achieving loose specimens for ideal determination of the soil critical state parameters of soils.

Furthermore, contractive and loose soil specimens may easily be prepared with the MT preparation technique. Viana da Fonseca et al. (2021) recommended that dense samples may not reach a critical state due to the strain limit of the utilized triaxial device for testing. The creation of extremely loose soils sample is a key criterion for the soils to reach the critical state and well within the limits of the triaxial equipment. All the tested soil samples have an approximate cylindrical dimension of 70mm diameter and 140mm height making up a ratio of 2:1. Some initial test trials using the wet pluviation (WP) preparation technique for the clean sand (ECS00) yielded rather dilative responses in the ICU tests and previous studies, e.g., Viana da Fonseca et al. (2021) have confirmed similar observations in their paper.

It is a well-established fact that the adopted soil sample remolding method in triaxial tests often determines their resulting strength behavior (Been & Jefferies, 1985; Yimsiri & Soga, 2010). Several researchers (Been et al. (1991); e.g., Bouckovalas et al. (2011); Dafalias and Manzari (2004); Papadimitriou et al. (2005), and Chaudhary et al. (2002)) indicated the inherent difference in the stress-strain behavior/response of soils even when tested under similar initial conditions (i.e., same void ratio, relative density, confining stress, and same strain shearing rate). However, it has also been reported that the primary factor responsible for non-consistent/diverse shear strength responses experienced in tested reconstituted soil samples in the laboratory is the ‘soil initial fabric structure’ formed by the various reconstitution methods (Dafalias et al., 2004).

The most utilized methods for remolding soil samples in triaxial testing may be classified into three categories (i) Pluviation (raining of sand through air), (ii) Tamping (compaction), and (iii) Vibration methods. All the above methods have some variants, and they are best illustrated with adopted abbreviations in Table 3.6.

Table 3.6 Types of soil sample reconstitution techniques in triaxial testing

Pluviation	Tamping	Vibration
Air or Dry (AP)	Dry (DT)	Dry (DV)
Wet (WP)	Wet or Moist (MT)	Moist (MV)
Dry Deposition (DD)	Under-Compaction (UC)	
Mixed Dry Deposition (MDD)		
Slurry Deposition (SD)		

Vaid et al. (1999) suggested that the WP-prepared samples closely simulate the in-situ fluvial and hydraulic fill sand except for the high possibility of fines segregation. The reason for the above assertion is that particles with higher densities will settle in the water faster than those with less density. One key advantage of the SD method over other remolding methods is its ability to prevent fines segregation, which is prevalent with sands containing fines during soil sample reconstitution in the laboratory. The MT reconstitution technique is mostly applicable especially when it is required to derive the critical state properties and calibrate soil parameters for the application of some advanced critical state compatible numerical constitution models.

First, after previously oven-drying the sand (ECS), it is sieved with a sieve of size 75 μ m to remove any existing fines or impurities from it to be sure it is clean sand. The sieved ECS were then subsequently mixed with various percentages of kaolin to create other clayey sand samples (i.e., sand matrix or mixed soil specimens). The oven-drying process is primarily to facilitate handling. An electronic weighing scale was utilized in measuring the masses of the triaxial specimens during the pre-moisturizing and forming process while using a split mold/sample former to mold the soil samples. The volume of the mold used is known by measuring each soil specimen's height in at least 4 different positions. For instance, a 70mm diameter and 140mm height soil sample would have an equivalent volume of 538,783.14mm³.

Ideally, the soil specimens were first conditioned to known moisture contents, typically ranging from 5 to 12% water content before embarking on the tamping process and depending on the kaolinite content in sand mixtures. The reason for the variation of the soils' initial water content is that samples with more kaolinite (clay) experienced significant volume changes throughout their testing life cycle, especially during the saturation and consolidation stage, hence, not matching the initially prepared dimension. In addition, the clayey sand samples would experience a high magnitude of physical instability if not prepared under certain workable moisture contents and densities under laboratory conditions. Hence, there are wide variations between the achieved densities of clean sands (ECS00) when compared with clayey sand matrix soils (i.e., ECS10 to ECS30) as the clayey sands prepared tends to become denser because of the kaolinite particles occupied or shared within the void spaces inside the sand fabric structure. The experienced instability of looser samples of clayey sands is simply because the clay particles have a greater affinity for water and besides, the clay particles lubricate the void spaces in between the sand

particles. Hence, a great reduction of total sample volume is experienced, and the consequent usually experienced physical instability.

Before commencing tamping, soil samples were stored in plastic bags for a minimum of 7-days to ensure that their premixed target initial moisture content was well equilibrated before the start of experiments. The triaxial soil specimens were then prepared with pre-weighed soil masses and compacted in six to seven layers with about 13 to 15 tamps per layer to the target void ratios. Viana da Fonseca et al. (2021) suggested that the thickness of the tamped layers should not be more than 25mm, hence the thickness of each tamped layer herein was within the range of 2.0 to 2.5mm. The top of each tamped layer was scarified (i.e., scratched) before additions of overlying layers to ensure homogeneity and uniformity in the densities of specimens created, and also prevent segregation of soil layer by formed weak planes.

A typical example of reconstituted soil after preparation and ready for testing is shown in Figure 3.19. Even though it has been reported by previous researchers that there is a tendency for each layer to reach a unique CSL irrespective of the varied internal distribution of the void ratios, efforts are made to ensure that uniform samples are created. Also worthy of note is that samples were kept in plastic bags during the tamping process to prevent air drying and hence maintain the initial moisture content.

It is importance to lubricate the specimen endplates to minimize friction and mitigate shear banding otherwise known as strain localization, and this was achieved by applying a thin film of silicone grease on the formed specimen's top and bottom platens. The lubrication is necessary to reduce friction at the endplates and enhance a uniform stress field in the specimen (Wichtmann, 2005); other previous research workers (e.g., Jefferies & Been, 2015; Viana da Fonseca et al., 2021) even recommended using end platens that are wider than the specimen's initial diameters. Loosely prepared specimens do not experience friction and shear banding, but dense specimens do. The required parameters to measure during sample preparations typically include the samples' dimensions (diameter and height) at a minimum of 5 different positions, wet mass, dry mass, and initial moisture content. The Alfa Triaxial machine software automatically computes the other key pre-test soil parameters, and these include the soil samples' initial void ratio, area, volume, bulk density, dry density, degree of saturation, etc., after inputting the formerly estimated properties.

The complete MT procedural details are not repeated here as they are available in several other references (e.g., Carraro, 2004; Jefferies & Been, 2015; Viana da Fonseca et al., 2021). The relevant applicable equations during the soil sample preparation and other test processes are summarized in Equations 3.4 to 3.7



Figure 3.19 A typical triaxial soil specimen after preparation

Assuming a constant cylindrical shape of the soil specimen along its length, the initial cross-sectional area A_0 is:

$$A_0 = \frac{\pi \times D_0^2}{4} (cm^2) \quad 3.4$$

The parameter D_0 in Equation 3.4 is the initial diameter of the soil specimen measured with a vernier caliper. The relative volume of the soil specimen is expressed in Equation 3.5 as:

$$V_0 = A_0 \times h_0 (cm^3) \quad 3.5$$

The parameter h_0 is the initial measured height of the soil specimen. Once A_0 and V_0 are computed, the initial dry density is defined according to Equation 3.6 as:

$$\gamma_d = \frac{W_s}{V_0} (g/cm^3) \quad 3.6$$

Where W_s is the initial dry weight of the soil specimen. Next, the initial void ratio e_0 is computed from Equation 3.7 as:

$$e_0 = \frac{\gamma_s}{\gamma_d} - 1 \quad 3.7$$

Where, γ_s is the soils' specific grain unit weight in (g/cm^3) .

Recalling that the relative density of the soil specimen is obtainable from Equation 2.11. The triaxial tester automatically computes the changes in the soil specimen's volume (ΔV) and height (ΔH) after the saturation, consolidation, and shear stage. The triaxial software also considers the membrane correction factor, the area, and volume corrections immediately after the saturation stage. Input combo-boxes are available in the software interface to enter the properties of the utilized membrane (e.g., thickness, perimeter, modulus of elasticity, and stiffness value).

Estimating the change in void ratio during the saturation stage can be often problematic. Researchers mostly adopt the method suggested by Verdugo and Ishihara (1996) in resolving this issue by utilizing the direct relationship between moisture content and void ratio for saturated soils. Typically, from the former author's method, the volume change is measured at the end of the saturation stage to be able to compute the final void ratio (e_f) from Equation 3.8, similar to the work done by Marcosanti (2011).

$$e = \frac{(V_1 - V_0 + \omega_r \times W_d)}{W_d} \cdot G_s \quad 3.8$$

In Equation 3.8, the subscripts 1 and 0 indicates the final and initial values of the volume, ω_r is the soil specimen's remaining moisture content, W_d is the dry weight of the soil specimen after testing, and G_s is the soil specimen's specific gravity.

Several other methods exist for computing the post-consolidation void ratio which is utilized in combination with the mean effective stress at critical state in obtaining the CSL locus in the $e - \log p'$ stress-space. Another method of computing void ratio, e is expressed in Equation 3.9 in which, the volume of voids = V_v , the volume of solids = V_s , the mass of water = m_w , the density of water = ρ_w , the density of solid = ρ_s , the mass of solids = m_s , ASTM-D4767-11 (2011).

$$e = \frac{V_v}{V_s} = \frac{m_w}{\rho_w} \times \frac{\rho_s}{m_s} \quad 3.9$$

The procedures for estimating the post-test void ratio in the drained and undrained tests follow closely those described in the work by Verdugo and Ishihara (1996) as specified in Equation 3.8. The Verdugo and Ishihara (1996) method may be summarized as simply closing the drainage valves of the triaxial device after tests, applying a very high confining stress (usually to the maximum capacity of the device), at the same time applying axial load and squeezing out the excess water in the sample into a safe measurement chamber (e.g., burette). The remaining moisture content of the sample is then determined, and the post-consolidation void ratios are subsequently estimated based on the measured excess water in the burette and the remaining moisture content in the sample. The above procedure for void ratio determination has been reported by Verdugo and Ishihara (1996) as similar to those obtained by the well-known freezing method. It is usually considered more realistic and accurate to utilize the obtained final moisture contents after tests to estimate the post-consolidation void ratios rather than using specimen dimensions which may introduce errors since it is almost impossible to measure the specimen dimensions during saturation.

3.5.2 The saturation stage

For critical state soil testing, the complete saturation of the pores or voids in the soil specimens' volume space is an essential prerequisite in completely removing air from them. In other words, all the existing air in the soils' void spaces must be replaced by de-aired water. Further, a complete undrained condition cannot be assumed unless complete saturation is achieved and this is more significant under the undrained condition because the evolution of pore water pressures mainly depends on the stiffness of the pore fluid (Viana da Fonseca et al., 2021). A minute amount of the presence of air in the soil voids has been reported to have significant effects on the PWP and volume change measurements.

The Alfa triaxial machine houses a water tank that produces completely de-aired water with a vacuum pump and a magnetic water stirrer positioned inside the tank. The soil specimens' complete saturation enables accurate measurements of the soils' effective shear strength parameters, the consolidation characteristics, volume change during drained shearing, and the pore water pressure measurements during undrained shearing. In this work, complete saturation was facilitated by bubbling carbon dioxide (CO_2) through the sample after tamping at the rate of about 3 to 5 bubbles per second as suggested by Jefferies and Been (2015). The subsequent application of backpressure to the specimens allowed pore water pressure increments in a controlled manner to force the remaining air bubbles in the soil sample into the de-aired water solution at reasonable low pore water pressures of between 50kPa to 300kPa for the clean sand (ECS00) and other clayey sand samples. More details on other methods of saturation are well-detailed elsewhere e.g., Viana da Fonseca et al. (2021).

In the current work, the assumed target initial effective stress during saturation ranges between 10kPa and 20kPa, always maintaining a positive effective stress for all the executed monotonic compressive tests. The specimen's cell pressure and pore water pressure were simultaneously increased while maintaining a low target effective stress as specified above ASTM-D4767-11 (2011) during the saturation process/stage. The reason for the choice of low target effective stress of 10kPa is not to induce further internal densification of the soil volume since the looseness of the prepared soil specimens needs to be maintained.

The complete and full-saturation of all tested soil specimens were confirmed with Skempton's B-value parameter-check expressed in Equation 3.10. According to ASTM-D4767-11 (2011), saturation is commonly assumed to be complete when the B-value greater than or equal to 0.95 is achieved but the adopted minimum B-value in this work is 0.98. The B-value is easily computed from the plot of applied pressures (pore water pressures or backpressures) on the ordinate against the cell pressures on the abscissa. The B-Value check was automatically computed, checked, and displayed at intervals of 5minutes by the triaxial software. In most cases, a B-value of about 1.0 was achieved. The next phase of the test, which is the consolidation stage, is initiated automatically by the computer software once the minimum Boolean for the set B-value (0.98)

check above is true and no further increase of the B-value has been observed in the plot of the B-value versus pore water pressure (kPa).

$$B = \frac{\Delta u}{\Delta \sigma_3} = \frac{u_i - u_0}{\Delta \sigma_3} \geq 0.98 \text{ to } 1.0 \quad 3.10$$

Where Δu is the change in pore water pressure, u_0 is the initial pore water pressure, u_i is the measured pore water pressure at any B-value check time, and $\Delta \sigma_3$ is the change in cell pressure.

3.5.3 The consolidation stage

The consolidation phase of the tested soil specimens is required to determine the time needed to complete the 100% consolidation process i.e., t_{100} . The above is required for computing the appropriate strain rates for the subsequent shearing stages. The implemented consolidation procedure follows the steps specified in ASTM-D4767-11 (2011) and the procedural methods found in Head (2014, pp. 222-223). In the triaxial software tools' option, an initial piston touching force of 5N was preset to automatically place the axial loading piston in contact with the specimen's top cap after the saturation stage. The device's piston rod stops moving once this magnitude of the force (i.e., 5N) is achieved/detected in the software. This feature ensures that no axial loads more than 0.5% of the estimated axial load at failure are possibly applied on the soil specimens at the initial stage.

Typically, the undrained tests were consolidated to constant, all-around, effective confining isotropic consolidation stress levels of 50kPa, 100kPa, 200kPa, 300kPa, 500kPa as required. In some cases, tests were performed to higher confining stress to study the effects of confining stress on the stress paths. The drained shear tests were mostly executed at 100kPa, 200kPa, and 400kPa initial consolidation/confining stresses for all tested samples. Jefferies and Been (2015) recommended obtaining data from very low to high-stress testing levels to enable the estimation of the state parameter (ψ) and critical state void ratios (e_{cs}) determined.

Applying the analogy of the one-dimensional consolidation tests, in the $v - \ln p$ space of the consolidation process, the slope of the virgin consolidation line (i.e., the normal compression line's slope) known as lambda (λ), and the slope of the swelling lines (also known as the unloading-reloading line's slope) often represented by kappa (κ) are useful soil's critical state parameters mostly utilized in the conventional CamClay models. The equations defining the lines named above are stated in Equations 3.11 & 3.12.

For the normal compression:

$$v = N - \lambda \ln(-p) \quad 3.11$$

For the swelling line or unloading-reloading:

$$v = v_s - \kappa \ln(-p) \quad 3.12$$

Where N is the corresponding specific volume at unit pressure (dependent on units of measurements), v_s is the relative specific volume to the swelling line (depends on the soil's loading history) as shown schematically in Figure 3.20.

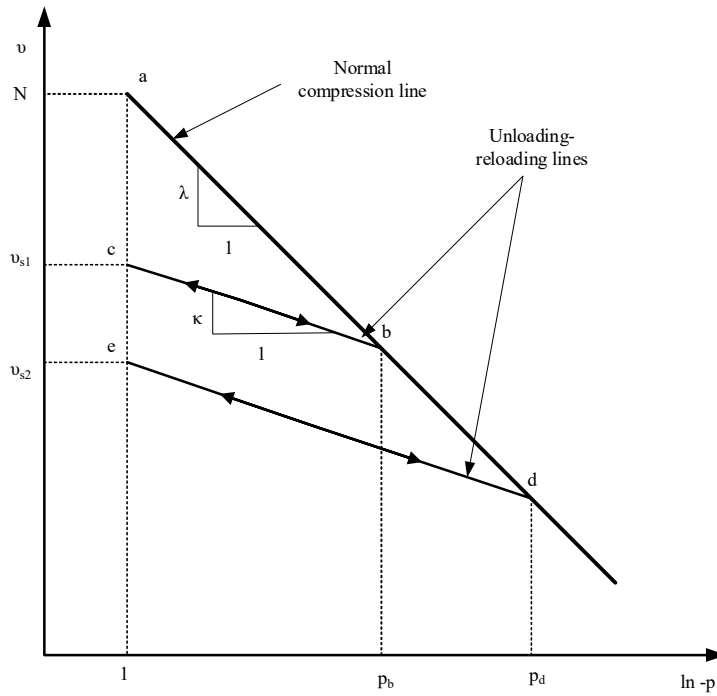


Figure 3.20 Schematics of soil behavior during compression and unloading in consolidation

The majority of the advanced critical state-compatible constitutive liquefaction soil models formulate the soil's hardening behavior based on elasticity's theoretical assumptions and the normal compression line. The soils' elastoplasticity characteristics usually are obtained from the swelling or unloading-reloading lines. However, no unload-reload loop was done under the triaxial condition to avoid complexities since maintaining the simplicity of the overall test procedure was necessary herein. The one-dimensional (1D) consolidation/oedometer test was carried out separately to study the consolidation characteristics of the studied soil specimens and its methodology are detailed in subsection 3.5.6. Other alternatives of deriving the critical state parameters from isotropically consolidated triaxial compression tests are available elsewhere such as Jefferies and Been (2015) and same is applied herein.

The derivation of time to failure of the soil specimens is commonly obtainable from the volume change plotted against the square root time. The computation of the appropriate strain rate for each soil sample followed closely the procedure found in Head (2014, pp. 225-227). Summarily, the first procedure is to plot the graph of volume change on the abscissa against the square root of time on the ordinate to derive the time required for 100% consolidation (i.e., t_{100}).

Secondly, the needed time to failure is calculated based on the factors summarized in Table 3.7 for a no use of side drains with filter paper during consolidation.

Table 3.7 Computation factors for failure time estimates

Test type	No use of side drain
ICU	$0.53 \times t_{100}$
ICD	$8.5 \times t_{100}$

Finally, the shearing strain rate is computed from Equation 3.13 as per Head (2014) as:

$$\frac{\varepsilon_f \times L}{100t_f} \quad 3.13$$

Where ε_f the assumed failure strain (typically 15%), L sample length, t_f the computed time to failure as summarized in Table 3-6 and the axial compression of samples correlating with $\varepsilon_f\%$ strain is $\frac{\varepsilon_f(\%)}{100} \times L$

The typical derived and applicable strain rates in all ICU and ICD tests are summarized in Table 3.8. It is well known that the consequence of an appropriate strain rate may not be critical in ICU tests, but it is in the ICD tests as excess PWP must not be generated during shearing.

Table 3.8 The applicable strain rates in the executed ICU and ICD tests

Sample Name	ICU Strain Rate (%/min)	ICD Strain Rate (%/min)
ECS00	0.2	0.01
ECS10	0.25	0.01
ECS15	0.02	0.08
ECS20	0.2	0.025
ECS30	0.1	0.01

3.5.4 The monotonic compression shearing stage

The monotonic compression shearing aimed at determining critical state parameters was achieved by axially loading the soil specimens until failure. Undrained tests on loosely prepared soil specimens would typically reach their corresponding critical state at axial strains less than 10% (Jefferies & Been, 2015). Shearing is initiated after completing the specified initial isotropic mean consolidation stress for a particular test. The computed and applied axial deformation's rate is tabulated in Table 3.8. The selected rate of the shearing shows to provide high-quality overall test results/outputs. Some tests ended at low strains typically between 2% to 5% axial strains once a flow failure is detected or the critical state is reached during the ICU testing. The condition to terminate tests is also based on the observed trend of the stress-strain graphs and maximum deviator stress achieved before the former starts to drop, and the eventual constant rate of deformation is evident during testing. As a result of physical instability, some soil samples did not reach the initial specified maximum strain levels before failure. In the conventional triaxial

testing techniques, a combination of the plots of shear stresses versus normal stresses for a minimum of three tests would normally produce the well-known shear envelope (Mohr circles) for a particular test sample and may subsequently be utilized in deriving their respective effective shear strength parameters (i.e., the angle of shearing resistance (Φ') and effective cohesion (c')). Other methods of deriving the shear strength parameters from stress paths plots are available in the literature.

Furthermore, in conventional triaxial testing, the test failure criteria may include (a) the total strain in the test sample hits 15%, and there is an evident drop in the deviator stress (b) the deviator stress descends by 20% after attaining the principal stress peak, and (c) the axial strain gets to 35% since the test started or the slope reaches 0% (Alyousif, 2015). Furthermore, a typical failure criterion may also be assumed when the stress ratio $[(\sigma'_1)/(\sigma'_3)]$ gets to peak value (Head, 2014). The stress ratio may also be adopted as an applicable proxy for determining when to decide to end the shearing stage of all tests.

The work according to Lade and Yamamuro (2011) reported three kinds of instabilities experienced in triaxial tests, namely (a) shear banding (b) smooth peak failure, and (c) instability inside the failure surface. The shear band mode of failure is mostly experienced with dense samples. However, the observed mode of physical failure for the majority of the tested soil samples herein is sideways bulging since most of the tested soil samples were loose. The pictures in Figure 3.21 provide typical examples of the physically observed failure modes for the tested specimens.



(a) Bulging failure (loosely prepared specimens)



(b) Shear banding (densely prepared specimens)

Figure 3.21 Examples of experienced physical failures of soil specimens after shearing

During undrained loading, the soil specimen's volume is assumed constant since pore water drainage is not allowed from the sample. Hence, there is no volume change and void ratios may be assumed constant. Hence, the $e - \log p'$ plot is a straight line that moves from left to right towards the critical state line. However, in the practical sense, some elements of change in void

ratio must occur during the initial test stage such as passing water from below sample, saturation, and during the consolidation phase. The above is the reason for utilizing the estimated post-consolidation void ratios with the corresponding mean effective stress at critical state in determining the state line.

The applicable compression load is slow enough (i.e., low to very low strain, ranging from 0.1%/min to 0.01%/min, respectively) to ensure the generated pore pressure's equilibration in the entire specimen's mass. The employed procedural shearing process followed closely the ones found in Head (2014, pp. 226-227), and are summarized as follows:

- 1) The shearing rate computation is typically derived from the consolidation graph or computing the shearing time for about 15% axial deformation.
- 2) The initiation of compression shearing and the required data for plotting against strain (%) were computed as the test proceeds while applying the applicable corrections. For instance, the stress invariants which include deviator stresses (kPa) and the mean effective stress, pore pressures (kPa), principal stress ratios $(\sigma'_1)/(\sigma'_3)$ e.t.c. Data for creating the stress path plot of q against p' are summarized in Equations 3.14 and 3.15 according to the Cambridge notation of stresses.

$$q = (\sigma'_1 - \sigma'_3) \quad 3.14$$

$$p' = \frac{(\sigma'_1 + 2\sigma'_3)}{3} \quad 3.15$$

- 3) The next stage is unloading, dismantling, and determining the final soil specimen's moisture content and void ratios after completing the shearing stage. There is an existing tab on the triaxial software for ending tests and these include the application of -50kPa to specimen, taking cell pressure down to zero, and initializing load piston. Following the above test instructions for ending tests will ensure no mess of the specimens were created during the process of specimen removal for moisture content determination, the above procedure was not applied herein though because after squeezing the excess water from the soil specimen, a negative PWP is already created in the soil sample and the soil specimens could be removed/retrieved for the subsequent moisture content determination easily. The evacuated soils specimens remain intact for moisture content determination and observations. There is no freezing facility in the AUT geotechnical lab which would have been the preferred method of determining the soil specimen moisture contents after testing for the subsequent determination of the corresponding post-consolidation void ratios. Hence, the previously explained method of void ratio determination as per Verdugo and Ishihara (1996) remained applicable.

3.5.5 The triaxial experimental result calculations and plotting formula

The real-time plots (graphs) were monitored on the computer software during testing and after testing, raw data were exported from the triaxial software data acquisition (DAQ) in typical .csv-

excel file format for further post-process and analysis. The results of the undrained behaviors of all the studied samples are comprehensively discussed in Chapter 4. In addition, a hybrid of analytical methods such as the critical state framework and numerical analyses are utilized to validate the result of typical clean sand and a clayey sand soil samples (i.e., ECS00 and ECS30). Equations 3.16 to 3.22 summarize the breakdown of other useful equations for deriving some key soil parameters as found in a typical reference such as Rees (2010).

The volume of the soil sample, V (After full saturation)

$$V = V_s + V_v = \frac{m_s}{\rho_s} + \frac{m_v}{\rho_v} \quad 3.16$$

Where, V_s is the volume of solid, V_v is the volume of the void, m_s and m_v are the masses of solids and voids respectively, and ρ_s and ρ_v are the densities of solids and voids.

Axial Strain, ε_a in which the specimen's initial height is h_0 , and the Δh is the axial displacement with a positive value indicating compression and a negative value signifying extension:

$$\varepsilon_a = \frac{\Delta h}{h_0} \quad 3.17$$

Corrected specimen Area, A_c - accounts for the average specimen area due to changes in specimens' dimensions.

$$A_c = \frac{V}{h_0(1 - \varepsilon_a)} \quad 3.18$$

The deviator stress, q - In which F is the applied axial force/load.

$$q = \frac{F}{A_e} = \sigma_1 - \sigma_3 \quad 3.19$$

The mean effective stress, p' - In which σ_3 is the cell pressure, u is the pore water pressure.

$$p' = \frac{1}{3}(q + 2\sigma_3) - u \quad 3.20$$

The static stress ratio, η - In which σ_1' and σ_3' are the major principal effective stresses.

$$\eta = \frac{\sigma_1'}{\sigma_3'} = \frac{q}{p'} \quad 3.21$$

The volumetric strain, ε_v - In which ΔV is the soil specimen change in volume and V_0 is its initial/original volume.

$$\varepsilon_v = \frac{\Delta V}{V_0} \quad 3.22$$

The procedures for estimating the post-consolidation void ratios have already been explained under section 3.5.1. Tables 3.9 and 3.10 summarize some crucial test information on both the executed undrained and drained monotonic tests that were used in discussing the experimental

results. Tables 3.11 and 3.12 summarize the information of tests executed for numerical model calibration and data validation purposes, respectively. e_0 is the initial void ratio, e is the estimated post-consolidation void ratio as per the Verdugo and Ishihara (1996) method, σ_3 is the radial effective consolidation stress in kPa, γ_d is the dry density in (g/cm^3), γ_0 is the initial unit weight in (g/cm^3), w_i is the initial moisture content in %, w_f is the final moisture content after tests in %, and B-Value is the Skempton parameter for confirming saturation. As can be seen in Tables 3.9 to 3.10, it makes sense to see that the void ratios decrease with an increase in testing mean effective stress levels because there would be reductions in the soil volume as its effective confining pressure increases.

Table 3.9 Summary of some initial soil parameters in the undrained monotonic tests (ICU) – Experimental evidence

Sample Name	σ_3 (kPa)	w_i (%)	w_f (%)	γ_0 (g/cm^3)	γ_d (g/cm^3)	e_0	e	B-Value
ECS00	50	5.00	31.27	1.330	1.269	1.049	0.813	1.00
ECS00	100	5.00	29.54	1.405	1.338	0.943	0.776	0.98
ECS00	200	5.00	26.31	1.436	1.368	0.901	0.683	1.00
ECS10	50	4.88	22.50	1.523	1.450	0.800	0.675	0.98
ECS10	100	5.00	25.29	1.527	1.454	0.795	0.657	0.98
ECS10	200	4.88	24.87	1.563	1.490	0.752	0.646	0.98
ECS15	50	8.36	24.78	1.597	1.474	0.716	0.644	1.00
ECS15	100	8.36	25.12	1.651	1.524	0.660	0.628	1.00
ECS15	200	8.36	25.04	1.633	1.507	0.679	0.610	1.00
ECS20	50	10.18	24.45	1.757	1.595	0.624	0.635	1.00
ECS20	100	10.10	22.40	1.778	1.614	0.605	0.570	1.00
ECS20	200	10.00	21.62	1.755	1.593	0.626	0.562	0.99
ECS30	50	7.32	26.60	1.633	1.522	0.820	0.691	1.00
ECS30	100	7.32	24.20	1.638	1.526	0.678	0.629	1.00
ECS30	200	10.00	20.47	1.536	1.396	0.834	0.524	0.99

Table 3.10 Summary of some initial soil parameters in the drained monotonic tests (ICD) – Experimental evidence

Sample Name	σ_3 (kPa)	Initial MC (%)	Final MC (%)	γ_0 (g/cm^3)	γ_d (g/cm^3)	e_0	e	B-Value
ECS00	100	5.00	28.59	1.441	1.372	0.895	0.743	1.00
ECS00	200	5.00	27.29	1.478	1.414	0.839	0.709	0.98
ECS00	400	5.00	25.24	1.466	1.396	0.862	0.656	0.98
ECS10	100	4.87	24.86	1.520	1.470	0.776	0.646	0.98
ECS10	200	6.00	26.88	1.511	1.425	0.832	0.698	0.98
ECS10	400	6.00	26.26	1.524	1.438	0.815	0.682	0.98
ECS15	100	11.70	23.99	1.762	1.577	0.604	0.623	0.99
ECS15	200	9.06	23.87	1.692	1.551	0.631	0.620	0.99
ECS15	400	8.36	23.49	1.606	1.482	0.707	0.610	1.00
ECS20	100	10.18	21.92	1.750	1.588	0.631	0.569	1.00
ECS20	200	10.18	21.30	1.744	1.583	0.636	0.553	1.00
ECS20	400	10.18	20.58	1.635	1.484	0.745	0.535	1.00
ECS30	100	7.32	24.57	1.631	1.520	0.664	0.638	1.00
ECS30	200	7.10	24.07	1.663	1.550	0.652	0.625	1.00
ECS30	400	7.30	22.99	1.545	1.440	0.778	0.597	1.00

Table 3.11 Summary of some initial soil parameters in the undrained monotonic tests (ICU) – Numerical model calibration purpose

Sample Name	σ_3 (kPa)	w_i (%)	w_f (%)	γ_0 (g/cm ³)	γ_d (g/cm ³)	e_0	e	B-Value
ECS00	50	6.00	36.08	1.403	1.324	0.964	0.938	1.00
ECS00	100	6.00	34.97	1.359	1.282	1.028	0.910	0.98
ECS00	200	6.00	35.63	1.371	1.293	1.011	0.840	1.00
ECS00	300	6.00	35.43	1.387	1.308	0.988	0.700	0.98
ECS30	50	10.00	21.42	1.633	1.522	0.820	0.548	1.00
ECS30	100	10.00	21.67	1.606	1.460	0.753	0.555	1.00
ECS30	200	10.00	20.47	1.536	1.396	0.834	0.524	0.99
ECS30	500	10.00	19.95	1.615	1.468	0.744	0.511	1.00

Table 3.12 Summary soil parameters in the drained monotonic tests (ICU) – Numerical model calibration purpose

Sample Name	σ_3 (kPa)	w_i (%)	w_f (%)	γ_0 (g/cm ³)	γ_d (g/cm ³)	e_0	e	B-Value
ECS00	50	6.00	29.83	1.578	1.489	0.746	0.775	1.00
ECS00	80	6.00	29.34	1.581	1.492	0.743	0.763	1.00
ECS00	100	6.00	29.68	1.405	1.325	0.752	0.771	1.00
ECS00_2	100	6.00	33.43	1.573	1.484	0.962	0.869	0.99
ECS00	300	6.00	30.98	1.423	1.342	0.937	0.806	1.00
ECS00	600	6.00	31.88	1.371	1.293	1.011	0.828	1.00
ECS30	80	9.00	16.59	1.880	1.725	0.409	0.467	1.00
ECS30	100	11.00	15.97	2.088	1.881	0.361	0.435	0.98
ECS30_2	100	11.00	15.84	1.870	1.645	0.664	0.538	1.00
ECS30_3	100	11.00	15.99	1.653	1.489	0.719	0.466	1.00
ECS30	200	11.00	16.07	1.663	1.550	0.728	0.445	1.00
ECS30	300	11.00	15.91	1.684	1.517	0.688	0.429	1.00
ECS30	400	7.32	15.90	1.545	1.440	0.778	0.495	1.00
ECS30	600	11.00	16.06	1.711	1.541	0.661	0.422	0.98

3.5.6 One-dimensional consolidation (oedometer) experiment

The 1D consolidation characteristics of the studied soils specimens (ECS00, ECS10, ECS15, ECS20, and ECS30) were investigated using a modified, calibrated, and automated conventional oedometer apparatus to facilitate an efficient and accurate data acquisition system, thereby ensuring the elimination of errors in test data records. The implemented automation follows a typical similar work as found in Gonçalves et al. (2017) by installing Linear Variable Differential Transformer (LVDT) sensors in place of the manual dial gauge for capturing the ensuing soil deformation/displacements inside the oedometer rings. A data acquisition (DAQ) system was designed and written with the National Instrument's LabView software program while utilizing a 16-bit data acquisition card. The pictorial setup of the system is shown in Figure 3.22.



Figure 3.22 The automated manual oedometer test setup

The above concept is particularly useful when a fully automated strain or stress-controlled oedometer device is not available in the geotechnical laboratory. The applicable test procedures follow closely those detailed in ASTM-D2435/D2435M (2011). It was ensured that water remains in the oedometer chamber throughout testing. The loading, unloading, and reloading test program are detailed in Table 3.13. Typically, data were captured for a 24h period within the intervals of 0s., 10s, 20s., 30s, 40s, 50s, 60s, 1min, 2min, 4min, 8min, 15min, 30min, 1h, 2h, 4h, 8h, 16h, and 24h, respectively for all the studied soil samples and each of the loads/stresses as detailed in Table 3.13.

Table 3.13 Consolidation test loading schedule for each soil sample

S/N.	Total Stress (kPa)	Equivalent mass (g) due to 10% Mechanical Advantage
1	15	300
2	25	500
3	50	1000
4	100	2000
5	200	4000
6	400	8000
7	800	16000
8	200	4000
9	400	8000
10	800	16000
11	1600	32000

The initial soil sample dimensions were approximately made of 50mm in diameter and about 20mm in height. Drainage was a two-way system at both the top and bottom of the specimens which were carefully guided by filter papers and porous stones. Soil samples were simply prepared into the oedometer ring by casting conditioned soil specimens to about 10% moisture contents. Typical results of the one-dimensional characteristics of the studied soil specimens are attached as Appendix I1 to I5 for ECS00, ECS10, ECS15, ECS20, and ECS30, respectively.

The usual reason for performing one-dimensional consolidation tests is mostly to determine the pre-consolidation stress (p_c), estimate the soil's compression index (C_c), and swelling index (C_s). The key reason for executing the oedometer tests herein is primarily to provide an estimate of the compression and swelling indices of the studied specimens. The compression index (C_c) otherwise known as kappa in the conventional CamClay numerical models, is the slope of the normal compression line (NCL) during loading and when plotted in the void ratio vs log of effective mean stress space ($e - \log P$). On the other hand, the swelling index (C_s) also known as lambda, is the slope of the unload-reload line. The breakdown of the above concept has earlier been summarized under section 3.5.3. The computed compression and swelling indices of the specimen are reported in Table 3.14.

Table 3.14 Estimated compression and swelling indices of the studied soil samples

Sample Name	Compression Index (C_c)	Swelling Index (C_s)
ECS00	0.000235	0.000059
ECS10	0.000100	0.000330
ECS15	0.000140	0.000320
ECS20	0.000069	0.001980
ECS30	0.000030	0.000390

The combined plot of the loading-unloading loop was not done because of the wide differences in the computed void ratios of the studied specimens. As a result of the addition of kaolinite to the sand, a wide range of void ratios results. The oedometer tests results suggest that the increase in the kaolinite-clay contents in the sand would increase the compression and swelling of the latter. The reported low values further indicate that the utilized kaolinite in the study was of low plasticity and would not make the sand behave in an unstable manner if existing under foundation loading.

3.6 The application of the Norsand advanced constitutive model for numerical soil modeling

According to the derived summary of some key features of some studied/reviewed advanced liquefaction constitutive models, as detailed in Table 2.3 of the executed critical literature review, the Norsand model was selected to validate two soil samples, first the clean sand (ECS00) and secondly, a typical clayey sand sample (ECS30) under the triaxial monotonic compression conditions. The reason for validating only two samples out of the studied five soil samples has

been stated earlier as limited budget and the requirements of several tests for calibrating the numerical models.

The Norsand is an advanced, critical state-compatible, and stress-dependent geomechanical numerical model (Been & Jefferies, 2004; Itasca, 2021; Jefferies & Been, 2015). Elaborate details of the model can be found in Jefferies and Been (2015) textbook on “Soil liquefaction: A critical state approach”, and only a quick breakdown/summary is provided herein. The model may be pictured/visualized as an improved and advanced CamClay model. It incorporated two major postulates of the CamClay model, namely: 1) the existence of a critical state (CS) and 2) the tendency of the soil behavior towards a critical state with rising shear deformation. A recent and additional established third postulate was the softening of the yield surface due to the principal stress rotation (PSR) (Jefferies et al., 2015) and this is only applicable to situations under cyclic loading. The motivation to utilize the Norsand model for simulating and validating the characteristic behavior of the studied samples was found in Jefferies et al. (2015, p. 74) where it was stated that “there is no reason for not applying the model in simulating clayey soil despite its current name, Norsand”. In addition, based on the critical review as summarized in Table 2.3, the Norsand model’s adoption was inherently visible for validating the soil’s critical state characteristic response in the current study.

3.6.1 Summary of Norsand model

The major frameworks that were incorporated in its formulation, as found in Itasca (2021), are enumerated in the equations below:

1. The theory of elasticity

The presumed elasticity depends on the shear modulus of the form expressed in Equation (3.23)

$$G = G_{ref} \left(\frac{p}{p_{ref}} \right)^m \quad 3.23$$

Where, p is the present mean stress, and G_{ref} and m are material property constants. A logical and acceptable recommended range of m is $0 \leq m \leq 1$. The reference atmospheric pressure, p_{ref} , is usually adopted with a value of 100kPa.

2. The critical state

A major requirement for the critical state is that $D^p = 0$; $\dot{D}^p / \dot{e}_q^p = 0$, where the stress dilatancy

D^p represented as $D^p = \frac{\dot{e}_v^p}{\dot{e}_q^p}$; where \dot{e}_v^p and \dot{e}_q^p denotes the respective plastic volumetric and deviatoric strain.

In the model, the critical state line expressed and fitted by Equation 3.24 is defined by the obtained semi-logarithmic straight-line idealization of the void ratio against the mean effective stress ($e - \log p'$ plot).

$$e_c(p) = \Gamma - \lambda \ln\left(\frac{100p}{p_{ref}}\right) \quad 3.24$$

Where Γ and λ are material property constants.

Alternatively, the critical state void ratio, e_c , may be represented by a three-parameter power idealization expressed in Equation 3.25, where C_1 , C_2 , and C_3 are soil material property constants.

$$e_c(p) = C_1 - C_2 \left(\frac{p}{p_{ref}}\right)^{C_3} \quad 3.25$$

3. The state parameter

The state parameter is simply explained as the variance between the present void ratio (e) that of the critical state void ratio (e_c). The state parameter is logically represented in the form shown in Equation 3.26 and is responsible for establishing the initial state of the soils in terms of void ratio or relative density:

$$\psi = e - e_c(p) \quad 3.26$$

4. The failure yield surface

The adopted outer yield in the Norsand model is similar to the bullet-shaped of that of the conventional CamClay model, expressed in Equation 3.27 as:

$$\frac{\eta}{M_i} = 1 - \ln\left(\frac{p}{P_i}\right) \quad 3.27$$

Where p_i , known as image stress, determining the magnitude of the outer yield, $\eta = \frac{q}{p}$, $q = \sqrt{3J_2}$, J_2 is the second invariant of the deviator, and M_i is expressed in Equation 3.28:

$$M_i = M \left(1 - \frac{N_{\chi i} |\psi_i|}{M_{tc}}\right) \quad 3.28$$

Where M_{tc} denotes a strength parameter corresponding to q/p' at critical state in the compressive triaxial (TC) condition, N a material constant is known as volumetric coupling coefficient, M the friction ratio at critical state with an account of the Lode's angle (θ) influence. Equation 3.29 shows this effect.

$$M = M_{tc} - \frac{M_{tc}^2}{3 + M_{tc}} \cos\left(\frac{3\theta}{2} + \frac{\pi}{4}\right) \quad 3.29$$

The derived parameter M_i for triaxial compression and extension are shown in Equation 3.30 and (3.31), respectively:

$$M_{i,tc} = M_{tc} - N_{\chi i} |\psi_i|, \text{ at } \theta = \pi/6 \quad 3.30$$

$$M_{i,tc} = M_{i,tc} - \frac{3M_{tc}}{3+M_{tc}}, \text{ at } \theta = -\pi/6 \quad 3.31$$

Where χ_i a stress/state dilatancy parameter may be approximated according to equation (3.32):

$$\chi_i = \frac{M_{tc}\chi_{tc}}{M_{tc} - \lambda\chi_{tc}} \quad 3.32$$

And χ_{tc} is a material constant determined from drained tests on both loosely and densely prepared soil specimens.

5. The stress-dilatancy theory

According to Jefferies and Been (2015), the stress-dilatancy while assuming associated flow rule can be represented in Equation 3.33:

$$D^p = \frac{\dot{\epsilon}_v^p}{\dot{\epsilon}_q^p} = M_i - \eta \quad 3.33$$

Where $\dot{\epsilon}_v^p$ and $\dot{\epsilon}_q^p$ are the plastic volumetric and deviatoric strain rate, respectively.

The derivations of the complex plastic strain rate ratios are detailed in Jefferies and Shuttle (2002).

6. The hardening rule

Norsand's hardening rule is directly related to the second postulate, and expressed in Equation 3.34:

$$\frac{\dot{p}_i}{P_i} = H \frac{M_i}{M_{i,tc}} \left(\frac{p}{p_i} \right)^2 \left(\frac{p_{i,max}}{p} - \frac{p_i}{p} \right) \dot{\epsilon}_q^p + ST_s + T_{PSR} \quad 3.34$$

Where H , the hardening modulus is expressed in Equation 3.35 as:

$$H = H_0 + H_{y\psi} \quad 3.35$$

H_0 and $H_{y\psi}$ are material constants. $p_{i,max}$ is expressed in Equation 3.36 as:

$$p_{i,max} = p \exp \left(-\frac{\chi_i \psi_i}{M_{i,tc}} \right) \quad 3.36$$

The input of $S = 0$ will nullify the effect of the optional cap softening term T_s . S is zero by default, and its permissible range is $0 \leq S \leq 1$. A high S value will lead to quicker softening of sand in typical undrained shear loading. $S > 0$ is not recommended for drained loading. The last term in Equation 3.34 captured the effects of principal stress rotation according to Jefferies et al. (2015) and expressed in Equation 3.37 as:

$$T_{PSR} = \left[-z \left(\frac{p_i}{p} - \frac{1}{r} \right) \left| \frac{\dot{\alpha}}{\pi} \right| + \frac{1}{r} \right] |\psi_i| \quad 3.37$$

Where z is a material property, $r = \exp(1) \approx 2.718$ is fixed value for the yield surface spacing ratio, α is the angle between the major principal stress direction and the referenced y-coordinate.

3.6.2 Breakdown of the calibration for the Norsand numerical model soil properties

The calibrated soil model properties for the Norsand numerical framework include mainly the soil's critical state parameters, theories of plasticity, elasticity, hardening rule, flow rule, soil state parameters, stress-dilatancy, and state-dilatancy based soil parameters. A breakdown and summary of how the key parameters were obtained are summarized in subsequent subsections. The majority of the soil model parameters were obtained from fitted data trendlines of the several executed drained and undrained tests. The software tool that was used for the calibration of the Norsand material model properties herein is an open-source excel program called NorTx12. NorTx12 is an excel program that is attached to the critical state textbook authored by Jefferies and Been (2015). The NorTx12 consists of a programmed visual basic application (VBA) which contains all the Norsand formulas, it computes the new stresses and strains by the Euler integration method. The NorTx12 itself simulates four different aspects of the soil behavior but does not simulate the generated excess PWP. The simulation of the generated excess PWP is a boundary value problem that can only be obtained by the application of either a finite element (FEM) or finite difference method (FDM) - based software. The categories of the soil samples that were validated with the Norsand model have been stated earlier as the primary soil sample (ECS00) and a clayey sand matrix specimen (ECS30).

In the current work, the finite difference method (FDM) – based software program FLAC (Fast Lagrangian Analysis of Continua) and FLAC3D authored by Itasca (2021) was applied to simulate a 1-zone soil elemental response to validate the studied specimens' stress-strain and pore water pressure characteristics. FLAC is a well-known numerical software for advanced geotechnical analyses of soils, rocks, groundwater/ support in two dimensions while FLAC3D is a three-dimensional version (Itasca, 2021). The author was opportune to apply both software through the provided academic license under the Itasca Education Partnership Program (IEP) with AUT. The soil bearing strength is most certainly dictated by stress and strain invariants, and not by the stresses themselves (Jefferies & Been, 2015). To achieve the above, the triaxial data is transformed from the laboratory-measured results to reflect these invariants. The strain invariants, i.e., the volumetric strain (ε_v) is correlated with the corresponding shear strain (ε_q) based on Equation 3.38, where ε_1 is the current strain state

$$\varepsilon_q = \varepsilon_1 - \varepsilon_v/3 \quad 3.38$$

From the fundamentals of the stress-dilatancy theory, the drained data were used to convert strain to dilatancy as a ratio of strain increments by the central difference method of differentiation in NorTx12. The parameter of particular interest here is the maximum stress ratio (η_{max}), and the corresponding magnitude of dilatancy known as minimum dilatancy (D_{min}). In theory, it is said

that stress dilatancy would have η_{max} corresponding with D_{min} (Jefferies & Shuttle, 2020). The primary reason for focusing on D_{min} is because the frictional ratio at the critical state (M) varies with the soil fabric.

In addition, the evolution of void ratios (e) during drained shearing is required, and it is computed from Equation 3.39 from the estimated post-consolidation void ratios (e_0) and the volumetric strain.

$$e = e_0 - (1 + e_0) \times \varepsilon_v \quad 3.39$$

Lastly, from the drained data, the state parameter corresponding to D_{min} is computed from Equation 3.40 as:

$$\Psi = e - (\Gamma - \lambda_{10} \times \log p') \quad 3.40$$

The transformation of stress invariants utilizes the well-known deviatoric stress (q) and mean effective stress (p'), and they are estimated from Equations 3.19 and 3.20, respectively for the undrained tests in the effective stress analyses. All the equations earlier described in previous and current sections have been embedded in the excel sheets of NorTx12 and underlying VBA codes to post-process both the drained and undrained tests data for the required soil properties. A breakdown of the calibration procedures for Norsand model parameters is enumerated in the subsequent subsections.

3.6.2.1 The critical state (CSL) parameters

The two key critical state parameters, the Gamma (Γ) and Lambda (λ_{10}) were determined mainly from the undrained test data as fitted in the $e - \log p'$ stress-space. Γ is the altitude of the CSL at a reference mean effective stress (p') corresponding to about 1kPa magnitude of stress level, and λ_{10} is the corresponding slope of the CSL in the mean effective stress – void ratio ($e - \log p'$) space (Been et al., 1991). In summary, the critical state parameters are considered intrinsic soil properties. First, the undrained tests were carefully examined to identify the mean effective stress at which the constant rate of deformation was initiated in the sample (i.e., the mean effective stress at the onset of the critical state), see annotated Figure 3.23 for an example of how this was derived. The identified mean effective stresses were then paired with their corresponding computed post-consolidation void ratios to define the CSL locus in the ($e - \log p'$) space. Overall, both the drained and undrained $e - \log p'$ were plotted and fitted with Equation 3.24 to obtain the best-fit linear relationship. The derived critical state line (CSL) for the validated clean sand (ECS00) and clayey sand (ECS30) are shown in Figures 3.24 (a) and (b).

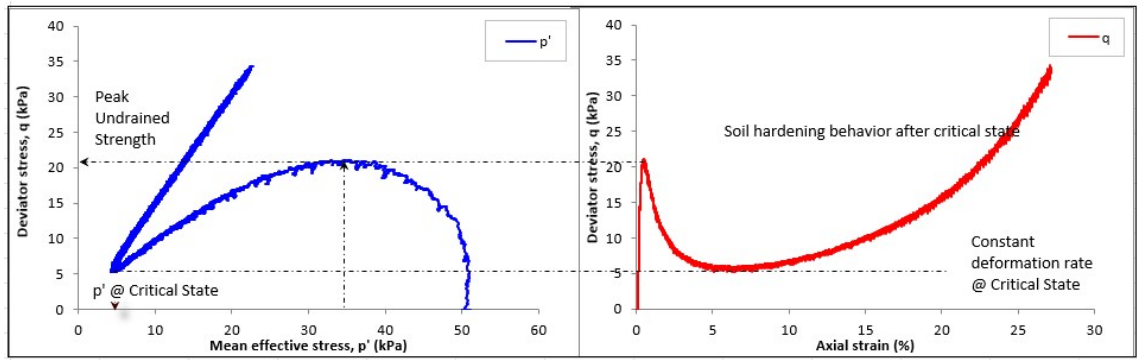
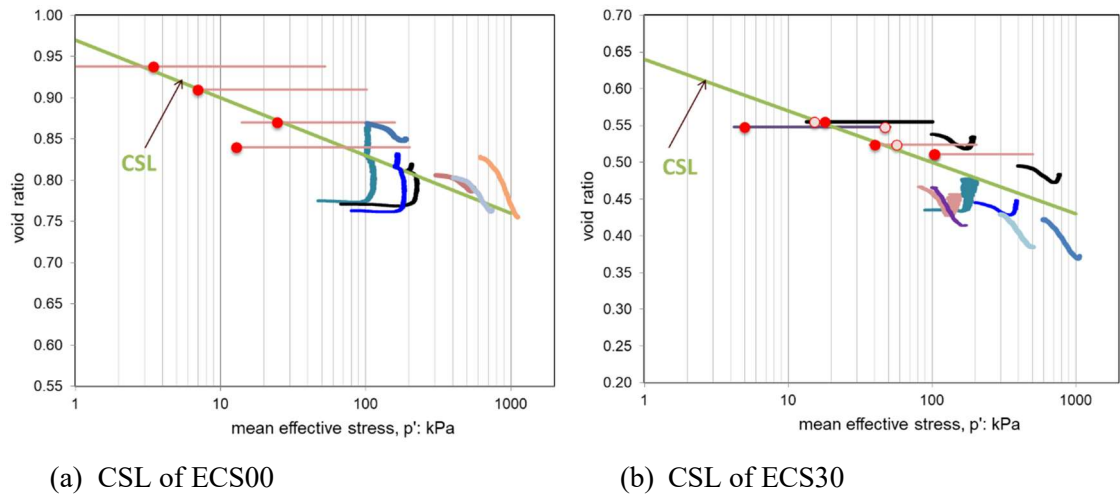


Figure 3.23 Evaluation of the soil critical state parameters from the stress invariants

A minimum of two test points are required to define the CSL in the $e - \log p'$ stress space, However, Jefferies and Shuttle (2020) recommended about 5 to 8 undrained tests at different stress levels to get the best possible fitted/refined line. The red dots in Figure 3.24 are indicative of the derived critical state locus in the $e - \log p'$ stress-space and the open circles are indicative of test start points for the drained tests. The intercept (Γ) and the slope (λ) of the CSL are easily read off after establishing the CSL by fitting the test data to it.



(a) CSL of ECS00

(b) CSL of ECS30

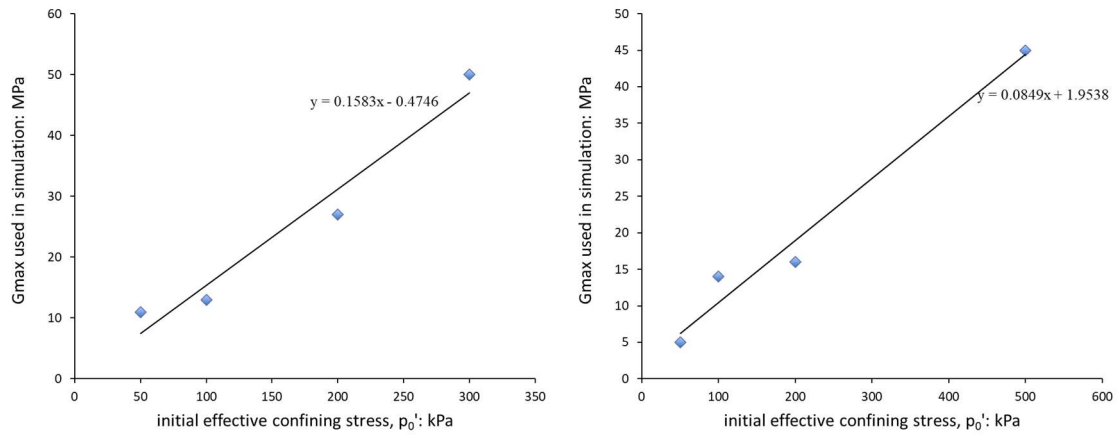
Figure 3.24 Derived critical state lines (CSL)

From the discerned CSL, one can see that engineering judgment is required when fitting to the experimental data trends. The undrained tests which are the horizontal lines that typically move from right towards the CSL (left) were the first factor to consider when fitting the CSL. The drained tests on the loosely prepared ECS00 samples fall above the CSL at the upper bottom right while the dense sample falls below the CSL at the bottom right.

3.6.2.2 The soil elasticity-based parameters

The relevant soil properties for the elasticity-based characteristics include the maximum shear elastic modulus at a reference initial effective stress ($G_{max} @ p_0$), the elastic exponent (G_{exp}), and the Poisson's ratio (ν). Most commonly, the G_{max} maybe determined in the laboratory by determining the shear wave velocities of the soil samples through the bender element tests. Alternatively, it may be derived by applying some existing correlation formula based on field data

(either CPT or SPT), resonant column tests, seismic shear wave velocity, etc. However, the bender element test was not carried out in the current work. Instead, a forward iterative modeling (FIM) was applied in correlation with data on similar soils from the elastic model in NorTx12 and deriving the best-fit value for the various soil models. See Figures 3-25 (a) and (b) for the elastic modulus check of ECS00 and ECS30 which can be linearly correlated with the stress levels. One can see that the elastic modulus is a function of the mean effective stress of the soil. Experiments for the determination of Poisson's ratio are extremely difficult to be executed in the laboratory, however, typical values in geotechnical engineering practice range between 0.15 to 0.3 for soils, a value of about 0.15 was adopted in the current study.



(a) Clean sand - ECS00

(b) Clayey sand - ECS30

Figure 3.25 Elastic modulus used during simulation

3.6.2.3 The soil plasticity-based parameters

The soil plasticity-based parameters include M_{tc} , N_{tc} , X_{tc} , H_0 , and H_ψ . The subscript tc in most parameters indicates the triaxial condition, however, some references in the literature may not include the subscript. The properties M_{tc} and N_{tc} are intrinsic stress-dilatancy properties, referred to as critical friction ratio and volumetric coupling coefficients, respectively. The stress-dilatancy theory already defined in Equation 3.33 is well explained in the work by Been and Jefferies (2004). First, the drained triaxial soil data is numerically differentiated (using the central difference approach) as detailed in Been and Jefferies (2004) to compute the dilatancy rate (D). The stress ratios ($\eta = q/p'$) is subsequently plotted against the corresponding minimum dilation (D_{min}). See Figure 3.26 and Figure 3.27 for the obtained dilatancy plot for ECS00 and ECS30, respectively. The details of this plot for other soil samples are attached as Appendix J1 to J3. The plots in Figures 3.26, 3.27 and Appendix J follow the developed stress dilatancy relationship as per the work of Been and Jefferies (2004). The parameter M_{tc} is obtained as the maximum stress ratio (η_{max}) corresponding to the respective minimum dilation (D_{min}). Figures 3.28 (a) and (b) indicates the instance applied in computing these parameters for sample ECS00 and ECS30, respectively. Theoretically, the η_{max} value corresponding to zero dilation is the M_{tc} value and

the fitted slope of the data trend line in Figures 3.28 (a) and (b) is the corresponding parameter N_{tc} . The minimum dilation (D_{min}) and corresponding maximum stress ratios (η_{max}) for each test are then determined and fitted plots of η_{max} vs D_{min} are created for picking the M_{tc} and N_{tc} . Equation 3.41 is used in computing this trendline in NorTx12.

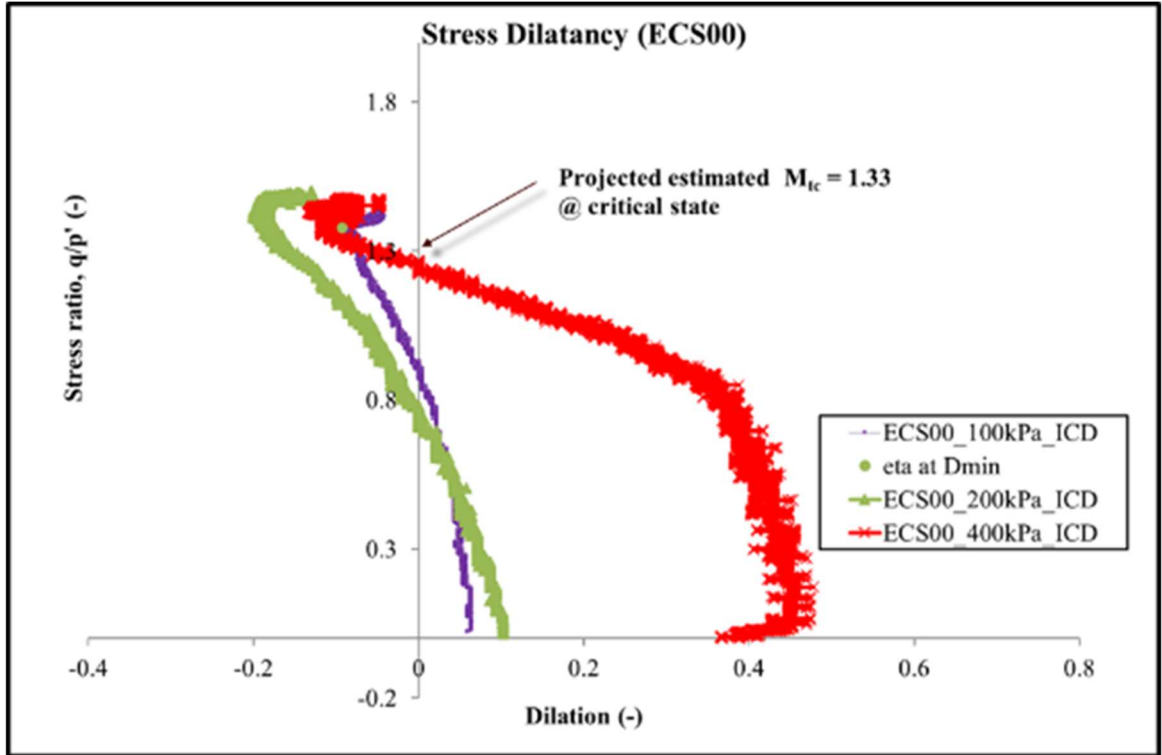


Figure 3.26 Stress dilatancy relationship measured in east coast sand (ECS00) with trendlines for CS selection of M_{tc} value

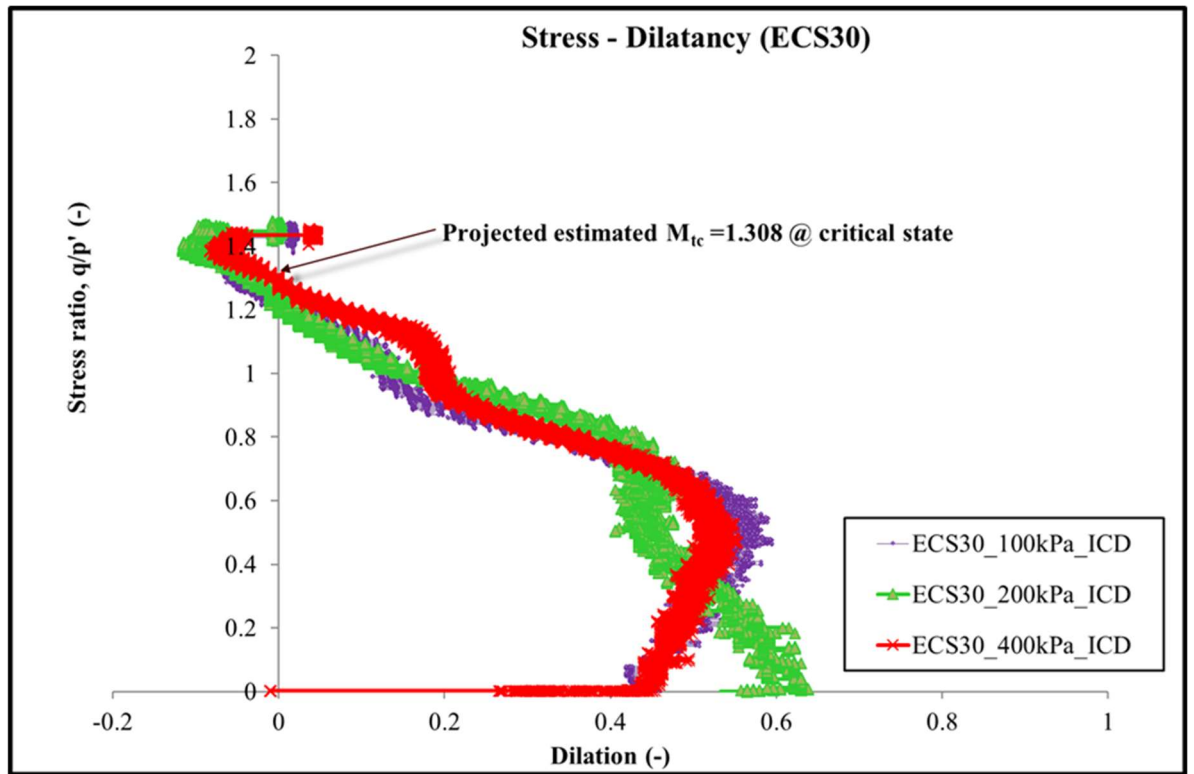


Figure 3.27 Stress dilatancy relationship measured in east coast sand (ECS30) with trendlines for the CS selection of M_{tc} value.

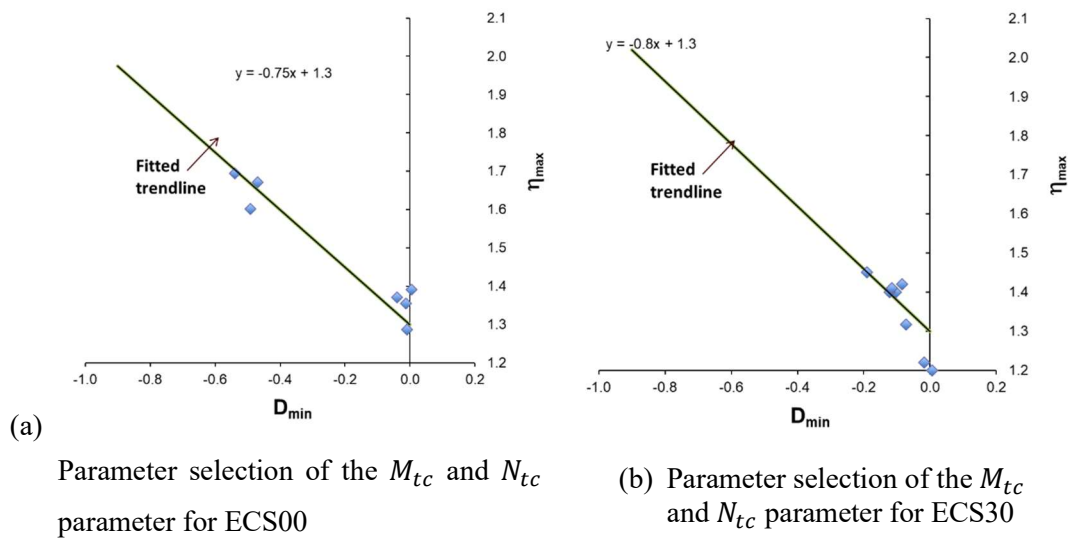
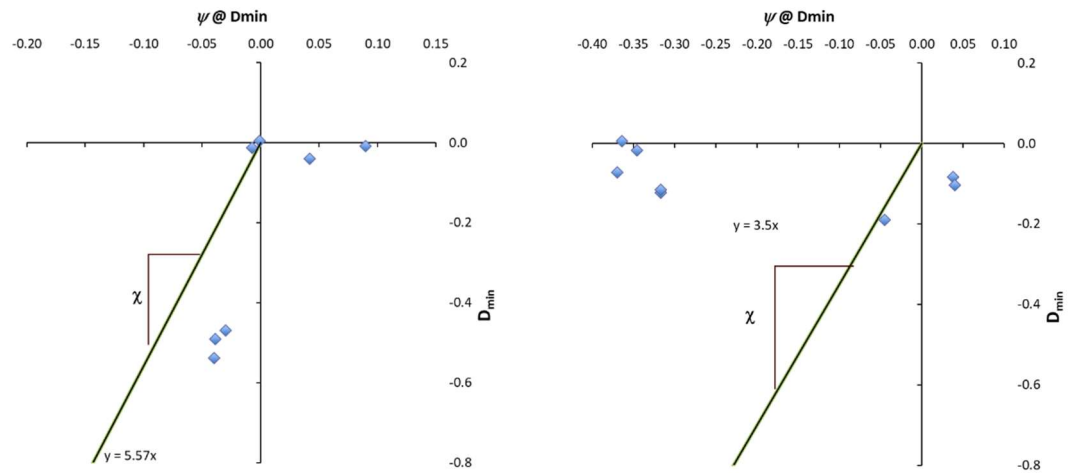


Figure 3.28 Calibration of stress dilatancy parameters of ECS00 and ECS30

The parameter X_{tc} , often called χ_{tc} , is the property defining the state-dilatancy of the soil. The determination of χ_{tc} (X_{tc}), similarly, follows the trendline of plotting D_{min} versus Ψ . The trendline plot works for both loosely and densely prepared soil samples. However, the data for the densely prepared samples in this study appeared to be sparse, hence, this plot was not used but applied an engineering judgment in selecting the applicable values in simulations using the forward iterative modeling (FIM), typical values of X_{tc} the range between 2.0 - 4.0 as found in Jefferies and Shuttle (2020). See Figure 3.29 (a) and (b) at the instance and attempted plots to calibrate the parameter χ_{tc} for ECS00 and ECS30, respectively. Equation 3.42 is the formula used in computing its trendline. One thing to note is that this trendline must pass through the point D_{min}, Ψ at (0,0) with tests datapoints fairly distributed or aligned with the line. The scatter data points of the drained tests herein are eminent, but engineering judgment was applied in approximating the best-fitted line to adequately represent the data. From Figures 3.29 (a) and (b), One can see why Jefferies and Been (2015) recommended that separate tests on dense samples be performed to estimate the soil property X_{tc} as data for loose drained tests tend to cluster towards the origin and negative side of the abscissa. In summary, the typical value of this parameter range between 0.2 to 0.4, therefore, it is intuitive to assume its value between this range for the validated soil samples and iterate with simulations to see the value that best fits the experimental data.

$$D_{min} = X_{tc} \cdot \Psi \quad 3.42$$

The parameter H , referred to as plastic modulus was derived simply by FIM (otherwise known as back analysis in routine engineering analyses) to determine its values that best fit the test/experimental data, this soil property is dependent on the soil fabric and consequently, it is a function of the state parameter.



(a) State-dilatancy of ECS00

(b) State Dilatancy of ECS30

Figure 3.29 State-dilatancy plot of ECS00 and ECS30

The theory of plasticity plays a significant role in the soil yield surface/behavior and this is explicitly explained in Jefferies and Been (2015).

3.6.2.4 The initial soil state-based parameters

The initial soil state parameters would normally include the state parameter- ψ (Ψ_0), post-consolidation void ratio (e_0), initial mean effective stress (p_0), and the overconsolidation ratio (OCR). The state parameter ψ , obtained from equation 3.26 is an important property relating to the soil fabric. A positive state parameter indicates a loose sample while a negative ψ indicates a dense soil material. Hence, the state parameter has been used as a quantifying index parameter for liquefiable soils in previous works. The best fit of the parameter ψ would usually compute the perfect match of all soil engineering properties as obtained from the simulations by iterations. For simplicity, it is assumed in all the analyses done that all the soil samples are normally consolidated (NCL) under isotropic triaxial conditions, hence, the overconsolidation ratio (OCR) that was utilized in all simulations ranges between 1.0 to 1.2. Although in-situ soils in the field would like to exhibit anisotropic behavior whose analyses are rather considered too complex for any realistic conclusion, hence simplifying the assumptions make more sense. By definition, OCR is simply the ratio of the pre-consolidation stress to the current mean effective stress in the soil element. All the advanced geomechanical soil parameters were collated and further discussed in chapter four.

3.6.3 Numerical modeling in the VBA and FLAC codes

The numerical validation tests include typically one-zone soil elemental simulation tests based on the conditions of static, loose, undrained triaxial compression conditions (TC) on the ECS00 and ECS30 soil specimens, with consideration that the so-called conditions best matched the state for static/flow liquefaction modeling and would mimic the same scenarios as found in the in-situ field conditions. Some comparison tests with the VBA code show a good agreement between the VBA and FLAC – codes-based simulations. The one-zone soil element numerical simulation carried out in the VBA-based code simulation is a straightforward process as only the relevant excel macro buttons such as ‘update model’ and ‘plot data’ need to be clicked/activated after entering the derived and calibrated soil properties under the ‘Params & Plots’ tab of NorTx12. The drainage mode can also be toggled between drained and undrained mode, the CSL idealization can also be toggled between the semi-log and curved CSL idealization. The semi-log CSL idealization was adopted and assumed reasonable for all the simulations done herein. The best-fit derived parameters set were subsequently tabulated and utilized also in the subsequent FLAC simulations.

The numerical simulation tests were carried out in FLAC by examining a one-zone soil model with an axisymmetric configuration, a unit dimension in the x- and y – directions. Figure 3.30 shows the typical configuration of the one-zone soil element boundary conditions and grid system in FLAC.

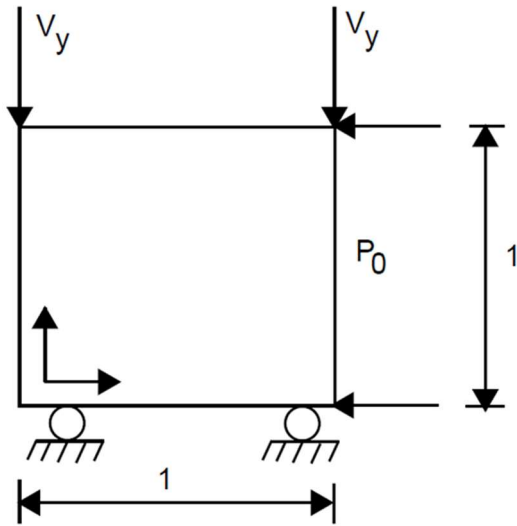


Figure 3.30 The specified boundary conditions in the FLAC software

The specified boundary condition in Figure 3.30 is such that the base of the model is a roller boundary, the side is subjected to the initial testing mean effective stress, p_0 , and fixed velocity boundary and strain rate of $1e-6$ applied at the top. A reasonable initial in-situ stress is specified in the FLAC code by FISH, an instance of specifying this in the FLAC is shown in Figure 3.31.

```
define ini_stress
  loop ii (1,izones)
    loop jj (1,jzones)
      _esxx = esxx(ii,jj)
      _esyy = esyy(ii,jj)
      _eszz = eszz(ii,jj)
      _esxy = sxy(ii,jj)
      z_prop(ii,jj,'sxx_ini')=_esxx
      z_prop(ii,jj,'syy_ini')=_esyy
      z_prop(ii,jj,'szz_ini')=_eszz
      z_prop(ii,jj,'sxy_ini')=_esxy
    endloop
  endloop
end
;
ini_stress
```

Figure 3.31 Specification of initial stress in FLAC using FISH

The groundwater configuration is set to a no-flow with its fluid properties: initial fluid tension and fluid modulus set as constants as $-1e20$ and $2e6$, respectively.

FISH is the programming language designed to work with the FLAC and FLAC3D software, it enables the user to define new functions and variables. For instance, new variables may be set, printed, or plotted, parametric studies may also be automated. The 3D-version of FLAC, FLAC3D apart from FISH can further utilize the Python programming language for further functionalities of the software. Table 3.15 defines and specifies the applicable material properties of the Norsand FISH material functions/codes as per Itasca (2021) in the FLAC software. Also, worthy of note is that the critical state soil mechanics (CSSM) often applies the upper case of the Greek words in the naming conventions of the soil parameters.

Table 3.15 Summary of the relevant material properties for the Norsand model as per Itasca (2021)

FISH Code	Material property
cs11	critical-state-1, C_1 . CSL determination parameter
cs12	critical-state-2, C_2 . CSL determination parameter
cs13	critical-state-3, C_3 . CSL determination parameter. Here, the $C_3 = 0$ (default), therefore CS is based on the semi-log equation where $C_1 = \Gamma$ and $C_2 = \lambda$
p_ref	Reference pressure, G_{ref}
poisson	Poisson's ratio, assumed herein as 0.15
rat_crit	Critical state ratio, M_{tc} , calibrated value for ECS00 and ECS30 ~ 1.30
fac_cp	Volumetric coupling-factor, N_{tc} , For ECS00 $N_{tc} = 0.25$, for ECS30 $N_{tc} = 0.20$
h0	Hardening-0, H_0 . Plastic hardening modulus when $\psi=0$.
hy	Hardening-y, H_y . Another hardening modulus parameter so that plastic hardening follows $H = H_0 - H_y \Psi$. Default = 0
Fac_dil	Factor-dilatancy, X_{tc} . This is the property relating the minimum dilatancy to the corresponding Ψ , TC is the reference condition, values typically range between 2.0 and 4.0.
gref	Reference shear modulus
exp_m	Pressure exponent dependence defining elasticity, m range between 0.2 and 0.8 in simulations
ocr	Overconsolidation ratio, OCR . OCR typically range between 1.1 and 1.2 in simulations.
Ind_soft	Index-softening, S . An additional softening term. The allowable range is $0 \leq S \leq 1$. A higher S will produce a faster softening of loose sand during undrained simulations. A reasonable value of S should be ≥ 0 for any case of drained loading.
sxx_ini	Stress-xx-initial, σ_{xx}^0
syy_ini	Stress-yy-initial, σ_{yy}^0
szz_ini	Stress-zz-initial, σ_{zz}^0
sp_ini	The initial state parameter Ψ_0 . When $e_0 \leq 0$, the soil initial state will use this initial state parameter and e_0 will be computed by Ψ_0 (updating)
void_ini	Initial void ratio, e_0 .

In summary, the utilized FLAC code for simulations was written as a batch file in a notepad document and called by the assigned file name into FLAC to run simulations subsequently. The obtained outputs from the FLAC plot histories were further exported into excel .csv files for further post-processing where comparisons of the simulations can be easily made with the VBA and FLAC code for further analytical discussions with the experimental results. The typical applicable FLAC code written for the undrained simulations is annexed as Appendix K. Further discussions are presented in Chapter 5 for the simulation results.

3.7 The physical model testing (shake table experiments)

The main objective of conducting the shake table experiments herein was to primarily evaluate the dynamically generated excess pore water pressure (PWP) characteristics of all the studied soil samples due to the varied clay contents in the fabrics of ECS. The physical model experiment for the shake table was achieved with the aid of a novel 600N rated-capacity, automated shaking table available at the AUT geotechnical laboratory. The decision to utilize the above device was based on the consideration of the associated existing limitations of the conventional large-scale shaking tables. Subsequently, parametric studies were carried out to determine the samples' dynamically generated excess PWP for comparative technical discussions.

The associated limitations of large-sized, shaking table models may include the increasingly high cost of procurement and maintenance of actuators as the number of required actuators and payload increases (Prasad et al., 2004). Besides, a large-size model often requires outsized space to fit (or accommodate) test setup, especially in small spaced laboratories; the unavoidable long durations and laborious requirements for sample preparations are notable limitations.

3.7.1 The 600N rated-capacity shaking table setup

A 20mm thick base plywood material measuring 1000mm x 450mm (i.e., length x breadth) houses the entire shaking table assembly (refer to Figure 3.33). The assembly of the simple system consists of a greater than or equal to 600N rated-capacity actuator (MS500-Series Modal Shakers), an amplifier (Series LA-500) from National Instruments, an H-section frictionless sliding mechanism, and a 25mm thick plywood upper base (measuring 520mm x 400mm) screwed to the actuator and sliding mechanism with four M-8 bolts. Four (4) numbers of hollow steel legs of a 200mm x 200mm cross-sectional area, filled with concrete, carried the entire device setup; the provided legs' function is to provide rigidity and prevent any relative movement of the device during operations. In summary, the table's primary function is to provide stability and prevent lateral movements of components of the device during its operations as a reaction mass.

The amplifier powers the actuator, which in turn moves the upper base plywood in a single degree of freedom (SDOF) simple harmonic motion. The theoretical concepts of SDOF vibration GM are well-detailed in several previous works; for instance, Chopra (1995), Kramer (1996), and well-summarized by Douglas (2003). Figure 3.32 shows the schematics and free body diagram of

the typical fundamental theory of SDOF motion following Newton's 2nd law of motion, and it typifies and mimics the utilized shaking table's physics and mechanism of operations. The shake table assembly and main components, shown in Figure 3.33, operate according to the SDOF ground motion.

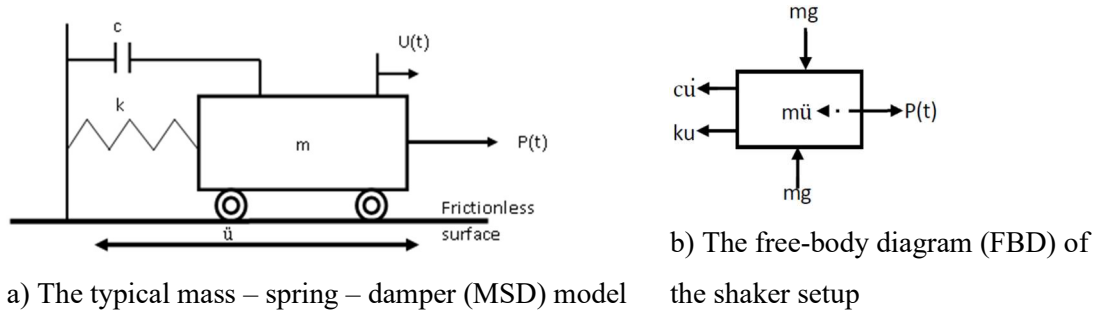


Figure 3.32 Mechanics of typical SDOF motion for earthquake ground motion modified after Chopra (1995)

If a body with mass m is driven by a horizontal ground motion of acceleration \ddot{u} on a surface with approximate zero friction, the horizontal displacement of the body is u assuming a spring of stiffness k and a provided viscous damping coefficient of c is given by the dashpot. Therefore, applying Newton's second law and equilibrium forces resolution in the horizontal direction gives:

$$m\ddot{u} + c\dot{u} + ku = P(t) \quad 3.43$$

In Equation 3.43, $P(t)$ is an externally applied dynamic load but in the case of the current shake table setup $P(t) = 0$ since there is no externally applied force to the system. Therefore, for force equilibrium, the sum of the inertia force, damping force, and spring force are equivalent to zero in Equation (3.21). Equation 3.43 is the governing physics for vibration motion mechanisms based on SDOF. The dot notation on symbols signifies the required integral steps to achieve the corresponding symbolic variable. Dividing Equation (3.43) by m yields Equation 3.44:

$$\ddot{u} + 2\xi_0\omega_0\dot{u} + \omega^2u = -\ddot{u} \quad 3.44$$

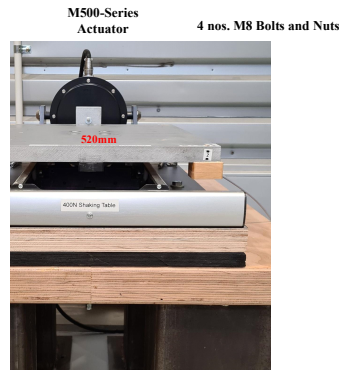
In Equation (3.44), $\omega_0^2 = \frac{k}{m}$ and $\xi_0 = c/2\omega_0m$.

Furthermore, the systems' undamped natural period is $T_0 = 2\pi\sqrt{m/k}$ and critical damping ratio is $\xi_0 = c/2\sqrt{km}$. More details of the above equations are available in Douglas (2003). Typically, transient GM parameters usually are based on amplitude, frequency content, and duration quantities. The peak ground accelerations (PGA), peak ground velocities (PGV), and peak ground displacements (PGD) are directly related to the derived amplitude parameters. In New Zealand geotechnical practice, the PGA, derived typically from inputs of the site sub-class, return period, design working life, and the importance level of the structure is a key parameter for seismic assessment and designs.

The frequency contents, routinely obtained from spectra data (e.g., Fourier Spectra, Fast Fourier Spectrum, response spectrum, etc.), and the duration parameters are concerned with how long the

earthquake is occurring (e.g., bracketed duration, the equivalent number of cycles). Other commonly used GM parameters are Arias intensity, which quantifies the amount of energy in an earthquake, the cumulative absolute velocity, etc.

In a bid to examine the pore pressure generation characteristics of ECS by using the 600N rated-capacity shaking table device, a rigid soil container was designed and fabricated (refer to Figure 3.34).



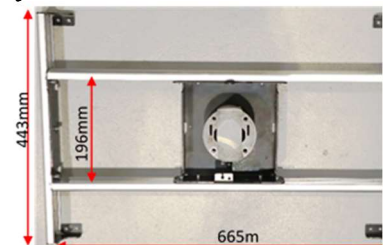
a) The shaking table assembly



(b) The data acquisition (DAQ) system



(c) The series LA-500 Ni amplifier



(d) H-section, sliding mechanism

Figure 3.33 The shaking table setup and main components

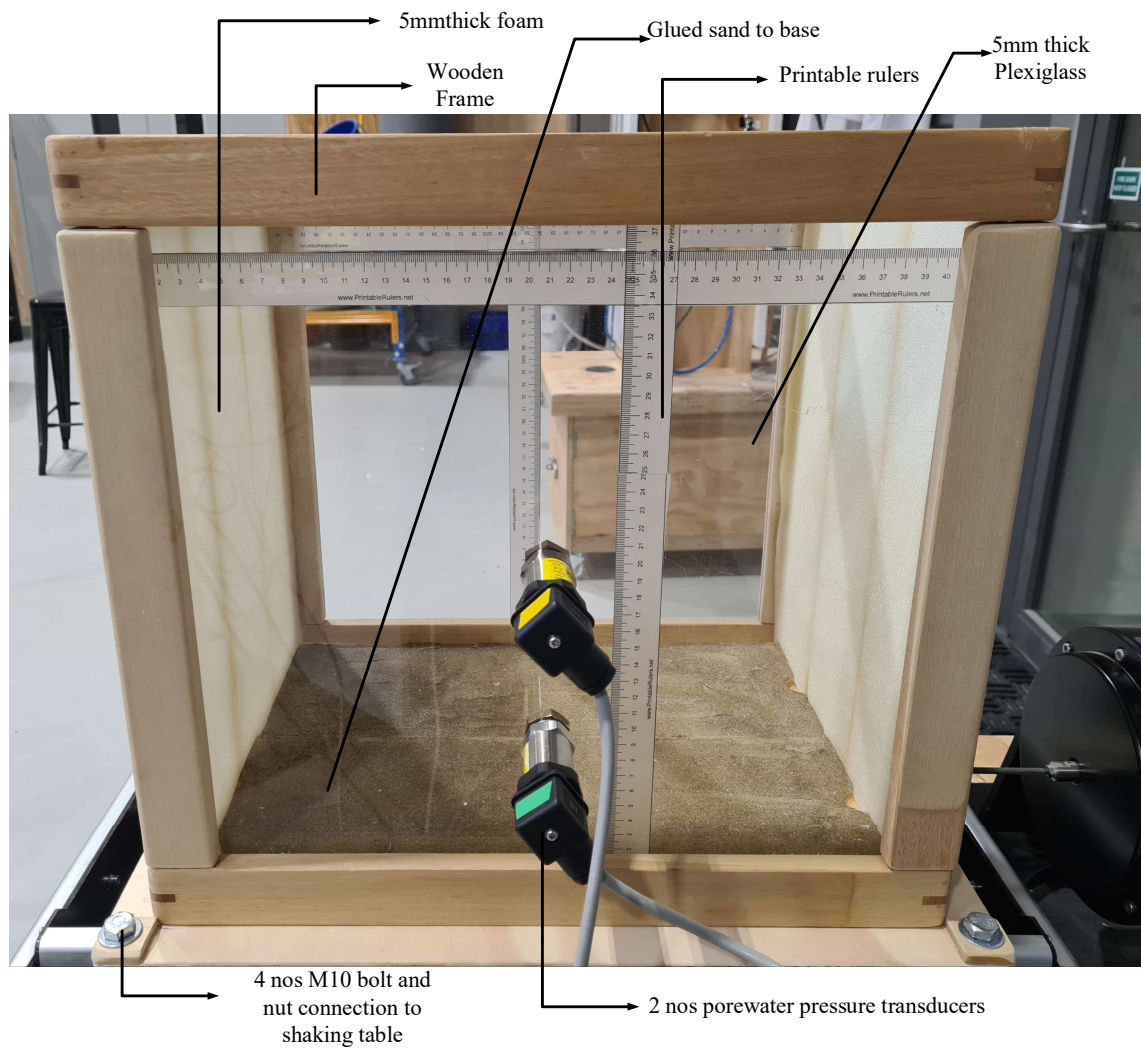


Figure 3.34 Details of the designed and fabricated soil model rigid box

The rigid box, made of a 5mm thick plexiglass material, has a total internal dimensional capacity of 395mm x 295mm x 400mm (i.e., length x breadth x height). The soil box (as shown in Figure 3.34) is brazed around its external corners/edges with timber frames to complement its strength and rigidity when subjected to shaking under vigorous shaking. The targeted prototype soil model's actual dimension is approximately 395mm x 295mm x (220 to 240mm), offering about 90mm clearance at the top of the model box to avoid spillage during shaking events.

Lombardi et al. (2015) suggested that an absorbing material be installed on the model container's internal transient boundaries to minimize the effects induced by the artificial boundaries on the soil model. Following the above work, a foam material with a thickness of 5mm was installed on the soil box internal transient boundaries. Dry sands were also glued to the box's base to aid the generation of upward shear stresses/waves in the specimen-soil model, as shown in Figure 3.34.

To assist with an accurate measurement of the container's internal size, soil sample heights, falling height during pluviation for easy estimation of densities, and water level, printable rulers were obtained from printablerulers.net and glued to the container's horizontal and vertical space inside. The soil container was calibrated by volume through comparisons made between the obtained

estimates from the direct calculation of volumes with the box dimension and water-filling calculation methods. A typical plot of the calculated and water-measurement volume calibration against dept is shown in Figure 3-35. The slight variation may be due to the space occupied by the protruding pore water pressure sensors inside the soil box. The chart shown in Figure 3.35 is useful for quick estimation of soil densities inside the model container.

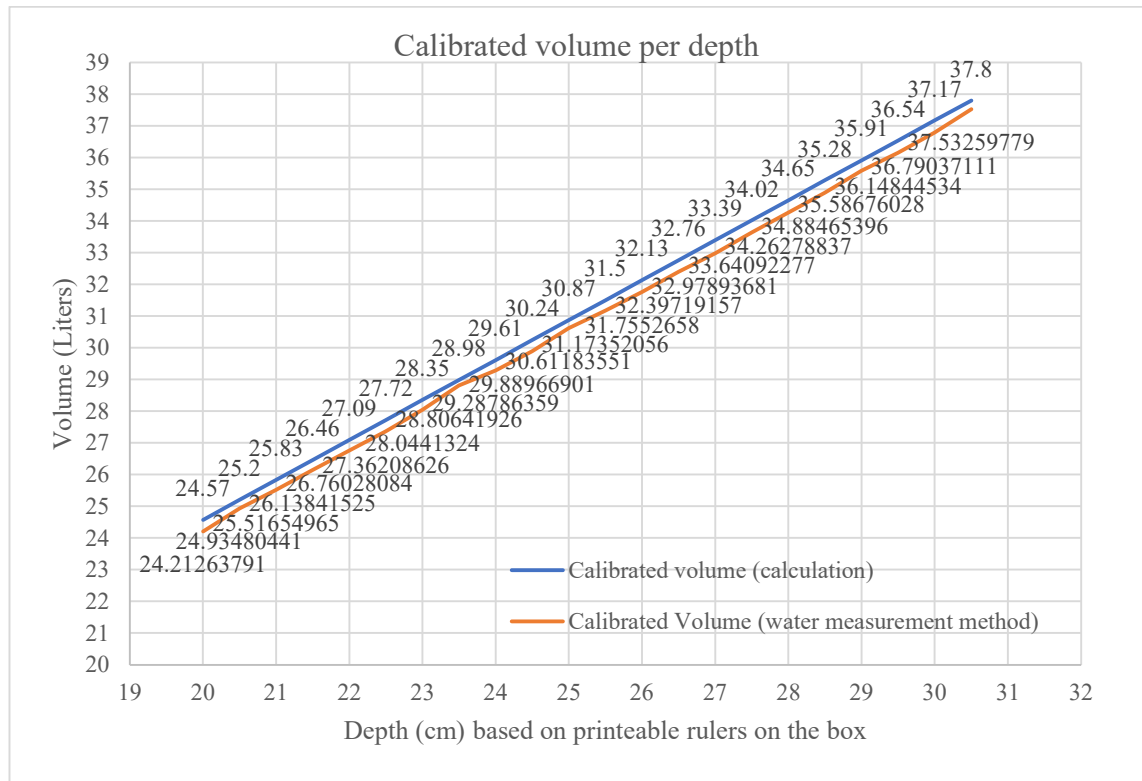


Figure 3.35 Calibration of soil model container volume by calculation and water-measuring method

3.7.2 The model setup, instrumentation, and data acquisition (DAQ) system

The applied instrumentation includes accelerometers of model 4030-series, manufactured by TE Connectivity (TE.com/sensorsolutions), and flush pressure sensors of SS402 series, manufactured by Sendo-Sensor (sendo-sensor.com). An accelerometer installed on the shaking table base allowed to measure/capture the input base motion of the acceleration-time histories. Another accelerometer was installed at approximately 200mm depth at the near-surface level inside the model to study the amplification and attenuation characteristics of the tested soils. In total, two PWP transducers were installed on the soil box at about 100mm and 200mm model depths levels to capture the PWP at the model's mid-depth and near-surface level, respectively. All the sensors were connected and calibrated with the LabView DAQ system. The DAQ system code was written in LabVIEW version 18.0.1. The program enables the development of an intuitive and interactive graphical user interface (GUI) for the test setup's various input and output interfaces. The utilized National instruments chassis is model PXIe-1078 coupled with suitable VI data cards and other hardware as schematically shown in Figure 3.36, the plan and longitudinal view of test instrumentation are shown in Figure 3.37 (a) and (b), respectively.

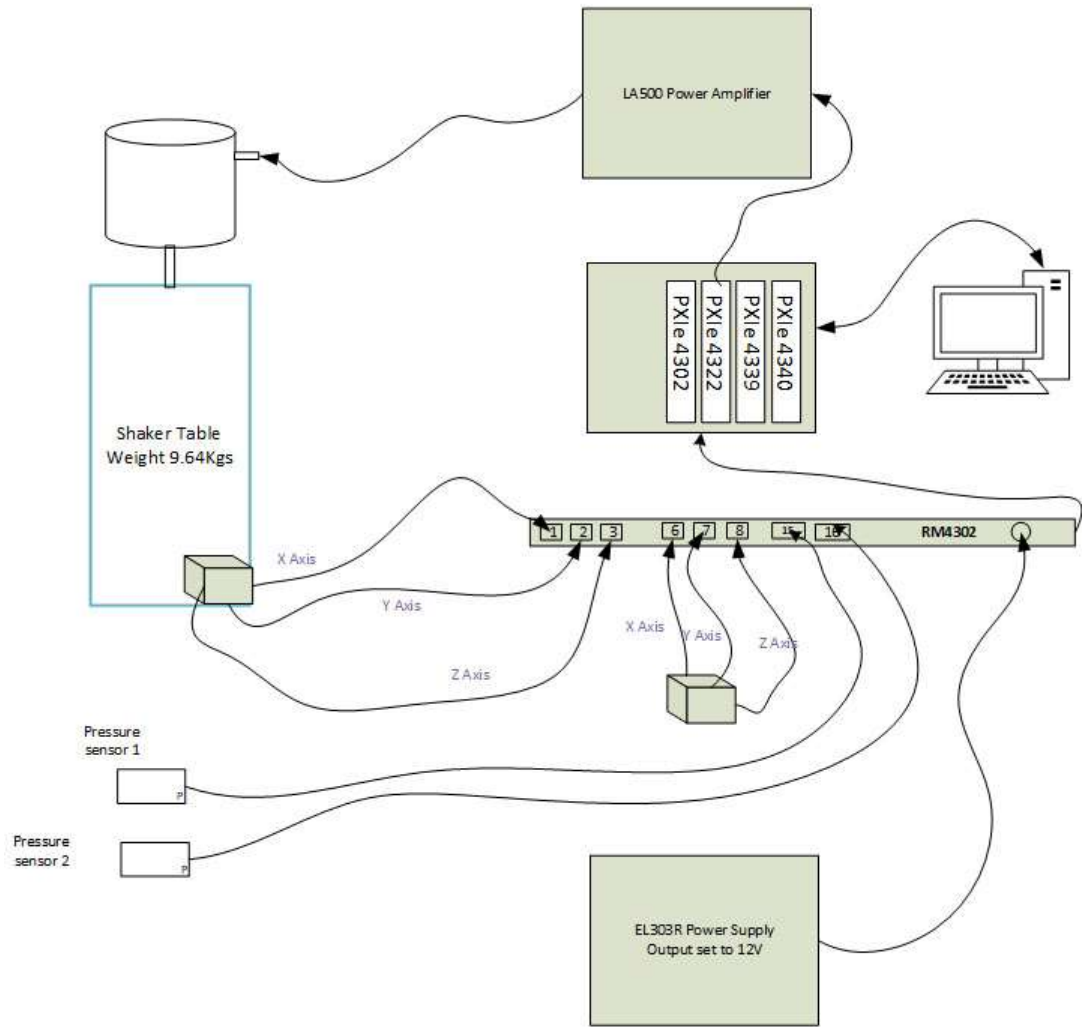


Figure 3.36 Schematics of the hardware setup

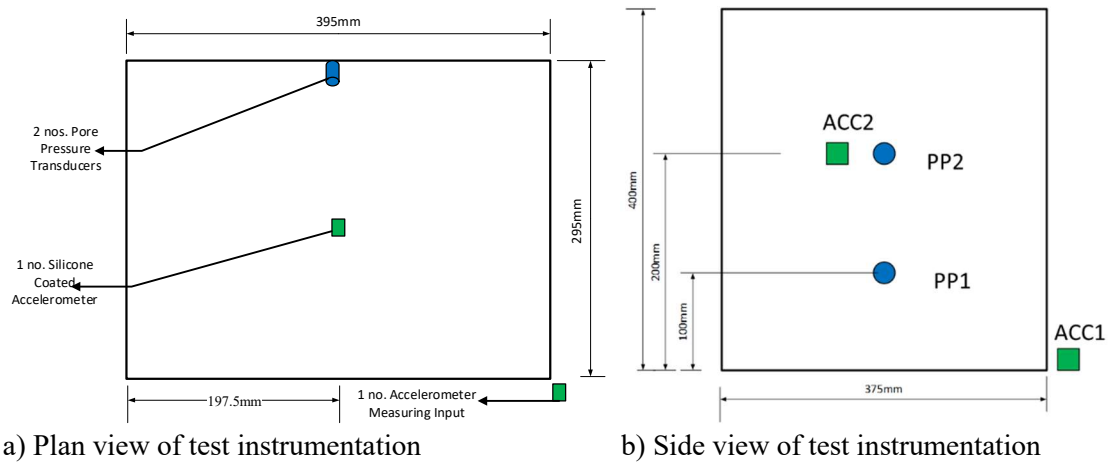


Figure 3.37 Layouts of the test instrumentation

3.7.3 The model sample preparation

To ensure the replicability/repeatability of tests, the majority of the prototype model setup procedures implemented herein followed the guidelines found in (Kutter, 2019; Kutter et al., 2020) of the liquefaction experiments and analysis project (LEAP). As per the preliminary sample preparations, both the clean sand (ECS) and the industrial kaolinite were oven-dried between 50

to 70°C for 24 hours. The most tasking part of the model preparation procedures is shown in Figure 3.38. Dry mixing by utilizing the mechanical mixer as shown in Figure 3.8(a) produced the mixed samples derived from both ECS and sand-kaolinite sand matrix mixtures. For all the studied soil samples, dried specimens were pluviated into the soil container by using a manual pluviator shown in Figure 3.38(b). Pluviated samples were then saturated with de-aired water from the side of the model and left to equilibrate for a minimum time of 72 hrs (Kutter et al., 2020). The soil models were then covered to prevent the evaporation and further aeration of the de-aired water. The utilized de-aired water facilitated saturation since it is impossible to carry out a B-value check to confirm saturation. The combined influence of effective confining stress and density/void ratios directly determines the liquefaction behavior of particulate materials such as sands. To mimic the in-situ evolution of excess PWP characteristics of liquefiable deposits in the laboratory, soil models were prepared with the configuration of low densities to make up for the effect of low confining stress and similar to the other previous works (Motamed et al., 2010; Varghese & Latha, 2014).



(a) Dry mixing of east coast sand and kaolinite (b) Dry pluviation of soil samples into the instrumented soil box.

Figure 3.38 Sample preparations of shake table experiment specimens

One key precaution taken during sample preparations of the soil models is controlling the mass of dried soil solids pluviated into the model container by a digital weighing scale with a precision of 0.01 kg. Approximately 40 kg each of all the dried soil particle masses were measured and utilized in the pluviation process. The reason for the above is to create constant masses for all the tested reconstituted specimens since it is considered that Equation 3.43 controls the force equilibrium of the ground motion intensities. The amount of water used in the saturation of all

models was similarly influenced by the above process and measured to enable computations of fairly conservative initial effective stresses in the models. The approximate total mass of each prepared model (i.e., the mass of empty box + mass of dried soil + mass of water) was approximately 60kg, which was within the rated force capacity ($\geq 600\text{N}$) of the applied actuator of the shaking table.

The soil-phase relationships were subsequently utilized in the computations of basic soil index model parameters, some of which are summarized in Table 3.16. Under laboratory conditions, it is particularly challenging to create similar overburden initial effective stresses as the depths of the soil models are very small as compared to actual in-situ soils. Observed from Table 3.16 is that the estimated void ratios are nearly the same except for that of ECS30 with minor deviation, which can be considered negligible. The same observation was found in the obtained corresponding submerged unit weights.

Table 3.16 Summary of experimental shaking table-physical model properties

Sample Name/ Properties	Dry Unit Weight (kN/m³)	Wet Unit Wt. (kN/m³)	Moisture Content (%)	Void Ratio	Specific Gravity	Relative Density	Average Permeability k (cm/s)
ECS00	14.00	19.80	29.50	0.600	2.60	0.52	4.55E-03
ECS05	13.70	19.90	24.20	0.600	2.54	0.77	3.67E-03
ECS10	13.40	19.40	23.70	0.600	2.61	0.72	2.28E-03
ECS15	12.40	19.30	23.30	0.590	2.53	0.76	1.22E-03
ECS20	12.00	19.30	25.30	0.650	2.59	0.68	4.73E-04
ECS30	10.20	17.70	23.70	0.540	2.56	0.77	7.35E-05

3.7.4 The scaling/similitude laws

The scaling laws otherwise known as the similitude laws are well-known key factors for consideration while interpreting the physical model results of particulate material such as soil in a shaking table testing with a finite boundary domain. This is simply because it is practically impossible to simulate the infinite lateral extents of in-situ soils in a finite boundary model container. The key factors determining similitude as per liquefaction physical models have already been discussed in the literature. The relevant and typical applicable scaling laws in the current study adopted those provided by Towhata (2008) and Iai (1989) and are summarized in Table 3.17 below.

The fundamental physics used for deriving the scaling laws as explained by Iai (1989) are typically governed by the fundamental laws of statics which simulate the mass and force equilibrium of the soil structure, pore water, and the soil constitutive laws (i.e., the stress-strain characteristics). It is not part of the scope of the current research to study the soils' deformation characteristics rather the main interest herein is the study of the evolution/generation of the soil-

fluid/excess (PWP) mechanisms. The soil-fluid similitude is complex, still controversial, and not well understood as stated in the literature.

Overall, the significance of the similitude laws is their requirements for the interpretation of the physical model results. Most importantly, the in-situ soil confining stresses are far greater than those produced in physical models. As found in Towhata (2008), some soil parameters are mentioned as significant parameters to scale with the similitude laws and they include the ground thickness, soil density, small strain shear modulus, large-strain damping ratio, shaking circular frequency, acceleration, cyclic displacements, shear strain, and reference strain. In summary, the time scale in the model is reduced by the square root of the prototype time, application of reduced soil densities (loose soils) in models for reasonable comparisons with prototype densities.

Table 3.17 Some applicable similitude laws as per (Iai, 1989; Towhata, 2008)

Quantity description	Symbol	Scaling factors (prototype/model)
Length	l	λ
Saturated soil mass density	ρ_{sat}	1
Shear strain	γ	$\lambda^{0.5}$
Shaking time	t	$\lambda^{0.75}$
Total stress	σ	λ
Effective stress	σ'	λ
The bulk modulus of soil solid particles	K_s	$\lambda^{0.5}$
Pore water pressure	u	λ
Soil permeability	k	$\lambda^{0.75}$
Soil velocity	\dot{u}	$\lambda^{0.75}$
Soil acceleration	\ddot{u}	1
The relative displacement of pore water to soil skeleton	w	$\lambda^{1.5}$
Rate of flow of pore water	\dot{w}	$\lambda^{0.75}$
Soil porosity	n	1
The bulk modulus of pore water	K_w	$\lambda^{0.5}$
Hydraulic gradient	i	1
Frequency	f	1
Shear modulus	G_{max}	$\lambda^{0.5}$

*Note: λ is the geometrical scale factor of the prototype soil to the soil model.

3.7.5 The shaking test information

Three consecutive shaking intensities were selected for operating the shaking table with a combination of sinusoidal motion derived by a constant frequency of 10Hz, varying amplitudes of (2, 3, 4), and a shaking duration of approximately 15s. The selected GM intensities were classified as a low shake (denoted as F10A2), intermediate shake (denoted as F10A3), and high shake (F10A4), respectively. It is intended to study the effects of the intensity of shaking on the PWP generation characteristics of the soil samples and their subsequent liquefaction responses. Shaking at varying GM intensities has been done by previous researchers (Kutter, 2019; Kutter et al., 2020; Rayhani & El Naggar, 2008). In summary, three shakings were executed on all the model samples to evaluate the dynamic soil PWP properties, their corresponding data captured by the DAQ at a high sampling rate of 1000 samples per second and saved for further post-processing. The obtained output raw test data of the accelerometers and PWP transducers were in voltages and exported from the LabView software by excel importer to .csv excel files. The acceleration-time histories were converted to g's using the calibration values of voltages per g and pore pressures converted to kPa. The achieved input base motion (i.e., the PGA) ranges between 0.1 to 0.2g.

The cumulative vertical settlements of the soil models after each shake (i.e., at F10A2, F10A3, and F10A4) were manually read off from the printable rulers installed on the soil box container and recorded. The effective stresses were estimated at the depth level of PWP measurements in the soil models. Typically, liquefaction was identified by the excess pore water pressure ratio (r_u) previously defined in Equation 2.1. The comprehensive results of the shaking table experiments are further discussed in detail in Chapter 4. Idriss and Boulanger (2008) have reported that the cyclic stress ratio (*CSR*) for the shake table may be defined in Equation 3.45. In which, τ_{cyc} is the cyclic shear stress in the horizontal direction and σ'_{vc} is the vertical effective stress. It implies that higher *CSR* will induce more liquefaction (i.e., $r_u = 100\%$ or when cyclic shear strain γ is 3%.

$$CSR = \tau_{cyc} / \sigma'_{vc} \quad 3.45$$

Typical liquefaction deformation analyses utilize the plots the *CSR* against the number of cycles N in either log or semi-logarithmic curves.

3.8 Summary

This chapter explains the applicable experimental and quantitative research methods that were applied in the current study. The investigated soil characteristic elements include the basic soil classification characteristics, permeability test, strength and deformation characteristics (advanced geomechanical properties under monotonic triaxial compression conditions), the dynamic shaking table experiments for measuring dynamically generated excess PWP, the applicable numerical framework that was utilized in the data validation process of the investigated static/flow liquefaction under monotonic triaxial compression conditions. The current chapter demonstrates typical applied scientific research through experimental and numerical modeling

tests for data validation while referring to the relevant established theoretical concepts as found in the relevant literature. Adequate references were made to the relevant tests standards including American Standards (ASTM), Australian Standards (AS), British Standards (BSI), and New Zealand Standards (NZS), the relevant geotechnical engineering modules of the New Zealand Ministry of Business, Innovation & Employment (popularly known as the MBIE modules), and other relevant references as related to some specific specialist experimental investigations.

In this Chapter, the relevant theoretical frameworks and laboratory testing methods were applied to derive the required advanced soil geomechanical data which are required to achieve the stated objectives as per section 1.4 of Chapter One. As a recap, the study objectives include deriving the critical state classification characteristics, evaluating the soil dynamic PWP properties, experimental study of the undrained static/flow liquefaction behavior of loose deposits of varieties of clayey sands, soil geomechanical data validation by numerical modeling with the application of a typical critical state-compatible advanced constitutive numerical model (i.e., the Norsand model). The current Chapter is considered the central processing unit in meeting the stated objectives.

CHAPTER 4: SHAKING TABLE DYNAMIC POREWATER CHARACTERISTIC TESTS

4.1 Introduction

In practice, in-situ soil tests are used in deriving the soil parameters with physical meanings for practical engineering applications. However, soil samples used in this study are laboratory-created samples and thus the results can not be directly compared with in-situ soils without reference to the relative densities at which tests were executed and applying the relevant similitude laws for the most suitable application interpretations. Moreover, a well-known issue is the problem of establishing correct model confining stresses relative to the high confining stresses inherent in prototype in-situ soils (Towhata, 2008). On this basis, model shaking tests are performed at low confining stresses (i.e., extremely loose deposits) for compensating for the effects of reduced geostatic stresses compared to that of in-situ soils. Therefore, the scaling or similarity laws, otherwise known as the similitude laws are relevant for logical interpretations of physical tests results. As it is practically impossible to meet all the scaling laws requirements, consequently, most researchers only select a few key model parameters for scaling.

The test procedures for executing the shake table experiments on all investigated soil samples have been previously discussed in chapter 3. The key elements for the investigation in the current study are itemized below as:

- 1) Investigating the dynamically generated excess porewater pressures (PWP) of the studied soil specimens as a result of the varied clay (kaolinite) contents embedded in the fabrics of the ECS,
- 2) Computing the amplification factors (AF) of all the studied soil samples,
- 3) Observations and records of the seismically induced immediate settlements based on the sensitivity influences of the varied kaolinite contents in ECS,
- 4) Studying the effects of recurring earthquakes on liquefaction extents by varying the intensities of base input motions successively. This scenario mostly referred to as aftershocks are most common during actual earthquake occurrences in real-life situations and it is of interest to understand the response of the nature of the investigated soil samples under this condition.

Other soil dynamic deformation properties were considered out of scope in the current study due to the availability of very limited research funds and other research resources. For instance, it is impossible herein to estimate the cyclic shear stresses which normally are computed from the small strain shear modulus (G_{max}), the G_{max} mostly are obtained by measured shear wave velocities (V_s), from either bender elements or resonant column test in typical laboratory settings. Following, the traditional liquefaction curves in the form of cyclic stress ratio (CSR) which

normally are plotted against the number of cycles causing liquefaction (N) are not considered here.

A more appropriate soil container to study the soil deformation properties have been explained in the literature and identified as the lamina shear box type. The soil samples' classification and permeability characteristics have been explained in chapter 3.

The main applicable proxy for identifying liquefaction herein include the liquefaction coefficient (r_u), already explained in section 2.1 of the literature and defined as the ratio of excess PWP to the initial effective stress, i.e., $r_u = \Delta u / \sigma'_0$.

4.2 The base input ground motions

As explained in section 3.7.5, a constant frequency of 10Hz was combined respectively with amplitude factors of 2, 3, and 4 to achieve three different cases of base input motions. The subsequently synthetic ground motions (acceleration time histories) were classified as a low-shake (tagged as F10A2), intermediate-shake (tagged as F10A3), and high-shake (tagged as F10A4), respectively. The typically derived input base motions for the above-specified motion intensities as captured by the installed accelerometer on the shake table which was named as ACC1 from Figure 3.33 are shown in Figure 4.1 to 4.3. The achieved testing maximum PGA ranged between 0.1 and 0.45g.

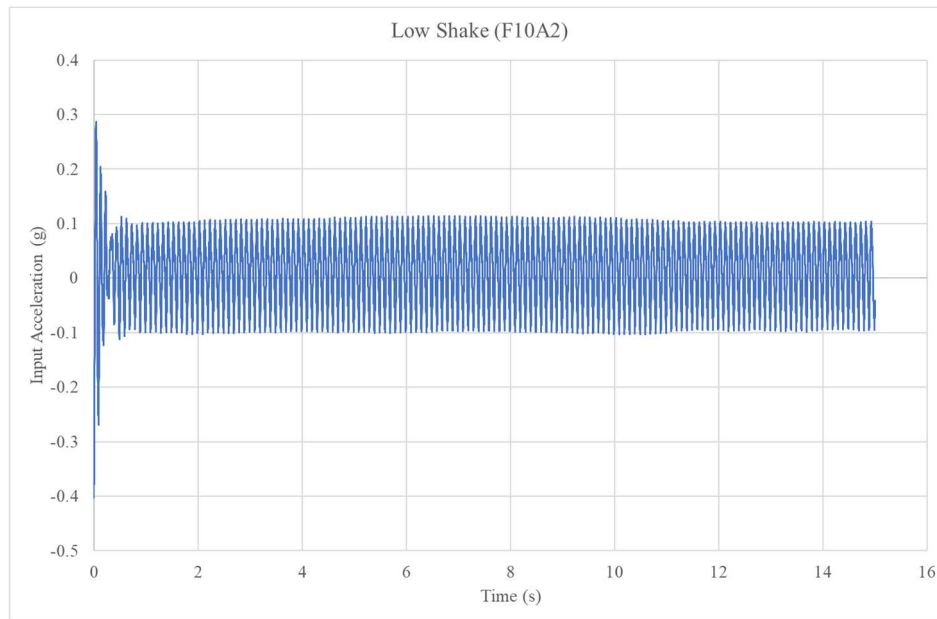


Figure 4.1 Base input motion for the low-shake (F10A2) case

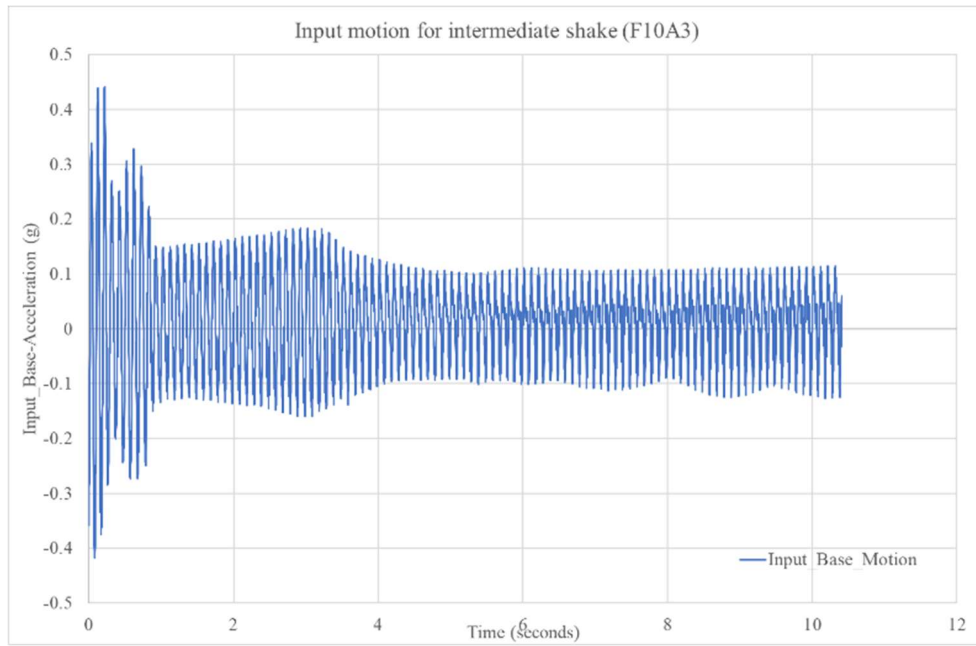


Figure 4.2 Base input motion for the intermediate-shake (F10A3) case

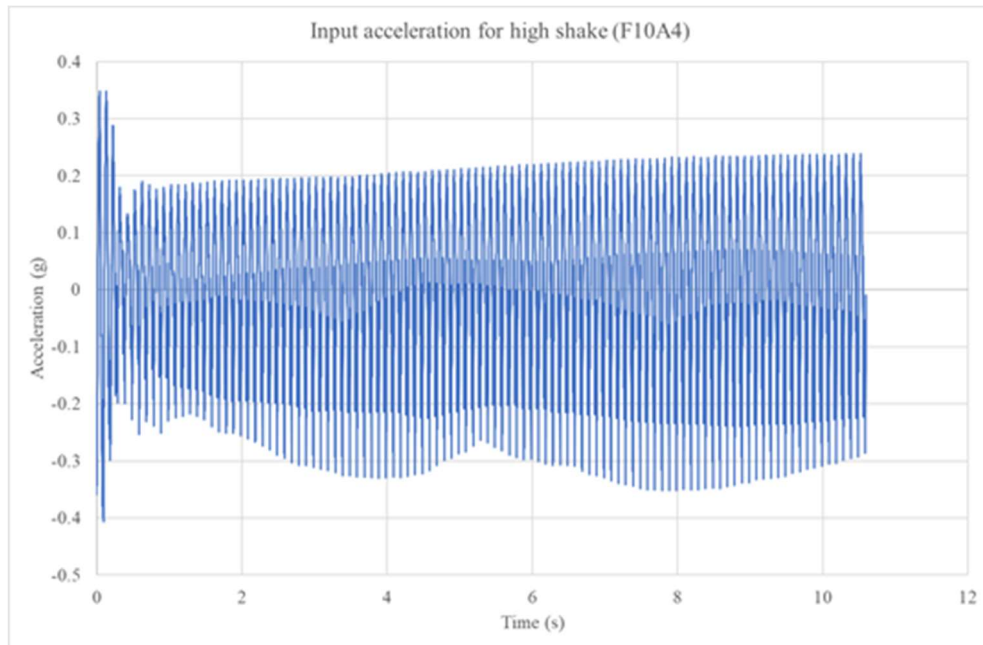


Figure 4.3 Base input motion for the high-shake (F10A4)

4.3 The excess porewater pressures characteristics

The excess porewater pressures (PWP) at the two transducers locations (i.e., PP1 and PP2) were simply derived as the difference between the measured PWP at every test point (denoted as u_i) and the initial PWP (denoted as u_0). It follows that excess PWP is denoted and expressed as $\Delta u = u_i - u_0$. Liquefaction and interpretation threshold range is such that when $r_u \geq 1$, full liquefaction is said to occur; when $r_u = 0.25$ to 0.70 , it implies that partial occurrence of liquefaction (cyclic mobility) has occurred and where $r_u = 0$, a condition of no liquefaction is reported.

4.3.1 Analyses and discussions of the low-shake case (F10A2)

As shown in Figure 3.37 of section 3.7.2, PP1 is the transducer measuring the PWP at about the models' mid-depth, and PP2 records the PWP at the model near-surface ground depth. All the derived parameters were subsequently converted to a prototype scale by applying the relevant scaling factors specified in Table 3.16 of section 3.7.4 to represent the prototype scale in the dynamic configuration domain. Specifically, the time scale was multiplied by $\lambda^{0.75}$ and the porewater pressure by λ . Figure 4.4 shows the measured excess PWP at both transducers during the low-shake intensity (F10A2).

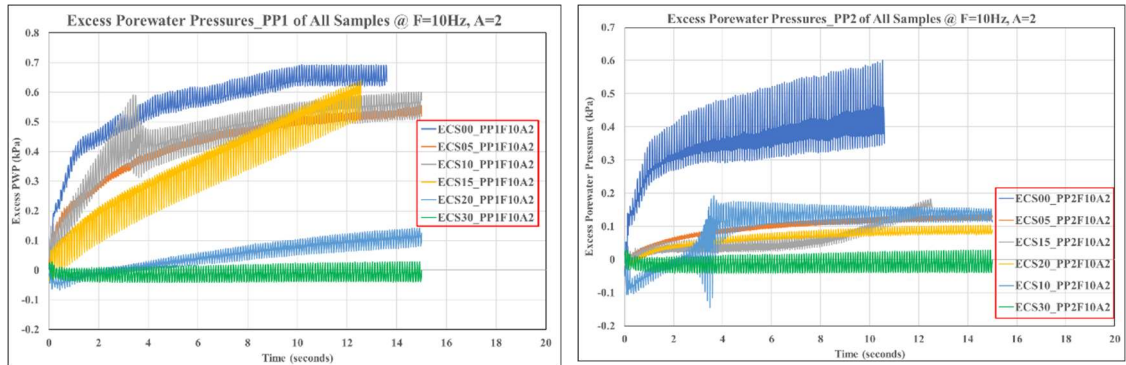


Figure 4.4 Excess porewater pressures (Δu) for the low-shake (F10A2) event @ PP1 and PP2

As can be seen from Figure 4.4, the clean sand (i.e., ECS00) has the most increased sensitivity response to change in PWP during the low-shake regime and shows the highest magnitude of excess PWP evolution in all the studied soil samples. Also noticeable is that the near-surface manifestation of liquefaction is highest in ECS00 (i.e., the clean sand sample). On the contrary, at PP2, other samples with more clay (kaolinite) showed a rather low excess PWP at the near ground surface of the models. Figure 4.5 shows the corresponding liquefaction coefficient (r_u) plots. According to the r_u -plots, ECS00, ECS05, and ECS10 first reached the condition of zero effective stress (i.e., $r_u = 1$) at the models' near-surface (i.e., the PP2-transducer) while the effective stresses at the models' mid-depth (PP1-transducer) did not reach this condition and subsequently, the confirmed manifestation and observation of liquefaction firstly at the near ground's surface for prototype soils. Recalling the specified interpretation range for r_u , a condition of partial liquefaction is recorded for ECS00, ECS05, ECS10, and ECS15 at the models' mid-depth (PP1) as can be seen in Figure 4.5(a), and no liquefaction for ECS20 and ECS30.

Furthermore, mostly observed at PP2 were the greatest change in porewater pressures than the estimated initial effective confining stress at the concerned elevation depth level. Realistically, the excess PWP should not be greater than the confining stresses because the rise in PWP usually is due to the increased effect of the overburden mass, the reason for this scenario may be identified as the rise in water-table elevation after the first shaking. A similar observation on the above situation has been formerly reported in previous studies such as that of Fiegel and Kutter (1994).

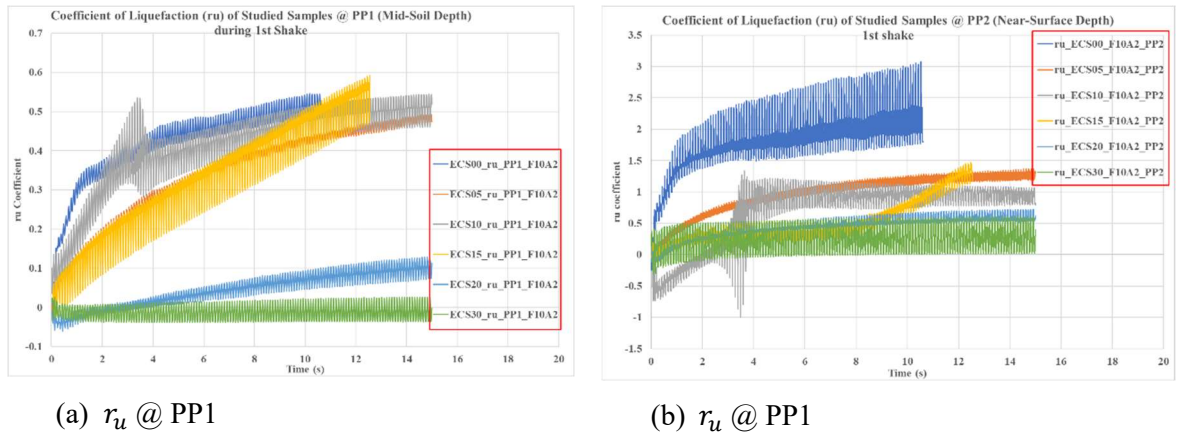


Figure 4.5 Liquefaction coefficient (r_u) for the low-shake (F10A4) events @ PP1 and PP2

4.3.2 Analyses and discussions of the intermediate-shake case (F10A3)

The excess PWP pressures during the intermediate-shake events are shown in Figure 4.6 and the coefficient of liquefaction is shown in Figure 4.7. As can be seen in Figure 4.6(a), a similar trend of the observed PWP behaviors in the low-shake case is reported at the models' mid-depth (PP1) except for the transitional characteristics which were observed between ECS10 and ECS15.

Further, the effect of sample densification as a result of the first shake is evident in both transducers during the 2nd intermediate shake events output and more evident at the near-surface transducer (PP2) with nearly flat characteristic curves. This is because the sample had already liquefied at the near-surface during the low-shake events. The samples that re-liquefied/liquefied at the PP2-transducer (near-surface) were the ECS00, ECS05, and ECS15 with ECS20 showing more of the cyclic softening phenomenon. The excess PWP plot indicates that ECS15 and ECS30 were dilative with evidence of negative pore pressures while other samples showed contractive behaviors on the contrary.

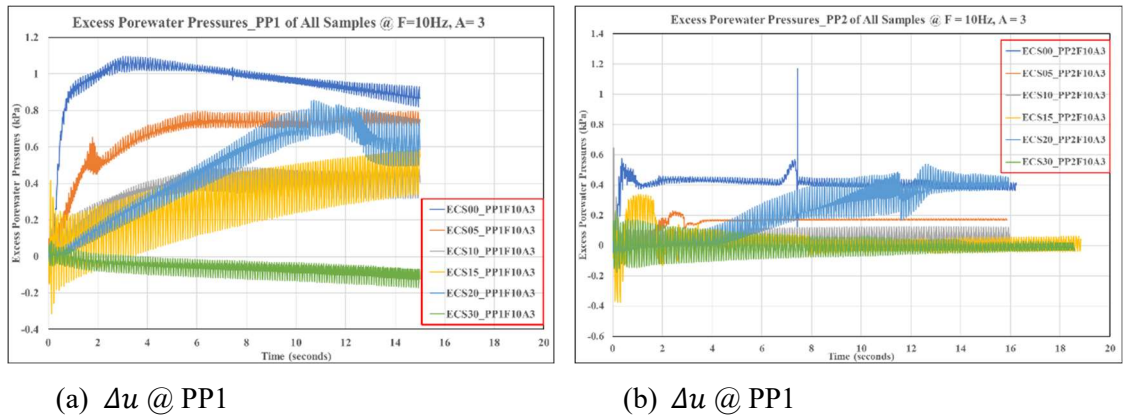


Figure 4.6 Excess porewater pressures (Δu) for the intermediate-shake (F10A3) event

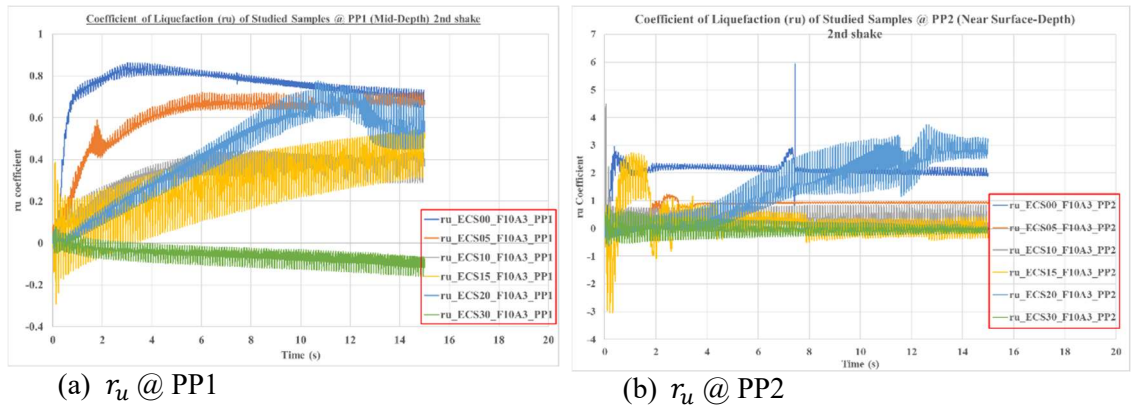


Figure 4.7 Liquefaction coefficient (r_u) for the intermediate-shake (F10A3) events

4.3.3 Analyses and discussions of the high-shake case (F10A4)

During the third case shaking, the majority of the samples had already densified due to previous shakes except for ECS00 and ECS05 which showed a rise in excess PWP. As can be seen in Figure 4.8 to 4.9, despite densification of the soil samples, the observed highest excess PWP occurred in the clean sand sample (ECS00) during the high-shake. The other key observation here is that the soil sample with the highest clay content (ECS30) exhibited the most dilative tendencies and softening confirming the phenomenon of cyclic softening in clayey samples at significantly high dynamic strains.

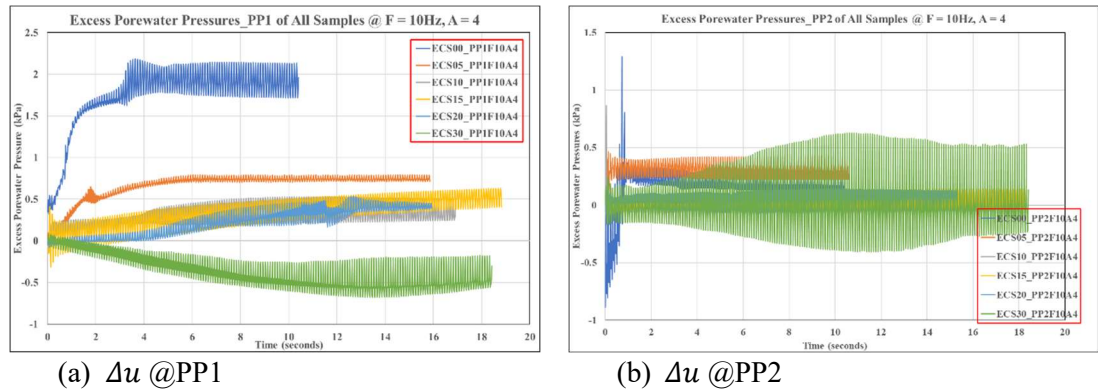


Figure 4.8 Excess porewater pressures (Δu) for the high-shake (F10A4) event

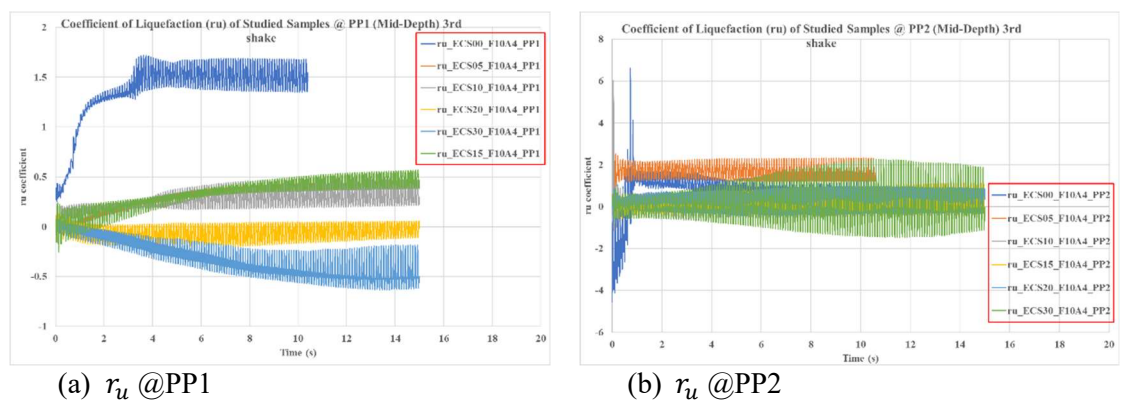
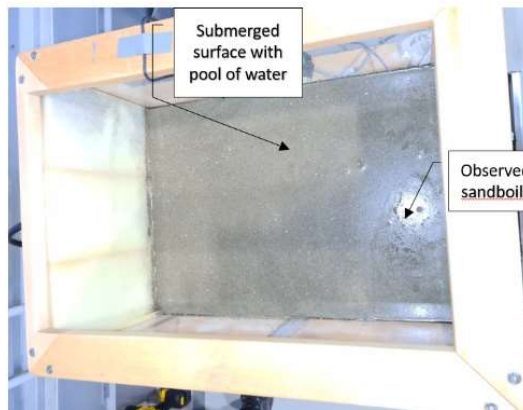


Figure 4.9 Liquefaction coefficient (r_u) for the high-shake (F10A4) events

4.3.4 Other observed key manifestations of liquefaction

Observations and pictures taken at the end of each shaking case indicated a descending order of the magnitude of extents of submerged soil model surface, deformation, and liquefaction extents from sand samples containing no kaolinites to the samples with the highest clay content (i.e., ECS30). Figure 4.10 shows the magnitude of the submerged soil model surface after the first shake



(a) ECS00 at the end of the low-shake case



(b) ECS05 at the end of the low-shake case



(c) ECS10 at the end of the low-shake case



(d) ECS15 at the end of the low-shake case



(e) ECS20 at the end of the low-shake case



(f) ECS30 at the end of the low-shake case

Figure 4.10 Observed surface manifestation of liquefaction in all the studied soil specimens

4.4 The seismically-induced immediate settlements

The cumulative seismically induced settlements at the soil model ground surface during the three shaking events were manually read-off from the printable rulers installed on the soil box. Observations from the settlement data indicate that the immediate settlement was highest in the clean sand sample (ECS00) and this confirms the typical expectations from a normally consolidated (NCL) soil such as sand. Even though compressibility is usually higher for clayey soils in a drained condition, the observed results herein under the undrained conditions indicated that the seismically induced immediate settlements decreased as the kaolinite contents increased. Refer to the statistical bar chart shown in Figure 4.11 for confirmation of the above inferences.

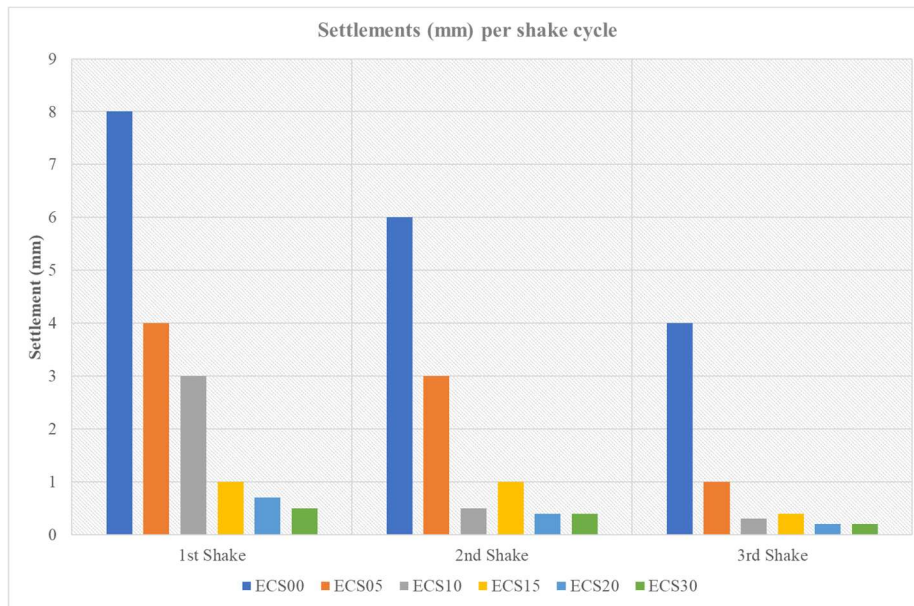


Figure 4.11 The immediate settlements for all samples

4.5 The soil amplification characteristics

The soil dynamic amplification factor (AF) is defined as the ratio of the horizontal peak ground acceleration (PGA) at the ground surface to the PGA from the bedrock or the earthquake acceleration ratio at which the earthquake acceleration would reach the ground surface (Özdağ et al., 2015). In earthquake-resistant designs, one of the key parameters for design is the PGA and this parameter helps to predict correctly when the magnitude of acceleration change coming from a bedrock would reach the ground surface. The AF values of the studied soil samples herein were computed as the ratio of the PGA from the ground accelerometer (AC2) to the PGA of the base input accelerometer (AC1). To view the amplification behavior of the studied soils more clearly, results were plotted on a three-dimensional bar chart plot in Figure 4.12.

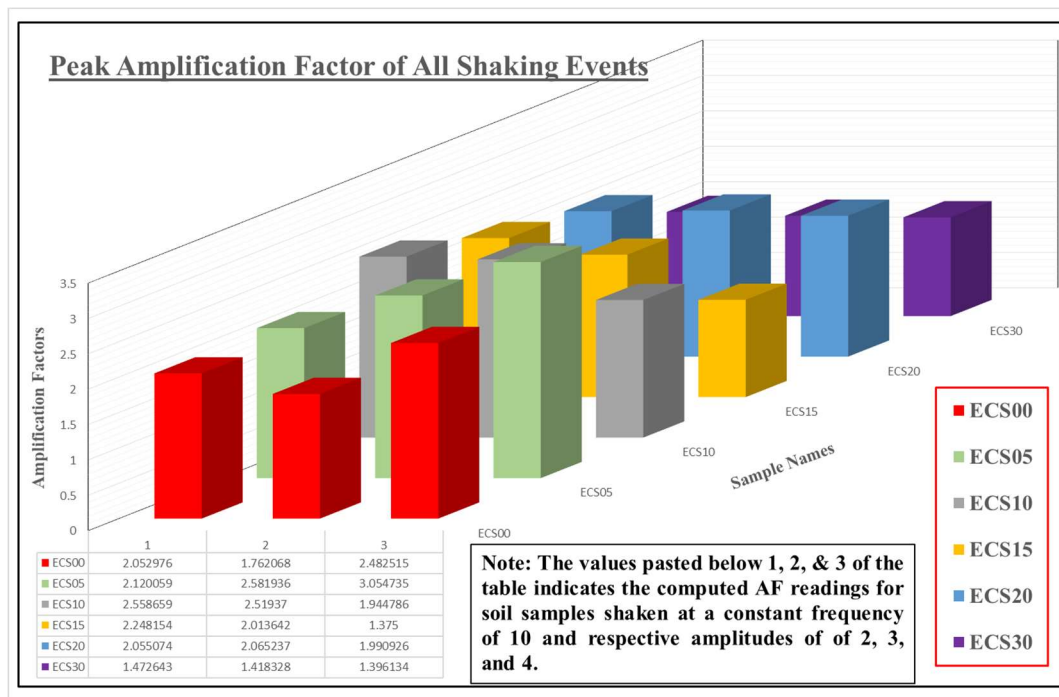


Figure 4.12 The computed amplification factors (AF) for all samples and shaking cases

As can be inferred from Figure 4.12, the soil sample with the highest amount of kaolinite exhibited the lowest AF suggesting that the PGA would likely travel slower in soils containing clays. The granular structural arrangements of cohesionless materials such as sand with particle-to-particle contact would experience faster travel of the PGA emanating from bedrocks.

4.6 Summary

This chapter explains a few significant dynamic characteristics of the studied remolded soil specimens while utilizing a 600N rated-capacity shaking table at the Geotechnical Laboratory of the Auckland University of Technology, New Zealand. The utilized proxy for interpreting the liquefaction characteristics of the soil samples is the liquefaction coefficient (r_u), simply expressed as the ratio of the change in PWP to the total effective confining stress. Observations from the study indicated and confirmed the comparative liquefaction characteristics of a wide range of samples with varying clay (kaolinite) contents. As expected, the sand sample with no clay content (ECS00) exhibited the highest manifestation of liquefaction susceptibilities and other seismically-induced failure-related mechanisms. Further analyses were carried under the undrained monotonic triaxial compression tests for the clean ECS00 and ECS30 as they showed the most extreme generated excess PWP characteristics. The shaking table device at AUT assisted in overcoming the previously highlighted limitations associated with large-shake devices and facilitated the parametric study of varieties of remolded soil samples in the laboratory. Such parametric studies with the application of large-scale, conventional shake tables are still relatively scarce in the literature. The reason for the scarcity of such studies is not far-fetched as such tests

could be overly costly, time-consuming, and laborious to prepare the required size of the physical soil models.

CHAPTER 5: THE STEADY/CRITICAL STATE UNDRAINED STRENGTH CHARACTERISTICS OF ECS AND CLAYEY-ECS

5.1 Introduction

A clearer assessment of the sudden transition of a stable ground from a drained state to a fully undrained/unstable one is still required for a realistic evaluation of the ground's overall stability and subsequent recommendation of suitable factors of safety in geotechnical engineering practices. Soil liquefaction is simply a different aspect of the soil behavior, and it is not by any means compulsory for an earthquake to occur before the former triggers; static loading under unfavorable soil conditions could trigger static, otherwise known as flow liquefaction, whereby the soil transits from a stable/drained to unstable/undrained state. The common consequences of a non-standardized assessment of the ground's stability may include but are not limited to failures due to landslides in steeped natural slopes, earth dams/tailings dams, hydraulically deposited artificial fills and reclaimed lands near coastlines (Verdugo & Ishihara, 1996). The above-mentioned failures can be very expensive and their effects on human lives sometimes lead to avoidable deaths and or fatalities.

In general, soil liquefaction is a major threat to engineering facilities/infrastructures constructed with or on saturated sandy soils (Robertson, 2010). The two well-known types of liquefaction failures include cyclic mobility or cyclic softening and flow or static liquefaction. A typical characteristic of the former liquefaction type may result in zero overburden stress due to cyclic/dynamic/earthquake loadings and the consequential loss of the soils' shear strength and zero or little effective stress whose principal function is to hold the soil grains together. A steep and high-magnitude strain-softening typifies the latter type of liquefaction failure with immediate loss of shear strength and it is also often referred to as flow liquefaction (e.g., Jefferies & Shuttle, 2020). The current research project focused more on the static liquefaction behavior of the studied reconstituted soil specimens by studying about five different aspects of the soil behavior under static/monotonic loads (i.e., triaxial compression conditions) including the deviatoric stress-strain relations, the ESPs, the volumetric strain, the consolidation characteristics, and the evolution of the excess PWP. Only one key aspect (i.e., the generation mechanism of excess pore water pressure, PWP) was investigated in the related earthquake-triggered liquefaction cases as explained in the previous Chapter 4, modeled through the physical model (shaking table tests).

A review of the subject literature indicated that several hybrids of proxies have been proposed in the past to analyze flow liquefaction-related mechanisms in sandy soils. However, it turns out that the concept of steady-state (Poulos, 1981), and the critical state (Schofield & Wroth, 1968) are the two most synchronized frameworks in the literature and have been widely referred to as the same. The key identifiable difference between the two as mentioned by Jefferies and Been (2015) is that the steady-state (SS) has no computable model while the critical state (CS) has. The similarity between the two is that during undrained compression loadings, a continuous state of

soil deformation is experienced at a constant specific volume (v), constant mean effective stress (p'), and deviatoric stress (q). In theory and practical computations, the critical state CS framework is a robust, tested, and well-established concept in the literature, correlating both the soil's consolidation, strength, and deformation characteristics. However, it is surprising to note that it is still rarely applied in practical geotechnical projects across the globe in 21st-century routine geotechnical engineering practice.

The current chapter first summarized the several proxies that were applied in interpreting the results of triaxial monotonic tests for an evaluation of the static/flow liquefaction behavior of all the studied soil specimens. The chapter focused on the discussions of the undrained monotonic CS responses of ECS and its clayey variants (or sand matrix soils or clayey sands). The numerical validation of the soil properties for all studied soil specimens was not possible as a result of research budget restraints since several triaxial monotonic tests are required for the correct calibration of the applied advanced numerical framework (Norsand model). Therefore, it was concluded in this research project to provide discussions based on 1) experimental evidence of the undrained monotonic behavior of five remolded soil samples executed at 50kPa, 100kPa, and 200kPa mean effective stresses in combination with a wide range of void ratios and 2) numerical validation of the selection of two observed extreme cases. The so-called extreme cases above are those of 1) the primary sand sample (ECS00) and 2) clayey variants of the former after mixing the same with 30% by weight of industrial kaolinite (ECS30) and the overall liquefaction behavior summary was 100% flow failure. The above selection decision was further based on the obtained undrained soil behavior responses/results from the previously executed physical model shaking table tests. From the shaking table tests, it was evident that the evolution of excess PWP decreased as the clay content increased when dynamic excitations were applied at the base of the model to mimic earthquake-induced liquefaction scenarios. In the shaking table tests, the ECS00 was observed to fall on the worst-case for typical cyclic liquefaction judging by the generated excess PWP. In addition, the ECS30 falls on the worst-case scenario of typical cyclic mobility otherwise known as cyclic softening.

The CS can be considered an intrinsic property of soils and can be determined unambiguously since they do not depend on the soil state, geology, or boundary conditions. The main quantifying parameter for the soil's initial state is the state parameter (ψ), simply defined as the difference between the current void ratio and the critical state void ratio.

The east coast sand (ECS), described in Chapters 1 and 3, is a typical example of clean sand that is utilized in local geotechnical-related construction practices around the Auckland region in New Zealand. The motivation for choosing this sand as the study's primary soil sample for investigation is that no publishable geotechnical engineering data currently exists in the literature database for the same. Therefore, this study seized it as an opportunity to utilize the ECS as a case study and determine its critical state characteristics and the ECS variants created by admixing varying

percentages by weight of a typical low-plastic fine (kaolinite). Under laboratory conditions, it is rather almost impossible to create the same state of some existing soft ground as sample handling in the laboratory becomes highly problematic.

One of the lessons learned in this study is that certain maximum void ratios must be targeted and attained during sample preparation for a successful workable critical state testing to logically provide the expected required data under the triaxial conditions. In an attempt to create very loose samples for critical state testing, several sample collapses were experienced even before the saturation was complete. Sand samples containing clayey fines are more difficult to handle in the laboratory when attempting to create non-dilating samples as they experience a significant amount of volume change and contraction throughout their testing cycle. The corresponding volume change and void ratios are very difficult to measure especially during saturation, even when the moist tamping technique of sample preparation is applied in its reconstitution process.

The interpretations of results follow closely those detailed in the SS/CS framework. The applied advanced numerical model, Norsand captures the key elements of the undrained soil characteristics ranging from no-plasticity to high-plasticity, softening to hardening, a combination of mean effective stresses and initial void ratios, typically ranging from as low as 50kPa to as high as 500kPa and 0.500 to 1.000, respectively. In addition, the Norsand is capable of capturing a wide range of generated excess PWP under varying mean effective confining stress. A summary of the Norsand model and calibration of model parameters have been presented earlier under sections 3.6.1 and 3.6.2 respectively. The numerical modeling methodology has been previously described under section 3.6.3, therefore, only the soil properties and output results are explained in the current Chapter.

The textbook soils (mostly referred to as clean sands and pure clays) are well-researched while in real world, the majority of the existing in-situ soils in the field situation exist as mixed soils, containing both coarse and fine-grained particles (e.g., sand admixed with some clayey fines), hence a key relevance of the current study. The latter type of soil is mostly referred to as non-textbook soils and understanding their sudden transition from a drained condition to an undrained state is crucial for providing a fairly accurate assessment of their critical state strength characteristics and liquefaction factors of safety (FOS) in designs during routine Geotechnical Engineering practice.

Several methods currently exist in the literature that are applied as an index for quantifying flow liquefaction susceptibilities and only a few are mentioned here. As found in Lade (2018), there are two common failure criteria for interpreting triaxial results, namely: 1) the occurrence of failure when the deviator stress gets to a limiting value, $(\sigma_1 - \sigma_3)_{\max}$ and 2) the occurrence of failure when the effective principal stress ratio gets to a limiting value, $(\sigma'_1/\sigma'_3)_{\max}$. Mostly, the first failure criterion is applicable in total stress analyses while the second criterion is utilized for

effective stress analyses. As suggested by the former author, what is responsible for static/flow liquefaction failure is termed instability and this is quite another different concept from the failure criteria earlier stated. Hence, liquefaction analyses are analogous to instability susceptibility and their consequent applications in several advanced numerical frameworks as a means of measuring the soil's undrained strength capacity (typically from the effective stress paths) to quantify liquefaction extents. One such proxy for identifying instability of soils is termed the instability line (IL), other schools of thought call this collapse line (CL) or flow liquefaction line (FLL), see Figure 5.1 as per J. Yang (2002) for the location of IL on typical effective stress path (ESP) in the $q - p'$ stress invariant space. One can see the IL simply as straight line passing through the origin

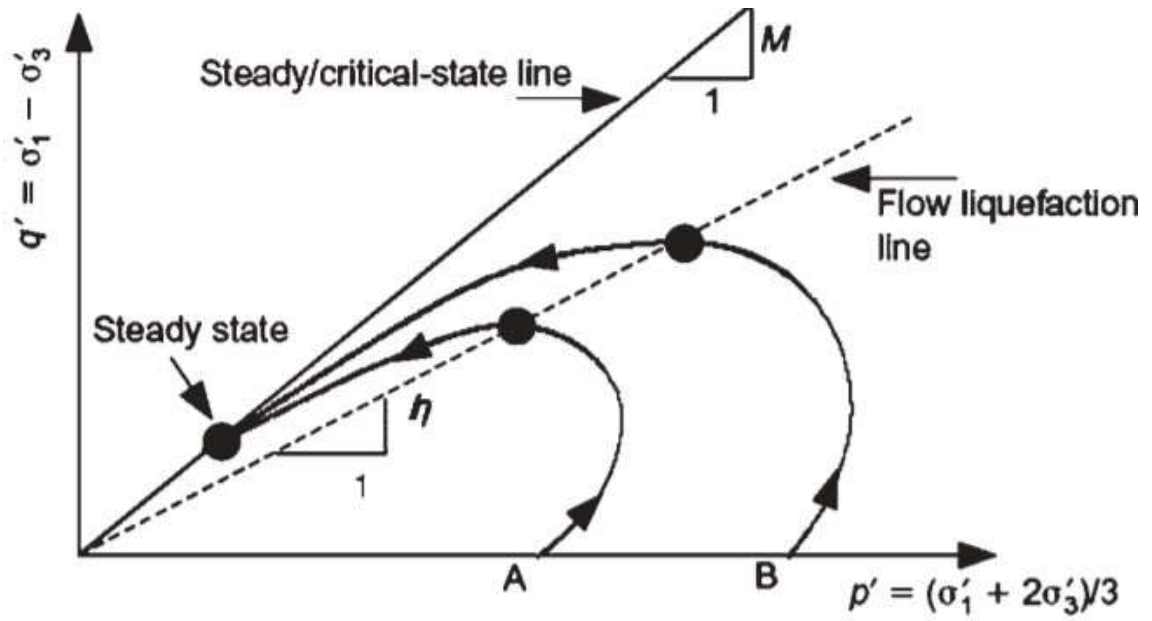


Figure 5.1 The schematics of locating the IL in q - p' stress space as per Yang (2002)

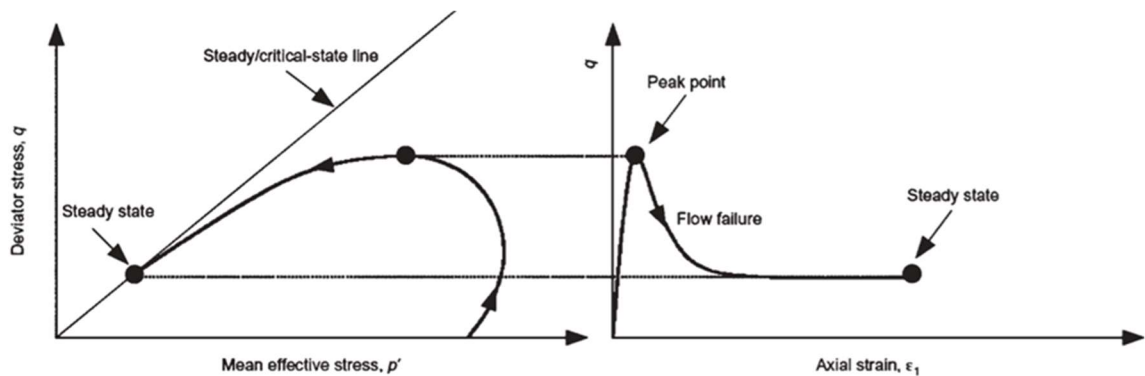


Figure 5.2 The schematics of locating the IL in q - p' stress space as per Yang (2002)

and the peak points of the effective stress path or the point of initial peak stress difference/deviator stress. The parameter for quantifying the magnitude of IL is termed " η_{IL} ", the maximum stress ratio. The IL delineates between unstable and stable states/zones of soil undrained behavior where the parts on the right-hand side of this line are termed stable and the part to the left-hand side of this line is regarded as unstable (Jafarian, Ghorbani, et al., 2013). The idealized behavior of loose

sand according to Sladen (1985), as shown in Figure 5.2, is very useful for understanding the undrained behavior of loose sands under the action of static loads. Static liquefaction corresponds to the point where the mean effective stress, $\sigma_3 = 0$ and $\sigma_1 - \sigma_3 = 0$, (Yamamuro & Lade, 1998). The simplest way to examine static liquefaction starts by examining the typical characteristic stress-strain curves in correlation with the $q - p'$ stress invariants charts, and the soils' steady-state or critical state properties. The mean effective stress at the onset of a constant rate of deformation with no change in deviator stress is referred to as the CS. The yield surface that is otherwise known as the effective stress path (ESP), i.e., the $q - p'$ stress invariant space may be viewed as the strength envelope or strength capacity of the soil (Jefferies & Been, 2015).

The phenomenon of static liquefaction metamorphizes at low confining stresses in very loose sands that are supposedly looser than their critical. The characteristic state otherwise known as the Mohr-Coulomb (MC) line is defined as the characteristic line that occurs at the point of transition from contraction to dilation through the origin of the stress path (Ibsen, 1999). Doanh et al. (1999) noted that static liquefaction in very loose sand is characterized by a sudden decrease in the deviatoric stress after achieving a peak value at the beginning of an undrained shearing. The above characteristic is followed by a rapid decrease in the shear stress until the steady state of deformation in which the undrained shear strength remains constant within a large range of axial strains. In addition, the generated excess PWP is characterized by a rapid increase to being constant over a range of axial strains. The state concept, otherwise, the CS is a very useful tool to characterize soil liquefaction behavior and determine possible factors of safety when the steady state of stress is compared with the applied field stress.

5.1.1 The state characterization

The indices of how loose or dense a sample is known as the state parameter and is widely considered a significant index of static liquefaction/flow failure in soils in critical state soil mechanics (CSSM). The applicable parameters for characterizing the initial state of the reconstituted soil specimens under the monotonic triaxial compression condition are the post-consolidation and critical state void ratios (e, e_{CS}), and the state parameter (ψ), respectively. The state parameter (ψ) is simply evaluated based on Equation 5.10, where the e_{CS} is the void ratio at the critical state.

$$\psi = e - e_{CS} \quad 5.10$$

In its simplest form, the inferred interpretation of the state parameter for quantifying flow liquefaction susceptibility is that a positive ψ implies a loose soil sample that is contractive while a negative ψ means a soil specimen that is dense and dilative (i.e., can experience volume expansion). One key fact established in the literature is that loose sand specimens would tend to contract while dense sand tends to dilate (Jefferies, 1993; Jefferies & Been, 2015).

5.1.2 The state concept as a basis of soil behavior type classification

Instances of varieties of flow liquefaction response types for sandy soil under undrained, triaxial, monotonic compression conditions with the ESP ($q - p'$) in correlation with the deviatoric stress strain as illustrated by Rees (2010) and Rahman et al. (2014a) is shown in Figures 5.3 (a) & (b), respectively. The flow responses are referred to as strain-softening otherwise known as flow failure (FF), strain-softening changing to strain-hardening (i.e., limited flow, LF), and complete strain-hardening (i.e., no flow, NF). The nominated abbreviations above are further applied in further discussions of this chapter as classifications of the undrained soil behavior exhibited by each studied soil specimen. The variations in the soil undrained strength characteristics between the three stress paths can be directly associated with the difference in relative densities, void ratios of the soil sample, state parameter, and the inter-particle mean effective stresses between the soil grains/fabric.

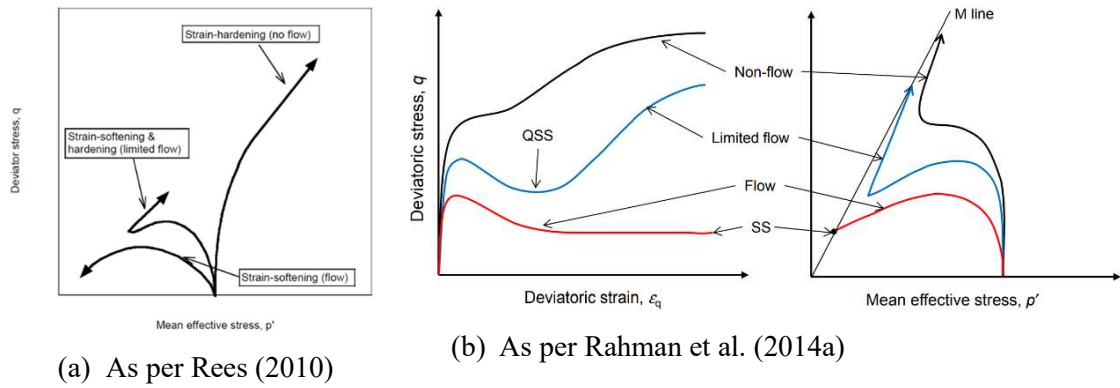


Figure 5.3 Typical undrained monotonic responses classification types for sands

Vaid et al. (1989) also provided similar schematics as shown in Figure 5.3 above for typical soil undrained behavior under triaxial compression load, and these are particularly useful as a template for interpreting the characteristics of the studied and obtained results herein. As explained by Rahman et al. (2014a), FF behavior is usually characterized by a rapid increase in deviator stress after which the soil softens to a residual value (SS/CS), and the constant rate of deformation sets in with no change in deviatoric stress (i.e., the so-called steady-state). Limited flow is characterized by softening of the soil element to a minimum state known as the quasi-steady state (QS) while further imposed shearing would cause the soil specimen to experience hardening, as shown by the black line in Figure 5.3 (b).

5.1.3 Reference to the critical state line (CSL)

The correct identification of the critical state is significant to be able to numerically compute the soil undrained behavior under static loads, especially when applying an advanced critical state-compatible constitutive model such as the Norsand model. Jefferies and Shuttle (2020) described how to identify the CS for both drained and undrained triaxial conditions. For the drained conditions, the stress-dilatancy concept is the most reliable for determining the CS, especially for medium dense soil samples or soil samples exhibiting a complex pattern identified as strain-

softening and hardening (limited flow) as shown in Figure 5.3. Firstly, the drained triaxial data is first converted into stress-dilatancy plots as a function of stress ratios (η) on the ordinate plotted against the dilatancy (D^P) on the abscissa, followed by reading off the η corresponding to $D^P = 0$. Hence, $D^P = 0$ at maximum stress ratios η_{max} . The transformation of triaxial data to dilatancy plots is well-explained in Been and Jefferies (2004) and it is simply the numerical differentiation (using the central difference method) to compute the dilatancy (D). The values of the maximum stress ratio (η_{max}) and their corresponding minimum dilation (D_{min}) obtained in the validated drained tests are then utilized to derive the M_{tc} and N parameters which are important parts of the Norsand model soil properties. As found in Jefferies and Shuttle (2020), two key conditions need to be met to confirm the CS and they are enumerated below as:

- i) The stress ratio value corresponding to the point at which dilatancy (D^P) is equal to zero is the CS, expressed in Equation 5.11 as:

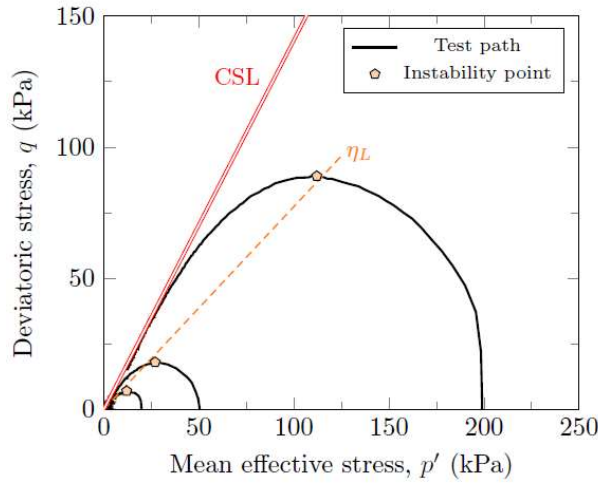
$$D^P = 0 \quad 5.11$$

- ii) The rate of change of the dilatancy with deviatoric strain must be equal to zero, expressed in Equation 5.12 as:

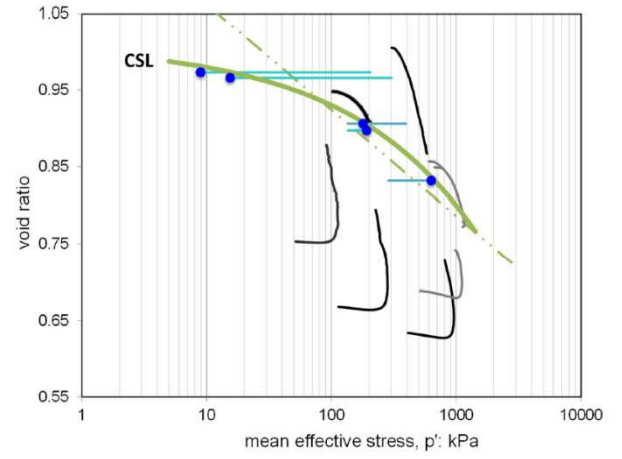
$$\delta D^P / \delta \varepsilon_q = 0 \quad 5.12$$

The point of stress reversal in the deviatoric – ESP stress-space, i.e., $q - p'$, is mostly referred to as the ‘pseudo-steady-state’ or ‘quasi-steady-state’ or ‘phase-change’ or ‘phase transformation’ in the literature (Jefferies & Been, 2015). It is considered crucial herein to depend on Equation 5.12 to derive accurate CS parameters for the validated selected soil specimens. The process that was followed to derive the CSL has been explained under subsection 3.6.2.

The key proxy for representing the CS is the CSL, from which the critical state parameters (Γ & λ) are calibrated and obtained for further computations of the soil behavior. The major application of the CSL is its usefulness to define a reference state for the onset of flow failure or static liquefaction and phase transformation in sands and quick clays. FF otherwise known as flow or static liquefaction is particularly identified as the behavior of very loose sands (i.e., sands that are looser than their critical). An example of the derived CSL by previous researchers for each of the stress-space representations is shown in Figures 5.4 (a) and (b) respectively.



(a) CSL in the $q - p'$ stress-space after Viana da Fonseca et al. (2021)



(b) CSL in the $e - \log p'$ stress-space after Jefferies and Shuttle (2020)

Figure 5.4 Illustration of the CSL in stress spaces

As shown in Figure 5.4 (a), the CSL, as a convention is mostly represented by double lines passing through the origin (i.e., 0,0) and the point of effective mean stress at the onset of CS. The instability line (IL) is shown in Figure 5.4 (a) as ηL , computed as the maximum stress ratios q/p' for all the undrained specimens.

The representation of the CSL in the SS $e - \log p'$ stress-space follows two types of methods as shown in Figure 5.4 (b), namely the semi-logarithmic and the power-law approach. The straight-line/semi-log method is assumed reasonable and appropriate enough herein for overconsolidated soils (OCC) or clays while the curved power law has been reported by several authors in the past, e.g., (Jefferies & Been, 2015; Jefferies & Shuttle, 2020; Viana da Fonseca et al., 2021) to best connect the CS points in the state plots, i.e., $e - \log p'$ stress-space. The relevant relation for the semi-log idealization is shown in Equation 5.13 and Equation 5.14 for the power law. Equation 5.13 has previously been described as Equation 2.19 in section 2.2.2 and Equation 5.14 is the same as Equation 2.22 and is only repeated here for brevity.

$$e = \Gamma - \lambda \ln p' \quad 5.13$$

$$e = A - B \left(\frac{p'}{100} \right)^c \quad 5.14$$

The evolution of the power-law curve was related to phenomena such as grain crushing effects, flow instability, low and high-stress states (Viana da Fonseca et al., 2021). For an undrained soil state in the monotonic compressive triaxial condition, the state point would normally move from an initial state (right) towards the critical state (left) as shown in Figure 5.4(b) since volume change is assumed zero during undrained shearing. On the other hand, in a drained condition, the state will move from the top to the bottom as a significant amount of volume change and void ratios is expected during drained shearing. Further, it is logical to say that the void ratios are

expected to decrease as effective confining stress of the soil increases thereby resulting in the sloping of the CSL from upper left to lower right on the $e - \log p'$ stress-space.

5.2 Discussions of the experimental static liquefaction behavior of the reconstituted soil specimens

The description of the studied reconstituted soil specimens has already been provided in subsections 1.6.1 and section 3.2. In addition, the details of the basic soil index classification characteristics and other relevant soil properties have been well-explained in Chapter 3. The order of the adopted naming nomenclature of the studied remolded soil specimens (i.e., ECS00, ECS10, ECS15, ECS20, and ECS30) is consequently followed in further discussions of the corresponding advanced soil geomechanical properties.

It is important to point out here that the majority of the obtained undrained stress-strain of the studied primary sand specimen (ECS00) did not show a constant rate of deformation, a notable feature of the SS. The above was due to two factors namely, the utilized triaxial device's load cell cannot measure a low change in deviatoric stress after FF has occurred. FF was the obtained typical characteristics of the investigated loose ECS, and tests were stopped immediately after the observed physical total collapse of the specimen inside the triaxial cell, which occurred mostly with the ECS00 (i.e., the clean sand specimens). Secondly, from an experimental perspective, SS implies that no change of deviatoric stress must be observed with shearing, meaning a constant rate of deformation on the deviatoric stress-strain plots must be attained with no re-gain of deviatoric stress with further shearing. The above condition was not achieved with the majority of the tested ECS00 during undrained shearing as this condition was only an approximation, similar observations have been reported in previous works (e.g., Rahman et al., 2014a). The typical characteristics of constant SS of deformation were rather achieved with other sand matrix specimens.

The key characteristic elements discussed under the obtained experimental evidence of the studied soil specimens herein include the deviatoric stress-strain and effective stress paths (ESP), the evolution of the excess PWP, and the corresponding critical state characteristics. The majority of the plots were annotated to provide clarity on several of the previously discussed indices of monotonic undrained soil behavior. Cross-examination and parametric comparisons of the undrained behavior of all studied five reconstituted sand specimens were carried out. Although, it is almost practically impossible to replicate the same void ratios for all soil specimens under laboratory conditions. Nevertheless, some comparisons were made by considering tests executed under the same initial mean effective stress levels, this is to enable some of the objectives of the current study to be achieved by studying the effects of the kaolinite clay on the geomechanical characteristics of the primary sand (ECS00).

5.2.1 Analyses of the deviatoric stress-strain, effective stress paths (ESPs), and excess PWP

The resulting deviatoric stress-strain(s) and ESPs for all the studied remolded sand specimens are consistent with other similar published results of typical sandy soils' monotonic behavior under the undrained static load condition. The characteristics charts of the primary sand sample (ECS00) is shown in Figure 5.5 to 5.7. The deviatoric stress-strain plots of all studied five soil specimens are annexed as Appendix L, the annotated ESP attached as Appendix M, and the evolution of the excess PWP as Appendix N. The key outputs of the undrained tests, executed at typical initial mean effective stresses of 50kPa, 100kPa, and 200kPa are summarized in Table 5.1. The above-specified mean effective stresses are more practicable for soils in routine geotechnical works and static failures are likely to occur in loose sandy soil deposits within the mentioned stress levels, hence, the justification for their selection for subsequent analyses.

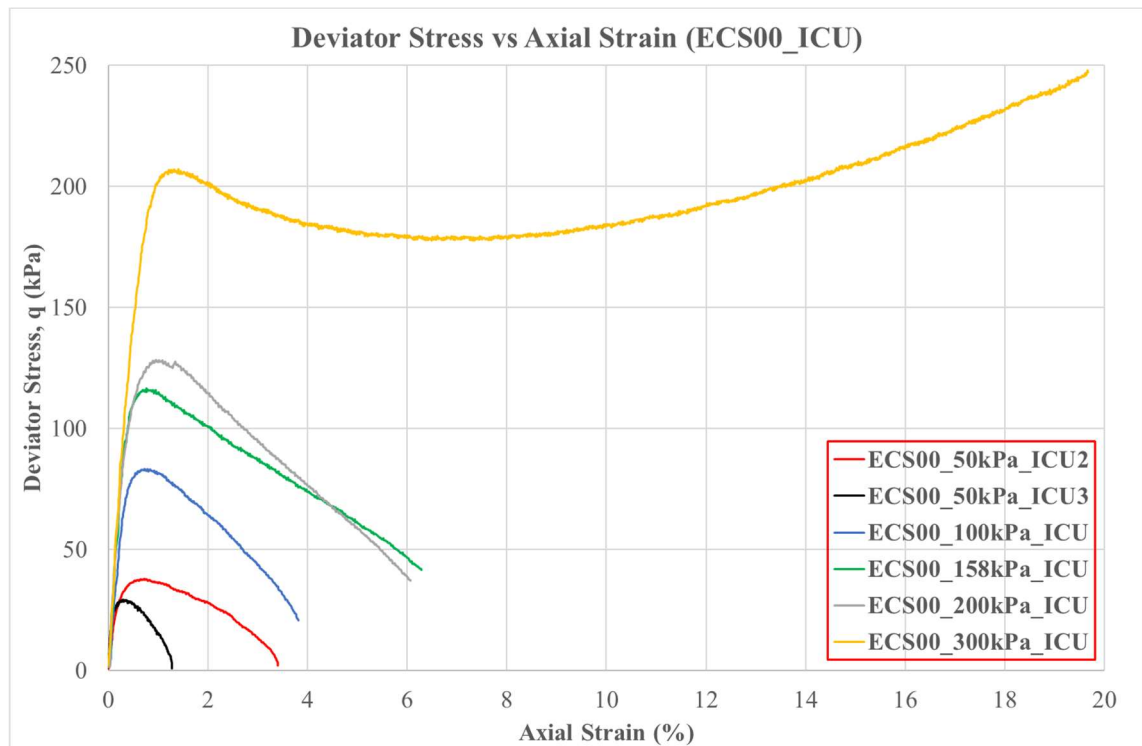


Figure 5.5 Deviatoric stress-strain of ECS00

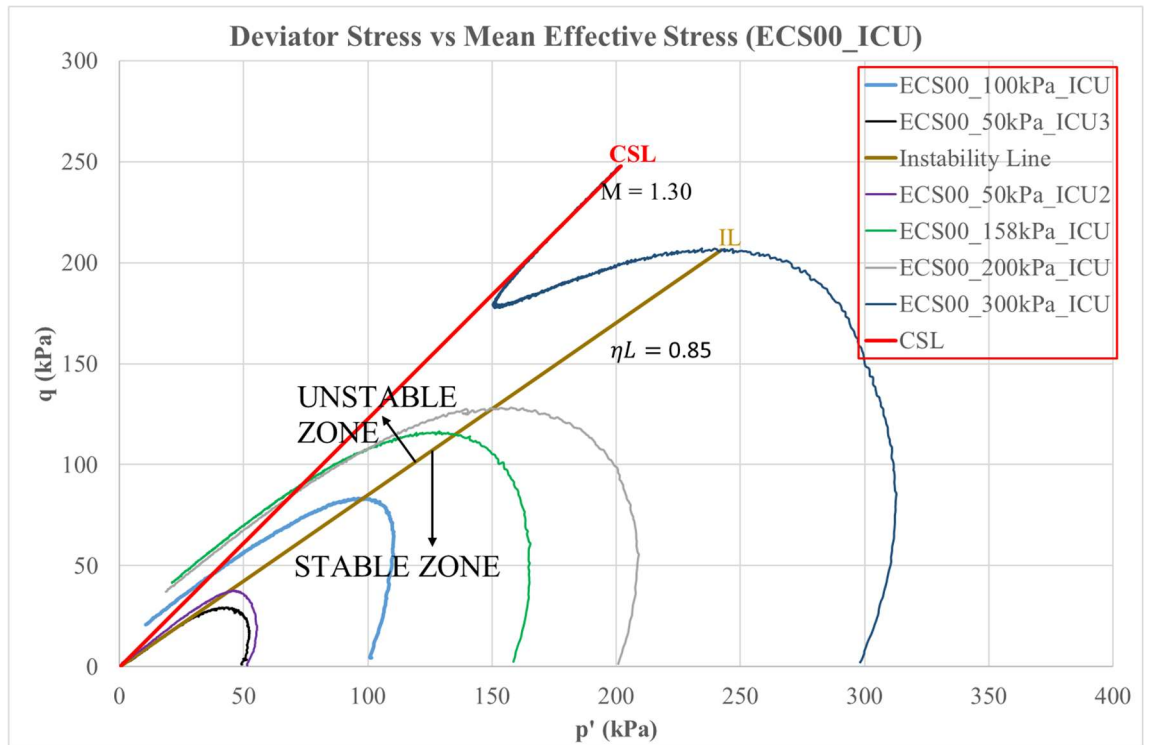


Figure 5.6 ESP of ECS00

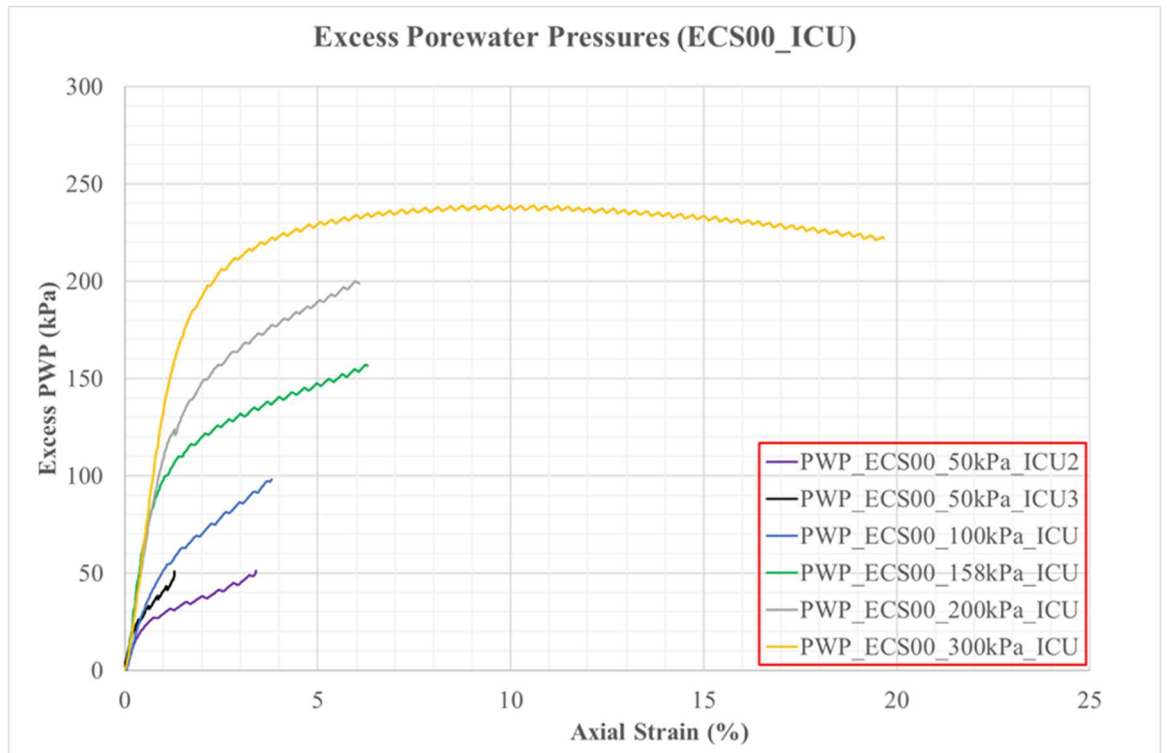


Figure 5.7 Generated excess PWP of ECS00 during monotonic shearing

In Table 5.1, all stresses are in kPa, p'_0 is the initial testing mean effective consolidation stress, e_{CS} is the estimated void ratio at the critical state (i.e., the post-consolidation void ratios for ICU), p'_{CS} is the estimated mean effective stress at the critical state as obtained from the ESPs and stress-

strain plots, q_{pk} is the peak deviatoric stress, p'_{pk} is the corresponding peak mean effective stress, PWP_{max} is the attained maximum excess pore water pressure, $M_{q-p'}$ is the critical stress ratio in the ESP stress-space (i.e., $q = Mp'$), η_L is the maximum stress ratio q/p' , and the subsequent failure types as deduced by comparisons with previous works (Rahman et al., 2014a; Rees, 2010).

One can see from Table 5.1 that the ECS00 and ECS30 soil specimens both experienced the fully contractive and FF behavior at all the testing stress levels with a positive state parameter indicating a loose state and a negative state a dense state. At a low mean effective confining stress of 50kPa, all the tested specimens typically experienced the contractive FF. ECS10 had a FF behavior at all testing P'_0 except at a higher testing P'_0 of 200kPa with LF characteristics with some trace of dilative tendencies. ECS15 only had a FF at a low 50kPa P'_0 , LF was the soil response at a higher P'_0 (100-200kPa). All the tested ECS20 had LF behavior at all testing stress levels with the soil specimen consistently showing dilation at approximately 20% axial strain for all stress levels. In summary, at higher testing pressures (i.e., ranging from 100kPa to 200kPa), the sand matrix soil specimens containing between 10% to 20% by weight kaolinite-clay content (i.e., ECS10, ECS15, & ECS20) showed some LF behavior, further confirming the fact obtained from the literature that sands containing plastic fines may not liquefy as fast as clean sand would do. The above-mentioned feature of sand matrix soils also indicates typical transitional soil properties. Transitional soils tend to exhibit undrained soil characteristics that are in between the contractive and dilative characteristics. Referring to the literature, the often-used term for the experienced FF type of the clayey sands is softening or cyclic softening/mobility particularly when soil liquefaction was induced by an earthquake.

Table 5.1 Result summary of undrained monotonic characteristics of tested soils

Sample Name	p'_0	e_{cs}	p'_{cs} (kPa)	q_{pk} (kPa)	p'_{pk} (kPa)	PWP_{max} (kPa)	$M_{q-p'}$	η_L	η_L Ave.	Failure type
ECS00	50	0.938	0	38.48	46.14	51.10	1.30	0.841	0.851	FF
ECS00	100	0.910	30	83.23	96.39	98.10		1.032		FF
ECS00	200	0.840	68	127.04	153.50	200.00		0.947		FF
ECS10	50	0.675	0	39.08	48.12	51.90	0.93	-	0.810	FF
ECS10	100	0.657	31	41.89	84.14	101.40		-		FF
ECS10	200	0.646	135	125.06	151.79	124.10		-		LF
ECS15	50	0.644	1	25.96	41.06	50.90	1.02	-	0.760	FF
ECS15	100	0.628	36	57.50	79.96	85.90		-		LF
ECS15	200	0.610	86	120.07	159.30	161.70		-		LF
ECS20	50	0.635	29	28.66	35.71	38.40	0.93	-	0.81	LF
ECS20	100	0.570	57	59.53	79.07	74.20		-		LF
ECS20	200	0.562	128	124.52	149.92	138.70		-		LF
ECS30	50	0.548	0	20.94	38.72	50.20	1.30	0.543	0.52	FF
ECS30	100	0.555	16	31.88	73.28	93.80		0.491		FF
ECS30	200	0.524	47	77.43	151.07	179.4		0.494		FF

The clean ECS sand specimen with no kaolinite in its fabrics, ECS00 recorded the peak deviator stress of 127kPa at a corresponding mean effective stress of 153.50kPa with testing confining

stress of 200kPa, suggesting that the ECS possesses the highest undrained effective strength when subjected to test at high mean effective stress, this fact further confirms the high probability of the occurrence static/flow liquefaction at low effective mean stress. The recorded highest effective strength in the ECS00 sand fabrics is due to the grain-to-grain contacts (friction) of the sand particles which enhances higher frictional resistance. On the other hand, for the case of the sand matrix specimens, the kaolinite-clay particles would most likely lubricate the void spaces of the sand fabrics in sand matrix soils samples thereby reducing the corresponding frictional resistance of the soil. On the contrary, the quick generation of excess PWP will be impeded as the clay content in the sand fabric increases.

One may also deduce from Table 5.1 that increasing the kaolinite content in the ECS00 sand would certainly decrease the magnitude of the critical state $M - line$ slope in the ESP stress-space. In addition, at the testing stress levels of 100kPa to 200kPa, the clayey sand specimens within the range of 10% to 20% kaolinite content (i.e., ECS10, ECS15, & ECS20) indicated the lowest evolution of excess PWP, which matched the observed undrained trend in dynamically generated excess PWP as per the shaking table physical models. The evolution of excess PWP is a well-known proxy for ascertaining the soil liquefaction state (i.e., either contractive or dilative) and a strong indicator of the liquefaction susceptibility in soils. The clean sand, ECS00 obviously had the highest excess PWP (~200kPa) at a testing stress level of 200kPa, further confirming that static liquefaction happens faster with clean sands due to either static or cyclic liquefaction. Figures 5.8 to 5.10 show the combined charts of all the studied soil specimens at the specified testing effective stresses for a clearer visualization of their corresponding flow liquefaction characteristics.

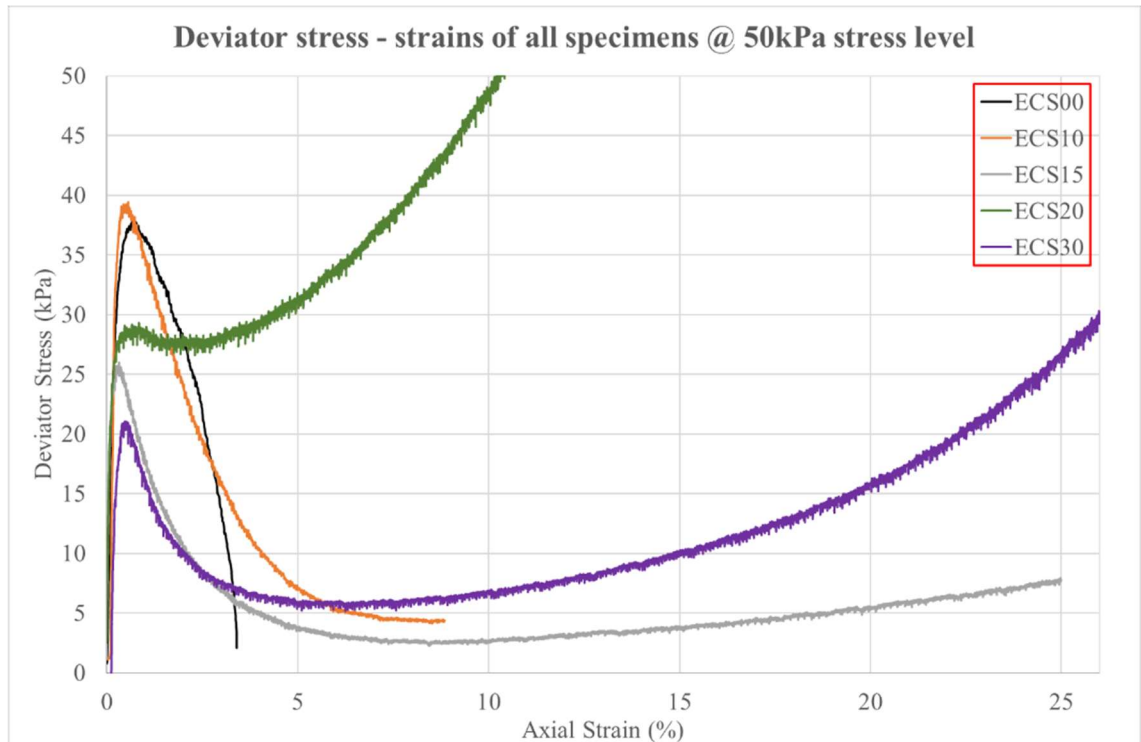


Figure 5.8 The deviatoric shear stresses of the soil specimens at 50kPa testing stress level

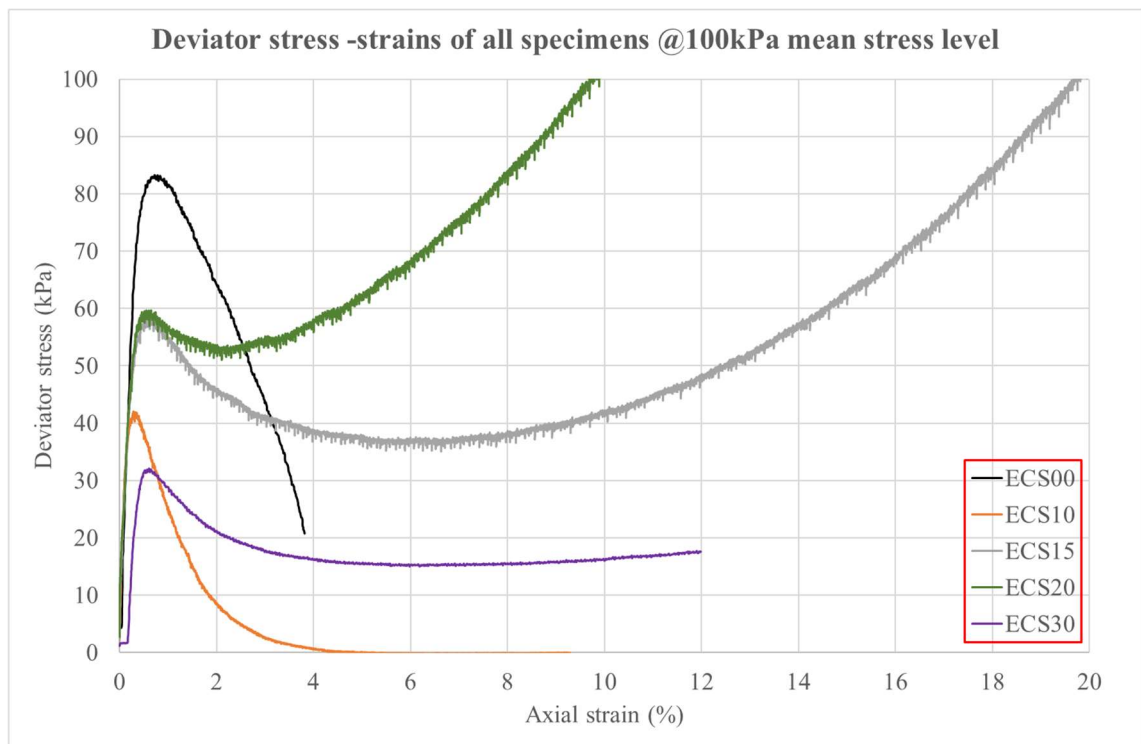


Figure 5.9 The deviatoric shear stresses of the soil specimens at 100kPa testing stress level

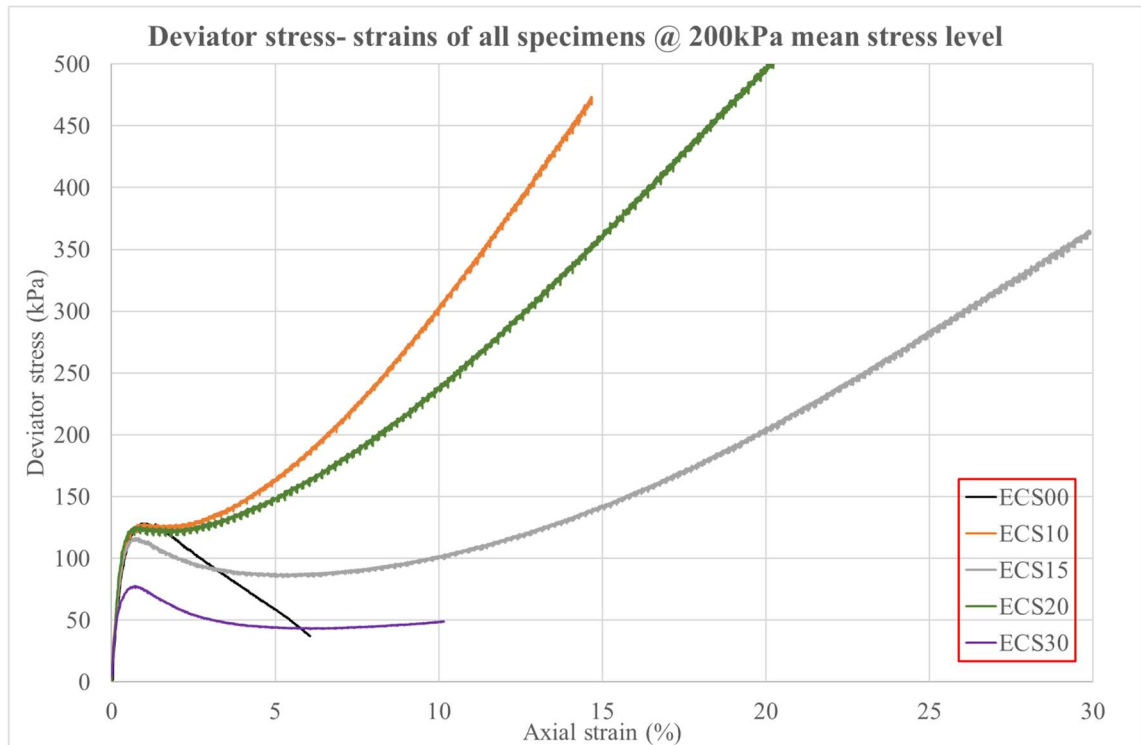


Figure 5.10 The deviatoric shear stresses of the soil specimens at 200kPa testing stress level

The softening phenomenon is a well-known characteristic of flow liquefaction in sandy soils, and it is characterized by a sharp drop of the deviatoric stress after attaining the first peak undrained shear strength. In Figure 5.8, all the tested soil specimens exhibited complete FF at an initial mean effective stress of 50kPa except the ECS20 soil sample which showed some element of soil hardening behavior after the initial peak shear strength was attained. At 100kPa mean confining stress, only ECS15 and ECS20 soils samples had the soil hardening features. At 200kPa mean effective stress, ECS10, ECS15, and ECS20 all had soil hardening characteristics.

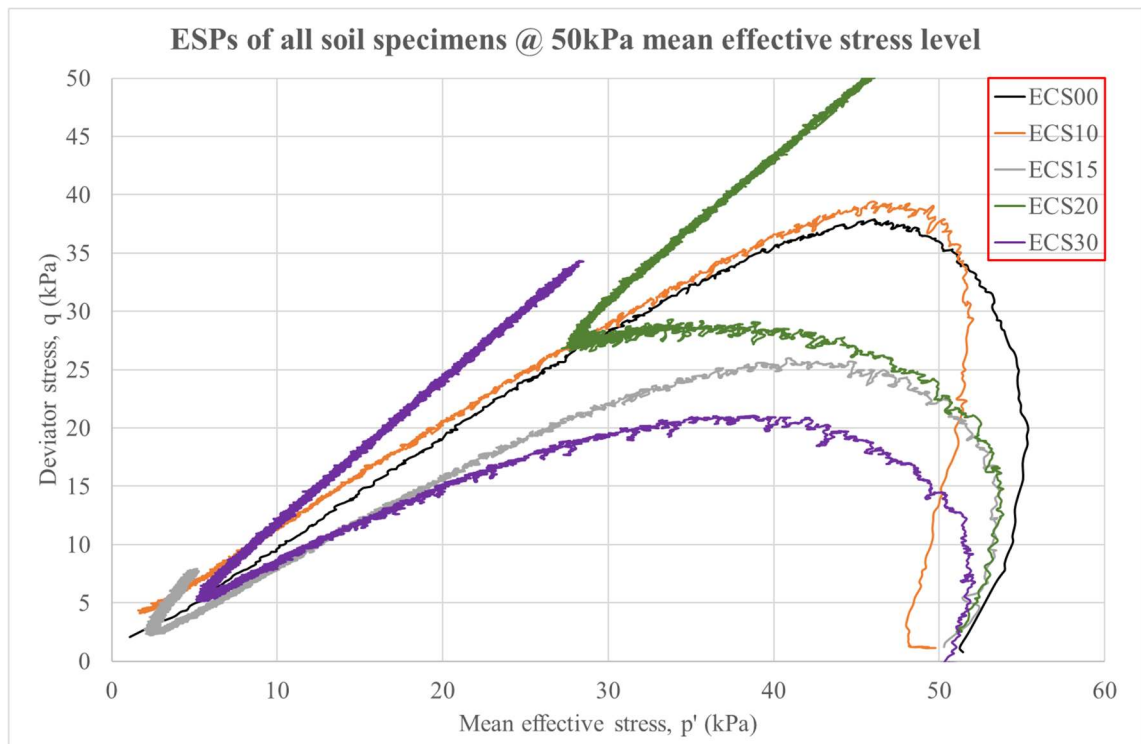


Figure 5.11 ESPs of all soil specimens at a mean effective stress level of 50kPa

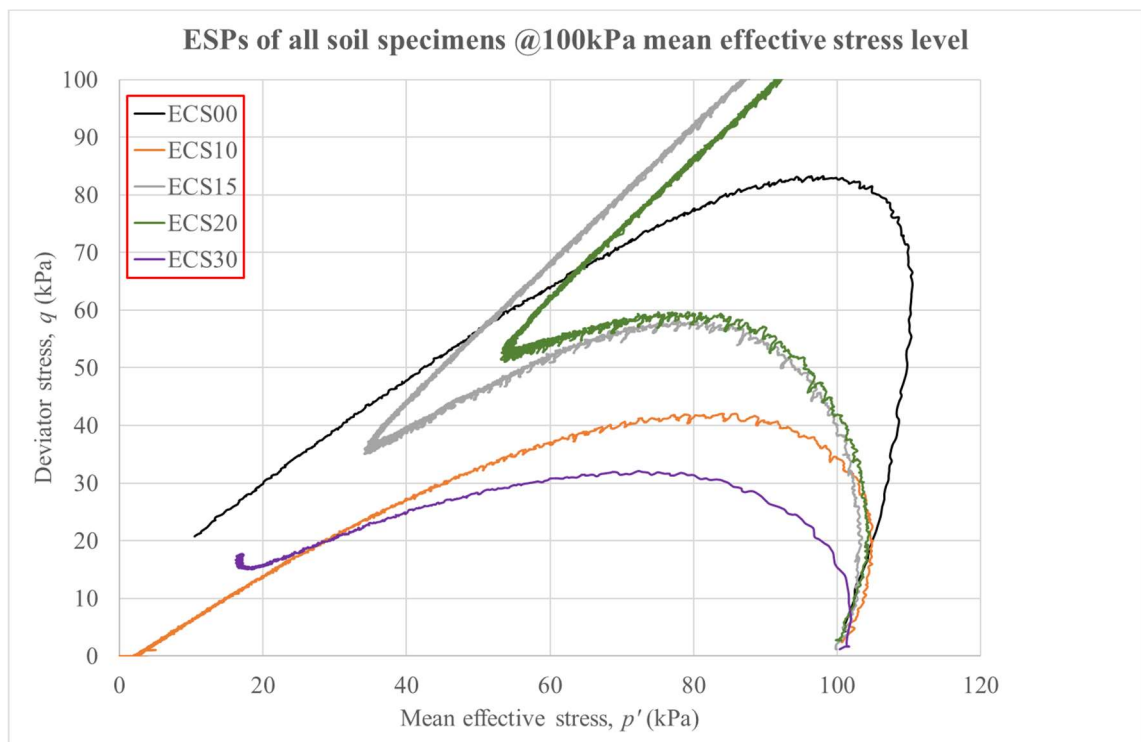


Figure 5.12 ESPs of all soil specimens at a mean effective stress level of 100kPa

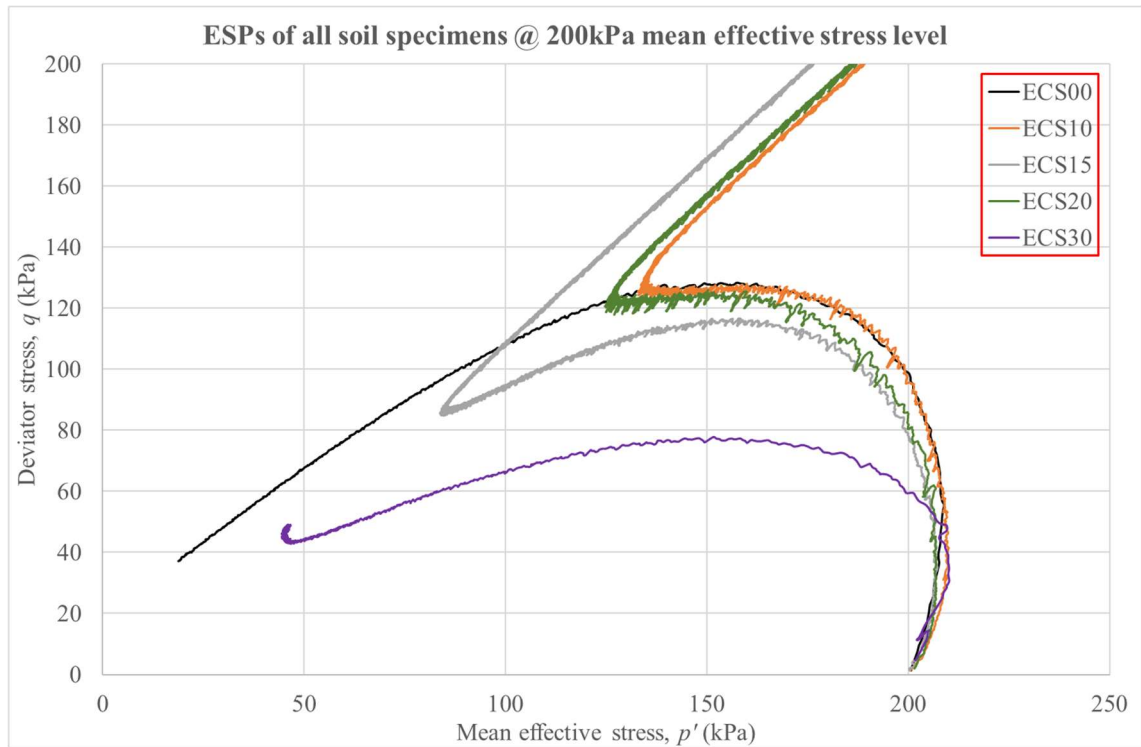


Figure 5.13 ESPs of all soil specimens at a mean effective stress level of 200kPa

The ESP plot is a significant chart that is required for the analyses of static liquefaction scenarios and the FF mechanisms in soils. Jefferies and Shuttle (2020) mentioned that the ESP can be seen as the strength capacity of the soil. When the derived ESPs from this study is compared with typical published types of analytical liquefaction charts as shown in Figure 5.3 (a) and (b) as per Rees (2010) and Rahman et al. (2014a), respectively, one can easily deduce the kind of flow liquefaction mechanism that represent any soil specimen in question. The ESP plot shows the transitional soil characteristics from a completely contractive state to a dilative one and the point of change between the above-mentioned states is mostly known in the literature as the ‘pseudo-steady-state’ or ‘phase change’ or ‘quasi steady state’ correspond to the point of minimum dilation, i.e., $D = 0$, (Jefferies & Shuttle, 2020). The majority of the tested loose soil specimens reached the CS at less than 5% axial strains. Some significant indicators of the soil strength characteristics as initially summarized at the beginning of this chapter are deduced from the ESP plot and consequently used in the calibrations of subsequent soil constitutive numerical models.

One obtainable key characteristic from the plots of the excess PWP versus axial strain is that one can deduce whether a sample is contractive or dilative. A contractive soil specimen would tend to have positive (+ve) excess PWP while a dilative soil would tend to have a negative (-ve) excess PWP. It can be seen in Figure 5.14 that only the ECS20 soil specimen had dilative properties, while other soil specimens maintained constant positive excess PWP. In Figure 5.15, only the ECS15 and ECS20 had a dilation behavior, and in Figure 5.16, ECS10, ECS15, and ECS20 possess strong dilative tendencies from 5% axial strain onwards as they approach negative excess PWP.

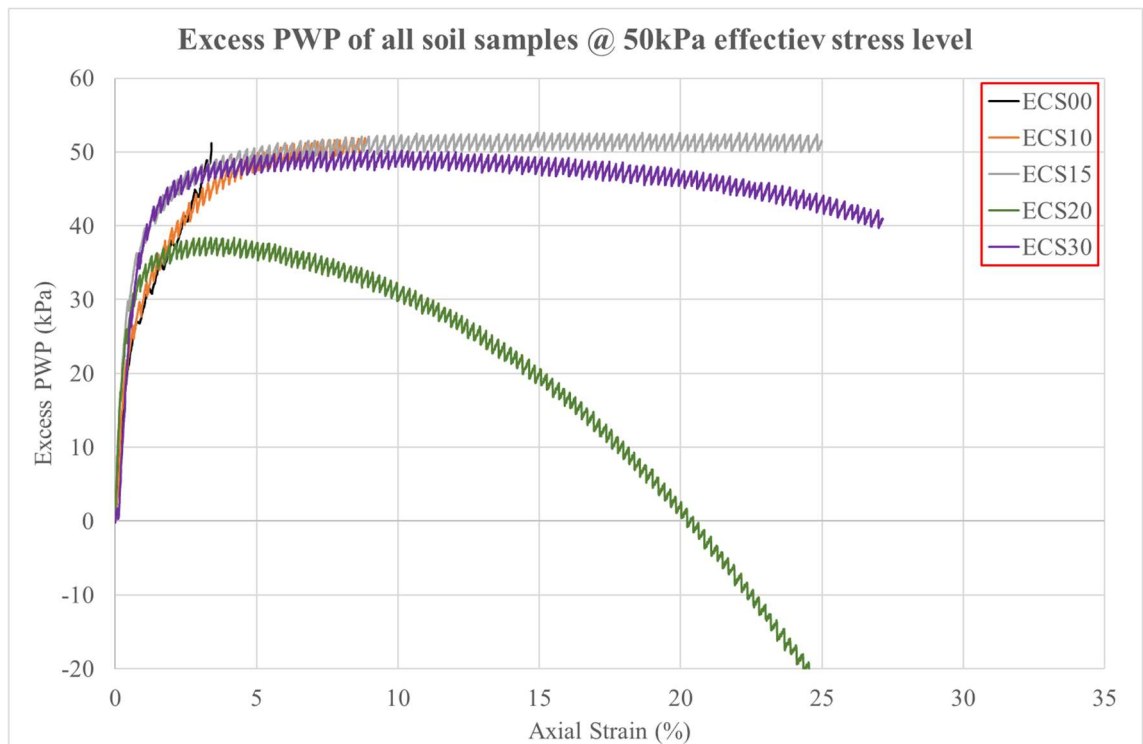


Figure 5.14 The evolution of excess PWP of all soil specimens at 50kPa mean effective stress

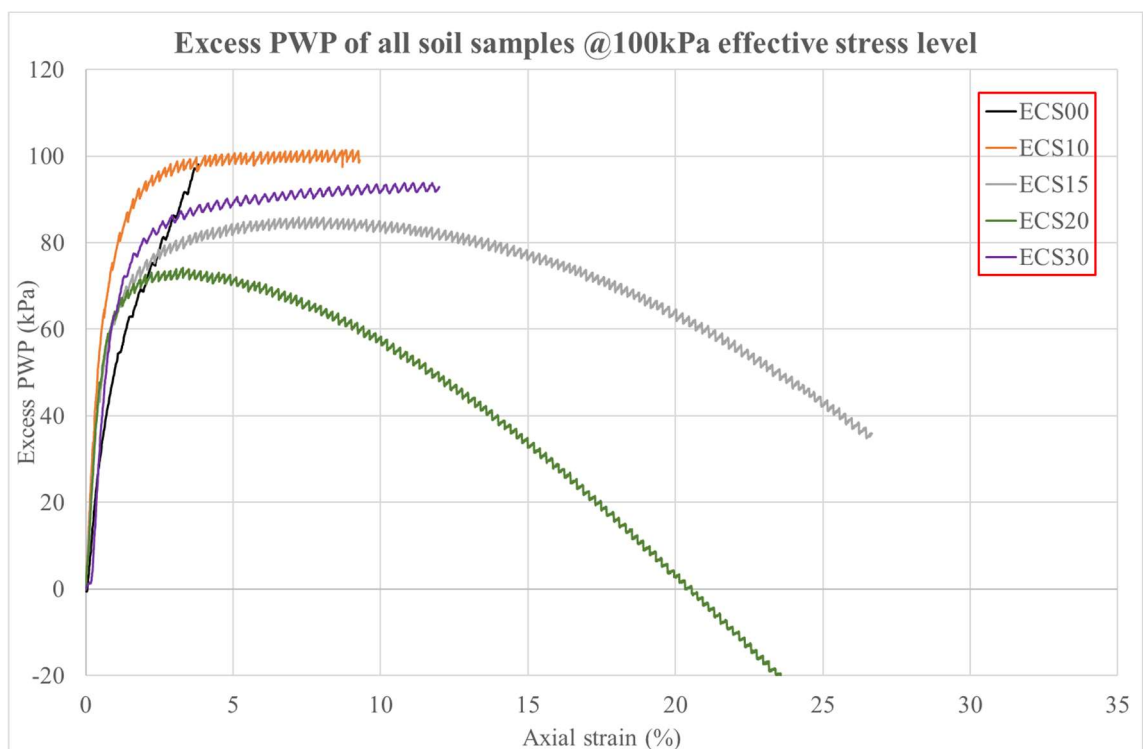


Figure 5.15 The evolution of excess PWP of all soil specimens at 100kPa mean effective stress

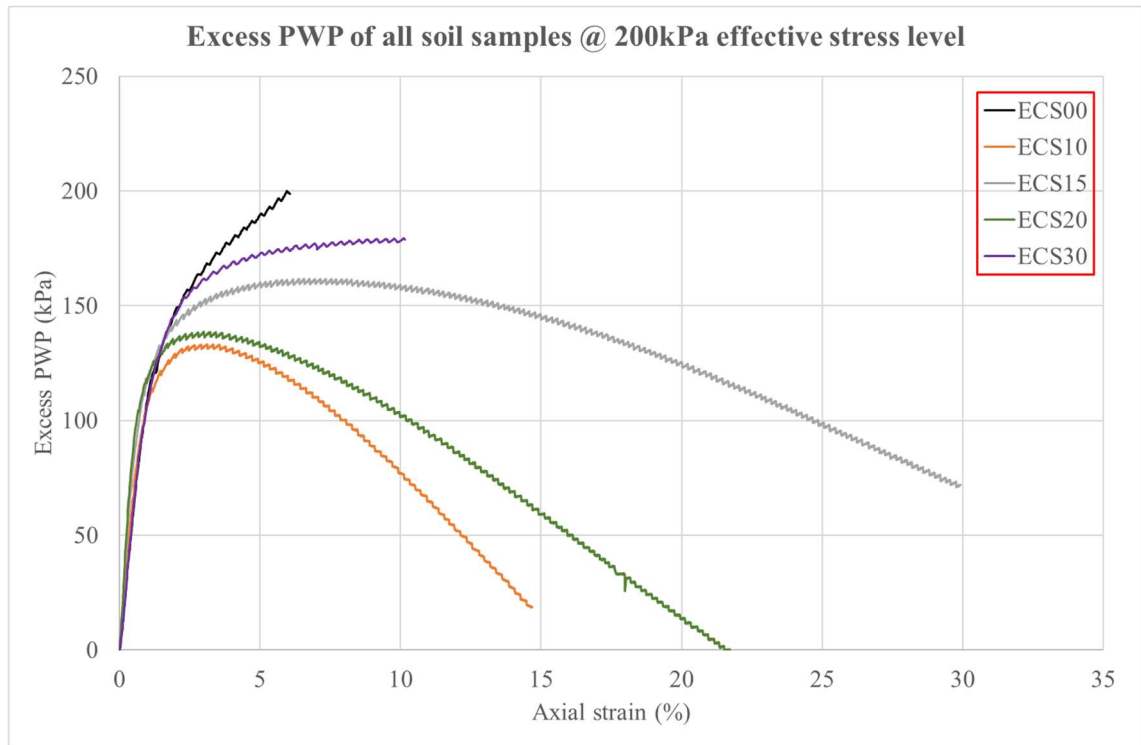


Figure 5.16 The evolution of excess PWP of all soil specimens at 200kPa mean effective stress

In summary, the initial introduction of kaolinite into the fabrics of the ECS reduces the undrained shear strength of the ECS, improved undrained shear strength was attained at a marginal optimal fine content (between 15-20%) and findings are strongly consistent with similar recently published works (e.g., Goudarzy et al., 2021) and previous works on the undrained strength characteristics of sand under static loads (e.g., Verdugo & Ishihara, 1996; Yoshimine & Ishihara, 1998). The clayey sand specimens (i.e., ECS10, ECS15, ECS20, and ECS30) exhibited more contractive tendencies than the clean sand (ECS00) because of the great affinity for water by the clay minerals within its fabric structure. In addition, the evolution of excess PWP was slower in the clayey sands than in the ECS suggesting that a marginal optimal undrained strength is required during the application of similar geomaterials in the field as soil replacement options.

5.3 Discussions of the numerically validated soil properties of ECS00 and ECS30

In this section, the obtained results from the executed numerical modeling and data validation for the advanced geomechanical parameters of soil specimens (ECS00 and ECS30) are discussed together with their corresponding calibrated properties as obtained from subsections 3.6.2 and 3.6.3. The details of the calibration of the Norsand soil model properties have been explained in the aforementioned subsections and therefore not repeated here, the reader may therefore refer to the details of model calibration in the appropriate section or subsection of Chapter 3. The Norsand numerical framework is a well-known advanced critical state-compatible, plasticity-based, stress-dependent constitutive model that captures realistic soil behavior. The current study further confirms that the model is capable of capturing the typical soil strength properties over a wide

range of mean effective confining stresses and void ratios, quantified through the state parameter (Ψ). The Norsand model has been implemented in several commercial geotechnical software which applies both the finite element method (FEM) and finite difference method (FDM) integration modes of implementation. Examples of popular FEM-based software with incorporated Norsand material models include PLAXIS (2D & 3D) and Rocscience (RS2, RS2, RSData). The Norsand model is also implemented in the FDM-based software (FLAC and FLAC3D). In addition, the Norsand formulas are made available in the visual basic application (VBA) codes in Microsoft excel of the NorTx12 in an open-source downloadable excel package.

In this study, the calibration of the Norsand soil properties was carried out in the NorTx12 excel program. The state plots and other key plots as detailed in Chapter 3 were easily derived with the aid of the NorTx12 program. Cross-verifications of the validated models were executed with both the VBA and FLAC codes by application of the Norsand model for the undrained characteristic simulations of ECS00 and EC30 under triaxial compression conditions for unit zone soil element response simulation tests at varying initial mean effective confining stress ranging between 50kPa and 500kPa. Five different aspects of the soil undrained behavior were modeled and they include the deviatoric stress-strain relations, the ESPs, the volumetric strain, the consolidation characteristics as derived by the critical state plot for each test, and the evolution of the excess PWP. It was concluded that the simulation results and experimental data were in good agreement, see Figures 5.17 to 5.20 for a gallery of simulation results of the first four (4) aspects as mentioned above for the ECS00 soil specimen and Figures 5.21 to 5.24 for ECS30, respectively. In Figures 5.17 to 5.24, the upper left graph is the stress-strain relation relationship, the upper right plot is the ESPs, the lower left plot is the constant volumetric strains versus axial strains, and the lower left graph shows the critical state line in the $e - \log P$ stress space for all the considered stress levels.

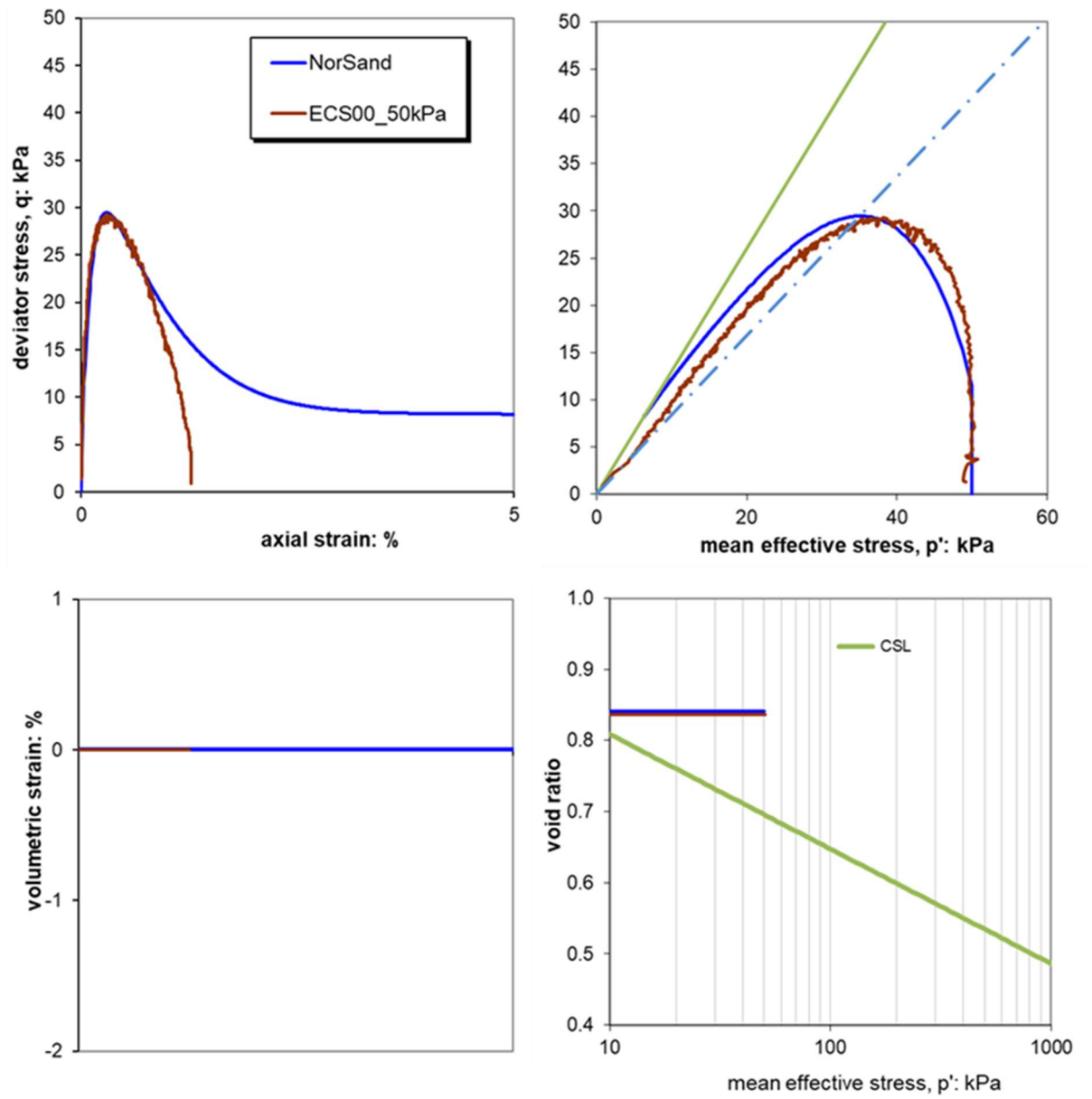


Figure 5.17 Simulation results of ECS00 at 50kPa mean confining stress level

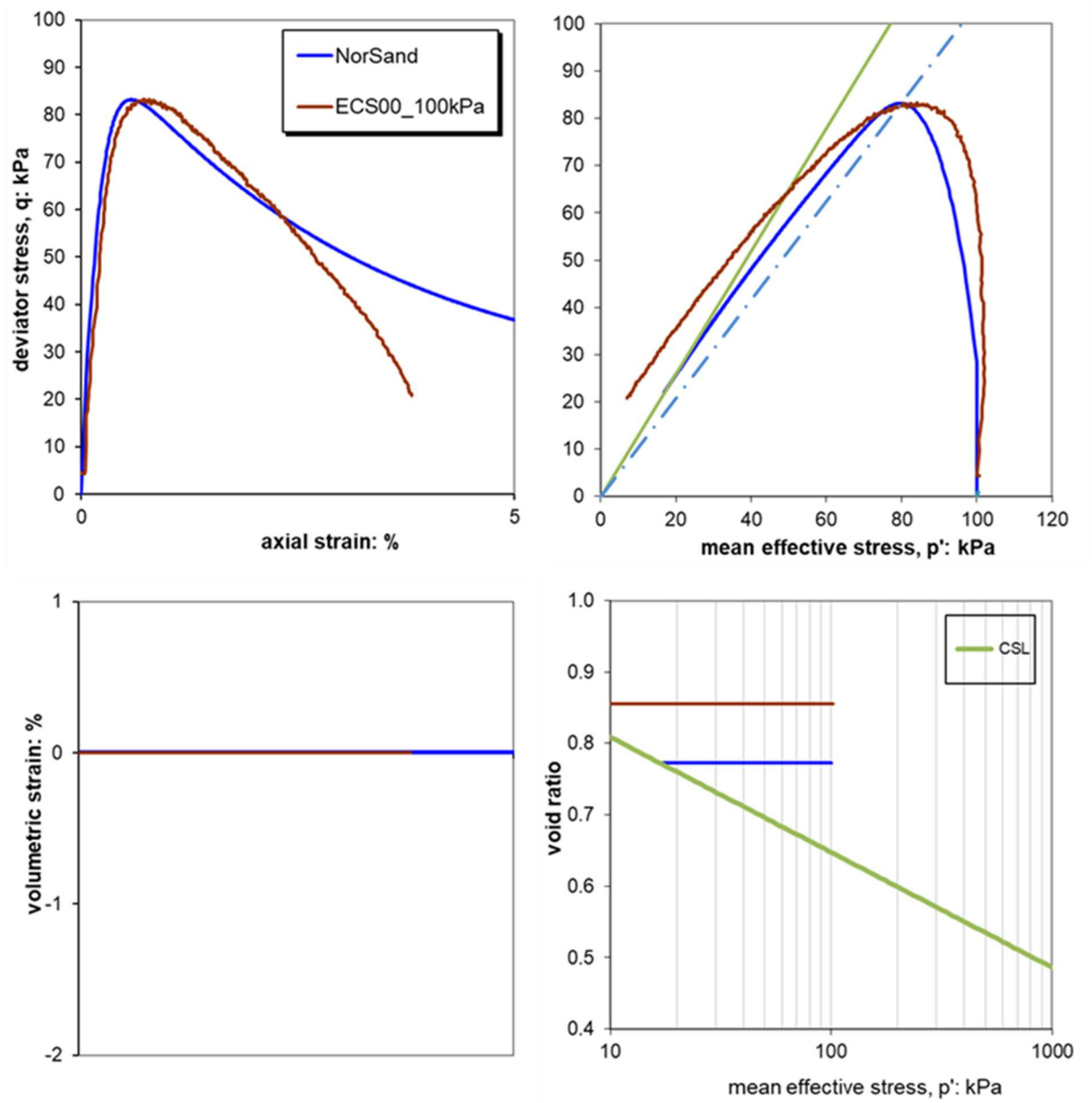


Figure 5.18 Simulation results of ECS00 at 100kPa mean confining stress level

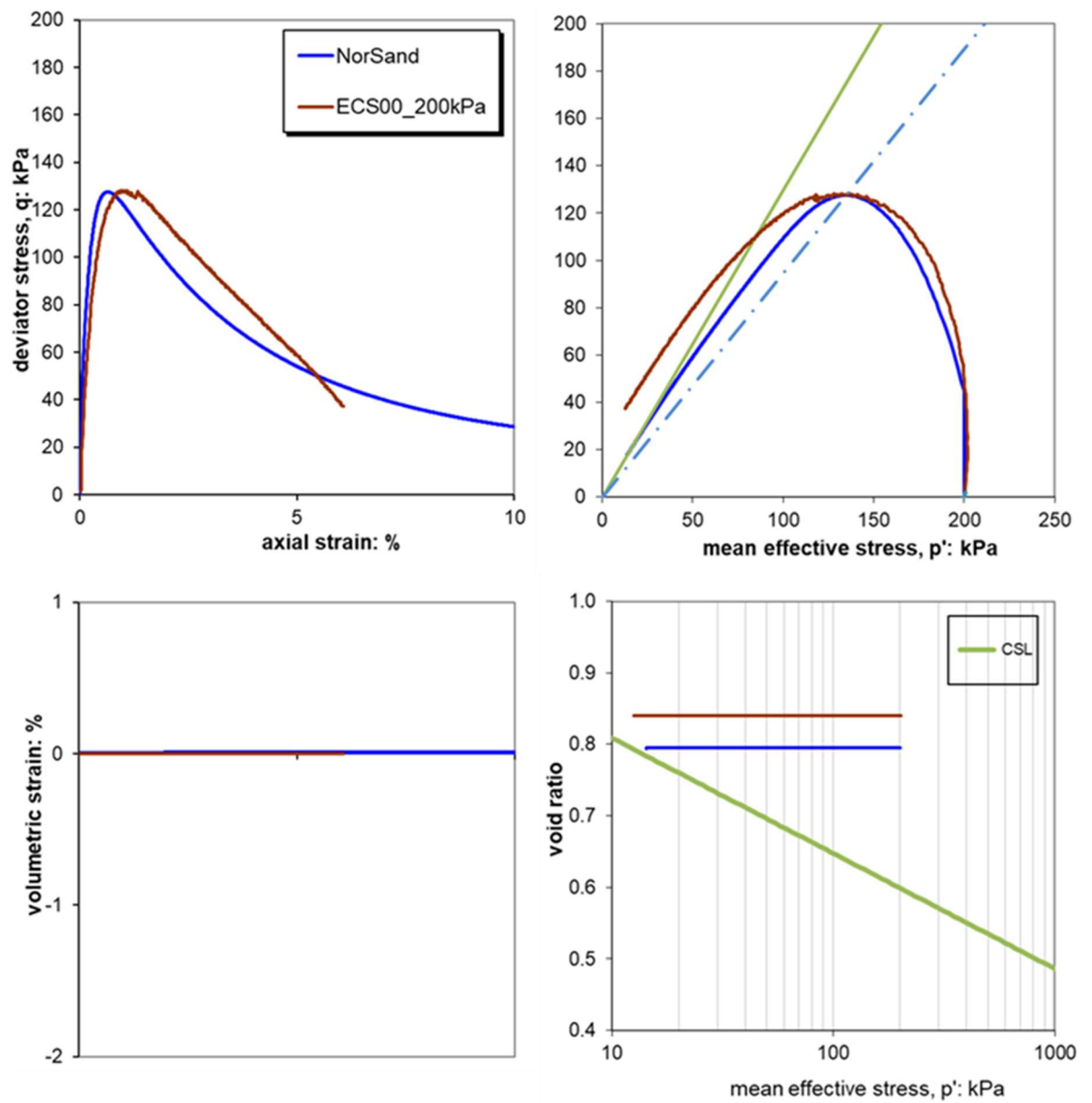


Figure 5.19 Simulation results of ECS00 at 200kPa mean confining stress level

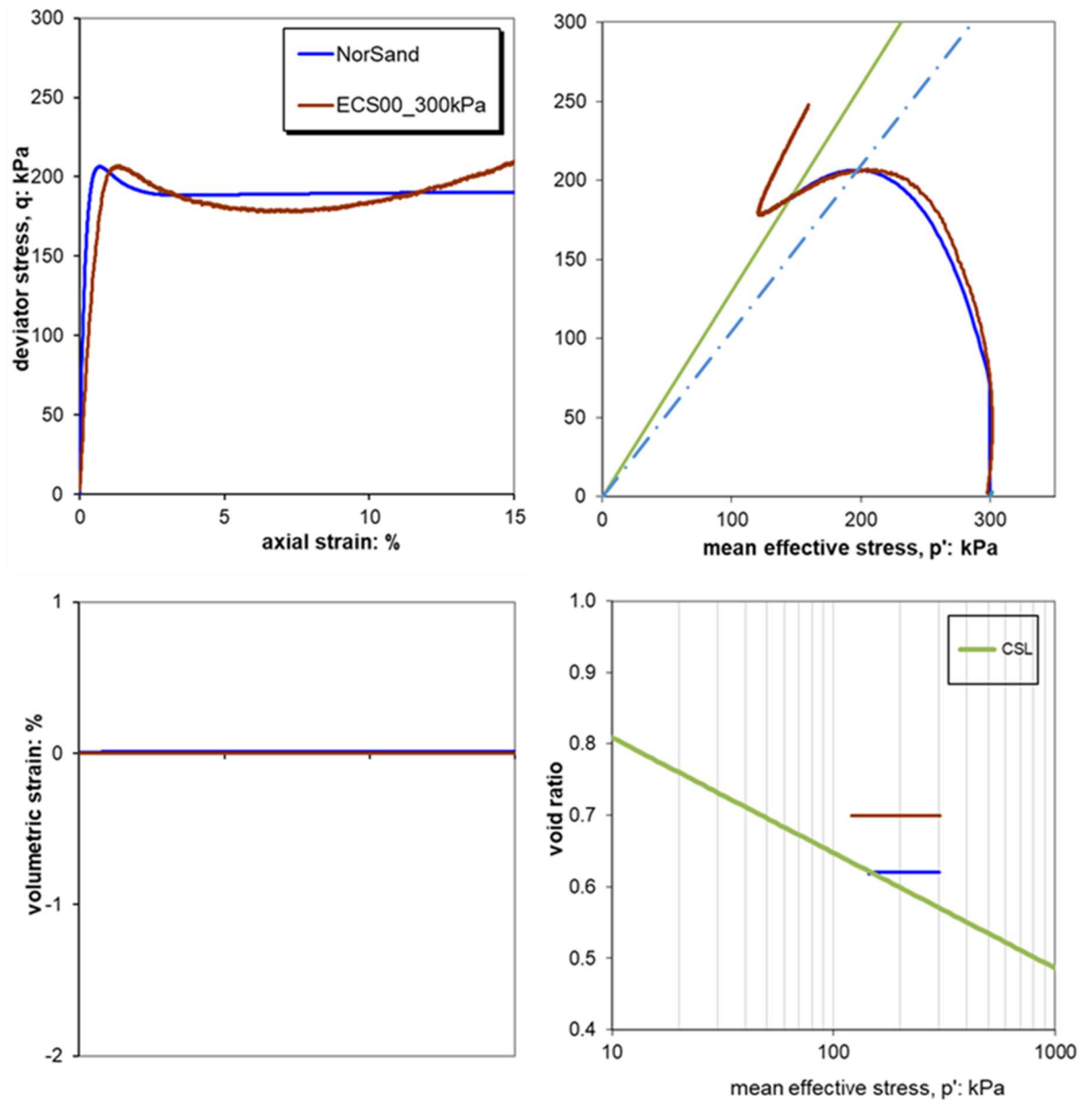


Figure 5.20 Simulation results of ECS00 at 300kPa mean confining stress level

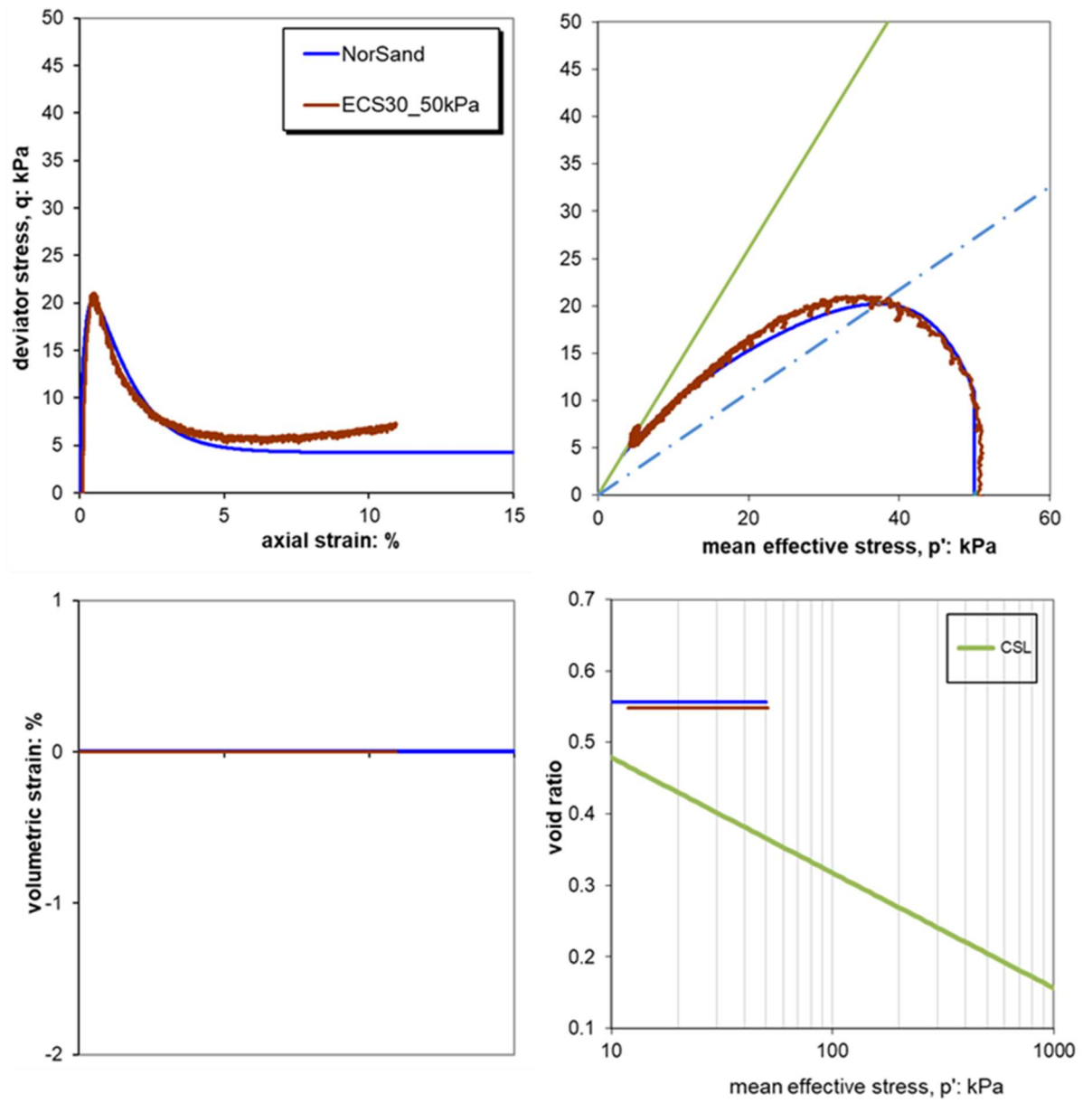


Figure 5.21 Simulation results of ECS30 at 50kPa mean confining stress level

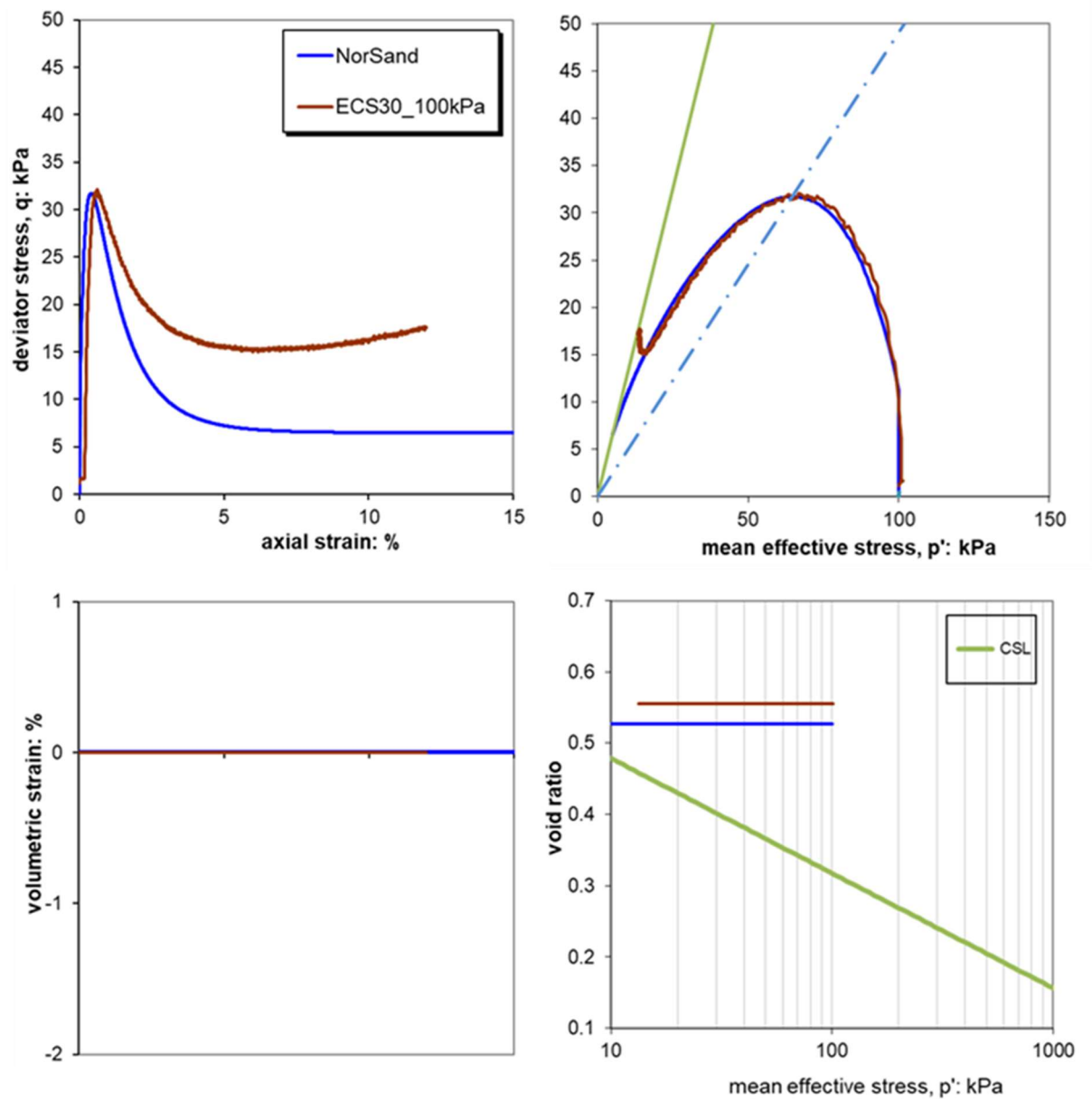


Figure 5.22 Simulation results of ECS30 at 100kPa mean confining stress level

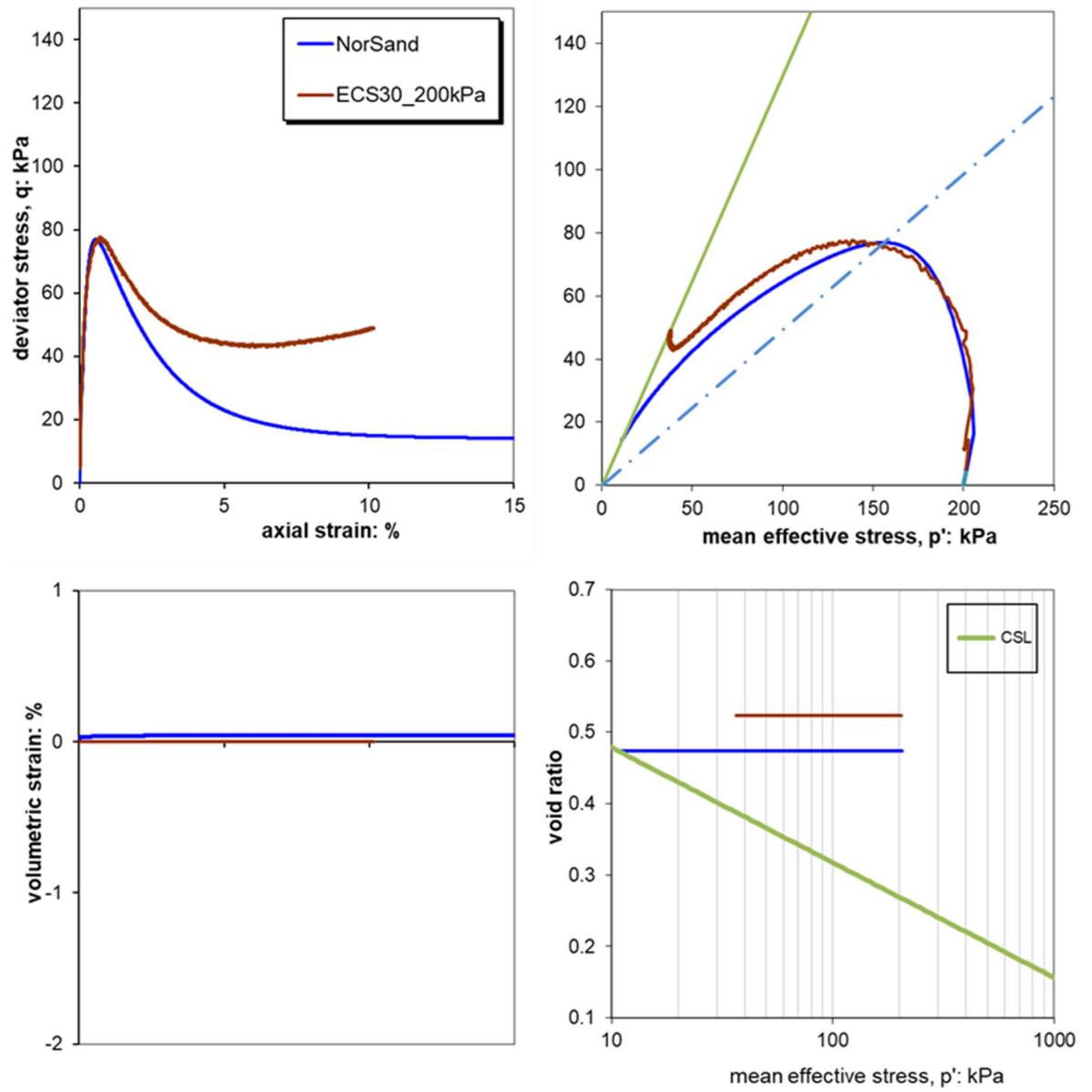


Figure 5.23 Simulation results of ECS30 at 200kPa mean confining stress level

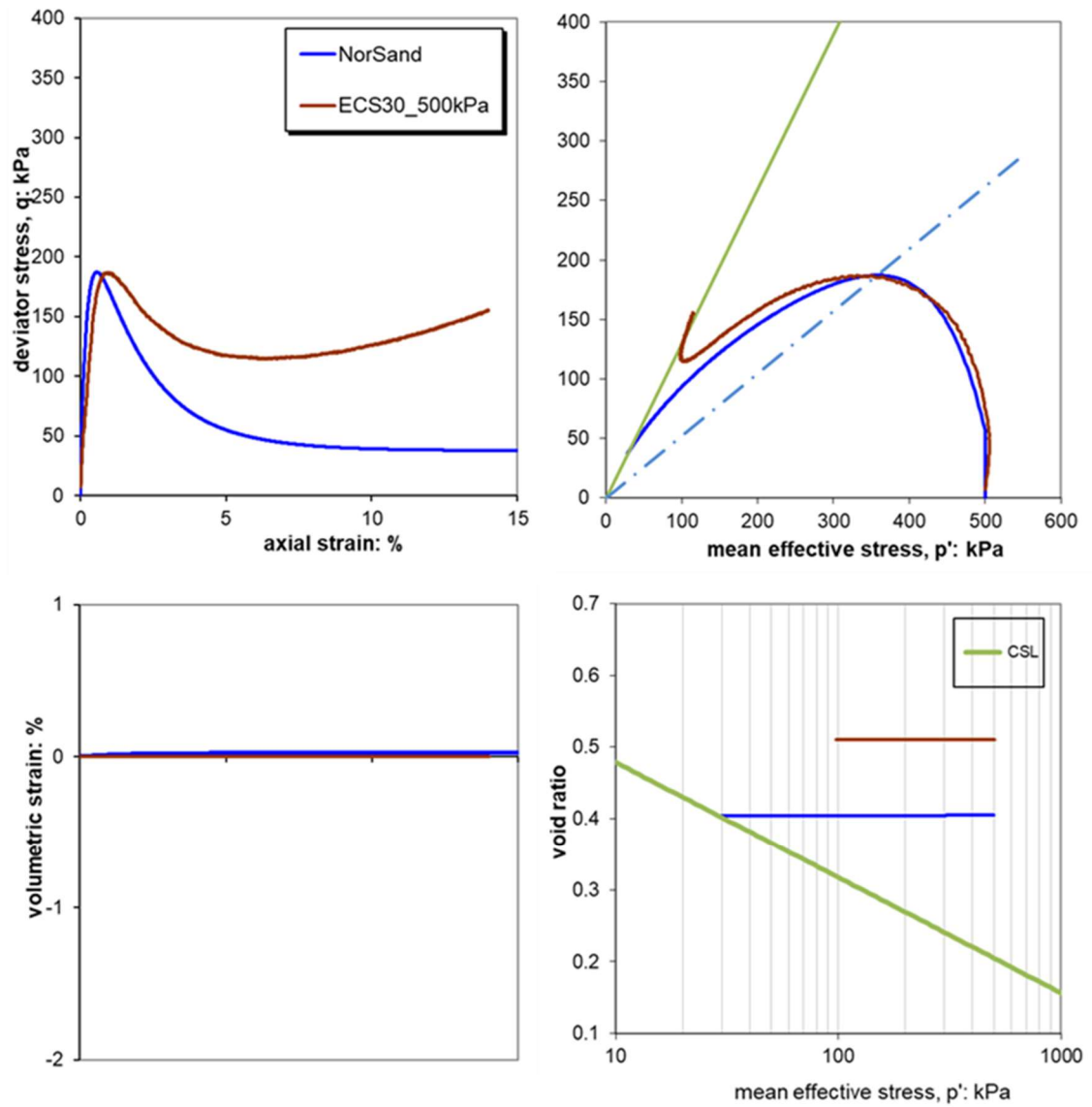


Figure 5.24 Simulation results of ECS30 at 500kPa mean confining stress

From Figures 5.17 to 5.24, One can see how the Norsand model captured the soil behavior within a wide range of confining pressures (50-500kPa) and void ratios (~ 0.500 to 1.000). For the ECS00, both completely contractive and dilative soil responses were modeled and the match is identical to the experimental data; additional simulations were executed at higher stresses 300kPa for the ECS00 and at 500kPa for ECS30, respectively to evaluate the soil behavior at higher mean effective stresses. The observed minor variations between the simulated and laboratory-measured void ratios in the $q - p'$ stress space can be attributed to the experienced slight errors within the range of -0.05 to $+0.05$ for laboratory-measured void ratios. Hence, it is highly recommended to apply the freezing method after tests to measure the void ratios of soil specimens after shearing. Figures 5.25 to 5.28 present the corresponding simulated and the laboratory-measured excess PWP for ECS00 while Figures 5.29 to 5.32 show the resulting simulation versus experimental data for the excess PWP for ECS30.

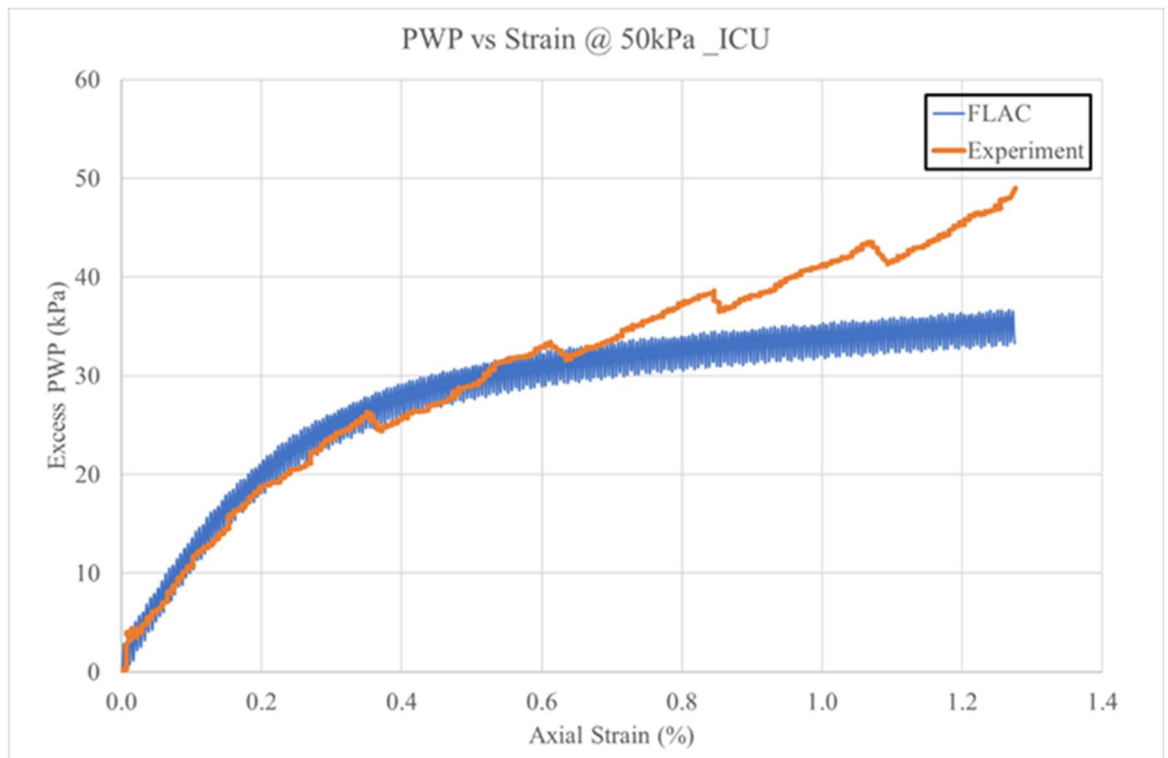


Figure 5.25 FLAC simulated versus experimental measured excess PWP for ECS00 @ 50kPa

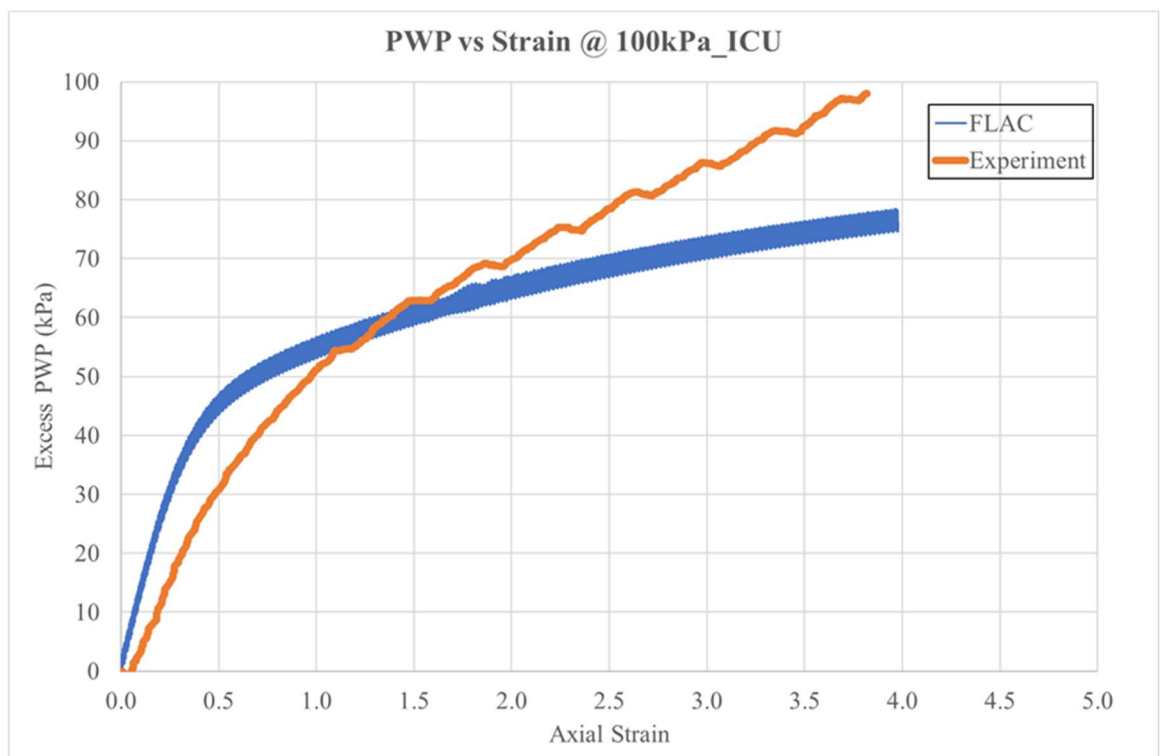


Figure 5.26 FLAC simulated versus experimental measured excess PWP for ECS00 @ 100kPa

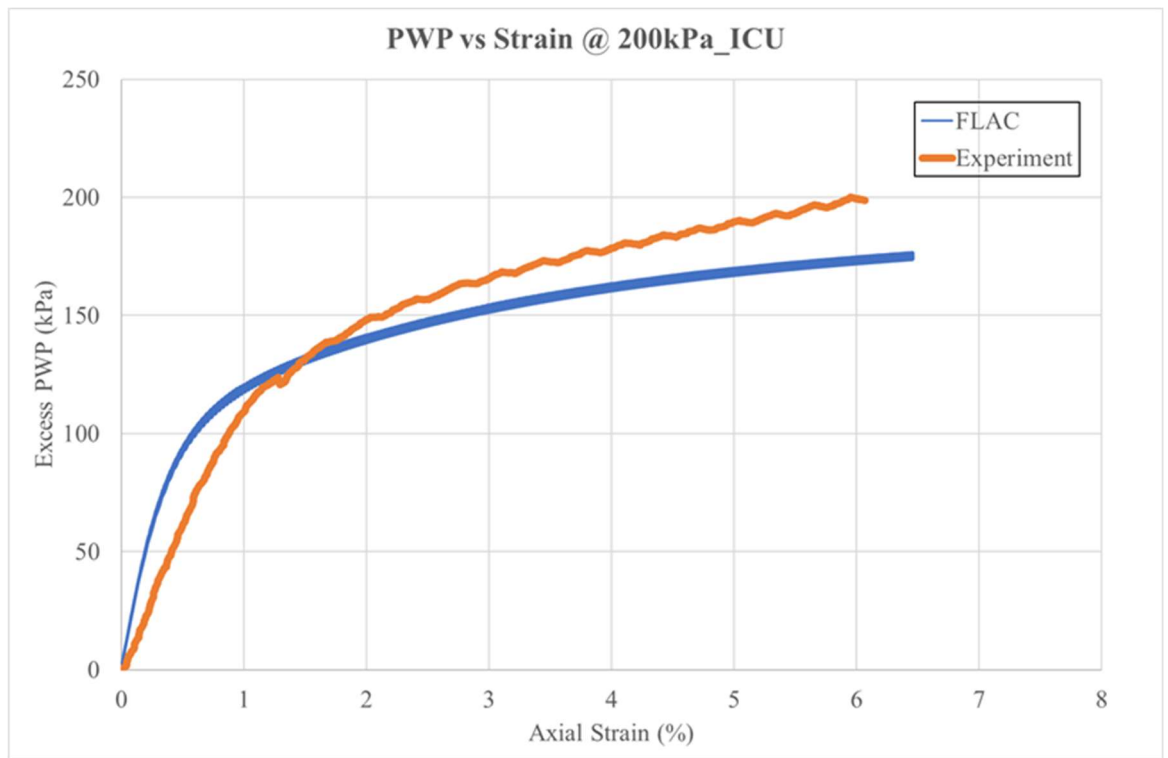


Figure 5.27 FLAC simulated versus experimental measured excess PWP for ECS00 @ 200kPa

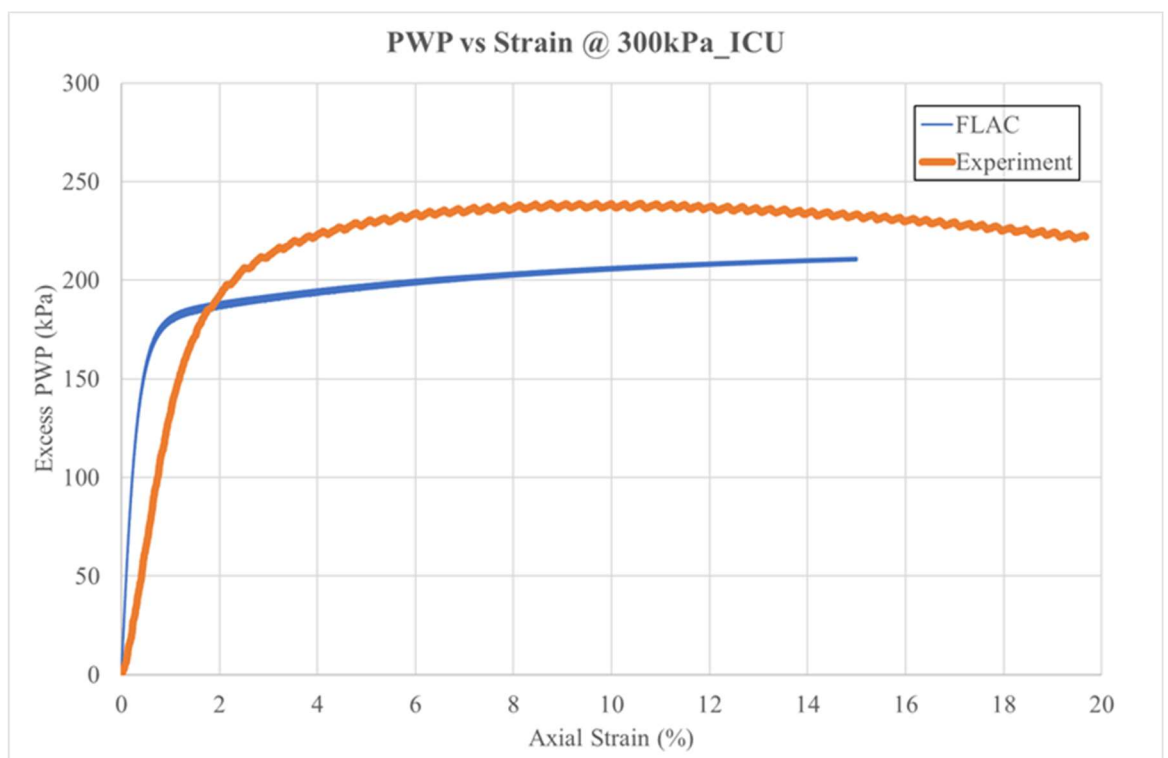


Figure 5.28 FLAC simulated versus experimental measured excess PWP for ECS00 @ 300kPa

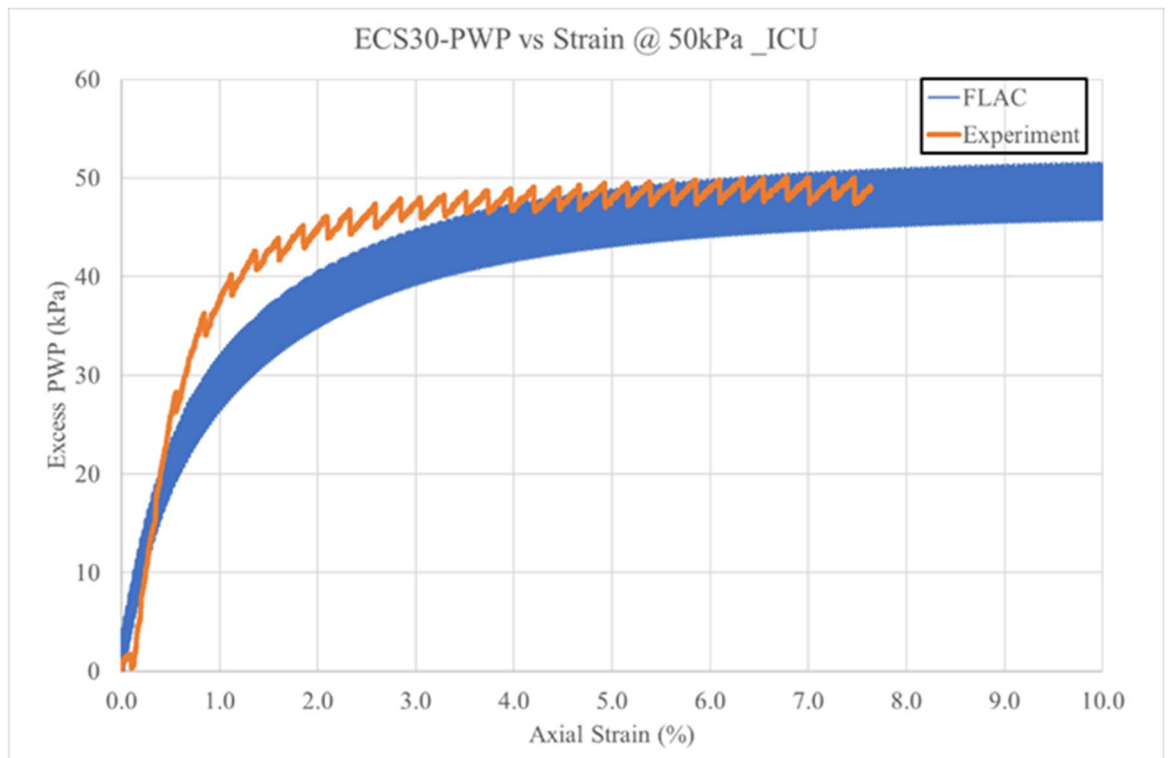


Figure 5.29 FLAC simulated versus experimental measured excess PWP for ECS30 @ 50kPa

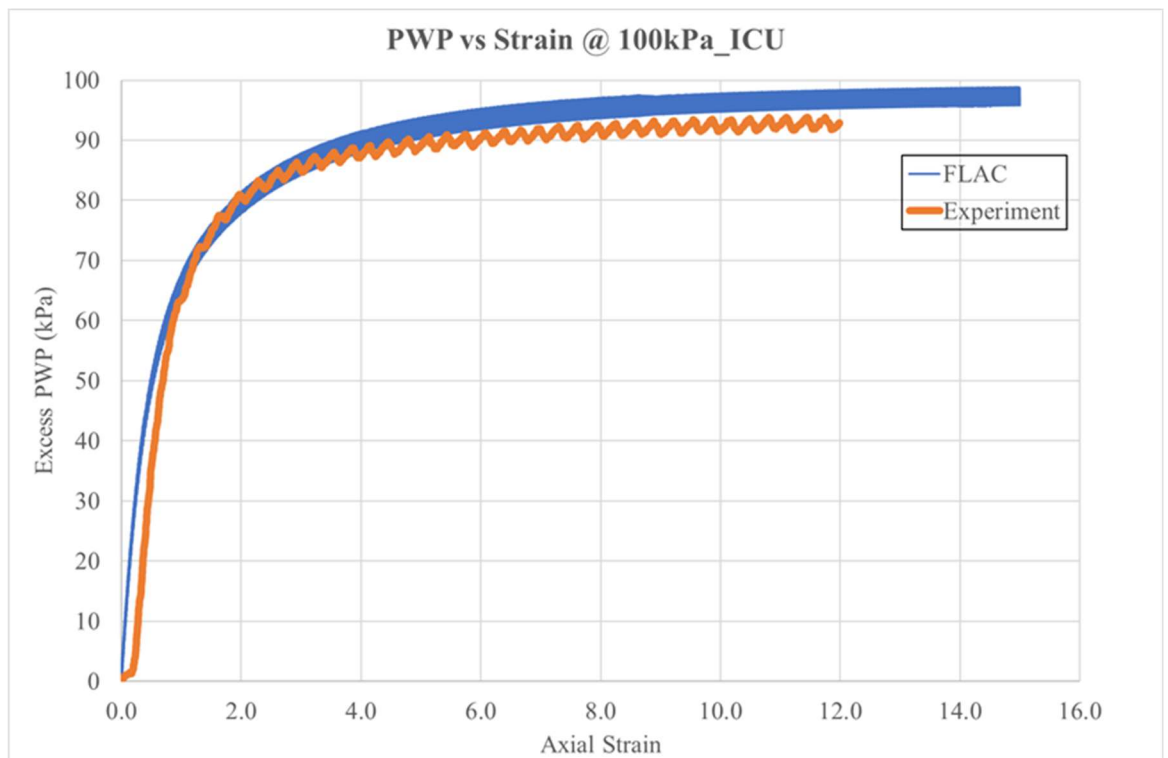


Figure 5.30 FLAC simulated versus experimental measured excess PWP for ECS30 @ 100kPa

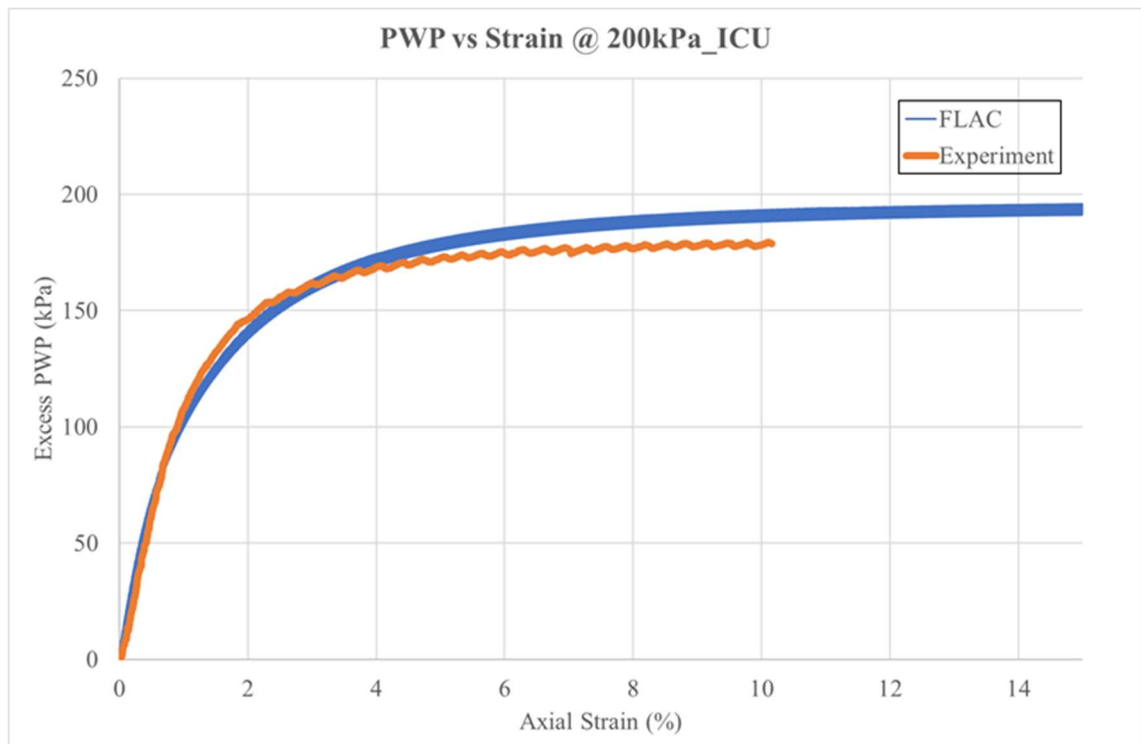


Figure 5.31 FLAC simulated versus experimental measured excess PWP for ECS30 @ 200kPa

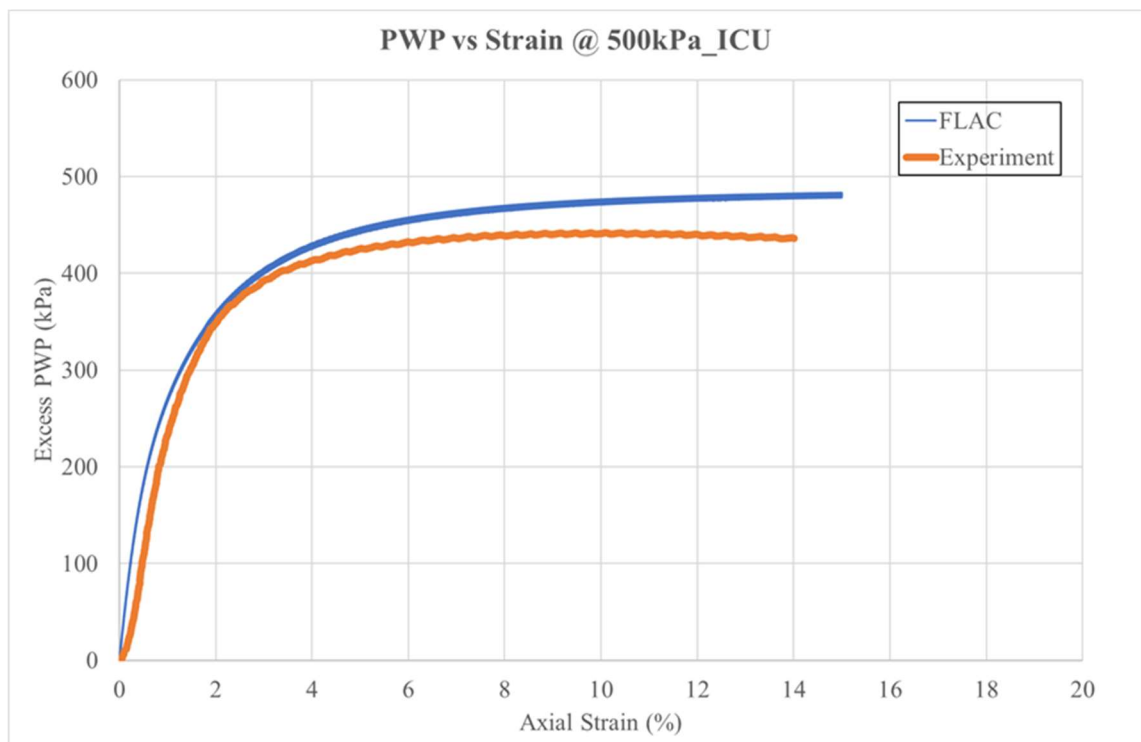


Figure 5.32 FLAC simulated versus experimental measured excess PWP for ECS30 @ 500kPa

The calibrated soil properties for the Norsand numerical model as detailed in subsection 3.6.2 are presented in Table 5.2. The majority of the soil properties detailed in Table 5.2 are familiar although a brief explanation of them is provided below. However, the interesting fact about the Norsand model is that only one set of soil parameters is required to simulate a particular soil

samples' behavior, the only changing variables are the state parameters, initial mean effective stress levels, elastic modulus, OCR, and the maximum elastic modulus. The calibrated soil model parameters may be classified as critical state-based, soil plasticity-based, soil elasticity-based, and the initial soil state parameters.

The CS-based parameters (Γ & λ), derived from the CSL have been previously explained in subsection 3.6.2, Γ is the altitude of the CSL at 1kPa mean stress, and λ the slope of the CSL. Based on the executed simulations for ECS00 and ECS30, Γ is found to be reduced by the inclusion of plastic fines (kaolinite), on the other hand, the same slope (λ) of the CSL was used in fitting the data for both specimens. Poulos et al. (1985) noted that the slope of the state line is only affected by the grain shapes of the soil, the added kaolinite fines would mostly occupy the void spaces of the ECS fabrics, therefore, the same grain shape of ECS is assumed workable for simulation purposes with the consideration that the Norsand works based on the particle-to-particle frictional contact principles for soils. Although there is an existing discrepancy about CSL for transitional soils not being unique, some previous workers have noted the existence of an infinity of CSL for transitional soils (Jefferies & Been, 2015; Viana da Fonseca et al., 2021). Another loophole is the accurate determination of void ratios is considered significant since the CSL is fitted in the $e - \log p'$ stress space, the estimated strength which is highly sensitive to the steady/critical state void ratios which is the equivalent of the post-consolidation void ratios in undrained triaxial conditions.

The plasticity theory related parameters include M_{tc} the critical friction ratio, N the volumetric coupling coefficient from Nova's flow rule at peak strength, H plastic hardening modulus, and X_{tc} χ_{tc} as often called is the parameter relating maximum dilatancy to Ψ . The calibration procedures for the plasticity-based parameters are well explained in subsection 3.6.2.3. The role of plasticity theory in simulating soil behavior dated back to the works of Drucker and Prager (1952). The H were derived by forward iterative modeling (FIM) and the subsequent best-fit data was adopted as calibrated data for applications in simulations. The plasticity theory revolves around the stress-dilatancy framework which provides the details about the soils' stress-strain relationships and the state dilatancy theory which provides the current undrained strength of the soil. The related elements to soils' plasticity include the yield surface, plastic flow, work hardening, and consistency condition (Jefferies & Shuttle, 2020). In soils, the deformations experienced are mostly irrecoverable, hence in the implementation of the soil plasticity, the shear strains are divided into elastic and plastic parts.

The Norsand model adopts its elasticity-based parameters to include I_r the shear rigidity computed as the ratio of shear modulus (G_{max}) to mean effective stress, and Poisson's ratio is often taken as 0.15 to 0.3 (Jefferies & Shuttle, 2020) for soils. The utilized G_{max} in simulations were derived by FIM since bender elements test was not carried out to estimate same and the best-fit values G_{max} of were adopted as calibrated for simulations. Overall the calibrated soil

parameters were compared with typical published values as found in Jefferies and Been (2015) and they fall within the range of published data for similar soils. The work hardening and the softening phenomenon is based on the so-called consistency condition and is related to the yield surface of the soil.

The state-related variables are the state parameter Ψ , the overconsolidation ratio, and the initial mean effective stress p'_0 . The comparison of the Norsand implementation in both the VBA and FLAC codes to the experimental data showed very good agreements and the match is something to behold. Figures 5.33 and 5.34 show some plots of the cross-comparisons made between the VBA and FLAC code simulations.

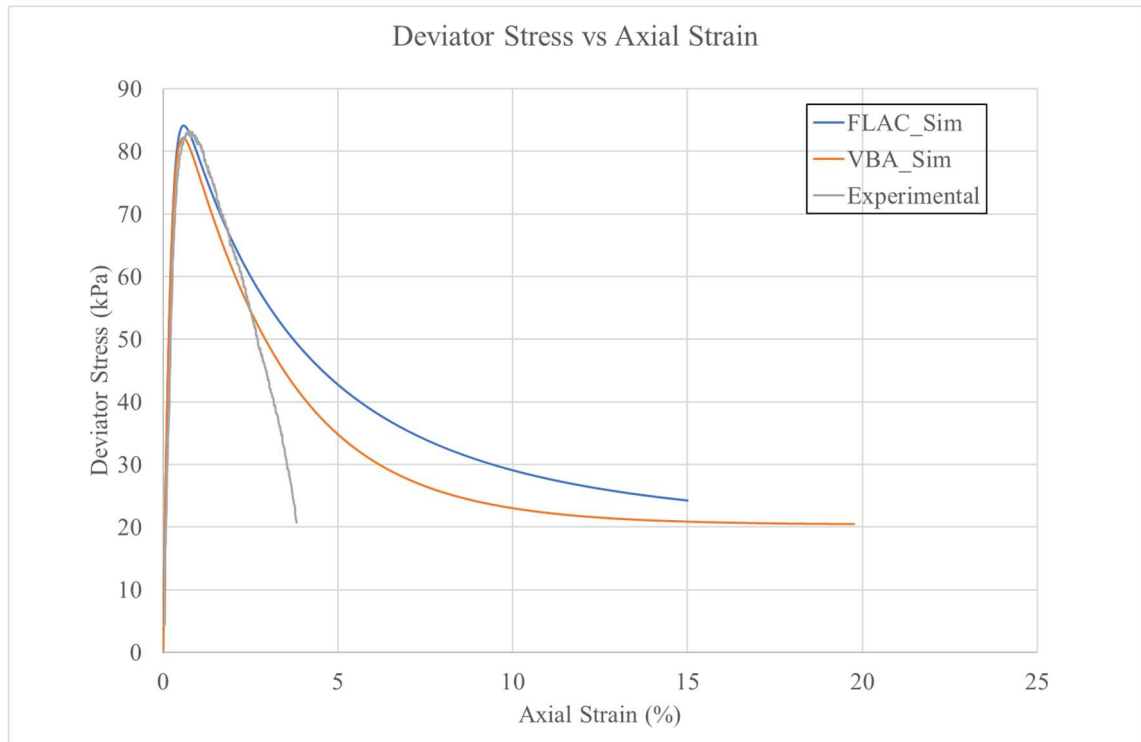


Figure 5.33 Cross-comparisons of VBA and FLAC simulated stress strains with Experimental data of ECS30 @ 100kPa

The consistency of the Norsand formula have been verified in previous studies (e.g., Cheng & Jefferies, 2020) for its implementation in the NorTx12, FLAC and FLAC3D software. As can be seen in Figure 5.33 and 5.34, the Norsand framework is consistent for the compared experimental data and simulated in both NorTx12 and FLAC.

In Table 5.2, the undrained strength ratios S_u/p'_0 , the drained strength ratio S_r/p'_0 , and the IL indices η_{IL} may all be regarded as substitutes for the conventional factors of safety (FOS) which are the preferred method for stability analyses for liquefaction analyses. The factors were all low since one of the aims of the study was to create loosely deposited specimens that are similar to the soft ground conditions in the field.

Table 5.2 The calibrated Norsand model soil properties

Parameters/ Sample Name	ECS00_50	ECS00_100	ECS00_200	ECS00_300	ECS30_50	ECS30_100	ECS30_200	ECS30_500
Test ID	7	8	9	11	4	5	6	7
M_{tc}	1.3	1.3	1.3	1.3	1.3	1.3	1.3	1.3
N	0.25	0.25	0.25	0.25	0.20	0.20	0.20	0.20
χ_{tc}	2.00	2.00	2.00	2.00	3.5	3.5	3.5	3.5
H₀	260	400	160	152	200	120	250	180
H_v	0	0	0	0	0	0	0	0
(H = H₀ - H_v)	260	400	160	152	200	120	250	180
Gamma (Γ)	0.97	0.97	0.97	0.97	0.640	0.640	0.640	0.640
Lambda (λ)	0.070	0.070	0.070	0.070	0.070	0.070	0.070	0.070
G_{max} @ p₀	11	13	27	50	5	14	16	45
G_{exp}	0.2	0.2	0.5	0.2	0.6	0.8	0.8	0.8
ν	0.15	0.15	0.15	0.15	0.15	0.15	0.15	0.15
(lr ...)	220	129.353	135	233.33	100	100	200	90
κ	0.008	0.013	0.012	0.006	0.014	0.014	0.017	0.014
ψ₀	0.145	0.13	0.196	0.05	0.191	0.210	0.205	0.200
e₀	0.841	0.777	0.795	0.621	0.557	0.557	0.474	0.405
p₀	50	100.5	200	300	50	100	200	500
K₀	0	0.01	0.01	0	0	0	0	0.01
(sig1...)	50	100	201	301.5	50	100.25	202	502.5
OCR ("R")	1.2	1.2	1.2	1.2	1.2	1.1	1.1	1.1
Key Results								
η_{IL}	0.841	1.032	0.947	1.048	0.543	0.491	0.494	0.523
s_u/p₀'	0.29	0.41	0.32	0.34	0.20	0.16	0.19	0.19
s_r/p₀'	0.082	0.102	0.045	0.314	0.042	0.032	0.035	0.038

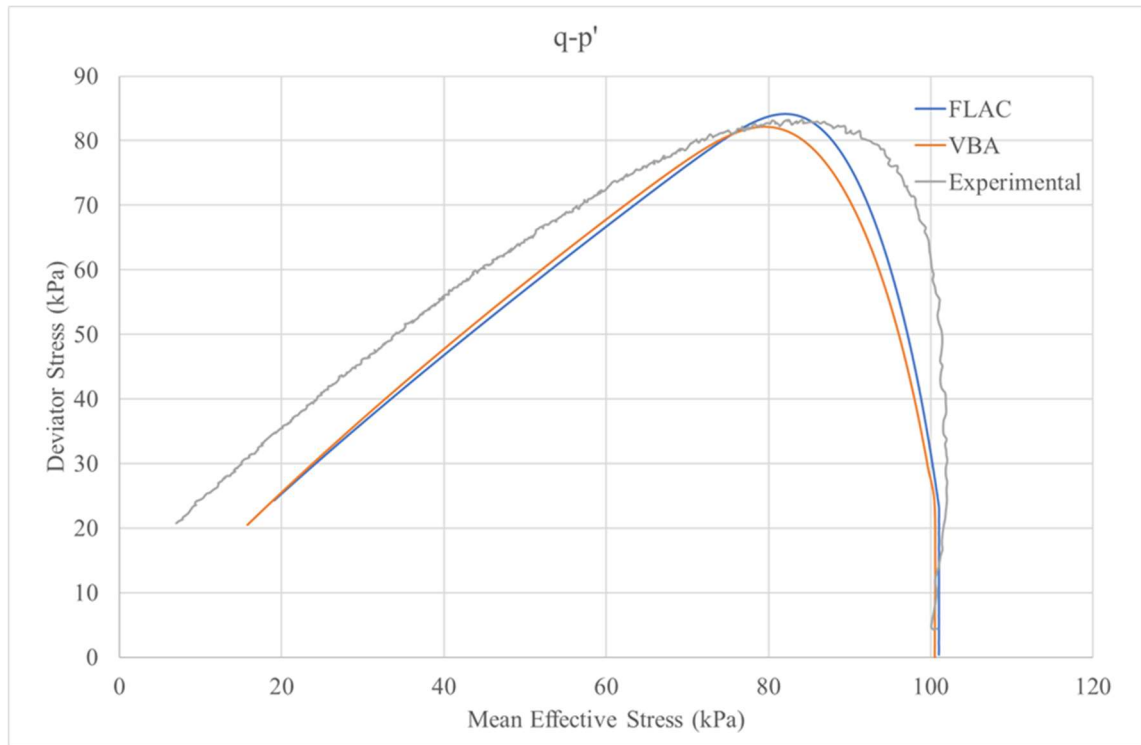


Figure 5.34 Cross-comparisons of VBA and FLAC simulated ESP with experimental data of ECS30 @ 100kPa confining stress

5.4 Summary

The experimental data were analyzed and discussed within the state concepts which corresponds to either the steady state of deformation or critical state. The useful insights gained from the study indicated that certain clayey sands may provide better strength characteristics where soil replacement methods are considered a priority during the construction and design phases of implementing some low-cost liquefaction mitigation procedures.

Overall, the undrained analyses of the studied remolded soil specimens indicated that the magnitude of flow failure reduces from FF to LF when the percentage content of kaolinite increased within the fabrics of the primary sand (ECS00) between 15% to 20% by weight of the kaolinite clay. The generated excess PWP do not particularly follow any specific pattern during the undrained shearing, rather at lower effective confining mean effective stress of 50kPa, ECS00 and ECS30 have the highest evolution of excess PWP. ECS20 showed the most dilatant tendencies at a testing pressure of 50kPa and 100kPa while ECS10 showed the most dilatant trend at higher confining stress of 200kPa. The experimental evidence further suggests that the undrained strength performance of ECS may improve with the inclusions of some plastic fines if further soil improvement methods such as densification are employed. The predicted improvement is based on certain factors that further influence the increase in the overall shear strength characteristics of the sand, such factors may include aging and overconsolidation due to

the effects of the clayey particles which enhance further adhesion and cohesion of the individual particles grains within the entire soil structure fabric.

Furthermore, numerical validation studies for transitional soils are still relatively scarce, hence, one of the objectives of this study is to validate the advanced soil parameters of typical clayey sand (ECS30) using the Norsand numerical model. This objective was met as the simulations all matched closely with the experimentally measured data. In addition, the calibrated soil model parameters were compared with previously published data on similar soils, and they are found to be consistent with typical published values. Personal communication with Dr. Michael Jefferies (the author of the Norsand Model) also commented that the parameters used were reasonable and consistent with previous soil data.

CHAPTER 6: CONCLUSIONS AND RECOMMENDATIONS

The textbook soils, otherwise known as clean sands and pure clay are well-researched while very limited studies have been focused on the computational numerical model validation of the experimentally-observed undrained flow behavior of transitional soils known as mixed soils (clayey sands as considered herein). The majority of in-situ soils in reality mostly exist as mixed fractions of both cohesionless and cohesive particles. Hence, the need for the selection of an appropriate advanced constitutive framework to capture the key soil undrained strength characteristics of mixed soils. A critical review of the subject of soil liquefaction mitigation further indicated that both the conventional and recent techniques to mitigate liquefaction may either be expensive or not environmentally sustainable. In the foregoing, suitable soil replacements may be sort to replace highly soils that are susceptible to static liquefaction otherwise known as flow failure (FF); therefore, the soil must be numerically validated to be able to fully predict its undrained flow strength characteristics as a replacement geomaterial. One of the key goals of the current research is to contribute to the existing state-of-the-art by demonstrating the appropriate selection procedures of an advanced numerical framework that captures the undrained behavior of mixed otherwise known as transitional soils. The formulated research objectives to help achieve the research goals are elaborated in the adjoining subsections of this chapter and were all met at different stages of the research project.

The current study examined the undrained flow failure behavior of east coast sand (ECS) from Auckland, New Zealand, and cross-comparisons were made with clayey variants of the sand, produced by the addition of some industrial kaolinite to the former. The key aspects examined included the undrained strength characteristics of the studied remolded soil specimens when subjected to both static and dynamic loads and the evolution of excess porewater pressures. The soil specimens included typical clean sand mostly called east coast sand (ECS) and other derived variants of clayey sands by admixing industrial kaolinite with the ECS by 10, 15, 20, and 30% by weight. ECS is available in large commercial quantities and utilized for local earthworks applications around the Auckland region of New Zealand. ECS's major geological origin source is from the Pakiri Group and has been commercially mined for decades to date with no known published geotechnical properties. To numerically validate the experimental data of clayey sands, the critical state soil mechanics (CSSM) framework was applied as the workable math/physics of the undrained flow failure (FF) mechanism of ECS00 and ECS30. The derived results of the cross-comparisons made between the laboratory obtained results and simulations for five different aspects of the soil undrained FF mechanisms were identical and the match was good for all studied five aspects.

6.1 The critical state characterization

The first objective was to provide the critical state characterization of the studied extreme cases. The identified so-called extreme cases here included typically those of clean sand (ECS00) and

clayey sand (ECS30) exhibiting complete contractive flow failure mechanisms at initial mean effective stresses (MES) ranging from 50kPa to 200kPa with the combination of loose void ratio configurations typically ranging from 0.84 to 1.000. The key idea derived from the above is to characterize the undrained soil behavior with different initial states. The most recognized test method for the determination of the soil critical state parameters is the conventional monotonic triaxial compressive test. The required monotonic tests for the determination of the critical state parameters are usually executed at a wide range of MES (say 50kPa to 1000kPa) and initial void ratios depending on the capacity of the equipment. The triaxial test data is normally used to derive the state line, otherwise known as the critical state line (CSL) which is a requirement for deriving the soil's intrinsic critical state parameters. The critical state parameters are majorly Gamma (Γ) and Lambda (λ), Γ is the altitude of the CSL at a reference mean effective stress (p') corresponding to about 1kPa magnitude of stress level, and λ_{10} is the corresponding slope of the CSL in the mean effective stress – void ratio ($e - \log p'$) space. The experimental evidence indicated that the addition of kaolinite to the fabrics of ECS would lower the altitude of the CSL (i.e., the Γ parameter). The major application of the CSL is its usefulness to define a reference state for the onset of flow failure or static liquefaction and phase transformation in soils. The addition of the kaolinite clay to the ECS produced more contractive characteristics under both the monotonic and dynamic (shaking table) loadings, this is consistent with the results obtained by similar studies from previous workers (e.g., Rees, 2010).

6.2 The dynamic excess pore water characteristics

The second objective herein was to study and analyze the dynamically generated excess pore water pressure (PWP) characteristics of all the studied remolded soil specimens. A 600N-rated capacity shaking table device was applied, coupled with a designed, fabricated, and sensors-instrumented rigid soil box. The rigid soil box was instrumented with pore water transducers to measure the evolution of excess PWP generated by soil specimens pluviated into the former. The implemented soil sample preparation technique is dry pluviation with the aid of a manual pluviator and subsequent saturation with a measured volume of de-aired water. It is important to make it clear that the soil's strength and deformation properties were not considered here as a result of the utilized rigid soil box, the laminar shear box is typically utilized in the former regard. The amplification factors were computed for all the soil specimens as a ratio of the measured horizontal peak ground acceleration (PGA) at the ground surface to the PGA from the base input acceleration.

The utilized proxy for interpreting the measured dynamically-induced excess PWP of all the soil samples is the well-known liquefaction coefficient (r_u), simply expressed as the ratio of the change in PWP to the initial total effective stress. The application of the relevant scaling laws was considered during all post-computations of the measured physical model data. The designed shaking intensity herein was classified as low, intermediate, and high shake. The analyses

indicated that the clean sand sample (ECS00) exhibited the most dynamic liquefaction potential with the highest magnitude of r_u as per the excess PWP criteria for evaluating liquefaction susceptibilities of granular soils. The soil samples with more kaolinite (e.g., ECS20 and ECS30) produced the least excess PWP as expected with rather softening tendencies, this is referred to as cyclic softening in practice. Shaking at higher intensities from the input base motion produced a rather complex excess PWP pattern that is difficult to interpret in correlation with the percentage kaolinite contents. The above was caused by the densification previously applied during shaking cycles as the soil has already liquefied in the previous shaking phases, hence, different soil fabrics from the initial soil state have been created. Soil specimens with the most kaolinite content exhibited the lowest amplification factors suggesting that the ground acceleration would likely travel slower in soil medium having clays in between the fabrics of the more granular particles (i.e., sand in this case). On the contrary, the clean sand specimen (ECS00) and sand specimen having 10% kaolinite possess the highest recorded amplification factor. This indicates that the peak ground acceleration (PGA) would travel faster in granular materials with little or no fines and rock than in clayey sands. Further observation indicated manifestation of liquefaction features such as sand boils were prominently more visible in the clean sand specimen (ECS00) and that trend decreases accordingly as the kaolinite content increases within the void spaces of ECS. The soil specimen containing the most kaolinite (ECS30) was highly contractive and sensitive to volume change, hence when such soils are applied as a backfilling material, densification is the best alternative to soil stabilization. In addition to the above, the global stability and settlements need to be checked to avoid the failure of structures built on them. Overall, the takeaway of the shaking table experiments demonstrated how parametric study could be easily implemented in the laboratory to study key soil dynamic characteristics, especially if the research budget is low. The limitations of utilizing the conventional shaking table were highlighted as the initial requirement of a huge research budget in terms of costs and the required lengthy test time while its key advantage is the ability to mimic near in-situ soil stresses. However, the issues of boundary conditions and similitude laws remain lingering research issues in either small or large size soil physical model studies as the in-situ field soils exist with infinite lateral boundary conditions which are challenging to model in soil boxes with finite boundaries. It is logical to say that when the required study objective is limited to issues like dynamic excess PWP mechanism in earth dams or designed fills, the small-scale model is a useful assessment tool.

6.3 The intrinsic advanced soil geomechanical characteristics

The third research study objective herein was to assess the required advanced soil intrinsic geomechanical parameters for numerical modeling and subsequent cross-comparisons made with the experimental measured undrained behavior of the studied remolded specimens. Apart from the critical state parameters as discussed in subsection 6.1, the derived relevant geomechanical parameters are directly related to the stress dilatancy, state dilatancy, the work hardening plasticity, elasticity, and the initial soil state parameters and are comprehensively explained in

subsection 5.3 of Chapter 5. The majority of the advanced intrinsic soil geomechanical parameters were derived from the curve fittings of both drained and undrained triaxial test data and deriving the corresponding slopes and intercepts of varieties of graphs. The soil's initial state parameters include those of the critical state void ratio, initial mean effective confining stress, the overconsolidation ratio ((OCR) mostly taken as 1-1.2 herein), and state parameter (Ψ). The state parameter is a useful proxy for characterizing flow failure mechanisms, a positive state parameter would indicate loose contractive undrained behavior and a negative Ψ would indicate likely dense dilative response.

The Norsand advanced numerical model was applied for the data validation of the obtained experimental evidence. The Norsand numerical framework is an advanced critical state-compatible, stress-dependent model which utilizes the state parameter in place of the void ratio or density. A critical review of some critical state-compatible advanced numerical soil liquefaction constitutive models and cross-examination of some key features in soil constitutive relations indicated that the Norsand numerical framework is capable of capturing the key aspects of the soil undrained behavior over a wide range of effective confining stress, at least tested and confirmed in the current study between the range of 50kPa and 500kPa with the combination of void ratios ranging between 0.500 and 1.0. The Norsand model captured the softening and hardening characteristics of the soils ranging from non-plastic to highly plastic, at least 30% by weight content of kaolinite as investigated herein as per the case of ECS30. The majority of factors affecting soil liquefaction behavior were summarized to include the soil gradation (PSD and fines content), relative densities/void ratios, the applied load types (static and dynamic), the soil drainage properties (degree of saturation), the initial mean effective confining stresses in the soil element, the intensity of dynamic and static loads, the soil stress-strain histories, the soil deposit thickness (the overburden stress/total stress), distance from earthquake source, the peak ground acceleration, to mention but a few.

The executed literature review elaborated on the most relevant laboratory testing techniques that were applied in the current work; the triaxial testing for the soils' critical state determination. A systematic literature review was carried out about the effects of the several existing soil sample reconstitution methods for soil triaxial testing before concluding herein to apply the moist tamping technique (MT) herein. The key advantage of the MT remolding method over the other soil remolding techniques for critical state testing is its ability to produce brittle, loose soil specimens that are contractive and suitable for the determination of the critical state parameters, further, the problem of fines segregation from the fabrics of the sand is completely mitigated with the MT remolding method. In addition, a systematic review was carried out on previous studies about the effects of plastic fines on the liquefaction behavior of sands. Contradictory facts exist in the current literature as to whether the presence of plastic fines in the fabrics of sands either increases or decreases the liquefaction resistance of sands. The experimental evidence presented herein

confirms that the liquefaction resistance of sands may reduce due to the introduction of plastic fines into the fabric structure of sands. Experimental findings further indicated that the undrained shear strength of sand would increase at some marginal optimal percentage inclusions of plastic fines/clay (detected at 15%-20% in the current study) after which the further additional increase of clay/plastic fines would result in the rapid strain-softening phenomenon, whereby the soil shear strength decreases and exhibit similar flow failure to the clean sand specimen. Soils with properties between the “sandlike” or “claylike” behavior often possess pseudo-static or quasi-static properties by exhibiting phase change between contractive and dilative tendencies and are mostly referred to as transitional soil characteristics.

6.4 The steady/critical state failure modes

The fourth research objective is to efficiently evaluate the critical state failure modes of the studied soil specimens to further justify observations and discussions. The literature appears to be congested with many theories on the liquefaction subject and it has gradually become a specialist field on its own. However, the state concept appears to be the only framework anchoring both the theories of the well-established steady-state (SS) and critical state (CS). In other words, both the SS and CS have assumed equivalent constant rates of soil deformation characteristics immediately after steady/critical state sets in, the notable difference between them is that the CS is a computable model while the SS is not. The critical state is a well-established framework as per the current literature and it synchronizes both the soils’ consolidation and strength characteristics. A typical variant of the state concept is the equivalent granular SS where fines contents were taken into consideration based on some empirical formulas. A compendium of soil liquefaction assessment techniques was classified herein from the executed literature review to include the stress-based, cyclic strain-based, energy approach, laboratory methods, in-situ testing (CPT, SPT, Shear Wave Velocity, etc.), physical modeling (e.g., shaking table and the centrifuge tests), and performance-based methods.

The applied abbreviations for result interpretation are such that: complete flow failure – FF, limited flow – LF, No flow – NF. The obtained experimental evidence from the executed undrained triaxial monotonic compression tests on the ECS00 and ECS30 indicated complete contractive flow failure (FF) for the considered soil’s initial mean effective stress levels of 50kPa to 200kPa. ECS10 exhibited a limited flow (LF) behavior at 200kPa effective stress level and FF at 50kPa and 100kPa testing stress level with some trace of dilative tendencies. ECS15 only experienced the FF mechanism at 50kPa mean stress and LF at 100kPa and 200kPa. EC20 was analyzed with typical LF at all testing stress levels and appears to be the sample with optimal strength characteristics based on the summary provided in Table 5.1. The experimental evidence further confirms the dependence of the undrained soil behavior more on the mean effective stresses and critical state void ratios rather than the percentage content of plastic fines in the sands’ fabrics. Other factors that would determine the soil's undrained strength behavior are related to

the previously discussed advanced geomechanical properties and they are broadly anchored to the elasticity and work-plasticity theories. It was clear that the added kaolinite clay had some impacts on the undrained behavior of the studied ECS and typical transitional soil characteristics were observed with samples having kaolinite contents by weight of between 15% and 20%. The obtained undrained responses of the studied reconstituted soil specimens were consistent with other similar published results on the topic of flow failure/static liquefaction (e.g., Bayat et al., 2014; Goudarzy et al., 2021; Verdugo & Ishihara, 1996; Yoshimine & Ishihara, 1998).

As a result of research budget restraints, numerical validation of the advanced soil geomechanical parameters could not be completed for all studied soil specimens in the current study. Therefore, a decision was made to numerically validate the two soil specimens with the extreme soil undrained behavior, namely the ECS00 and ECS30. The so-called extreme soil behavior above implies that the ECS00 was the most contractive and the ECS30 was characterized by both softening and contraction. The executed simulation outputs in the VBA and FLAC codes were cross-compared with the experimental data. Overall, the model outputs were in good agreement with the laboratory-measured properties for the examined five different aspects of the soil's undrained strength characteristics. The investigated characteristics herein include the complex non-linear stress-strain relations, the effective stress paths, the state and stress dilatancies, the critical state lines as per obtained void ratio-mean effective stress $e - \log p_0'$ stress space, and the generated excess PWP. One striking feature of the applied Norsand model is that only one set of soil model properties is required to simulate a particular soil specimen, the only required variables during simulations are the soil initial state properties which include typically the state parameter Ψ , the initial mean effective stress, the soil hardening modulus (soil plasticity), and the G_{max} . It was further confirmed found from the executed iterative forward modeling that the G_{max} is a function of the mean effective stress for the soil element and may be approximated as linear proportionality. Table 5-2 in Chapter 5 contains the important inputs and outputs as obtained from the numerical simulation procedures.

Overall, the derived key insights from the current study indicate that sands with some marginal clay contents are capable of providing better liquefaction resistance when used as soil replacement methods instead of hydraulically placed sands. Factors like aging and further soil remediation measures like densification would certainly improve the strength performance of clayey sands as compared with clean sands with no plastic content in routine geotechnical engineering works. From the above, it is evident that all the designed research objectives were achieved and answers are provided for the corresponding adjoining research questions.

The monotonic compressive triaxial tests may be regarded as physical modeling of the soil behavior as well since they simulate typical effective confining stress of soil elements and they may be compared with similar existing in-situ grounds with similar effective stresses to understand the soils' relative undrained behavior under static loads. Although, there are

controversies surrounding its applicability for mostly sandlike soil specimens due to the difficulty in obtaining completely undisturbed samples in the field, however, several advanced sampling techniques such as gel-push sampling technique and soil freezing technology have been recently invented to circumvent this limitation but not completely eradicated. The application of the aforementioned soil sampling techniques is still relatively expensive especially when working on large projects. On the contrary, it is easier to obtain undisturbed soil specimens with soils of more claylike behavior and the triaxial soil model is capable of mimicking the typical soil behavior relative to its in-situ ground conditions. The monotonic triaxial compression test is the universally recognized test for critical state determination of soils and calibration of the advanced soil geomechanical parameters in numerical liquefaction constitutive models. Although it is almost practically impossible to mimic every field state such as extremely soft ground in the laboratory, the typical undrained soil behavior at the specified and investigated initial mean effective stresses (50kPa-500kPa) in the current study were reliably captured and bracketed, at least for ECS containing kaolinite fines content between 0% and 30% .

The shaking table physical model tests have been extensively applied in the literature to study varieties of soil behavior under dynamic loads. The current study utilized a 600N-capacity shaking table to evaluate the dynamically generated excess pore water pressures of the soil specimens with the aid of a designed and fabricated rigid soil box with installed sensors (pore pressure transducers and accelerometers). The strength and deformation characteristics of soils are best studied with the lamina shear box based on the obtained facts from the literature. The observed results from the executed series of shaking tests herein indicated reductions in the generation of excess PWP in the studied soil specimens as the clay contents in the fabrics of ECS increased, further confirming that clean sands with little or no plastic fines are more susceptible to earthquake-induced liquefaction. The soil specimens ECS00 and ECS30 entail the most extreme contractive and softening characteristics, both samples were numerically validated to provide complete comprehensive information on sandlike and claylike geomaterials, respectively.

6.5 Recommendations

Liquefaction mitigation methods were classified and summarized in this study as conventional methods and new emerging methods. While some of the conventional methods have the limitations of cost-effectiveness, sustainability, and applicability issues, cautions must also be taken into consideration concerning some emerging new mitigation techniques such as the application of tire chips which have environmentally friendliness issues. The tire chips include poisonous chemicals such as lead (Pb) which may cause poisoning of the groundwater if extensively utilized for liquefaction mitigation. The derived summary is that liquefaction mitigation techniques in the 21st century meeting the multicriteria of environmental friendliness, cost-effectiveness, fostering zero-emissions of greenhouse gases (e.g., CO₂) and sustainability are still relatively scarce, hence the need for extensive research on varieties of mixed geomaterials as

alternatives for possible soil replacement applications, especially for small projects including hydraulic fills, earth dams, tailing dams, and other earthworks applications where flow failure is eminent.

The implemented research methodology herein elaborates more on the involving experimental methods, physical modeling, and numerical modeling that were applied during the study. The above-mentioned approaches were utilized in studying the remolded soil specimens to have a better understanding of their undrained shear strength performance when subjected to both statically and dynamically induced loads. The research methods were designed in such a way to meet the earlier-stated research objectives. The relevant experimental methods include the basic soil classification tests, scanning electron microscopy (SEM), permeability tests, one-dimensional consolidation tests, both drained and undrained monotonic triaxial compression tests, and shaking table tests.

It is however recommended in future studies that further numerical validation studies be executed for the range of sand-clay soil mixtures (i.e., 10% to 20% by weight kaolinite) by applying the Norsand model. Numerical validation studies are still relatively scarce in the literature for clayey sands and other transitional soils. Transitional soils with optimal undrained strength performance are capable of replacing the highly liquefaction-susceptible clean sands in the field. Hence, the need for a better understanding of their undrained shear strength characteristics.

6.6 The practical applicability of the research and notable limitations

Possible instances of the applicability of the current work are the evaluation of possible static flow failure of embankments in either earth or tailing dams to inform rational design decisions. In practice, it is common to apply the limit equilibrium approach coupled with the Mohr-Coulomb model for assessing the global stability factors of safety in earth embankments. The findings in the current work suggest that it may be more appropriate to apply the soil shear strength reduction method with fully coupled finite element or finite difference numerical models to evaluate the desired factors of safety. In summary, the method outlined herein describes how to adequately capture the important complex soils' undrained strength characteristics when model calibration is followed correctly.

On the other hand, the notable limitations of the research application are summarized in the following few sentences. The applicability of the prescribed static triaxial experiments and numerical model calibration in practice are subject to site-specific geological and groundwater conditions. Due to the usually experienced physical instability in geomaterials (i.e., soils), the applicability of the numerical framework is subject to calibration of site-specific conditions that need to be modelled. In addition, due to the requirements of high numbers of triaxial tests for model calibration, the initial costs of design would be on the high side during concept designs. However, the high initial cost of designs would later pay off in the long run than the impending

failure risks that would occur as a result of inadequate assessment of the project. Apart from economic loss, high numbers of deaths have been recorded in previous dam failures.

References

- Alainachi, I., & Mamadou, F. (2019). *Liquefaction Potential of Cementing Tailing Backfill: Shaking Table Test Results*. <https://doi.org/10.3233/STAL190254>
- Alyousif, M. (2015). *Development of computer-controlled triaxial test setup and study on multistage triaxial test on sand*. Middle East Technical University. Retrieved from <https://open.metu.edu.tr/bitstream/handle/11511/25345/index.pdf>
- Amini, F., & Qi, G. Z. (2000). Liquefaction testing of stratified silty sands. *Journal of Geotechnical and Geoenvironmental Engineering*, 126(3), 208-217.
- Anastasopoulos, I., Georgarakos, T., Georgiannou, V., Drosos, V., & Kourkoulis, R. (2010). Seismic performance of bar-mat reinforced-soil retaining wall: Shaking table testing versus numerical analysis with modified kinematic hardening constitutive model. *Soil Dynamics and Earthquake Engineering*, 30(10), 1089-1105.
- Ancheta, T. D., Darragh, R. B., Stewart, J. P., Seyhan, E., Silva, W. J., Chiou, B. S., . . . Boore, D. M. (2014). NGA-West2 database. *Earthquake Spectra*, 30(3), 989-1005.
- Andrews, D. C. A., & Martin, G. R. (2000). Criteria for liquefaction of silty soils. *NZ Soc. for EQ Engrg. Upper Hutt, New Zealand*. Symposium conducted at the meeting of the Proc., 12th World Conf. on Earthquake Engineering Retrieved from <https://www.iitk.ac.in/nicee/wcee/article/0312.pdf>
- Andrianopoulos, K. I., Papadimitriou, A. G., & Bouckovalas, G. D. (2010a). Bounding surface plasticity model for the seismic liquefaction analysis of geostructures. *Soil Dynamics and Earthquake Engineering*, 30(10), 895-911. <https://doi.org/10.1016/j.soildyn.2010.04.001>
- Andrianopoulos, K. I., Papadimitriou, A. G., & Bouckovalas, G. D. (2010b). Explicit integration of bounding surface model for the analysis of earthquake soil liquefaction. *International Journal for Numerical and Analytical Methods in Geomechanics*, 34(15), 1586-1614. <https://doi.org/10.1002/nag.875>
- Andrus, R. D., & Stokoe, K. H. (1999). *Liquefaction resistance based on shear wave velocity*: United State Department of Transportation. Retrieved from <https://rosap.nrl.bts.gov/view/dot/13896>
- Andrus, R. D., & Stokoe, K. H. (2000). Liquefaction resistance of soils from shear-wave velocity. *Journal of Geotechnical and Geoenvironmental Engineering*, 126(11), 1015-1025. [https://doi.org/Doi 10.1061/\(Asce\)1090-0241\(2000\)126:11\(1015\)](https://doi.org/Doi 10.1061/(Asce)1090-0241(2000)126:11(1015))
- Andrus, R. D., Stokoe, K. H., & Juang, C. H. (2004). Guide for shear-wave-based liquefaction potential evaluation. *Earthquake Spectra*, 20(2), 285-308. <https://doi.org/10.1193/1.1715106>
- Arnedo, D., Alonso, E. E., Olivella, S., & Romero, E. (2008). Gas injection tests on sand/bentonite mixtures in the laboratory. Experimental results and numerical modelling. *Physics and Chemistry of the Earth, Parts A/B/C*, 33, S237-S247. <https://doi.org/10.1016/j.pce.2008.10.061>
- AS 1289.6.7.1. (2001). Methods of testing soils for engineering purposes Soil strength and consolidation tests *Determination of permeability of a soil - Constant head method for a remoulded specimen*.
- AS 1289.6.7.2. (2001). Methods of testing soils for engineering purposes Soil strength and consolidation tests *Determination of permeability of a soil - Falling head method for a remoulded specimen*.
- Askari, F., Dabiri, R., Shafiee, A., & Jafari, M. K. (2011). Liquefaction resistance of sand-silt mixtures using laboratory based shear Wave velocity.
- ASTM-D698-12. (2012). Standard Test Methods for Laboratory Compaction Characteristics of Soil Using Standard Effort (12 400 ft-lbf/ft³ (600 kN-m/m³)), . West Conshohocken, PA, USA.: ASTM International.
- ASTM-D854-14. (2014). Standard test methods for specific gravity of soil solids by water pycnometer. West Conshohocken, PA: ASTM International.
- ASTM-D2435/D2435M. (2011). Standard test method for onedimensional consolidation properties of soils using incremental loading *Standard test method for onedimensional consolidation properties of soils using incremental loading. Annual Book of ASTM (American Society of Testing Material) Standards* (Vol. 4).
- ASTM-D4253-16. (2016). Standard test methods for maximum index density and unit weight of soils using vibratory table. West Conshohocken, PA: ASTM International.

- ASTM-D4254-16. (2016). Standard test method for minimum index density and unit weight of soils and calculation of relative density. West Conshohocken, PA: ASTM International.
- ASTM-D4767-11. (2011). Consolidated undrained triaxial compression test for cohesive soils (pp. 929-935). West Conshohocken, PA: ASTM International.
- ASTM. (2017). Standard test methods for particle-size distribution (gradation) of soils using sieve analysis *D6913/D6913M – 17*. West Conshohocken, United States.: ASTM International.
- ASTM. (2019). Annual Book of ASTM Standards *Volume 04.08 & 04.09 Soils and Rocks - Part (I) and (II)*. West Conshohocken, PA 19428-2959: ASTM International.
- Bao, X., Jin, Z., Cui, H., Chen, X., & Xie, X. (2019). Soil liquefaction mitigation in geotechnical engineering: An overview of recently developed methods. *Soil Dynamics and Earthquake Engineering*, 120, 273-291.
- Bayat, M., Bayat, E., Aminpour, H., & Salarpour, A. (2014). Shear strength and pore-water pressure characteristics of sandy soil mixed with plastic fine. *Arabian Journal of Geosciences*, 7(3), 1049-1057.
- Been, K., & Jefferies, M. G. (1985). A State Parameter for Sands. *Geotechnique*, 35(2), 99-112. <https://doi.org/DOI> 10.1680/geot.1985.35.2.99
- Been, K., & Jefferies, M. G. (2004). Stress dilatancy in very loose sand. *Canadian Geotechnical Journal*, 41(5), 972-989.
- Been, K., Jefferies, M. G., & Hachey, J. (1991). The Critical State of Sands. *Geotechnique*, 41(3), 365-381. <https://doi.org/DOI> 10.1680/geot.1991.41.3.365
- Belkhatir, M., Arab, A., Della, N., Missoum, H., & Schanz, T. (2010). Liquefaction resistance of Chlef river silty sand: effect of low plastic fines and other parameters. *Acta Polytechnica Hungarica*, 7(2), 119-137.
- Benghalia, Y., Bouafia, A., Canou, J., & Dupla, J. (2015). Liquefaction susceptibility study of sandy soils: effect of low plastic fines. *Arabian Journal of Geosciences*, 8(2), 605-618.
- Beroya, M. A. A., Aydin, A., & Katzenbach, R. (2009). Insight into the effects of clay mineralogy on the cyclic behavior of silt-clay mixtures. *Engineering Geology*, 106(3-4), 154-162.
- Bhattacharya, S., Lombardi, D., Dihoru, L., Dietz, M. S., Crewe, A. J., & Taylor, C. A. (2012). Model container design for soil-structure interaction studies. In *Role of seismic testing facilities in performance-based earthquake engineering* (pp. 135-158): Springer.
- Blatz, J. A., Graham, J., & Chandler, N. A. (2002). Influence of suction on the strength and stiffness of compacted sand-bentonite. *Canadian Geotechnical Journal*, 39(5), 1005-1015. <https://doi.org/10.1139/t02-056>
- Bobei, D. C., Lo, S. R., Wanatowski, D., Gnanendran, C. T., & Rahman, M. M. (2009). Modified state parameter for characterizing static liquefaction of sand with fines. *Canadian Geotechnical Journal*, 46(3), 281-295.
- Boivin, P., Garnier, P., & Tessier, D. (2004). Relationship between clay content, clay type, and shrinkage properties of soil samples. *Soil Science Society of America Journal*, 68(4), 1145-1153.
- Bolarinwa, A., Kalatehjari, R., Poshdar, M., Tookey, J., & Al-Dewani, S. (2019). *A compendium of soil liquefaction potential assessment methods*. presented at the meeting of the Pacific Conference on Earthquake Engineering, Auckland, New Zealand.
- Bolarinwa, A., Kalatehjari, R., Poshdar, M., Tookey, J., Rashid, A. S., & Al-Dewani, S. (2021). *The porewater pressure characteristics of east coast sand (ECS) with different clay (Kaolinitic) contents from shaking table physical tests*. presented at the meeting of the Mediterranean Geosciences Union, Annual Meeting, Istanbul, Turkey.
- Boore, D. M., & Bommer, J. J. (2005). Processing of strong-motion accelerograms: needs, options and consequences. *Soil Dynamics and Earthquake Engineering*, 25(2), 93-115.
- Bouckovalas, G. D., Papadimitriou, A. G., Niarchos, D. G., & Tsiapas, Y. Z. (2011). Sand fabric evolution effects on drain design for liquefaction mitigation. *Soil Dynamics and Earthquake Engineering*, 31(10), 1426-1439. <https://doi.org/10.1016/j.soildyn.2011.05.019>
- Bouferra, R., & Shahrour, I. (2004). Influence of fines on the resistance to liquefaction of a clayey sand. *Proceedings of the Institution of Civil Engineers-Ground Improvement*, 8(1), 1-5.

- Boulanger, R. W., & Idriss, I. M. (2006). Liquefaction susceptibility criteria for silts and clays. *Journal of Geotechnical and Geoenvironmental Engineering*, 132(11), 1413-1426. [https://doi.org/10.1061/\(ASCE\)1090-0241\(2006\)132:11\(1413\)](https://doi.org/10.1061/(ASCE)1090-0241(2006)132:11(1413))
- Boulanger, R. W., & Idriss, I. M. (2014). CPT and SPT based liquefaction triggering procedures. *Report No. UCD/CGM-14, 1*.
- Boulanger, R. W., & Idriss, I. M. (2015). CPT-based liquefaction triggering procedure. *Journal of Geotechnical and Geoenvironmental Engineering*, 142(2), 04015065.
- Boulanger, R. W., Wilson, D. W., & Idriss, I. M. (2011). Examination and reevaluation of spt-based liquefaction triggering case histories. *Journal of Geotechnical and Geoenvironmental Engineering*, 138(8), 898-909.
- Boulanger, R. W., & Ziotopoulou, K. (2015). PM4Sand (Version 3): A sand plasticity model for earthquake engineering applications. *Center for Geotechnical Modeling Report No. UCD/CGM-15/01, Department of Civil and Environmental Engineering, University of California, Davis, Calif.*
- Bradley, B. A., & Hughes, M. (2012). Conditional peak ground accelerations in the Canterbury earthquakes for conventional liquefaction assessment. *University of Canterbury, Christchurch, New Zealand*.
- Bradshaw, A. S., & Baxter, C. D. P. (2007). Sample preparation of silts for liquefaction testing. *Geotechnical Testing Journal*, 30(4), 324-332.
- Brandon, T. L., Duncan, J. D., & Cadden, A. W. (1990). Automatic back-pressure saturation device for triaxial testing. *Geotechnical Testing Journal*, 13(2), 77-82.
- Bray, J. D., & Sam, R. B. (2006). Assessment of the liquefaction susceptibility of fine-grained soils. *Journal of Geotechnical and Geoenvironmental Engineering*, 132(9), 1165-1177. [https://doi.org/10.1061/\(ASCE\)1090-0241\(2006\)132:9\(1165\)](https://doi.org/10.1061/(ASCE)1090-0241(2006)132:9(1165))
- Bray, J. D., Sancio, R. B., Riemer, M. F., & Durgunoglu, T. (2004). Liquefaction susceptibility of fine-grained soils. *Stallion Press, Singapore*. Symposium conducted at the meeting of the Proc., 11th Int. Conf. on Soil Dynamics and Earthquake Engineering and 3rd Int. Conf. on Earthquake Geotechnical Engineering
- BS/EN/ISO-17892-1. (2014). Part 1: Determination of water content *Geotechnical investigation and testing - laboratory testing of soil* (pp. 5): British Standard Institution (BSI).
- BS/EN/ISO-17892-12. (2018). Part 12: Determination of liquid and plastic limits *Geotechnical investigation and testing - laboratory testing of soil*: British Standard Institution (BSI).
- Byrne, P. M., Park, S. S., & Beaty, M. (2003). Seismic liquefaction: centrifuge and numerical modeling Symposium conducted at the meeting of the Proceedings of 3rd International FLAC Symposium, Sudbury
- Byrne, P. M., Park, S. S., Beaty, M., Sharp, M., Gonzalez, L., & Abdoun, T. (2004). Numerical modeling of liquefaction and comparison with centrifuge tests. *Canadian Geotechnical Journal*, 41(2), 193-211. <https://doi.org/10.1139/T03-088>
- Byrne, P. M., & Seid-Karbasi, M. (2003). Seismic stability of impoundments Symposium conducted at the meeting of the 17th Annual Symposium, Vancouver Geotechnical Society
- Carraro, J. A. H. (2004). *Mechanical behavior of silty and clayey sands*. Purdue University, Purdue e-pubs. Retrieved from <https://docs.lib.purdue.edu/dissertations/AAI3154640/>
- Carraro, J. A. H., & Prezzi, M. (2007). A new slurry-based method of preparation of specimens of sand containing fines. *Geotechnical Testing Journal*, 31(1), 1-11.
- Carraro, J. A. H., Prezzi, M., & Salgado, R. (2009). Shear strength and stiffness of sands containing plastic or nonplastic fines. *Journal of Geotechnical and Geoenvironmental Engineering*, 135(9), 1167-1178.
- Castro, G., & Poulos, S. J. (1977). Factors affecting liquefaction and cyclic mobility. *Journal of Geotechnical and Geoenvironmental Engineering*, 103(6).
- Castro, G., Seed, R. B., Keller, T. O., & Seed, H. B. (1992). Steady-state strength analysis of lower San Fernando Dam slide. *Journal of Geotechnical Engineering*, 118(3), 406-427.
- Centrallandscapesupplies. (2020). *East coast sand*. Retrieved 2020, from <https://centrallandscapes.co.nz/products/east-coast-sand>
- Cetin, K. O., Seed, R. B., Der Kiureghian, A., Tokimatsu, K., Harder, L. F., Kayen, R. E., & Moss, R. E. S. (2004). Standard penetration test-based probabilistic and deterministic assessment of seismic soil liquefaction potential. *Journal of Geotechnical and*

- Geoenvironmental Engineering*, 130(12), 1314-1340.
[https://doi.org/10.1061/\(Asce\)1090-0241\(2004\)130:12\(1314\)](https://doi.org/10.1061/(Asce)1090-0241(2004)130:12(1314))
- Chaudhary, S. K., Kuwano, J., Hashimoto, S., Hayano, Y., & Nakamura, Y. (2002). Effects of initial fabric and shearing direction on cyclic deformation characteristics of sand. *Soils and Foundations*, 42(1), 147-157. <https://doi.org/DOI.10.3208/sandf.42.147>
- Chen, G., Zuo, X., Zhuang, H., & DU, X. (2008). A comparison between large-size shaking table test results and numerical simulation of a subway station structure. *Earthquake Engineering and Engineering Vibration - Chinese Edition*, 28(1), 157.
- Chen, S., Tang, B., Zhao, K., Li, X. S., & Zhuang, H. (2020). Seismic response of irregular underground structures under adverse soil conditions using shaking table tests. *Tunnelling and Underground Space Technology*, 95, 103145.
- Cheng, Z. (2013). Application of SANISAND Dafalias-Manzari model in FLAC3D (pp. 09-03): Paper.
- Cheng, Z. (2018). A practical 3D-bounding surface plastic sand model for geotechnical earthquake engineering application. In *Geotechnical Earthquake Engineering and Soil Dynamics V: Numerical Modeling and Soil Structure Interaction* (pp. 37-47): American Society of Civil Engineers Reston, VA.
- Cheng, Z., & Detournay, C. (2021). Formulation, validation and application of a practice-oriented two-surface plasticity sand model. *Computers and Geotechnics*, 132, 103984.
- Cheng, Z., & Jefferies, M. G. (2020). *Implementation and verification of NorSand model in general 3D framework*. presented at the meeting of the Geo-Congress, Minneapolis. <https://doi.org/doi.org/10.1061/9780784482810.002>
- Chopra, A. K. (1995). *Dynamics of structures theory and applications to earthquake engineering*. Eaglewood NJ: Prentice Hall International.
- Chouw, N., Orense, R., Barrios, G., & Larkin, T. (2017). *Improved understanding of liquefaction effects on shallow foundations for enhanced seismic design*: The University of Auckland, New Zealand.
- Christie, A. B., Thompson, B., & Brathwaite, B. (2000). Mineral commodity report 20—clays. *New Zealand Mining*, 27, 26-43.
- Conlee, C. T., Gallagher, P. M., Boulanger, R. W., & Kamai, R. (2012). Centrifuge modeling for liquefaction mitigation using colloidal silica stabilizer. *Journal of Geotechnical and Geoenvironmental Engineering*, 138(11), 1334-1345. [https://doi.org/10.1061/\(Asce\)Gt.1943-5606.0000703](https://doi.org/10.1061/(Asce)Gt.1943-5606.0000703)
- Cornejo, F. A. O. (2015). *Cyclic behavior of sands with superplastic fines*. Purdue University, Purdue e-pubs.
- COSMOS Virtual Data Center. (n.d.). Center for Strong Ground Motion Retrieved March, 2020. <https://strongmotioncenter.org/vdc/scripts/default.plx>
- Cubrinovski, M., Bray, J. D., de-la-Torre, C., Olsen, M., Bradley, B. A., Chiaro, G., . . . Krall, T. (2018). Liquefaction-induced damage and CPT characterization of the reclamations at centre port, Wellington, New Zealand. *Bulletin of the Seismological Society of America*, 108(3B), 1695-1708.
- Cubrinovski, M., Bray, J. D., Torre, C., Olsen, M., Bradley, B. A., Chiaro, G., . . . Wotherspoon, L. M. (2017). Liquefaction effects and associated damages observed at the Wellington Centreport from the 2016 Kaikoura earthquake.
- Cubrinovski, M., Henderson, D., & Bradley, B. A. (2012). Liquefaction impacts in residential areas in the 2010-2011 Christchurch earthquakes.
- Cubrinovski, M., & Ishihara, K. (2002). Maximum and minimum void ratio characteristics of sands. *Soils and Foundations*, 42(6), 65-78.
- D2487-17, A. (2017). Standard practice for classification of soils for engineering purposes (Unified Soil Classification System): ASTM International.
- D7928-16. (2017). Standard test method for particle-size distribution (gradation) of fine-grained soils using the sedimentation (hydrometer) analysis. West Conshohocken, PA 19428-2959, United States.: ASTM.
- Dafalias, Y. F., & Manzari, M. T. (2004). Simple plasticity sand model accounting for fabric change effects. *Journal of engineering mechanics*, 130(6), 622-634. [https://doi.org/10.1061/\(Asce\)0733-9399\(2004\)130:6\(622\)](https://doi.org/10.1061/(Asce)0733-9399(2004)130:6(622))

- Dafalias, Y. F., Papadimitriou, A. G., & Li, X. S. (2004). Sand plasticity model accounting for inherent fabric anisotropy. *Journal of engineering mechanics*, 130(11), 1319-1333.
- Dave, T. N., & Dasaka, S. M. (2012). Assessment of portable traveling pluviator to prepare reconstituted sand specimens. *Geomechanics and Engineering*, 4(2), 79-90.
- Dawson, E. M., & Mejia, L. H. (2012). Updates to a practice-oriented liquefaction model. In *GeoCongress 2012: State of the Art and Practice in Geotechnical Engineering* (pp. 2118-2127)
- DeGregorio, V. B. (1990). Loading systems, sample preparation, and liquefaction. *Journal of Geotechnical Engineering*, 116(5), 805-821.
- Derakhshandi, M., Rathje, E. M., Hazirbaba, K., & Mirhosseini, S. M. (2008). The effect of plastic fines on the pore pressure generation characteristics of saturated sands. *Soil Dynamics and Earthquake Engineering*, 28(5), 376-386.
- Dihoru, L., Taylor, C. A., Bhattacharya, S., Wood, D. M., Simonelli, A., Moccia, F., & Mylonakis, G. (2010). Shaking table testing of free field response in layered granular deposits Symposium conducted at the meeting of the Proceedings of the 14th international conference of earthquake engineering, Ohrid, paper
- Dinh, D. N., Kobayashi, K., Murakami, S., & Yasuhara, K. (2020). 1G laboratory-scale shaking table tests on reduction of liquefaction damage in sand using short gravel compaction piles. In *Geotechnics for Sustainable Infrastructure Development* (pp. 635-639): Springer.
- Dixit, J., Dewaikar, D. M., & Jangid, R. S. (2012). Assessment of liquefaction potential index for Mumbai city. *Natural Hazards and Earth System Sciences*, 12(9), 2759-2768. <https://doi.org/10.5194/nhess-12-2759-2012>
- Dizhur, D., Giaretton, M., & Ingham, J. M. (2017). Damage Observations Following the M w 7.8 2016 Kaikoura Earthquake *Springer*. Symposium conducted at the meeting of the International Conference on Earthquake Engineering and Structural Dynamics
- Doanh, T., Ibraim, E., Dubujet, P. H., Mattiotti, R., & Herle, I. (1999). Static liquefaction of very loose Hostun RF sand: Experiments and modelling. In *Physics and Mechanics of Soil Liquefaction* (pp. 17-28): Routledge.
- Donaghe, R. T., Chaney, R. C., & Silver, M. L. (1988). *Advanced triaxial testing of soil and rock*: ASTM.
- Douglas, J. (2003). Earthquake ground motion estimation using strong-motion records: a review of equations for the estimation of peak ground acceleration and response spectral ordinates. *Earth-Science Reviews*, 61(1-2), 43-104.
- Drucker, D. C., & Prager, W. (1952). Soil mechanics and plastic analysis or limit design. *Quarterly of applied mathematics*, 10(2), 157-165.
- Duputel, Z., & Rivera, L. (2017). Long-period analysis of the 2016 Kaikoura earthquake. *Physics of the Earth and Planetary Interiors*, 265, 62-66.
- Ecemis, N. (2013). Simulation of seismic liquefaction: 1-g model testing system and shaking table tests. *European Journal of Environmental and Civil Engineering*, 17(10), 899-919.
- Edbrooke, S. W., & Brook, F. J. (2009). Geology of Auckland. Lower Hutt, New Zealand.: Institute of Geological and Nuclear Sciences.
- Ehrgott, J. Q. (1971). *Calculation of stress and strain from triaxial test data on undrained soil specimens*: Waterways Experiment Station.
- El-Mohtar, C. S., Bobet, A., Drnevich, V. P., Johnston, C. T., & Santagata, M. C. (2014). Pore pressure generation in sand with bentonite: from small strains to liquefaction. *Geotechnique*, 64(2), 108.
- El-Mohtar, C. S., Bobet, A., Santagata, M. C., Drnevich, V. P., & Johnston, C. T. (2012). Liquefaction mitigation using bentonite suspensions. *Journal of Geotechnical and Geoenvironmental Engineering*, 139(8), 1369-1380.
- Fad, Z. G., Takaki, M., & Junichi, K. (2015). 1G Shaking table test and its numerical simulation on effect of input acceleration on liquefaction of embankment Symposium conducted at the meeting of the Geo Kanto Conference, Tokyo.
- Fairless, G. J., & Berrill, J. B. (1984). Liquefaction during historic earthquakes in New Zealand. *Bulletin of the New Zealand Society for Earthquake Engineering*, 17(4), 280-291.
- Fang, H. Y. (2013). *Foundation engineering handbook*: Springer Science & Business Media.

- Fiegel, G. L., & Kutter, B. L. (1994). Liquefaction mechanism for layered soils. *Journal of Geotechnical Engineering*, 120(4), 737-755.
- Figueroa, J. L., Saada, A. S., Liang, L. Q., & Dahisaria, N. M. (1994). Evaluation of Soil Liquefaction by Energy Principles. *Journal of Geotechnical Engineering-Asce*, 120(9), 1554-1569. [https://doi.org/Doi.10.1061/\(Asce\)0733-9410\(1994\)120:9\(1554\)](https://doi.org/Doi.10.1061/(Asce)0733-9410(1994)120:9(1554))
- Fishman, K. L., Mander, J. B., & R., R. J. (1995). Laboratory study of seismic free-field response of sand. *Soil Dynamics and Earthquake Engineering*, 14(1), 33-43.
- Gajo, A., Piffer, L., & De-Polo, F. (2000). Analysis of certain factors affecting the unstable behaviour of saturated loose sand. *Mechanics of Cohesive-frictional Materials: An International Journal on Experiments, Modelling and Computation of Materials and Structures*, 5(3), 215-237.
- Ganainy, H. E., Abdoun, T., & Dobry, R. (2012). Centrifuge study of the effect of permeability and other soil properties on the liquefaction and lateral spreading of dense sand. In *GeoCongress 2012: State of the Art and Practice in Geotechnical Engineering* (pp. 1998-2007)
- Gautam, D., de-Magistris, F. S., & Fabbrocino, G. (2017). Soil liquefaction in Kathmandu valley due to 25 April 2015 Gorkha, Nepal earthquake. *Soil Dynamics and Earthquake Engineering*, 97, 37-47.
- Ghahremani, M., & Ghalandarzadeh, A. (2006). Effect of plastic fines on cyclic resistance of sands. In *Soil and rock behavior and modeling* (pp. 406-412)
- Gonçalves, J., Batista, J., Paula, M., & César, M. B. (2017, 2017). One dimensional consolidation properties of solid using incremental loading test: experimental setup based on a labview approach Symposium conducted at the meeting of the Proceedings of the 7th International Conference on Mechanics and Materials in Design, Albufeira/Portugal. Retrieved from https://paginas.fe.up.pt/~m2d/Proceedings_M2D2017/data/papers/6739.pdf
- GoogleEarthPro. (2022). Map of Auckland. GoogleEarth.
- Goudarzy, M., Sarkar, D., Lieske, W., & Wichtmann, T. (2021). Influence of plastic fines content on the liquefaction susceptibility of sands: monotonic loading. *Acta Geotechnica*. <https://doi.org/10.1007/s11440-021-01283-w>
- Guo, T., & Prakash, S. (2000). Liquefaction of silt-clay mixtures. *Proceedings of the 12th World Conference Earthq. Eng., New Zealand*.
- Guoxing, C., Su, C., Xi, Z., Xiuli, D., Chengzhi, Q., & Zhihua, W. (2015). Shaking-table tests and numerical simulations on a subway structure in soft soil. *Soil Dynamics and Earthquake Engineering*, 76, 13-28.
- Gutierrez, M. (2005). Mixture theory characterization and modeling of soil mixtures. In *Geomechanics: Testing, modeling, and simulation* (pp. 600-616)
- Harder, L. F. (1997). *Application of the Becker penetration test for evaluating the liquefaction potential of gravelly soils* (1088-3800).
- Head, K. H. (2006). *Manual of soil laboratory testing* (Vol. 1). Scotland, UK: Whittles Publishing.
- Head, K. H. (2011). *Manual of soil laboratory testing* (Vol. 2). Scotland, UK.: Whittles Publishing.
- Head, K. H. (2014). *Manual of soil laboratory testing* (Vol. 1). Scotland, UK.: Whittles Publishing.
- Hird, C. C., & Hassona, F. (1990). Some factors affecting the liquefaction and flow of saturated sands in laboratory tests. *Engineering Geology*, 28(1-2), 149-170.
- Ho, D. Y. F., & Fredlund, D. G. (1982). A multistage triaxial test for unsaturated soils. *Geotechnical Testing Journal*, 5(1/2), 18-25.
- Hollingsworth, J., Ye, L., & Avouac, J. P. (2017). Dynamically triggered slip on a splay fault in the Mw 7.8, 2016 Kaikoura (New Zealand) earthquake. *Geophysical Research Letters*, 44(8), 3517-3525.
- Huang, Y., & Wang, L. (2016). Laboratory investigation of liquefaction mitigation in silty sand using nanoparticles. *Engineering Geology*, 204, 23-32. <https://doi.org/10.1016/j.enggeo.2016.01.015>
- Huang, Y., & Wen, Z. Q. (2015). Recent developments of soil improvement methods for seismic liquefaction mitigation. *Natural Hazards*, 76(3), 1927-1938. <https://doi.org/10.1007/s11069-014-1558-9>

- Iai, S. (1989). Similitude for shaking table tests on soil-structure-fluid model in 1g gravitational field. *Soils and Foundations*, 29(1), 105-118.
- Ibrahim, A. A., & Kagawa, T. (1991). Microscopic measurement of sand fabric from cyclic tests causing liquefaction. *Geotechnical Testing Journal*, 14(4), 371-382.
- Ibraim, E., Diambra, A., Russell, A. R., & Wood, D. M. (2012). Assessment of laboratory sample preparation for fibre reinforced sands. *Geotextiles and Geomembranes*, 34, 69-79.
- Ibsen, L. B. (1994). The stable state in cyclic triaxial testing on sand. *Soil Dynamics and Earthquake Engineering*, 13(1), 63-72.
- Ibsen, L. B. (1999). The mechanism controlling static liquefaction and cyclic strength of sand. In *Physics and mechanics of soil liquefaction* (pp. 29-39): Routledge.
- Idriss, I. M., & Boulanger, R. W. (2006). Semi-empirical procedures for evaluating liquefaction potential during earthquakes. *Soil Dynamics and Earthquake Engineering*, 26(2-4), 115-130. <https://doi.org/10.1016/j.soildyn.2004.11.023>
- Idriss, I. M., & Boulanger, R. W. (2008). *Soil liquefaction during earthquakes*: Earthquake Engineering Research Institute.
- Idriss, I. M., & Boulanger, R. W. (2010). SPT-based liquefaction triggering procedures. *Rep. UCD/CGM-10*, 2, 4-13.
- Imerys. (2020). *Industrial Kaolin*. Retrieved from <https://www.imerys-performance-additives.com/our-minerals/kaolin>
- Ishihara, K. (1996). Soil behaviour in earthquake geotechnics.
- Itasca. (2021). Fast Lagrangian analysis of continua. *Itasca Consulting Group Inc., Minneapolis, Minn.*
- Iwasaki, T., Arakawa, T., & Tokida, K. (1984). Simplified procedures for assessing soil liquefaction during earthquakes. *International Journal of Soil Dynamics and Earthquake Engineering*, 3(1), 49-58.
- Jafarian, Y., Ghorbani, A., Salamatpoor, S., & Salamatpoor, S. (2013). Monotonic triaxial experiments to evaluate steady-state and liquefaction susceptibility of Babolsar sand. *Journal of Zhejiang University SCIENCE A*, 14(10), 739-750.
- Jafarian, Y., Vakili, R., Abdollahi, A. S., & Baziar, M. H. (2013). Simplified soil liquefaction assessment based on cumulative kinetic energy density: attenuation law and probabilistic analysis. *International Journal of Geomechanics*, 14(2), 267-281.
- Jefferies, M. G. (1993). NorSand: A simple critical state model for sand. *Geotechnique*, 43(1), 91-103.
- Jefferies, M. G., & Been, K. (2015). *Soil liquefaction: a critical state approach*: CRC press.
- Jefferies, M. G., & Shuttle, D. A. (2002). Dilatancy in general Cambridge-type models. *Geotechnique*, 52(9), 625-638.
- Jefferies, M. G., & Shuttle, D. A. (2020). *Critical soil mechanics* [Course Notes]. Vancouver Geotechnical Society Workshop. (Available from the Subsection of the Canadian Geotechnical Society)
- Jefferies, M. G., Shuttle, D. A., & Been, K. (2015). Principal stress rotation as cause of cyclic mobility. *Geotechnical Research*, 2(2), 66-96.
- Jiang, M. J., Yu, H. S., & Leroueil, S. (2007). A simple and efficient approach to capturing bonding effect in naturally microstructured sands by discrete element method. *International Journal for Numerical Methods in Engineering*, 69(6), 1158-1193. <https://doi.org/10.1002/nme.1804>
- Juang, C. H., Yang, S. H., & Yuan, H. M. (2005). Model uncertainty of shear wave velocity-based method for liquefaction potential evaluation. *Journal of Geotechnical and Geoenvironmental Engineering*, 131(10), 1274-1282. [https://doi.org/10.1061/\(ASCE\)1090-0241\(2005\)131:10\(1274\)](https://doi.org/10.1061/(ASCE)1090-0241(2005)131:10(1274))
- Kalatehjari, R. (2020). *The permeability device flow chart* [Unpublished]. (Available from the Auckland University of Technology, Auckland, New Zealand.)
- Kanıbir, A., Ulusay, R., & Aydan, Ö. (2006). Assessment of liquefaction and lateral spreading on the shore of Lake Sapanca during the Kocaeli (Turkey) earthquake. *Engineering Geology*, 83(4), 307-331.
- Kayen, R. E., & Mitchell, J. K. (1997). Assessment of liquefaction potential during earthquakes by Arias intensity. *Journal of Geotechnical and Geoenvironmental Engineering*, 123(12), 1162-1174. <https://doi.org/Doi> 10.1061/(ASCE)1090-0241(1997)123:12(1162)

- Kayen, R. E., Moss, R. E. S., Thompson, E. M., Seed, R. B., Cetin, K. O., Kiureghian, A. D., . . . Tokimatsu, K. (2013). Shear-wave velocity-based probabilistic and deterministic assessment of seismic soil liquefaction potential. *Journal of Geotechnical and Geoenvironmental Engineering*, 139(3), 407-419.
- Khari, M., Kassim, K. A., & Adnan, A. (2014). Sand samples' preparation using mobile pluviator. *Arabian Journal for Science and Engineering*, 39(10), 6825-6834.
- Khoshnevisan, S., Juang, H., Zhou, Y. G., & Gong, W. (2015). Probabilistic assessment of liquefaction-induced lateral spreads using CPT—focusing on the 2010–2011 Canterbury earthquake sequence. *Engineering Geology*, 192, 113-128.
- Knappett, J., & Craig, R. (2012). *Craig's Soil Mechanics*: Oxford: Spon Press (Taylor & Francis Group).
- Koester, J. P. (1994). The influence of fines type and content on cyclic strength. *ASCE. Symposium conducted at the meeting of the Ground failures under seismic conditions*
- Kolay, P. K., & Ramesh, K. C. (2016). Reduction of expansive index, swelling and compression behavior of kaolinite and bentonite clay with sand and class C fly ash. *Geotechnical and Geological Engineering*, 34(1), 87-101.
- Kongar, I., Rossetto, T., & Giovinazzi, S. (2017). Evaluating simplified methods for liquefaction assessment for loss estimation. *Natural Hazards and Earth System Sciences*, 17(5), 781-800.
- Kramer, S. L. (1996). *Geotechnical earthquake engineering*. New Jersey: Prentice Hall.
- Kuerbis, R., & Vaid, Y. P. (1988). Sand sample preparation-the slurry deposition method. *Soils and Foundations*, 28(4), 107-118.
- Kutter, B. L. (2019). *Model Tests and Numerical Simulations of Liquefaction and Lateral Spreading*: Springer Nature.
- Kutter, B. L., Carey, T. J., Stone, N., Bonab, M. H., Manzari, M. T., Zeghal, M., . . . Hung, W. Y. (2020). LEAP-UCD-2017 V. 1.01 Model Specifications. In *Model Tests and Numerical Simulations of Liquefaction and Lateral Spreading* (pp. 3-29): Springer. Retrieved 14th February 2021. [https://doi.org/https://doi.org/10.1007/978-3-030-22818-7_1](https://doi.org/10.1007/978-3-030-22818-7_1)
- Kwong, N. S. (2015). *Selection and scaling of ground motions for nonlinear response history analysis of buildings in performance-based earthquake engineering*. University of California, Berkeley, UC Berkeley Electronic Theses and Dissertations. Retrieved from <http://escholarship.org/uc/item/4vq6b08x>. Available from Google Scholar database.
- Ladd, R. S. (1978). Preparing test specimen using undercompaction. *Geotechnical Testing Journal*, 1(1), 16-23.
- Lade, P. V. (2018). *Physics and mechanics of soil liquefaction*: Routledge.
- Lade, P. V., Liggio, C. D., & Yamamuro, J. A. (1998). Effects of non-plastic fines on minimum and maximum void ratios of sand. *Geotechnical Testing Journal*, 21, 336-347.
- Lade, P. V., & Yamamuro, J. A. (1997). Effects of nonplastic fines on static liquefaction of sands. *Canadian Geotechnical Journal*, 34(6), 918-928. <https://doi.org/DOI.10.1139/cgj-34-6-918>
- Lade, P. V., & Yamamuro, J. A. (2011). Evaluation of static liquefaction potential of silty sand slopes. *Canadian Geotechnical Journal*, 48(2), 247-264.
- Law, K. T., & Ling, Y. H. (1992). Liquefaction of granular soils with non-cohesive and cohesive fines Symposium conducted at the meeting of the Proceedings of the tenth world conference on earthquake engineering, Rotterdam
- Le-Hir, P., Cayocca, F., & Waeles, B. (2011). Dynamics of sand and mud mixtures: A multiprocess-based modelling strategy. *Continental Shelf Research*, 31(10), S135-S149. <https://doi.org/10.1016/j.csr.2010.12.009>
- Lee, K. M., Shen, C. K., Leung, D. H. K., & Mitchell, J. K. (1999). Effects of placement method on geotechnical behavior of hydraulic fill sands. *Journal of Geotechnical and Geoenvironmental Engineering*, 125(10), 832-846.
- Li, X. S., Dafalias, Y. F., & Wang, Z. L. (1999). State-dependant dilatancy in critical-state constitutive modelling of sand. *Canadian Geotechnical Journal*, 36(4), 599-611.
- Li, X. S., & Ming, H. Y. (2000). Unified modeling of flow liquefaction and cyclic mobility. *Soil Dynamics and Earthquake Engineering*, 19(5), 363-369.

- Lombardi, D., Bhattacharya, S., Scarpa, F., & Bianchi, M. (2015). Dynamic response of a geotechnical rigid model container with absorbing boundaries. *Soil Dynamics and Earthquake Engineering*, 69, 46-56.
- Ltifi, M., Abichou, T., & Tisot, J. P. (2014). Effects of soil aging on mechanical and hydraulic properties of a silty soil. *Geotechnical and Geological Engineering*, 32(4), 1101-1108.
- Luzi, L., Pacor, F., & Puglia, R. (2017). Italian Accelerometric Archive v 2.2. (Publication no. 10.13127/ITACA.2.2).
- Maeda, Y., Yamato, S., Sugano, Y., Sakai, G., Suemasa, N., & Tanaka, N. (2015). Evaluation of soil liquefaction potential by screw driving sounding test in residential areas Symposium conducted at the meeting of the 6th International Conference on Earthquake Geotechnical Engineering
- Marcosanti, A. (2011). *Experimental study of the transitional behaviour of the silty soils from the Venice lagoon*. Università di Bologna.
- Martin, G. R., Finn, W. D. L., & Seed, H. B. (1975). Fundamentals of liquefaction under cyclic loading. *Journal of Geotechnical and Geoenvironmental Engineering*, 101(ASCE# 11231 Proceeding).
- Marto, A., & Tan, C. S. (2012). Short review on liquefaction susceptibility. *International Journal of Engineering Research and Applications*, 2(3), 2115-2119.
- Maurer, B. W., Green, R. A., Cubrinovski, M., & Bradley, B. A. (2014). Evaluation of the liquefaction potential index for assessing liquefaction hazard in Christchurch, New Zealand. *Journal of Geotechnical and Geoenvironmental Engineering*, 140(7), 04014032. <https://doi.org/Artn> 04014032
- 10.1061/(Asce)Gt.1943-5606.0001117
- Maurer, B. W., Green, R. A., Cubrinovski, M., & Bradley, B. A. (2015). Fines-content effects on liquefaction hazard evaluation for infrastructure in Christchurch, New Zealand. *Soil Dynamics and Earthquake Engineering*, 76, 58-68. <https://doi.org/10.1016/j.soildyn.2014.10.028>
- Maurer, B. W., Green, R. A., & Taylor, O. D. S. (2015). Moving towards an improved index for assessing liquefaction hazard: Lessons from historical data. *Soils and Foundations*, 55(4), 778-787. <https://doi.org/10.1016/j.sandf.2015.06.010>
- MBIE. (2016a). *Module 2 - Geotechnical investigations for earthquake engineering*. Wellington: Ministry of Business Innovation and Employment.
- MBIE. (2016b). *Module 3: Identification, assessment and mitigation of liquefaction hazards*. Wellington: Ministry of Business Innovation and Employment.
- Mirjafari, Y., Orense, R. P., & Suemasa, N. (2016). Evaluation of liquefaction susceptibility of soils using screw driving sounding method. *Japanese Geotechnical Society Special Publication*, 2(32), 1160-1164.
- Miura, S., & Toki, S. (1982). A sample preparation method and its effect on static and cyclic deformation-strength properties of sand. *Soils and Foundations*, 22(1), 61-77.
- Miura, S., & Toki, S. (1984). Anisotropy in mechanical properties and its simulation of sands sampled from natural deposits. *Soils and Foundations*, 24(3), 69-84.
- Miura, S., Yagi, K., & Kawamura, S. (1995). Liquefaction damage of sandy and volcanic grounds in the 1993 Hokkaido Nansei-Okai earthquake Symposium conducted at the meeting of the International Conference on Recent Advances in Earthquake Engineering and Soil Dynamics Retrieved from <https://scholarsmine.mst.edu/icrageesd/03icrageesd/session03/3/>
- Mizuno, H., Sugimoto, M., Mori, T., Iiba, M., & Hirade, T. (2000). Dynamic behaviour of pile foundation in liquefaction process—Shaking table tests utilising big shear box Symposium conducted at the meeting of the Proc., 12th World Conf. on Earthquake Engineering Retrieved from <http://www.iitk.ac.in/nicee/wcee/article/1883.pdf>
- Mohammadi, A., & Qadimi, A. (2015). Characterizing the process of liquefaction initiation in Anzali shore sand through critical state soil mechanics. *Soil Dynamics and Earthquake Engineering*, 77, 152-163.
- Moretti, M., Alfaro, P., Caselles, O., & Canas, J. A. (1999). Modelling seismites with a digital shaking table. *Tectonophysics*, 304(4), 369-383.

- Morikawa, Y., & Cho, H. (2020). Numerical analysis on mechanism of dewatering as a mitigation method against liquefaction. *International Journal of Geomate*, 18(66), 68-75.
- Motamed, R., Sesov, V., Towhata, I., & Anh, N. T. (2010). Experimental modeling of large pile groups in sloping ground subjected to liquefaction-induced lateral flow: 1-G shaking table tests. *Soils and Foundations*, 50(2), 261-279.
- Mulilis, J. P., Seed, B., Clarence, K. C., Mitchell, J. K., & Arulanandan, K. (1977). Effects of sample preparation on sand liquefaction. *Journal of the Geotechnical Engineering*, 103(GT2), 91-105.
- Murao, H., Nakai, K., Noda, T., & Yoshikawa, T. (2018). Deformation–failure mechanism of saturated fill slopes due to resonance phenomena based on 1 g shaking-table tests. *Canadian Geotechnical Journal*, 55(11), 1668-1681.
- Naesgaard, E. (2011). *A hybrid effective stress–total stress procedure for analyzing soil embankments subjected to potential liquefaction and flow*. University of British Columbia, UBC, Canada. Retrieved from <http://hdl.handle.net/2429/34004>
- Nagaraj, H. B. (2016). Influence of gradation and proportion of sand on stress–strain behavior of clay–sand mixtures. *International Journal of Geoengineering*, 7(1), 19.
- NASEM. (2016). *State of the art and practice in the assessment of earthquake-induced soil liquefaction and its consequences*. Washington, DC.
- O'Donnell, S. T. (2016). *Mitigation of earthquake-induced soil liquefaction via microbial denitrification: A two-stage process*: Arizona State University.
- Okochi, Y., & Tatsuoka, F. (1984). Some factors affecting K₀-values of sand measured in triaxial cell. *Soils and Foundations*, 24(3), 52-68.
- Olson, R. S., Green, R. A., Lasley, S., Martin, N., Cox, B. R., Rathje, E. M., . . . French, J. (2011). Documenting liquefaction and lateral spreading triggered by the 12 January 2010 Haiti earthquake. *Earthquake Spectra*, 27(S1), S93-S116.
- Orense, R., Asadi, M., Stringer, M. E., & Pender, M. (2020). Evaluating liquefaction potential of pumiceous deposits through field testing. *NZSEE Bulletin*, 53(2). <https://doi.org/doi.org/10.5459/bnzsee.53.2.101-110>
- Orfeus. (n.d.). ESM - Engineering Strong-Motion database. Retrieved March, 2020. <https://www.orfeus-eu.org/data/>
- Othman, B. A., & Marto, A. (2018). Laboratory test on maximum and minimum void ratio of tropical sand matrix soils *IOP Publishing*. Symposium conducted at the meeting of the IOP Conference Series: Earth and Environmental Sciences
- Özdağ, Ö. C., Gönenç, T., & Akgün, M. (2015). Dynamic amplification factor concept of soil layers: a case study in İzmir (Western Anatolia). *Arabian Journal of Geosciences*, 8(11), 10093-10104.
- Özener, P. T., Greenfield, M. W., Sideras, S. S., & Kramer, S. L. (2020). Identification of time of liquefaction triggering. *Soil Dynamics and Earthquake Engineering*, 128, 105895.
- Pacific Earthquake Engineering Research Center (PEER). (2020). PEER NGA Ground Motion Database. Retrieved March 2020 <https://peer.berkeley.edu/peer-strong-ground-motion-databases>
- Papadimitriou, A. G., Dafalias, Y. F., & Yoshimine, M. (2005). Plasticity modeling of the effect of sample preparation method on sand response. *Soils and Foundations*, 45(2), 109-123.
- Papadopoulou, A. I., & Tika, T. (2008). The effect of fines on critical state and liquefaction resistance characteristics of non-plastic silty sands. *Soils and Foundations*, 48(5), 713-725.
- Papathanassiou, G., Ganas, A., & Valkaniotis, S. (2016). Recurrent liquefaction-induced failures triggered by 2014 Cephalonia, Greece earthquakes: spatial distribution and quantitative analysis of liquefaction potential. *Engineering Geology*, 200, 18-30. <https://doi.org/https://doi.org/10.1016/j.enggeo.2015.11.011>
- Papathanassiou, G., Mantovani, A., Tarabusi, G., Rapti, D., & Caputo, R. (2015). Assessment of liquefaction potential for two liquefaction prone areas considering the May 20, 2012 Emilia (Italy) earthquake. *Engineering Geology*, 189, 1-16. <https://doi.org/10.1016/j.enggeo.2015.02.002>
- Papazafeiropoulos, G., & Plevris, V. (2018). OpenSeismoMatlab: A new open-source software for strong ground motion data processing. *Heliyon*, 4(9), e00784. <https://doi.org/10.1016/j.heliyon.2018.e00784>

- Park, S. S., & Kim, Y. (2012). Liquefaction resistance of sands containing plastic fines with different plasticity. *Journal of Geotechnical and Geoenvironmental Engineering*, 139(5), 825-830.
- Peacock, W. H. (1968). Sand liquefaction under cyclic loading simple shear conditions. *Journal of Soil Mechanics & Foundations Div.*
- Phan, V. T. A., Hsiao, D. H., & Nguyen, P. T. (2016). Critical state line and state parameter of sand-fines mixtures. *Procedia engineering*, 142, 299-306.
- Plaxis. (2019). *Plaxis User Manuals*.
- Polito, C. P. (1999). *The effects of non-plastic and plastic fines on the liquefaction of sandy soils*. Virginia Tech.
- Polito, C. P. (2001). Plasticity based liquefaction criteria.
- Polito, C. P., Green, R. A., & Lee, J. (2008). Pore pressure generation models for sands and silty soils subjected to cyclic loading. *Journal of Geotechnical and Geoenvironmental Engineering*, 134(10), 1490-1500. [https://doi.org/10.1061/\(ASCE\)1090-0241\(2008\)134:10\(1490\)](https://doi.org/10.1061/(ASCE)1090-0241(2008)134:10(1490))
- Polito, C. P., & Martin, J. R. (2001). Effects of nonplastic fines on the liquefaction resistance of sands. *Journal of Geotechnical and Geoenvironmental Engineering*, 127(5), 408-415.
- Potter, S. H., Becker, J. S., Johnston, D. M., & Rossiter. (2015). An overview of the impacts of the 2010-2011 Canterbury earthquakes. *International Journal of Disaster Risk Reduction*, 14(2015), 6-4.
- Poulos, S. J. (1981). The steady state of deformation. *Journal of Geotechnical and Geoenvironmental Engineering*, 107(ASCE 16241 Proceeding). <https://doi.org/https://ascelibrary.org/doi/abs/10.1061/AJGEB6.0001129>
- Poulos, S. J., Castro, G., & France, J. W. (1985). Liquefaction evaluation procedure. *Journal of Geotechnical Engineering-Asce*, 111(6), 772-792. [https://doi.org/Doi10.1061/\(ASCE\)0733-9410\(1985\)111:6\(772\)](https://doi.org/Doi10.1061/(ASCE)0733-9410(1985)111:6(772))
- Prasad, S. K., Towhata, I., Chandradhara, G. P., & Nanjundaswamy, P. (2004). Shaking table tests in earthquake geotechnical engineering. *Current Science*, 87(10), 1398-1404.
- Puebla, H. (1999). *A constitutive model for sand and the analysis of the CanLex embankments*. University of British Columbia.
- Raghunandan, M., Juneja, A., & Hsiung, B. (2012). Preparation of reconstituted sand samples in the laboratory. *International Journal of Geotechnical Engineering*, 6(1), 125-131.
- Rahman, M. M., Baki, M., & Lo, S. R. (2014a). Prediction of undrained monotonic and cyclic liquefaction behavior of sand with fines based on the equivalent granular state parameter. *International Journal of Geomechanics*, 14(2), 254-266.
- Rahman, M. M., & Lo, S. R. (2008a). Effect of sand gradation and fines type on liquefaction behaviour of sand-fines mixture. In *Geotechnical earthquake engineering and soil dynamics IV* (pp. 1-11)
- Rahman, M. M., & Lo, S. R. (2008b). The prediction of equivalent granular steady state line of loose sand with fines. *Geomechanics and Geoengineering*, 3(3), 179-190.
- Rahman, M. M., & Lo, S. R. (2011). Predicting the onset of static liquefaction of loose sand with fines. *Journal of Geotechnical and Geoenvironmental Engineering*, 138(8), 1037-1041. [https://doi.org/https://ascelibrary.org/doi/abs/10.1061/\(asce\)gt.1943-5606.0000661](https://doi.org/https://ascelibrary.org/doi/abs/10.1061/(asce)gt.1943-5606.0000661)
- Rahman, M. M., Lo, S. R., & Dafalias, Y. F. (2014b). Modelling the static liquefaction of sand with low-plasticity fines. *Geotechnique*, 64(11), 881-894.
- Rayhani, M. H. T., & El Naggar, H. (2008). Physical and numerical modeling of dynamic soil-structure interaction. In *Geotechnical earthquake engineering and soil dynamics IV* (pp. 1-11)
- Reddy, K. R., Saxena, S. K., & Budiman, J. S. (1992). Development of a true triaxial testing apparatus. *Geotechnical Testing Journal*, 15(2), 89-105.
- Rees, S. D. (2010). *Effects of fines on the undrained behaviour of Christchurch sandy soils*. University of Canterbury. Civil and Natural Resources, University of Canterbury.
- Riemer, M. F., & Seed, R. B. (1997). Factors affecting apparent position of steady-state line. *Journal of Geotechnical and Geoenvironmental Engineering*, 123(3), 281-288. [https://doi.org/https://ascelibrary.org/doi/abs/10.1061/\(ASCE\)1090-0241\(1997\)123:3\(281\)](https://doi.org/https://ascelibrary.org/doi/abs/10.1061/(ASCE)1090-0241(1997)123:3(281))

- Robertson, P. K. (2010). Evaluation of flow liquefaction and liquefied strength using the cone penetration test. *Journal of Geotechnical and Geoenvironmental Engineering*, 136(6), 842-853.
- Robertson, P. K., & Wride, C. E. (1998). Evaluating cyclic liquefaction potential using the cone penetration test. *Canadian Geotechnical Journal*, 35(3), 442-459. <https://doi.org/DOI10.1139/cgj-35-3-442>
- Rollins, K. M., & Seed, H. B. (1990). Influence of buildings on potential liquefaction damage. *Journal of Geotechnical Engineering*, 116(2), 165-185.
- Roscoe, K. H., Schofield, A., & Wroth, P. (1958). On the yielding of soils. *Geotechnique*, 8(1), 22-53.
- Rosser, B. J., & Dellow, S. (2017). *Assessment of liquefaction risk in Hawke's Bay*. Lower Hutt (NZ): GNS Science Consultancy Report.
- Rugg, D. A., Yoon, J., Hwang, H., & El-Mohtar, C. S. (2011). Undrained shearing properties of sand permeated with a bentonite suspension for static liquefaction mitigation. *Proceedings of the Geo-Frontiers, Dallas, Tex*, 13-16.
- Sadek, S., & Saleh, M. (2007). The effect of carbonaceous fines on the cyclic resistance of poorly graded sands. *Geotechnical and Geological Engineering*, 25(2), 257.
- Sadigh, K., Chang, C., Egan, J. A., Makdisi, F., & Youngs, R. R. (1997). Attenuation relationships for shallow crustal earthquakes based on California strong motion data. *Seismological Research Letters*, 68(1), 180-189.
- Sana, H., & Nath, S. K. (2016). Liquefaction potential analysis of the Kashmir valley alluvium, NW Himalaya. *Soil Dynamics and Earthquake Engineering*, 85, 11-18.
- Sasaki, Y., & Taniguchi, E. (1982). Shaking table tests on gravel drains to prevent liquefaction of sand deposits. *Soils and Foundations*, 22(3), 1-14. https://doi.org/https://doi.org/10.3208/sandf1972.22.3_1
- Schmertmann, J. H. (1991). The mechanical aging of soils. *Journal of Geotechnical Engineering*, 117(9), 1288-1330.
- Schmertmann, J. H. (1993). Update on the mechanical aging of soils Symposium conducted at the meeting of the "Sobre Envejecimiento de Suelos," The Mexican Society of Soil Mechanics, Mexico City
- Schofield, A., & Wroth, P. (1968). *Critical state soil mechanics* (Vol. 310): McGraw-Hill London. Retrieved from http://www-civ.eng.cam.ac.uk/geotech_new/publications/schofield_wroth_1968.pdf
- Seed, H. B. (1982). Ground motions and soil liquefaction during earthquakes. *Earthquake engineering research insitutue*.
- Seed, H. B., & Idriss, I. M. (1971). Simplified procedure for evaluating soil liquefaction potential. *Journal of Soil Mechanics & Foundations Div.* <https://doi.org/https://ascelibrary.org/doi/abs/10.1061/JSFEAQ.0001662>
- Seed, H. B., Idriss, I. M., & Arango, I. (1983). Evaluation of Liquefaction Potential Using Field Performance Data. *Journal of Geotechnical Engineering-Asce*, 109(3), 458-482. [https://doi.org/Doi10.1061/\(Asce\)0733-9410\(1983\)109:3\(458\)](https://doi.org/Doi10.1061/(Asce)0733-9410(1983)109:3(458))
- Seed, R. B., Cetin, K. O., Moss, R. E. S., Kammerer, A. M., Wu, J., Pestana, J. M., . . . Kayen, R. E. (2003). Recent advances in soil liquefaction engineering: a unified and consistent framework Symposium conducted at the meeting of the Proceedings of the 26th Annual ASCE Los Angeles Geotechnical Spring Seminar: Long Beach, CA Retrieved from https://digitalcommons.calpoly.edu/cgi/viewcontent.cgi?article=1007&context=cenv_fa
- Silver, M. L., & Park, T. K. (1976). Liquefaction potential evaluated from cyclic strain-controlled properties tests on sands. *Soils and Foundations*, 16(3), 51-65.
- Silver, M. L., Tatsuoka, F., Phukunhaphan, A., & Avramidis, A. S. (1980). Cyclic undrained strength of sand by triaxial test and simple shear test Symposium conducted at the meeting of the Proceedings of the 7th World Conference on Earthquake Engineering
- Sivapullaiah, P. V., Sridharan, A., & Stalin, V. K. (2000). Hydraulic conductivity of bentonite-sand mixtures. *Canadian Geotechnical Journal*, 37(2), 406-413. <https://doi.org/10.1139/t99-120>
- Sladen, J. A. (1985). The liquefaction of sands, a collapse surface approach. *Canadian Geotechnical Journal*, 22(4), 564-578.

- Smitha, S., Rangaswamy, K., & Keerthi, D. S. (2021). Triaxial test behavior of silty sands treated with agar biopolymer. *International Journal of Geotechnical Engineering*, 15(4), 11. <https://doi.org/doi-org.ezproxy.aut.ac.nz/10.1080/19386362.2019.1679441>
- Stringer, M. E., Bastin, S., McGann, C., Cappellaro, C., El Kortbawi, M., McMahon, R., . . . Davis, R. (2017). Geotechnical aspects of the 2016 Kaikōura Earthquake on the South Island of New Zealand.
- Sy, A., & Campanella, R. G. (1994). Becker and standard penetration tests (BPT–SPT) correlations with consideration of casing friction. *Canadian Geotechnical Journal*, 31(3), 343-356.
- Sze, H. Y., & Yang, J. (2013). Failure modes of sand in undrained cyclic loading: impact of sample preparation. *Journal of Geotechnical and Geoenvironmental Engineering*, 140(1), 152-169.
- Tabatabaiefar, S. H. R., Fatahi, B., & Samali, B. (2014). Numerical and experimental investigations on seismic response of building frames under influence of soil-structure interaction. *Advances in structural Engineering*, 17(1), 109-130.
- Taiebat, M., & Dafalias, Y. F. (2008). SANISAND: Simple anisotropic sand plasticity model. *International Journal for Numerical and Analytical Methods in Geomechanics*, 32(8), 915-948. <https://doi.org/10.1002/nag.651>
- Taiebat, M., Jeremic, B., Dafalias, Y. F., Kaynia, A. M., & Cheng, Z. (2010). Propagation of seismic waves through liquefied soils. *Soil Dynamics and Earthquake Engineering*, 30(4), 236-257. <https://doi.org/10.1016/j.soildyn.2009.11.003>
- Taiebat, M., Shahir, H., & Pak, A. (2007). Study of pore pressure variation during liquefaction using two constitutive models for sand. *Soil Dynamics and Earthquake Engineering*, 27(1), 60-72. <https://doi.org/10.1016/j.soildyn.2006.03.004>
- Talamkhani, S., & Naeini, S. A. (2018). Effect of Plastic Fines on Undrained Behavior of Clayey Sands. *International Journal of Geotechnical and Geological Engineering*, 12(8), 519-522.
- Tan, C. S., Marto, A., Leong, T. K., & Teng, L. S. (2013). The role of fines in liquefaction susceptibility of sand matrix soils. *Electronic Journal of Geotechnical Engineering*, 18, 2355-2368.
- Tatsuoka, F., Iwasaki, T., Yoshida, S., Fukushima, S., & Sudo, H. (1979). Shear modulus and damping by drained tests on clean sand specimens reconstituted by various methods. *Soils and Foundations*, 19(1), 39-54.
- Tatsuoka, F., Muramatsu, M., & Sasaki, T. (1982). Cyclic undrained stress-strain behavior of dense sands by torsional simple shear test. *Soils and Foundations*, 22(2), 55-70.
- Tatsuoka, F., Ochi, K., Fujii, S., & Okamoto, M. (1986). Cyclic undrained triaxial and torsional shear strength of sands for different sample preparation methods. *Soils and Foundations*, 26(3), 23-41.
- Taylor, M. L., Cubrinovski, M., & Bradley, B. A. (2015). *Earthquake-induced liquefaction triggering of Christchurch sandy soils*. presented at the meeting of the NZSEE Conference,
- Terzaghi, K. (1943). *Theoretical soil mechanics* (Vol. 18). New York: Wiley.
- Thevanayagam, S., & Mohan, S. (2000). Intergranular state variables and stress–strain behaviour of silty sands. *Geotechnique*, 50(1), 1-23. <https://doi.org/doi-abs/10.1680/geot.2000.50.1.1>
- Thevanayagam, S., Shenthan, T., Mohan, S., & Liang, J. (2002). Undrained fragility of clean sands, silty sands, and sandy silts. *Journal of Geotechnical and Geoenvironmental Engineering*, 128(10), 849-859. [https://doi.org/doi/pdf/10.1061/\(ASCE\)1090-0241\(2002\)128:10\(849\)](https://doi.org/doi/pdf/10.1061/(ASCE)1090-0241(2002)128:10(849))
- Towhata, I. (2008). *Geotechnical Earthquake Engineering* (Vol. 1). Verlag Berlin Heidelberg: Springer. <https://doi.org/10.1007/978-3-540-35783-4>
- Towhata, I., Otsubo, M., Uchimura, T., Shimura, M., Liu, B. G., Hayashida, T., . . . Cauvin, B. (2015). Shaking model tests on liquefaction mitigation of embedded lifeline. In *Perspectives on Earthquake Geotechnical Engineering* (pp. 311-341): Springer.
- Towhata, I., Yasuda, S., Yoshida, K., Motohashi, A., Sato, S., & Arai, M. (2016). Qualification of residential land from the viewpoint of liquefaction vulnerability. *Soil Dynamics and*

- Troncoso, J. H. (1985). Silt content and dynamic behavior of tailing sands Symposium conducted at the meeting of the Proc. 11th ICSMFE
- Tsai, P. H., Lee, D. H., Kung, G. T. C., & Hsu, C. H. (2010). Effect of content and plasticity of fines on liquefaction behaviour of soils. *Quarterly Journal of Engineering Geology and Hydrogeology*, 43(1), 95-106.
- Uchimura, T., Chi, N., Nirmalan, S., Sato, T., Meidani, M., & Towhata, I. (2007). Shaking table tests on effect of tire chips and sand mixture in increasing liquefaction resistance and mitigating uplift of pipe Symposium conducted at the meeting of the Proceedings, international workshop on scrap tire derived geomaterials—opportunities and challenges, Yokosuka, Japan
- Ueng, T. S. (2010). Shaking table tests for studies of soil liquefaction and soil-pile interaction. *Geotechnical Engineering*, 41(1), 29.
- Ueng, T. S., Wang, M. H., Chen, M. H., Chen, C. H., & Peng, L. H. (2005). A large biaxial shear box for shaking table test on saturated sand. *Geotechnical Testing Journal*, 29(1), 1-8.
- Upreti, S. (2016). *Effects of plasticity on liquefaction characteristics of fine-grained soils*: Southern Illinois University at Carbondale.
- Vaid, Y. P. (1994). *Liquefaction of silty soils*. presented at the meeting of the Ground failures under seismic conditions,
- Vaid, Y. P., Chung, E. K. F., & Kuerbis, R. H. (1989). Preshearing and undrained response of sand. *Soils and Foundations*, 29(4), 49-61.
- Vaid, Y. P., & Sivathayalan, S. (2000). Fundamental factors affecting liquefaction susceptibility of sands. *Canadian Geotechnical Journal*, 37(3), 592-606. <https://doi.org/doi/abs/10.1139/t00-040>
- Vaid, Y. P., Sivathayalan, S., & Stedman, D. (1999). Influence of specimen-reconstituting method on the undrained response of sand. *Geotechnical Testing Journal*, 22(3), 187-195.
- vanBallegooy, S., Green, R. A., Lees, J., Wentz, F., & Maurer, B. W. (2015). Assessment of various CPT based liquefaction severity index frameworks relative to the Ishihara (1985) H1–H2 boundary curves. *Soil Dynamics and Earthquake Engineering*, 79, 347-364. <https://doi.org/doi.org/10.1016/j.soildyn.2015.08.015>
- vanBallegooy, S., Malan, P., Lacrosse, V., Jacka, M. E., Cubrinovski, M., Bray, J. D., . . . Cowan, H. (2014). Assessment of liquefaction-induced land damage for residential Christchurch. *Earthquake Spectra*, 30(1), 31-55. <https://doi.org/doi/pdf/10.1193/031813EQS070M>
- Varghese, R. M., & Latha, G. M. (2014). Shaking table tests to investigate the influence of various factors on the liquefaction resistance of sands. *Natural Hazards*, 73(3), 1337-1351. <https://doi.org/10.1007/s11069-014-1142-3>
- Verdugo, R., & Ishihara, K. (1996). The steady state of sandy soils. *Soils and Foundations*, 36(2), 81-91. https://doi.org/doi.org/10.3208/sandf.36.2_81
- Viana da Fonseca, A., Cordeiro, D., & Molina-Gómez, F. (2021). Recommended procedures to assess critical state locus from triaxial tests in cohesionless remoulded samples. *Geotechnics*, 1(1), 95-127. <https://doi.org/doi.org/10.3390/geotechnics1010006>
- Vytiniotis, A. (2011). *Contributions to the analysis and mitigation of liquefaction in loose sand slopes*. Massachusetts Institute of Technology.
- Wan, R. G., & Guo, P. J. (2001). Effect of microstructure on undrained behaviour of sands. *Canadian Geotechnical Journal*, 38(1), 16-28.
- Wang, J., Salam, S., & Xiao, M. (2020). Evaluation of the effects of shaking history on liquefaction and cone penetration resistance using shake table tests. *Soil Dynamics and Earthquake Engineering*, 131, 106025. <https://doi.org/doi.org/10.1016/j.soildyn.2019.106025>
- Wang, W. (1979). *Some findings in soil liquefaction*: Earthquake Engineering Department, Water Conservancy and Hydroelectric Power
- Wang, Z. L., Dafalias, Y. F., & Shen, C. K. (1990). Bounding Surface Hypoplasticity Model for Sand. *Journal of Engineering Mechanics-Asce*, 116(5), 983-1001. [https://doi.org/Doi10.1061/\(Asce\)0733-9399\(1990\)116:5\(983\)](https://doi.org/Doi10.1061/(Asce)0733-9399(1990)116:5(983))
- Wichtmann, T. (2005). *Explicit accumulation model for non-cohesive soils under cyclic loading*. Inst. für Grundbau und Bodenmechanik Bochum University, Germany.

- Wijewickreme, D., Srischandakumar, S., & Byrne, P. (2005). Cyclic loading response of loose air-pluviated Fraser River sand for validation of numerical models simulating centrifuge tests. *Canadian Geotechnical Journal*, 42(2), 550-561. <https://doi.org/doi/abs/10.1139/t04-119>
- Wood, D. M. (1990). *Soil behaviour and critical state soil mechanics*: Cambridge university press.
- Wood, F. M., Yamamuro, J. A., & Lade, P. V. (2008). Effect of depositional method on the undrained response of silty sand. *Canadian Geotechnical Journal*, 45(11), 1525-1537. <https://doi.org/10.1139/T08-079>
- Woods, R. J., McBride, S. K., Wotherspoon, L. M., Beaven, S. J., Potter, S. H., Johnston, D. M., . . . Brackley, H. (2017). Science to emergency management response: Kaikoura earthquakes 2016.
- Wotherspoon, L. M., Orense, R. P., Bradley, B. A., Cox, B. R., Wood, C. M., & Green, R. A. (2015). Soil profile characterisation of Christchurch central business district strong motion stations. *Bulletin of the New Zealand Society for Earthquake Engineering*, 48(3).
- Wotherspoon, L. M., Orense, R. P., Green, R. A., Bradley, B. A., Cox, B. R., & Wood, C. M. (2015). Assessment of liquefaction evaluation procedures and severity index frameworks at Christchurch strong motion stations. *Soil Dynamics and Earthquake Engineering*, 79, 335-346. <https://doi.org/10.1016/j.soildyn.2015.03.022>
- Xenaki, V. C., & Athanasopoulos, G. A. (2003). Liquefaction resistance of sand-silt mixtures: an experimental investigation of the effect of fines. *Soil Dynamics and Earthquake Engineering*, 23(3), 1-12. [https://doi.org/10.1016/S0267-7261\(02\)00210-5](https://doi.org/10.1016/S0267-7261(02)00210-5)
- Xiao, P., Liu, H. L., Xiao, Y., Stuedlein, A. W., & Evans, T. M. (2018). Liquefaction resistance of bio-cemented calcareous sand. *Soil Dynamics and Earthquake Engineering*, 107, 9-19. <https://doi.org/10.1016/j.soildyn.2018.01.008>
- Xu, H., & VanDeventer, J. S. J. (2002). Microstructural characterisation of geopolymers synthesised from kaolinite/stilbite mixtures using XRD, MAS-NMR, SEM/EDX, TEM/EDX, and HREM. *Cement and Concrete research*, 32(11), 1705-1716.
- Yamamuro, J. A., & Lade, P. V. (1998). Steady-state concepts and static liquefaction of silty sands. *Journal of Geotechnical and Geoenvironmental Engineering*, 124(9), 868-877. [https://doi.org/Doi 10.1061/\(Asce\)1090-0241\(1998\)124:9\(868\)](https://doi.org/Doi 10.1061/(Asce)1090-0241(1998)124:9(868))
- Yamamuro, J. A., & Lade, P. V. (1999). Experiments and modelling of silty sands susceptible to static liquefaction. *Mechanics of Cohesive-frictional Materials: An International Journal on Experiments, Modelling and Computation of Materials and Structures*, 4(6), 545-564.
- Yamamuro, J. A., & Wood, F. M. (2004). Effect of depositional method on the undrained behavior and microstructure of sand with silt. *Soil Dynamics and Earthquake Engineering*, 24(9-10), 751-760. <https://doi.org/10.1016/j.soildyn.2004.06.004>
- Yang, J. (2002). Non-uniqueness of flow liquefaction line for loose sand. *Geotechnique*, 52(10), 757-760. <https://doi.org/doi.org/10.1680/geot.2002.52.10.757>
- Yang, S. L., Sandven, R., & Grande, L. (2006). Steady-state lines of sand-silt mixtures. *Canadian Geotechnical Journal*, 43(11), 1213-1219. <https://doi.org/doi.org/10.1139/t06-069>
- Yasuda, S., Nagase, H., Kiku, H., & Uchida, Y. (1992). The mechanism and a simplified procedure for the analysis of permanent ground displacement due to liquefaction. *Soils and Foundations*, 32(1), 149-160.
- Ye, B., Ye, G. L., Zhang, F., & Yashima, A. (2007). Experiment and numerical simulation of repeated liquefaction-consolidation of sand. *Soils and Foundations*, 47(3), 547-558. <https://doi.org/DOI 10.3208/sandf.47.547>
- Yegian, M. K., Eseller-Bayat, E., Alshawabkeh, A., & Ali, S. (2007). Induced-partial saturation for liquefaction mitigation: Experimental investigation. *Journal of Geotechnical and Geoenvironmental Engineering*, 133(4), 372-380. [https://doi.org/10.1061/\(Asce\)1090-0241\(2007\)133:4\(372\)](https://doi.org/10.1061/(Asce)1090-0241(2007)133:4(372))
- Yimsiri, S., & Soga, K. (2010). DEM analysis of soil fabric effects on behaviour of sand. *Geotechnique*, 60(6), 483-495. <https://doi.org/10.1680/geot.2010.60.6.483>
- Yoshimine, M., & Ishihara, K. (1998). Flow potential of sand during liquefaction. *Soils and Foundations*, 38(3), 189-198.

- Yoshimine, M., Ishihara, K., & Vargas, W. (1998). Effects of principal stress direction and intermediate principal stress on undrained shear behavior of sand. *Soils and Foundations*, 38(3), 179-188.
- Youd, T. L. (1999). Updating assessment procedures and developing a screening guide for liquefaction *Research Progress* (pp. 79).
- Youd, T. L., & Idriss, I. M. (2001). Liquefaction resistance of soils: summary report from the 1996 NCEER and 1998 NCEER/NSF workshops on evaluation of liquefaction resistance of soils. *Journal of Geotechnical and Geoenvironmental Engineering*, 127(4), 297-313.
- Youd, T. L., Idriss, I. M., Andrus, R. D., Arango, I., Castro, G., Christian, J. T., . . . Hynes, M. E. (2003). Closure to “liquefaction resistance of soils: summary report from the 1996 NCEER and 1998 NCEER/NSF workshops on evaluation of liquefaction resistance of soils” *Journal of Geotechnical and Geoenvironmental Engineering*, 129(3), 284-286. [https://doi.org/doi/pdf/10.1061/\(ASCE\)1090-0241\(2003\)129:3\(284\)](https://doi.org/doi/pdf/10.1061/(ASCE)1090-0241(2003)129:3(284))
- Yu, H. S., Zeng, X., Li, B., & Ming, H. Y. (2012). Effect of fabric anisotropy on liquefaction of sand. *Journal of Geotechnical and Geoenvironmental Engineering*, 139(5), 765-774. [https://doi.org/10.1061/\(ASCE\)GT.1943-5606.0000807](https://doi.org/10.1061/(ASCE)GT.1943-5606.0000807)
- Yusa, M. (2015). *Aging and creep of non-plastic silty sand*. University of Canterbury, Christchurch New Zealand., UC Research Repository.
- Zealand, G.-G. H. I. f. N. (n.d.). Strong Motion Data Products. Retrieved March, 2020.
- Zheng, J., & Hryciw, R. D. (2018). Identification and characterization of particle shapes from images of sand assemblies using pattern recognition. *Journal of Computing in Civil Engineering*, 32(3), 04018016.

APPENDICES

APPENDIX A – Particle size analysis (PSD) of ECS00

A1: Test 1

AUT		Sieve Analysis Data Sheet			
		ASTM D6913M-17(2019)			
Project Name:	PhD Research	Tested By:	A. Bolarinwa	Date:	6/08/2019
Location:	City Campus	Checked By:	R. Kalatehjari	Date:	6/08/2019
Sample No:	ECS00	Test Number:	1		
USCS Soil Classification:		SP			
AASHTO Soil Classification:					
Weight of Container (g):	499.19	Weight of Container & Soil (g):		1127.73	
Weight of Dry Sample (g):	628.54				

Sieve Number	Diameter (mm)	Mass of Sieve (g)	Mass of Sieve & Soil (g)	Soil Retained (g)	Soil Retained (%)	Soil Passing (%)
#4	4.75	584.27	584.27	0.00	0.00	100.0
#8	2.36	532.33	532.63	0.30	0.05	100.0
#10	2.00	536.06	536.38	0.32	0.05	99.9
#20	0.850	492.98	497.31	4.33	0.69	99.2
#40	0.425	453.63	497.57	43.94	6.98	92.2
#60	0.250	450.51	682.79	232.28	36.90	55.3
#100	0.150	416.69	727.74	311.05	49.41	5.9
#140	0.106	410.80	443.52	32.72	5.20	0.7
#200	0.075	456.80	460.18	3.38	0.54	0.2
Pan		499.16	500.40	1.24	0.20	
TOTAL				629.56	100.00	

Grain Size

% Gravel:	0	D ₁₀ :	0.162	C _u :	1.62
% Sand:	99.8	D ₃₀ :	0.202	C _c :	0.95
% Fines:	0.2	D ₆₀ :	0.263		
		D ₅₀ :	0.245		

A2: Test 2

AUT		Sieve Analysis Data Sheet			
ASTM D6913M-17(2019)					
Project Name:	PhD Research	Tested By:	A. Bolarinwa	Date:	7/08/2019
Location:	AUT City Campus	Checked By:	R. Kalatehjari	Date:	7/08/2019
Sample No:	ECS00	Test Number:	2		
USCS Soil Classification:		SP			
AASHTO Soil Classification:					
Weight of Container (g):	499.19	Weight of Container & Soil (g):	1103.49		
Weight of Dry Sample (g):	604.30				

Sieve Number	Diameter (mm)	Mass of Sieve (g)	Mass of Sieve & Soil (g)	Soil Retained (g)	Soil Retained (%)	Soil Passing (%)
#4	4.75	584.30	584.32	0.02	0.00	100.0
#8	2.36	532.38	532.51	0.13	0.02	100.0
#10	2.00	536.12	536.42	0.30	0.05	99.9
#20	0.850	492.99	497.33	4.34	0.72	99.2
#40	0.425	453.79	497.15	43.36	7.17	92.0
#60	0.250	450.58	679.46	228.88	37.87	54.2
#100	0.150	416.72	712.75	296.03	48.98	5.2
#140	0.106	410.82	440.11	29.29	4.85	0.3
#200	0.075	456.82	458.38	1.56	0.26	0.1
Pan		499.21	499.67	0.46	0.08	
TOTAL				604.37	100.00	

Grain Size Distribution Curve Results:

% Gravel:	0	D ₁₀ :	0.164	C _u :	1.62
% Sand:	99.8	D ₃₀ :	0.203	C _c :	0.94
% Fines:	0.2	D ₆₀ :	0.266		
		D ₅₀ :	0.245		

A3: Test 3

		<h2 style="margin: 0;">Sieve Analysis Data Sheet</h2> <p style="margin: 0;">ASTM D6913M-17(2019)</p>			
Project Name:	PhD Research	Tested By:	A. Bolarinwa	Date:	7/08/2019
Location:	AUT City Campus	Checked By:	R. Kalatehjari	Date:	7/08/2019
Sample No:	ECS00	Test Number:	3		
USCS Soil Classification:		SP			
AASHTO Soil Classification:					
Weight of Container (g):	499.21	Weight of Container & Soil (g):		1112.22	
Weight of Dry Sample (g):	613.01				

Sieve Number	Diameter (mm)	Mass of Sieve (g)	Mass of Sieve & Soil (g)	Soil Retained (g)	Soil Retained (%)	Soil Passing (%)
#4	4.75	584.24	584.26	0.02	0.00	100.0
#8	2.36	532.31	532.43	0.12	0.02	100.0
#10	2.00	536.06	536.44	0.38	0.06	99.9
#20	0.850	493.07	496.89	3.82	0.62	99.3
#40	0.425	453.72	495.86	42.14	6.87	92.4
#60	0.250	450.59	671.29	220.70	35.97	56.5
#100	0.150	416.70	718.25	301.55	49.14	7.3
#140	0.106	410.83	451.41	40.58	6.61	0.7
#200	0.075	456.81	460.37	3.56	0.58	0.1
Pan		499.21	499.96	0.75	0.12	
TOTAL				613.62	100.00	

The graph plots % Passing (0 to 100) against Particle Diameter (mm) on a semi-logarithmic scale (10.00 to 0.01). The curve starts at 100% passing for diameters down to approximately 0.25 mm, then drops sharply to about 0.1% passing at 0.075 mm. Soil classification zones are indicated: GRAVEL (> 4.75 mm), Coarse SAND (2.0 - 4.75 mm), Medium SAND (0.425 - 2.0 mm), Fine SAND (0.075 - 0.425 mm), and SILT/CLAY (< 0.075 mm). Key sieve numbers #4, #10, #40, and #200 are marked on the curve.

Grain Size Distribution Curve Results:					
% Gravel:	0	D ₁₀ :	0.158	C _u :	1.65
% Sand:	99.83	D ₃₀ :	0.199	C _c :	0.96
% Fines:	0.17	D ₆₀ :	0.26		
		D ₅₀ :	0.245		

APPENDIX B – Atterberg's' Limits

Atterberg limits for Kaolinite (Casagrande's method)

B1: Test 1 for Kaolinite (100% by weight)

<div style="display: flex; justify-content: space-between; align-items: center;"> <div style="background-color: black; color: white; padding: 5px; font-weight: bold; font-size: 1.2em;">AUT</div> <div> Atterberg Limits Data Sheet BS EN ISO 17892-12:2018 </div> </div>										
Project Name:			PhD Research				Tested By:		A. Bolarinwa	
Test Location:			AUT City Campus				Checked By:		R. Kalatehjari	
Sample Description:			Industrial kaolinite				Test Number:		1	
Sample No:			K-00							
USCS Soil Classification:			Inorganic Clay (CL)							

TEST			PLASTIC LIMIT				LIQUID LIMIT			
Variable	NO		1	2	3	4	1	2	3	4
	Var.	Units								
Number of Blows	N	blows					27	20	22	35
Log (N)							1.43	1.30	1.34	1.54
Can Number	---	---	C-1	C-2	C-3		T-1	T-2	T-3	T-4
Mass of Empty Can	M _C	(g)	21.04	6.28	6.15		13.81	14.88	20.53	17.53
Mass Can & Soil (Wet)	M _{CMS}	(g)	23.10	9.45	8.00		20.44	23.14	27.62	24.45
Mass Can & Soil (Dry)	M _{CDS}	(g)	22.57	8.67	7.54		18.45	20.54	25.45	22.40
Mass of Soil	M _S	(g)	1.53	2.39	1.39		4.64	5.66	4.92	4.87
Mass of Water	M _W	(g)	0.53	0.78	0.46		1.99	2.60	2.17	2.05
Water Content	w	(%)	34.6	32.6	33.1		42.9	45.9	44.1	42.1

Liquid Limit (LL or w _L) (%)	44
Plastic Limit (PL or w _P) (%)	33
Plasticity Index (PI) (%)	10
USCS Classification:	CL

PI at "A" Line = 0.73(LL-20)

One Point Liquid Limit Calculation:

$$LL = w_p (N/25)^{0.12}$$

PROCEDURE USED	
<input checked="" type="checkbox"/>	Casagrande Method
<input type="checkbox"/>	Fall Cone Method
<input type="checkbox"/>	
<input type="checkbox"/>	

Regression Analysis

Slope: -14.457

64.06423

B2: Test 2 for Kaolinite

AUT			Atterberg Limits Data Sheet BS EN ISO 17892-12:2018							
Project Name: PhD Research			Tested By: A. Bolarinwa			Date: 15-Jul-2019				
Location: AUT City Campus			Checked By: R. Kalatehjari			Date: 16-Jul-2019				
Sample Description: Industrial kaolinite			Test Number: 2							
Sample No: K-00										
USCS Soil Classification:			Inorganic Clay (CL)							
TEST			PLASTIC LIMIT				LIQUID LIMIT			
Variable	NO		1	2	3	4	1	2	3	4
	Var.	Units								
Number of Blows	N	blows					20	18	17	16
Log (N)							1.30	1.26	1.23	1.20
Can Number	---	---	C-1	C-2	C-3		T-1	T-2	T-3	T-4
Mass of Empty Can	M _C	(g)	21.04	6.28	6.15		13.80	14.87	20.51	17.54
Mass Can & Soil (Wet)	M _{CMS}	(g)	22.67	7.59	8.54		21.93	24.80	30.80	24.87
Mass Can & Soil (Dry)	M _{CDS}	(g)	22.25	7.23	7.92		19.41	21.74	27.58	22.58
Mass of Soil	M _S	(g)	1.21	0.95	1.77		5.61	6.87	7.07	5.04
Mass of Water	M _W	(g)	0.42	0.36	0.62		2.52	3.06	3.22	2.29
Water Content	w	(%)	34.7	37.9	35.0		44.9	44.5	45.5	45.4
Liquid Limit (LL or w _L) (%):							44			
Plastic Limit (PL or w _P) (%):							36			
Plasticity Index (PI) (%):							8			
USCS Classification:							CL			
<p>PI at "A" Line = 0.73(LL-20)</p> <p>One Point Liquid Limit Calculation:</p> $LL = w_p(N/25)^{0.12}$										
PROCEDURE USED										
X	Casagrande Method									
	Fall Cone Method									
<p>Regression Analysis</p> <p>Slope: -7.09557</p> <p>53.96386</p>										

B3: Test 3 for Kaolinite

<div style="display: inline-block; background-color: black; color: white; padding: 5px; font-weight: bold; font-size: 1.2em;">AUT</div>			Atterberg Limits Data Sheet BS EN ISO 17892-12:2018											
Project Name:			PhD Research				Tested By:		A. Bolarinwa		Date:		17-Jul-2019	
Location:			AUT City Campus				Checked By:		R. Kalatehjari		Date:		18-Jul-2019	
Sample Description:			Industrial kaolinite				Test Number:		3					
Sample No:			K-00											
USCS Soil Classification:			Inorganic Clay (CL)											
TEST			PLASTIC LIMIT				LIQUID LIMIT							
Variable	NO		1	2	3	4	1	2	3	4				
	Var.	Units												
Number of Blows	N	blows					27	24	21	31				
Log (N)							1.43	1.38	1.32	1.49				
Can Number	—	—	C-1	C-2	C-3		T-1	T-2	T-3	T-4				
Mass of Empty Can	M _C	(g)	21.07	6.30	6.18		13.82	14.89	20.53	17.56				
Mass Can & Soil (Wet)	M _{CMS}	(g)	22.52	8.22	6.96		19.32	21.65	25.50	23.04				
Mass Can & Soil (Dry)	M _{CDS}	(g)	22.16	7.71	6.75		17.61	19.51	23.93	21.33				
Mass of Soil	M _S	(g)	1.09	1.41	0.57		3.79	4.62	3.40	3.77				
Mass of Water	M _W	(g)	0.36	0.51	0.21		1.71	2.14	1.57	1.71				
Water Content	W	(%)	33.0	36.2	36.8		45.1	46.3	46.2	45.4				
Liquid Limit (LL or w _L) (%):							46							
Plastic Limit (PL or w _P) (%):							35							
Plasticity Index (PI) (%):							10							
USCS Classification:							CL							
PI at "A" Line = 0.73(LL-20) One Point Liquid Limit Calculation: $LL = w_p(N/25)^{0.12}$														
PROCEDURE USED														
<div style="border: 1px solid black; padding: 5px; font-size: 1.5em; width: 30px; height: 30px; display: flex; align-items: center; justify-content: center;">X</div>		Casagrande Method												
<div style="border: 1px solid black; padding: 5px; font-size: 1.5em; width: 30px; height: 30px; display: flex; align-items: center; justify-content: center;"> </div>		Fall Cone Method												
<div style="border: 1px solid black; padding: 5px; font-size: 1.5em; width: 30px; height: 30px; display: flex; align-items: center; justify-content: center;"> </div>														
<div style="border: 1px solid black; padding: 5px; font-size: 1.5em; width: 30px; height: 30px; display: flex; align-items: center; justify-content: center;"> </div>														
<div style="border: 1px solid black; padding: 5px; font-size: 1.5em; width: 30px; height: 30px; display: flex; align-items: center; justify-content: center;"> </div>														
<div style="border: 1px solid black; padding: 5px; font-size: 1.5em; width: 30px; height: 30px; display: flex; align-items: center; justify-content: center;"> </div>														
<div style="display: flex; justify-content: space-between;"> <div> <p>Regression Analysis</p> <p>Slope: -6.39792</p> <p>54.74073</p> </div> <div> </div> </div>														
<div style="display: flex; justify-content: space-between;"> <div> </div> <div> <p>Water Content (%)</p> <p>Number of Blows (N)</p> </div> </div>														

The fall-cone liquid limit method and plastic limit of kaolinite

B4: Consistency limits of Kaolinite (Clay)

AUT		Atterberg Limits Data Sheet		BS EN ISO 17892-12:2018	
Project Name:	PhD Research	Tested By:	A. Bolarinwa	Date:	13-Sep-2019
Location:	AUT City Campus	Checked By:	R. Kalatehjari	Date:	14-Sep-2019
Sample Description:	Kaolinite	Test Trial Numbers:	3		
Sample No:	KK-00				
USCS Soil Classification:		CL			
LL Determination by Cone Penetration Method		Plastic Limit Determination			
Avg. Penetration (mm)	Avg. Moisture content (%)	Description/Test Trials	1	2	3
17.5	45.52	Mass of tar + wet soil (M ₁) g	11.29	11.77	10.88
15.5	45.76	Mass of tar + dry soil (M ₂) g	10.72	11.1	10.52
21.73	47.57	Mass of container (M _c) g	9.04	9	9.39
18.7	46.86	Mass of water (M _w) g	0.57	0.67	0.36
21.32	46.9	Mass of dried soil (M _d) g	1.68	2.10	1.13
		Plastic Limit (w _p) %	33.93	31.90	31.86
		Average	31.88		
<p>Linear (moisture content against penetration)</p> <p>$y = 0.2848x + 41.125$ $R^2 = 0.7562$</p>					
Moisture content @ 20mm penetration using equation 'y' =		47			
Liquid Limit (LL or w _L) (%)	47				
Plastic Limit (PL or w _P) (%)	32				
Plasticity Index (PI) (%)	15				
USCS Classification:					

B5: Consistency limits of ECS05

		Atterberg Limits Data Sheet BS EN ISO 17892-12:2018	
Project Name:	PhD Research	Tested By:	A. Bolarinwa
Location:	AUT City Campus	Checked By:	R. Kalatehjari
Sample Description:	Mixed sand-clay matrix soil	Test Trial Numbers:	3
Sample No:	ECS-05		
USCS Soil Classification:		SP	
LL Determination by Cone Penetration Method		Plastic Limit Determination	
Avg. Penetration (mm)	Avg. Moisture content (%)	Description/Test Trials	
15.5	19.05		
18.29	20.2		
20.52	21.63		
22.52	22.84		
Proportion of Samples Less than 0.425mm Sieve			
Description	Values		
Water content of test specimen (w) %	0.42		
Mass of undried test specimen (g)	643.06		
Dried mass of coarse soil retained on 0.425mm sieve	171.52		
Percentage smaller than 0.425mm sieve (K)	73.22		
Moisture content corresponding to 20mm penetration using equation 21			
Liquid Limit (LL or w_L) (%):	21.00		
Plastic Limit (PL or w_P) (%):	NA		
Plasticity Index (PI) (%):	NA		
USCS Classification:	SP		

B6: Consistency limits of ECS10

Atterberg Limits Data Sheet BS EN ISO 17892-12:2018	
Project Name:	PhD Research
Location:	AUT City Campus
Sample Description:	Mixed sand-clay matrix soil
Sample No:	ECS-10
Tested By:	A. Bolarinwa
Checked By:	R. Kalatehjari
Test Trial Numbers:	3
USCS Soil Classification:	SP-SC

LL Determination by Cone Penetration Method		Plastic Limit Determination			
Avg. Penetration (mm)	Avg. Moisture content (%)	Description/Test Trials	1	2	3
24.85	23.37	Mass of tar + wet soil (M ₁) g	28.1	22.55	18.3
23.67	22.76	Mass of tar + dry soil (M ₂) g	26.96	21.34	17.62
23.38	22.35	Mass of container (M _c) g	20.97	14.88	13.79
		Mass of water (M _w) g	1.14	1.21	0.68
		Mass of dried soil (M _d) g	5.99	6.46	3.83
		Plastic Limit (w _p) %	19.03	18.73	17.75
		Average	18.39		

Proportion of Samples Less than 0.425mm Sieve	
Description	Values
Water content of test specimen (w) %	0.15
Mass of undried test specimen (g)	477.40
Dried mass of coarse soil retained on 0.425mm sieve (g)	260.60
Percentage smaller than 0.425mm sieve (K)	45.33

Linear (moisture content against penetration)

Moisture content @ 20mm penetration using equation y =	20.28
Liquid Limit (LL or w _L) (%):	20
Plastic Limit (PL or w _p) (%):	18
Plasticity Index (PI) (%):	2
USCS Classification:	

B7: Consistency limits of ECS15

AUT		Atterberg Limits Data Sheet	
		BS EN ISO 17892-12:2018	
Project Name:	PhD Research	Tested By:	A. Bolarinwa
Location:	AUT City Campus	Checked By:	R. Kalatehjari
Sample Description:	Mixed sand-clay matrix soil	Test Trial Numbers:	3
Sample No:	ECS-15		
USCS Soil Classification:		SC	
LL Determination by Cone Penetration Method		Plastic Limit Determination	
Avg. Penetration (mm)	Avg. Moisture content (%)	Description/Test Trials	1 2 3
19.26	21.00	Mass of tar + wet soil (M ₁) g	22.95 8.85 7.94
18.08	20.86	Mass of tar + dry soil (M ₂) g	22.65 8.49 7.69
17.17	20.76	Mass of container (M _c) g	20.97 6.05 6.19
		Mass of water (M _w) g	0.3 0.36 0.25
		Mass of dried soil (M _d) g	1.68 2.44 1.50
		Plastic Limit (w _p) %	17.86 14.75 16.67
		Average	16.43
Proportion of Samples Less than 0.425mm Sieve			
Description	Values		
Water content of test specimen (w) %	0.35		
Mass of undried test specimen (g)	449.91		
Dried mass of coarse soil retained on 0.425mm	104.1		
Percentage smaller than 0.425mm sieve (K)	76.78		
Moisture content @ 20mm penetration using equation 'y' =		21.16	
Liquid Limit (LL or w _L) (%)	21		
Plastic Limit (PL or w _p) (%)	16		
Plasticity Index (PI) (%)	5		
USCS Classification:			

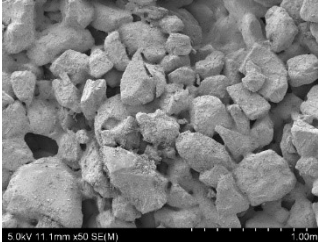
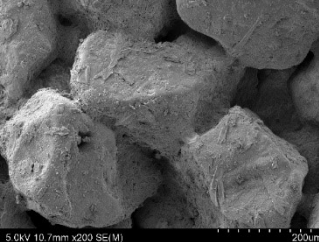
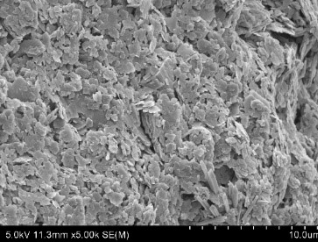
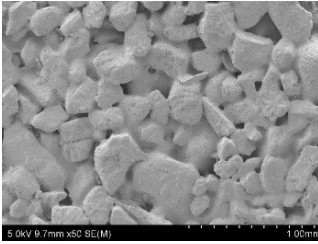
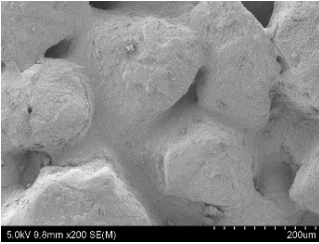
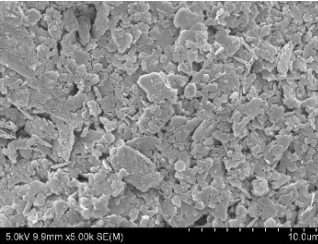
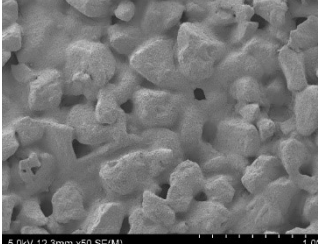
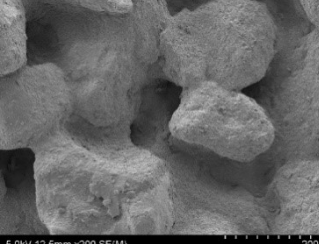
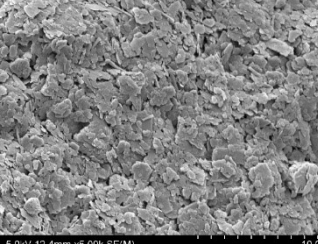
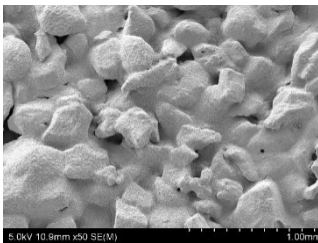

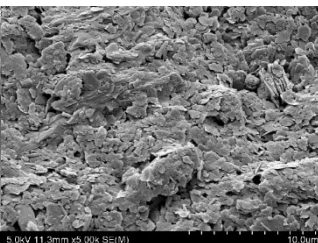

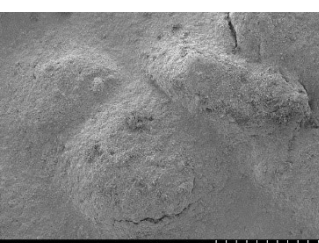
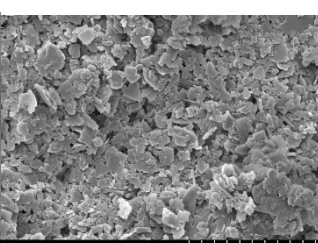
B8: Consistency limits of ECS20

AUT		Atterberg Limits Data Sheet		BS EN ISO 17892-12:2018	
Project Name:	PhD Research	Tested By:	A. Bolarinwa	Date:	
Location:	AUT City Campus	Checked By:	R. Kalatehjari	Date:	
Sample Description:	Mixed sand-clay matrix soil	Test Trial Numbers:	3		
Sample No:	ECS-20				
USCS Soil Classification:		SC			
LL Determination by Cone Penetration Method		Plastic Limit Determination			
Avg. Penetration (mm)	Avg. Moisture content (%)	Description/Test Trials	1	2	3
17.8	22.13	Mass of tar + wet soil (M ₁) g	11.03	10.67	12.37
19.21	22.64	Mass of tar + dry soil (M ₂) g	10.77	10.45	11.96
20.94	22.86	Mass of container (M _c) g	9.02	8.97	9.39
21.27	23.25	Mass of water (M _w) g	0.26	0.22	0.41
24.68	23.78	Mass of dried soil (M _d) g	1.75	1.48	2.57
Proportion of Samples Less than 0.425mm Sieve		Plastic Limit (w _p) %	14.86	14.86	15.57
Description	Values	Average	14.86		
Water content of test specimen (w) %	0.29				
Mass of undried test specimen (g)	502.58				
Dried mass of coarse soil retained on 0.425mm sieve	116.97				
Percentage smaller than 0.425mm sieve	76.66				
<p>Linear (Series1)</p> <p>moisture content (%)</p> <p>penetration (mm)</p> <p>$y = 0.2349x + 18.051$ $R^2 = 0.9523$</p>					
Moisture content @ 20mm penetration using equation y =		22			
Liquid Limit (LL or w _L) (%):	22				
Plastic Limit (PL or w _P) (%):	15				
Plasticity Index (PI) (%):	7				
USCS Classification:					

B9: Consistency limits of ECS30

		Atterberg Limits Data Sheet BS EN ISO 17892-12:2018	
Project Name:	PhD Research	Tested By:	A.Bolarinwa
Location:	AUT City Campus	Checked By:	R. Kalatehjari
Sample Description:	Mixed sand-clay matrix soil	Test Trial Numbers:	3
Sample No:	ECS-30		
USCS Soil Classification:		SC	
LL Determination by Cone Penetration Method		Plastic Limit Determination	
Avg. Penetration (mm)	Avg. Moisture content (%)	Description/Test Trials	
18.79	24.58	Mass of tar + wet soil (M_1) g	1
20.37	26.65	Mass of tar + dry soil (M_2) g	2
20.97	27.08	Mass of container (M_c) g	3
23	27.43	Mass of water (M_w) g	
		Mass of dried soil (M_d) g	
		Plastic Limit (w_p) %	
		Average	
Proportion of Samples Less than 0.425mm Sieve			
Description	Values		
Water content of test specimen (w) %	0.6		
Mass of undried test specimen (g)	404.02		
Dried mass of coarse soil retained on 0.425mm	51.36		
Percentage smaller than 0.425mm sieve (K)	87.21		
Moisture content @ 20mm penetration using equation 'y' =		25	
Liquid Limit (LL or w_L) (%):	25		
Plastic Limit (PL or w_p) (%):	16		
Plasticity Index (PI) (%):	9		
USCS Classification:			

APPENDIX C - The scanning electron micrograph (SEM) of sand matrix soils

S/ N	Sample No	Magnification		
		X 50	X 200	X 5000
1.	ECS05			
2.	ECS10			
3.	ECS15			
4.	ECS20			
5.	ECS30			

APPENDIX D - Specific gravity test datasheets

D1: Specific gravity of kaolinite (clay)

AUT		Specific Gravity Determination Data Sheet				ASTM D854-14	
Project Name:	PhD Research	Tested By:	A. Bolarinwa	Date:	3/09/2019		
Location:	AUT, City Campus	Checked By:	R. Kalatehjari	Date:	3/09/2019		
Sample Name:	Kaolinite	No. of Density Bottles:	2Nos.				
Sample Number:	K-00	Nos of Repeatability.:	4				
USCS Soil Classification:		CL					
DENSITY BOTTLE CALIBRATION				1	2	3	4
Average Mass of Density Bottle (M_p) (g):				171.41	172.13	171.43	172.1
Mass of Density Bottle + Water (M_{pw}) (g):				1161.72	1170.39	1160.8	1167.7
Observed Water Temperature (T_i) (°C):				27.2	27.2	27.2	27.2
Density of water at calibrated temp. (ρ_{wt}) Table 2, ASTM D854				0.99646	0.99646	0.99646	0.99646
Calibrated volume of density bottle (V_p)(mL)				993.83	1001.81	992.88	999.14
SPECIFIC GRAVITY DETERMINATION							
Measurement/Calculation	Variable	Units	Test Trial Number/Density Bottle Number				
			1/6	2/7	3/6	4/7	
Mass of d. bottle + Water + Soil	M_{pws}	---	1226.09	1233.83	1225.94	1234.44	
Temperature	T_x	(°C)	27.20	27.20	27.20	27.20	
Mass of d. bottle+ Water @ T_x	M_{pw}	(g)	1161.690	1170.360	1160.770	1167.670	
Dish Number	---	---	1.00	1.00	1.00	1.00	
Mass of Dish	M_d	(g)	499.20	499.20	499.20	499.20	
	M_{ds}	(g)	609.50	609.40	608.36	611.42	
Mass of Oven Dry Soil	M_s	(g)	110.30	110.20	109.16	112.22	
Conversion Factor @ T_x (ASTM D854 Table 2)	K	---	0.99825	0.99825	0.99825	0.99825	
Specific Gravity of Soil	G_s	---	2.40	2.35	2.48	2.46	
Average Specific Gravity of Soil			2.42				
<p>NOTES: $M_{pw} = \frac{\gamma_w @ T_x}{\gamma_w @ T_i} [M_{pw} @ T_i - M_p] + M_p$</p> <p>$G_s = \frac{KM_s}{M_s + M_{pw} - M_{pws}}$</p>							

D2: Specific gravity of east coast sand (ECS00)

AUT		Specific Gravity Determination Data Sheet			
		ASTM D854-14			
Project Name:	PhD Research	Tested By:	A. Bolarinwa	Date:	4/09/2019
Location:	AUT, City Campus	Checked By:	R. Kalatehjari	Date:	4/09/2019
Sample Name:	East Coast Sand	No. of Density Bottles:	2Nos.		
Sample Number:	ECS-00	Nos of Repeatability.:	3		
USCS Soil Classification:		SP			
DENSITY BOTTLE CALIBRATION					
			1	2	3
	Average Mass of Density Bottle (M_p) (g):		171.43	172.13	171.39
	Mass of Density Bottle + Water (M_{pw}) (g):		1160.96	1169.92	1160.8
	Observed Water Temperature (T_i) (°C):		27.2	27.2	27.2
	Density of water at calibrated temp. (ρ_w) Table 2, ASTM D854		0.99646	0.99646	0.99646
	Calibrated volume of density bottle (V_p)(mL)		993.05	1001.33	992.92
SPECIFIC GRAVITY DETERMINATION					
Measurement/Calculation	Variable	Units	Test Trial Number/Density Bottle Number		
			1/6	2/7	3/6
Mass of d. bottle + Water + Soil	M_{pws}	—	1231.33	1239.69	1231.81
Temperature	T_x	(°C)	27.20	27.20	27.20
Mass of d. bottle+ Water @ T_x	M_{pw}	(g)	1160.930	1169.890	1160.770
Dish Number	—	—	1.00	1.00	1.00
Mass of Dish	M_d	(g)	499.20	499.20	499.20
	M_{ds}	(g)	613.14	613.38	613.92
Mass of Oven Dry Soil	M_s	(g)	113.94	114.18	114.72
Conversion Factor @ T_x (ASTM D854 Table 2)	K	—	0.99825	0.99825	0.99825
Specific Gravity of Soil	G_s	—	2.61	2.57	2.62
Average Specific Gravity of Soil			2.60		
<div style="display: flex; justify-content: space-between;"> <div> <p>NOTES: $M_{pw} = \frac{\gamma_w @ T_x}{\gamma_w @ T_i} [M_{pw} @ T_i - M_p] + M_p$</p> </div> <div> <p>$G_s = \frac{KM_s}{M_s + M_{pw} - M_{pws}}$</p> </div> </div>					

D3: Specific gravity of sand matrix sample (ECS05)

AUT		Specific Gravity Determination Data Sheet			
		ASTM D854-14			
Project Name:	PhD Research	Tested By:	A. Bolarinwa	Date:	5/09/2019
Location:	AUT, City Campus	Checked By:	R. Kalatehjari	Date:	5/09/2019
Sample Name:	Sand Matrix	No. of Density Bottles:	2Nos.		
Sample Number:	ECS-05	Nos of Repeatability.:	3		
USCS Soil Classification:		SP			
DENSITY BOTTLE CALIBRATION					
			1	2	3
	Average Mass of Density Bottle (M_p) (g):		171.41	172.15	172.15
	Mass of Density Bottle + Water (M_{pw}) (g):		1161.72	1167.70	1170.39
	Observed Water Temperature (T_i) (°C):		27.2	27.2	27.2
	Density of water at calibrated temp. (ρ_w) Table 2, ASTM D854		0.99646	0.99646	0.99646
	Calibrated volume of density bottle (V_p)(mL)		993.83	999.09	1001.79
SPECIFIC GRAVITY DETERMINATION					
Measurement/Calculation	Variable	Units	Test Trial Number/Density Bottle Number		
			1/6	2/7	3/7
Mass of d. bottle + Water + Soil	M_{pws}	—	1231.54	1237.86	1240.31
Temperature	T_x	(°C)	27.20	27.20	27.20
Mass of d. bottle+ Water @ T_x	M_{pw}	(g)	1161.69	1167.67	1170.36
Dish Number	—	—	1.00	1.00	1.00
Mass of Dish	M_d	(g)	499.20	499.20	499.20
	M_{ds}	(g)	614.36	614.61	614.30
Mass of Oven Dry Soil	M_s	(g)	115.16	115.41	115.10
Conversion Factor @ T_x (ASTM D854 Table 2)	K	—	0.99825	0.99825	0.99825
Specific Gravity of Soil	G_s	—	2.54	2.55	2.54
Average Specific Gravity of Soil			2.54		
<div style="display: flex; justify-content: space-between;"> <div> <p>NOTES: $M_{pw} = \frac{\gamma_w @ T_x}{\gamma_w @ T_i} [M_{pw} @ T_i - M_p] + M_p$</p> </div> <div> <p>$G_s = \frac{KM_s}{M_s + M_{pw} - M_{pws}}$</p> </div> </div>					

D4: Specific gravity of sand matrix sample (ECS10)

AUT		Specific Gravity Determination Data Sheet			
		ASTM D854-14			
Project Name:	PhD Research	Tested By:	A. Bolarinwa	Date:	6/09/2019
Location:	AUT, City Campus	Checked By:	R. Kalatehjari	Date:	6/09/2019
Sample Name:	Sand Matrix	No. of Density Bottles:	2Nos.		
Sample Number:	ECS-10	Nos of Repeatability.:	3		
USCS Soil Classification:		SP-SC			
DENSITY BOTTLE CALIBRATION					
			1	2	3
	Average Mass of Density Bottle (M_p) (g):		171.76	172.15	171.46
	Mass of Density Bottle + Water (M_{pw}) (g):		1161.01	1170.39	1161.01
	Observed Water Temperature (T_i) (°C):		27.2	27.2	27.2
	Density of water at calibrated temp. (ρ_w) Table 2, ASTM D854		0.99646	0.99646	0.99646
	Calibrated volume of density bottle (V_p)(mL)		992.76	1001.79	993.07
SPECIFIC GRAVITY DETERMINATION					
Measurement/Calculation	Variable	Units	Test Trial Number/Density Bottle Number		
			1/6	2/7	3/6
Mass of d. bottle + Water + Soil	M_{pws}	—	1232.85	1240.97	1231.55
Temperature	T_x	(°C)	27.20	27.20	27.20
Mass of d. bottle+ Water @ T_x	M_{pw}	(g)	1160.98	1170.36	1160.98
Dish Number	—	—	1.00	1.00	1.00
Mass of Dish	M_d	(g)	499.20	499.20	499.20
	M_{ds}	(g)	614.31	614.16	614.31
Mass of Oven Dry Soil	M_s	(g)	115.11	114.96	115.11
Conversion Factor @ T_x (ASTM D854 Table 2)	K	—	0.99825	0.99825	0.99825
Specific Gravity of Soil	G_s	—	2.66	2.59	2.58
Average Specific Gravity of Soil			2.61		
NOTES: $M_{pw} = \frac{\gamma_w @ T_x}{\gamma_w @ T_i} [M_{pw} @ T_i - M_p] + M_p$ $G_s = \frac{KM_s}{M_s + M_{pw} - M_{pws}}$					

D5: Specific gravity of sand matrix sample (ECS15)

AUT		Specific Gravity Determination Data Sheet			
		ASTM D854-14			
Project Name:	PhD Research	Tested By:	A. Bolarinwa	Date:	9/09/2019
Location:	AUT, City Campus	Checked By:	R. Kalatehjari	Date:	9/09/2019
Sample Name:	Sand Matrix	No. of Density Bottles:	2Nos.		
Sample Number:	ECS-15	Nos of Repeatability.:	3		
USCS Soil Classification:		SC			
DENSITY BOTTLE CALIBRATION			1	2	3
Average Mass of Density Bottle (M_p) (g):			171.40	172.13	172.13
Mass of Density Bottle + Water (M_{pw}) (g):			1161.72	1169.92	1169.92
Observed Water Temperature (T_i) (°C):			27.2	27.2	27.2
Density of water at calibrated temp. (ρ_{wt}) Table 2, ASTM D854			0.99646	0.99646	0.99646
Calibrated volume of density bottle (V_p)(mL)			993.84	1001.33	1001.33
SPECIFIC GRAVITY DETERMINATION					
Measurement/Calculation	Variable	Units	Test Trial Number/Density Bottle Number		
			1/6	2/7	3/6
Mass of d. bottle + Water + Soil	M_{pws}	---	1231.78	1239.15	1239.65
Temperature	T_x	(°C)	27.20	27.20	27.20
Mass of d. bottle+ Water @ Tx	M_{pw}	(g)	1161.690	1169.890	1169.890
Dish Number	---	---	1.00	1.00	1.00
Mass of Dish	M_d	(g)	499.20	499.20	499.20
	M_{ds}	(g)	614.38	614.20	614.17
Mass of Oven Dry Soil	M_s	(g)	115.18	115.00	114.97
Conversion Factor @ Tx (ASTM D854 Table 2)	K	---	0.99825	0.99825	0.99825
Specific Gravity of Soil	G_s	---	2.55	2.51	2.54
Average Specific Gravity of Soil			2.53		
<div style="display: flex; justify-content: space-between;"> <div style="width: 60%;"> <p>NOTES: $M_{pw} = \frac{\gamma_w @ T_x}{\gamma_w @ T_i} [M_{pw} @ T_i - M_p] + M_p$</p> </div> <div style="width: 35%;"> <p>$G_s = \frac{KM_s}{M_s + M_{pw} - M_{pws}}$</p> </div> </div>					

D6: Specific gravity of sand matrix sample (ECS20)

AUT		Specific Gravity Determination Data Sheet			
		ASTM D854-14			
Project Name:	PhD Research	Tested By:	A. Bolarinwa	Date:	10/09/2019
Location:	AUT, City Campus	Checked By:	R. Kalatehjari	Date:	10/09/2019
Sample Name:	Sand Matrix	No. of Density Bottles:	2Nos.		
Sample Number:	ECS-20	Nos of Repeatability.:	3		
USCS Soil Classification:		SC			
DENSITY BOTTLE CALIBRATION			1	2	3
Average Mass of Density Bottle (M_p) (g):			171.41	172.09	172.1
Mass of Density Bottle + Water (M_{pw}) (g):			1161.70	1169.92	1169.89
Observed Water Temperature (T_i) (°C):			27.2	27.2	27.2
Density of water at calibrated temp. (ρ_w) Table 2, ASTM D854			0.99646	0.99646	0.99646
Calibrated volume of density bottle (V_p)(mL)			993.81	1001.37	1001.33
SPECIFIC GRAVITY DETERMINATION					
Measurement/Calculation	Variable	Units	Test Trial Number/Density Bottle Number		
			1/6	2/7	3/7
Mass of d. bottle + Water + Soil	M_{pws}	---	1232.30	1240.87	1240.34
Temperature	T_x	(°C)	27.20	27.20	27.20
Mass of d. bottle+ Water @ T_x	M_{pw}	(g)	1161.670	1169.890	1169.860
Dish Number	---	---	1.00	1.00	1.00
Mass of Dish	M_d	(g)	499.20	499.20	499.20
	M_{ds}	(g)	614.31	614.36	614.33
Mass of Oven Dry Soil	M_s	(g)	115.11	115.16	115.13
Conversion Factor @ T_x (ASTM D854 Table 2)	K	---	0.99825	0.99825	0.99825
Specific Gravity of Soil	G_s	---	2.58	2.60	2.57
Average Specific Gravity of Soil			2.59		
<div style="display: flex; justify-content: space-between;"> <div> <p>NOTES: $M_{pw} = \frac{\gamma_w @ T_x}{\gamma_w @ T_i} [M_{pw} @ T_i - M_p] + M_p$</p> </div> <div> <p>$G_s = \frac{KM_s}{M_s + M_{pw} - M_{pws}}$</p> </div> </div>					

D7: Specific gravity of sand matrix sample (ECS30)

AUT		Specific Gravity Determination Data Sheet			
		ASTM D854-14			
Project Name:	PhD Research	Tested By:	A. Bolarinwa	Date:	11/09/2019
Location:	AUT, City Campus	Checked By:	R. Kalatehjari	Date:	11/09/2019
Sample Name:	Sand Matrix	No. of Density Bottles:	2Nos.		
Sample Number:	ECS-30	Nos of Repeatability.:	3		
USCS Soil Classification:		SC			
DENSITY BOTTLE CALIBRATION					
		1	2	3	
Average Mass of Density Bottle (M_p) (g):		171.43	172.13	171.4	
Mass of Density Bottle + Water (M_{pw}) (g):		1160.96	1170.3	1161.7	
Observed Water Temperature (T_i) (°C):		27.2	27.2	27.2	
Density of water at calibrated temp. (ρ_w) Table 2, ASTM D854		0.99646	0.99646	0.99646	
Calibrated volume of density bottle (V_p)(mL)		993.05	1001.72	993.82	
SPECIFIC GRAVITY DETERMINATION					
Measurement/Calculation	Variable	Units	Test Trial Number/Density Bottle Number		
			1/6	2/7	3/6
Mass of d. bottle + Water + Soil	M_{pws}	---	1230.16	1240.79	1232.41
Temperature	T_x	(°C)	27.20	27.20	27.20
Mass of d. bottle+ Water @ Tx	M_{pw}	(g)	1160.930	1170.270	1161.670
Dish Number	---	---	1.00	1.00	1.00
Mass of Dish	M_d	(g)	499.20	499.20	499.20
	M_{ds}	(g)	614.11	614.39	614.26
Mass of Oven Dry Soil	M_s	(g)	114.91	115.19	115.06
Conversion Factor @ Tx (ASTM D854 Table 2)	K	---	0.99825	0.99825	0.99825
Specific Gravity of Soil	G_s	---	2.51	2.57	2.59
Average Specific Gravity of Soil			2.56		
<p>NOTES: $M_{pw} = \frac{\gamma_w @ T_x}{\gamma_w @ T_i} [M_{pw} @ T_i - M_p] + M_p$</p> <p>$G_s = \frac{KM_s}{M_s + M_{pw} - M_{pws}}$</p>					

APPENDIX E - Test datasheets for maximum index density parameters

E1: Maximum index density of ECS00

AUT		Maximum Index Density of Soil Samples				
		ASTM D4253-16				
Project Name:	PhD Research	Tested By:	A. Bolarinwa	Date:	16/09/2019	
Location:	AUT, City Campus	Checked By:	R. Kalatehjari	Date:	17/09/2019	
Sample Name:	East Coast Sand	No. of Moulds:	1			
Sample Number:	ECS-00	Nos of Repeatability.:	3			
Method Used:	Method A					
USCS Soil Classification:	Poorly graded sand (SP)					
CALIBRATION OF VOLUME OF MOULD			1	2	3	
Mass of mould, M_1 (g):			5020	5020	5020	
Mass of mould + water, M_2 (g):			6020	6020	6020	
Mass of water (g):			1000	1000	1000	
Temperature of water at calibration ($^{\circ}\text{C}$):			20	20	20	
Unit Vol. of water at calibrated temp. (mL/g) Table 2, ASTM 4254-16			1.001800	1.001800	1.001800	
Calibrated volume of water in mould, V_c (mL or cm^3):			1004	1004	1004	
Average calibrated volume of water (mL or cm^3):			1004			
Volume of soil = $V_c - (A \cdot H \cdot \text{Conversion factor from table 3})$ (cm^3):			1004			
Specific gravity of soil sample, G_s :			2.6			
Determination of Maximum Index Density						
Number of Test Trials:			1	2	3	
Mass of compacted Soil + Mould, M_3 (g):			6700	6680	6700	
Mass of Compacted Soil, m_4 (g):			1680	1660	1680	
Maximum density index ($\rho_{d\max,n}$), g/cm^3 :			1.67	1.65	1.67	
Average $\rho_{d\max,3}$ (g/cm^3):			1.67			
Average maximum index unit weight (kN/m^3):			16.35			
Average minimum-index void ratio e_{\min}			0.56			

E2: Maximum index density of ECS05

AUT		Maximum Index Density of Soil Samples			
		ASTM D4253-16			
Project Name:	PhD Research	Tested By:	A. Bolarinwa	Date:	16/09/2015
Location:	AUT, City Campus	Checked By:	R. Kalatehjari	Date:	17/09/2015
Sample Name:	Mixed Soil	No. of Moulds:	1		
Sample Number:	ECS-05	Nos of Repeatability.:	3		
Method Used:	Method A				
USCS Soil Classification:	Poorly graded sand (SP)				
CALIBRATION OF VOLUME OF MOULD			1	2	3
	Mass of mould, M ₁ (g):		5020	5020	5020
	Mass of mould + water, M ₂ (g):		6020	6020	6020
	Mass of water (g):		1000	1000	1000
	Temperature of water at calibration (°C):		20	20	20
	Unit Vol. of water at calibrated temp. (mL/g, Table 2, ASTM 4254-16)		1.001800	1.001800	1.001800
	Calibrated volume of water in mould, V _c (mL or cm ³)		1004	1004	1004
	Average calibrated volume of water (mL or cm ³)		1004		
	Volume of soil = V _c - (A _c *H*Conversion factor from table 3) (cm ³):		1003.9		
	Specific gravity of soil sample, G _s :		2.54		
Determination of Maximum Index Density					
Number of Test Trials:			1	2	3
Mass of compacted Soil + Mould, M ₃ (g):			6660	6620	6720
Mass of Compacted Soil, m ₄ (g):			1640	1600	1700
Maximum density index (ρ _{dmax,n}), g/cm ³ :			1.63	1.59	1.69
Average ρ _{dmax,3} , (g/cm ³)			1.64		
Average maximum index unit weight (kN/m ³):			16.09		
Average minimum-index void ratio e _{min}			0.55		

E3: Maximum index density of ECS10

AUT		Maximum Index Density of Soil Samples			
		ASTM D4253-16			
Project Name:	PhD Research	Tested By:	A. Bolarinwa	Date:	16/09/2019
Location:	AUT, City Campus	Checked By:	R. Kalatehjari	Date:	17/09/2019
Sample Name:	Mixed Soil	No. of Moulds:	1		
Sample Number:	ECS-10	Nos of Repeatability.:	3		
Method Used:	Method A				
USCS Soil Classification:		SP-SC			
CALIBRATION OF VOLUME OF MOULD			1	2	3
	Mass of mould, M ₁ (g):		5020	5020	5020
	Mass of mould + water, M ₂ (g):		6020	6020	6020
	Mass of water (g):		1000	1000	1000
	Temperature of water at calibration (°C):		20	20	20
	Unit Vol. of water at calibrated temp. (mL/g, Table 2, ASTM 4254-16)		1.001800	1.001800	1.001800
	Calibrated volume of water in mould, V _c (mL or cm ³)		1004	1004	1004
	Average calibrated volume of water (mL or cm ³)			1004	
	Volume of soil = V _c - (A _c *H*Conversion factor from table 3) (cm ³):			1003.9	
	Specific gravity of soil sample, G _s :		2.61		
Determination of Maximum Index Density					
Number of Test Trials:			1	2	3
Mass of compacted Soil + Mould, M ₃ (g):			6580	6640	6580
Mass of Compacted Soil, m ₄ (g):			1560	1620	1560
Maximum density index (ρ _{dmax,n}), g/cm ³ :			1.55	1.61	1.55
Average ρ _{dmax,3s} (g/cm ³)			1.57		
Average maximum index unit weight (kN/m ³):			15.43		
Average minimum-index void ratio e _{min}			0.66		

E4: Maximum index density of ECS15

AUT		Maximum Index Density of Soil Samples			
		ASTM D4253-16			
Project Name:	PhD Research	Tested By:	A. Bolarinwa	Date:	16/09/2019
Location:	AUT, City Campus	Checked By:	R. Kalatehjari	Date:	17/09/2019
Sample Name:	Mixed Soil	No. of Moulds:	1		
Sample Number:	ECS-15	Nos of Repeatability.:	3		
Method Used:	Method A				
USCS Soil Classification:		Clayey Sand (SC)			
CALIBRATION OF VOLUME OF MOULD			1	2	3
	Mass of mould, M ₁ (g):		5020	5020	5020
	Mass of mould + water, M ₂ (g):		6020	6020	6020
	Mass of water (g):		1000	1000	1000
	Temperature of water at calibration (°C):		20	20	20
	Unit Vol. of water at calibrated temp. (mL/g, Table 2, ASTM 4254-16)		1.001800	1.001800	1.001800
	Calibrated volume of water in mould, V _c (mL or cm ³)		1004	1004	1004
	Average calibrated volume of water (mL or cm ³)		1004		
	Volume of soil = V _c - (A _c *H*Conversion factor from table 3) (cm ³):		1003.88		
	Specific gravity of soil sample, G _s :		2.53		
Determination of Maximum Index Density					
Number of Test Trials:			1	2	3
Mass of compacted Soil + Mould, M ₃ (g):			6460	6460	6460
Mass of Compacted Soil, m ₄ (g):			1440	1440	1440
Maximum density index (ρ _{dmax,n}), g/cm ³ :			1.43	1.43	1.43
Average ρ _{dmax,3s} (g/cm ³)			1.43		
Average maximum index unit weight (kN/m ³):			14.07		
Average minimum-index void ratio e _{min}			0.76		

APPENDIX F - Tests datasheets for standard compaction tests

F1: Maximum index density of ECS20

Project Name:	PhD Research	Tested By:	A. Bolarinwa	Date:	20/00/2020
Location:	AUT, City Campus	Checked By:	R. Kalatehjari	Date:	20/01/2020
Sample Name:	Mixed Soil	No. of Moulds:	1		
Sample Number:	ECS-20				
Method Used:					
USCS Soil Classification:	Clayey Sand (SC)	G_s:	2.59		
Test Standard:	D698	Mold Height (mm):	115.62		
Test Method:	Method A	Mold Dia. (mm):	105.04		
		Mold Vol. (cm³):	1001.918		
Description					
Mass of Soil & Mold (M_t) (g):	4091.81	4154.50	4197.52	4133.25	4041.70
Mass of Mold (M_{mold}) (g):	2078.64	2078.64	2078.64	2078.64	2078.64
Mass of Soil (M_s) (g):	2013.17	2075.86	2118.88	2054.61	1963.06
Wet Density (γ_{wet}) (g/cm³):	2.01	2.07	2.11	2.05	1.96
Water Content w (%)	15.27	13.52	11.50	9.58	7.19
As Per ASTM D2216-19					
Dry Density (γ_{dry}) (g/cm³)	1.74	1.83	1.95	1.87	1.83
ECS20 data					
MC	DD				
15.27	1.74				
13.52	1.88				
11.50	1.95				
9.58	1.87				
7.19	1.83				

F2: Maximum index density of ECS30

Project Name:	PhD Research	Tested By:	A. Bolarinwa	Date:	20/00/2020
Location:	AUT, City Campus	Checked By:	R. Kalatehjari	Date:	20/01/2020
Sample Name:	Mixed Soil	No. of Moulds:	1		
Sample Number:	ECS-30				
Method Used:					
USCS Soil Classification:	Clayey Sand (SC)	G_s:	2.56		
		Mold Height (mm):	115.62		
Test Standard:	D698	Mold Dia. (mm):	105.04		
Test Method:	Method A	Mold Vol. (cm³):	1001.918		
Description					
Mass of Soil & Mold (M_p) (g):	4201.48	4223.00	4233.35	4159.86	4087.52
Mass of Mold (M_{mold}) (g):	2078.64	2078.64	2078.64	2078.64	2078.64
Mass of Soil (M_s) (g):	2122.84	2144.36	2154.71	2081.22	2008.88
Wet Density (γ_{wet}) (g/cm³):	2.12	2.14	2.15	2.08	2.01
Water Content w (%)	13.50	11.80	10.75	10.14	8.84
As Per ASTM D2216-19					
Dry Density (γ_{dry}) (g/cm³)	1.87	1.91	1.95	1.89	1.84
ECS30 Data					
MC	DD				
13.5	1.87				
11.8	1.91				
10.75	1.94				
10.14	1.89				
8.84	1.84				

APPENDIX G - Tests datasheets for minimum index density

G1: Minimum index density of ECS00

AUT		Minimum Index Density of Soil Samples			
		ASTM D4254-16			
Project Name:	PhD Research	Tested By:	A. Bolarinwa	Date:	3/09/2019
Location:	AUT, City Campus	Checked By:	R. Kalatehjari	Date:	3/09/2019
Sample Name:	East Coast Sand	No. of Moulds:	1		
Sample Number:	ECS-00	Nos of Repeatability.:	3		
Method Used:	Method C				
USCS Soil Classification:		SP			
CALIBRATION OF VOLUME OF MOULD			1	2	3
	Mass of Mould, M_1 (g):		5020	5020	5020
	Mass of Mould + Water, M_2 (g):		6020	6020	6020
	Mass of Water (g):		1000	1000	1000
	Temperature of water at Calibration ($^{\circ}\text{C}$):		20	20	20
	Unit Vol. of water at calibrated temp. (mL/g, Table 2, ASTM 4254-16)		1.001800	1.001800	1.001800
	Corrected volume of water in mould (mL or cm^3)		1002	1002	1002
	Average Volume of Water (mL or cm^3)		1002		
	Specific Gravity of Soil Sample, G_s :		2.6		
Determination of Minimum Index Density					
Number of Test Trials:			1	2	3
Mass of Loose Soil + Mould, M_3 (g):			6440	6460	6460
Mass of Loose Soil, m_4 (g):			1420	1440	1440
Minimum density index ($\rho_{\text{dmin},n}$), g/cm^3 :			1.42	1.44	1.44
Average $\rho_{\text{dmin},3}$, (g/cm^3)			1.43		
Average minimum index unit weight (kN/m^3):			14.03		
Average maximum -index void ratio e_{max} :			0.82		

G2: Minimum index density of ECS05

<div style="background-color: black; color: white; padding: 5px; font-weight: bold; font-size: 1.2em;">AUT</div>		Minimum Index Density of Soil Samples ASTM D4254-16			
Project Name:	PhD Research	Tested By:	A. Bolarinwa	Date:	3/09/2019
Location:	AUT, City Campus	Checked By:	R. Kalatehjari	Date:	3/09/2019
Sample Name:	Mixed Soil	No. of Moulds:	1		
Sample Number:	ECS-05	Nos of Repeatability.:	3		
Method Used:	Method C				
USCS Soil Classification:		SP			
CALIBRATION OF VOLUME OF MOULD					
			1	2	3
	Mass of Mould, M_1 (g):		5020	5020	5020
	Mass of Mould + Water, M_2 (g):		6020	6020	6020
	Mass of Water (g):		1000	1000	1000
	Temperature of water at Calibration ($^{\circ}\text{C}$):		20	20	20
	Unit Vol. of water at calibrated temp. (mL/g, Table 2, ASTM 4254-16)		1.001800	1.001800	1.001800
	Corrected volume of water in mould (mL or cm^3)		1002	1002	1002
	Average Volume of Water (mL or cm^3)		1002		
	Specific Gravity of Soil Sample, G_s :		2.54		
Determination of Minimum Index Density					
Number of Test Trials:			1	2	3
Mass of Loose Soil + Mould, M_3 (g):			6340	6340	6340
Mass of Loose Soil, m_4 (g):			1320	1320	1320
Minimum density index ($\rho_{\text{dmin},n}$), g/cm^3 :			1.32	1.32	1.32
Average $\rho_{\text{dmin},3}$, (g/cm^3)			1.32		
Average minimum index unit weight (kN/m^3):			12.92		
Average maximum -index void ratio e_{max} :			0.93		

G3: Minimum index density of ECS10

AUT		Minimum Index Density of Soil Samples			
		ASTM D4254-16			
Project Name:	PhD Research	Tested By:	A. Bolarinwa	Date:	3/09/2019
Location:	AUT, City Campus	Checked By:	R. Kalatehjari	Date:	3/09/2019
Sample Name:	Mixed Soil	No. of Moulds:	1		
Sample Number:	ECS-10	Nos of Repeatability.:	3		
Method Used:	Method C				
USCS Soil Classification:		SP-SC			
CALIBRATION OF VOLUME OF MOULD			1	2	3
	Mass of Mould, M_1 (g):	5020	5020	5020	
	Mass of Mould + Water, M_2 (g):	6020	6020	6020	
	Mass of Water (g):	1000	1000	1000	
	Temperature of water at Calibration ($^{\circ}\text{C}$):	20	20	20	
	Unit Vol. of water at calibrated temp. (mL/g, Table 2, ASTM 4254-16)	1.001800	1.001800	1.001800	
	Corrected volume of water in mould (mL or cm^3)	1002	1002	1002	
	Average Volume of Water (mL or cm^3)	1002			
	Specific Gravity of Soil Sample, G_s :	2.61			
Determination of Minimum Index Density					
Number of Test Trials:		1	2	3	
Mass of Loose Soil + Mould, M_3 (g):		6240	6240	6240	
Mass of Loose Soil, m_4 (g):		1220	1220	1220	
Minimum density index ($\rho_{\text{dmin},n}$), g/cm^3 :		1.22	1.22	1.22	
Average $\rho_{\text{dmin},3}$, (g/cm^3)		1.22			
Average minimum index unit weight (kN/m^3):		11.94			
Average maximum -index void ratio e_{max} :		1.14			

G4: Minimum index density of ECS15

AUT		Minimum Index Density of Soil Samples			
		ASTM D4254-16			
Project Name:	PhD Research	Tested By:	A. Bolarinwa	Date:	3/09/2019
Location:	AUT, City Campus	Checked By:	R. Kalatehjari	Date:	3/09/2019
Sample Name:	Mixed Soil	No. of Moulds:	1		
Sample Number:	ECS-15	Nos of Repeatability.:	3		
Method Used:	Method C				
USCS Soil Classification:		SC			
CALIBRATION OF VOLUME OF MOULD			1	2	3
	Mass of Mould, M_1 (g):	5020	5020	5020	
	Mass of Mould + Water, M_2 (g):	6020	6020	6020	
	Mass of Water (g):	1000	1000	1000	
	Temperature of water at Calibration ($^{\circ}\text{C}$):	20	20	20	
	Unit Vol. of water at calibrated temp. (mL/g, Table 2, ASTM 4254-16)	1.001800	1.001800	1.001800	
	Corrected volume of water in mould (mL or cm^3)	1002	1002	1002	
	Average Volume of Water (mL or cm^3)	1002			
	Specific Gravity of Soil Sample, G_s :	2.53			
Determination of Minimum Index Density					
Number of Test Trials:		1	2	3	
Mass of Loose Soil + Mould, M_3 (g):		6200	6200	6200	
Mass of Loose Soil, m_4 (g):		1180	1180	1180	
Minimum density index ($\rho_{\text{dmin},n}$), g/cm^3 :		1.18	1.18	1.18	
Average $\rho_{\text{dmin},3}$, (g/cm^3)		1.18			
Average minimum index unit weight (kN/m^3):		11.55			
Average maximum -index void ratio e_{max} :		1.15			

G5: Minimum index density of ECS20

AUT		Minimum Index Density of Soil Samples			
		ASTM D4254-16			
Project Name:	PhD Research	Tested By:	A. Bolarinwa	Date:	3/09/2019
Location:	AUT, City Campus	Checked By:	R. Kalatehjari	Date:	3/09/2019
Sample Name:	Mixed Soil	No. of Moulds:	1		
Sample Number:	ECS-20	Nos of Repeatability.:	3		
Method Used:	Method C				
USCS Soil Classification:		SC			
CALIBRATION OF VOLUME OF MOULD			1	2	3
	Mass of Mould, M_1 (g):	5020	5020	5020	
	Mass of Mould + Water, M_2 (g):	6020	6020	6020	
	Mass of Water (g):	1000	1000	1000	
	Temperature of water at Calibration ($^{\circ}\text{C}$):	20	20	20	
	Unit Vol. of water at calibrated temp. (mL/g, Table 2, ASTM 4254-16)	1.001800	1.001800	1.001800	
	Corrected volume of water in mould (mL or cm^3)	1002	1002	1002	
	Average Volume of Water (mL or cm^3)	1002			
	Specific Gravity of Soil Sample, G_s :	2.59			
Determination of Minimum Index Density					
Number of Test Trials:		1	2	3	
Mass of Loose Soil + Mould, M_3 (g):		6120	6120	6120	
Mass of Loose Soil, m_4 (g):		1100	1100	1100	
Minimum density index ($\rho_{\text{dmin},n}$), g/cm^3 :		1.10	1.10	1.10	
Average $\rho_{\text{dmin},3}$, (g/cm^3)		1.10			
Average minimum index unit weight (kN/m^3):		10.77			
Average maximum -index void ratio e_{max} :		1.36			

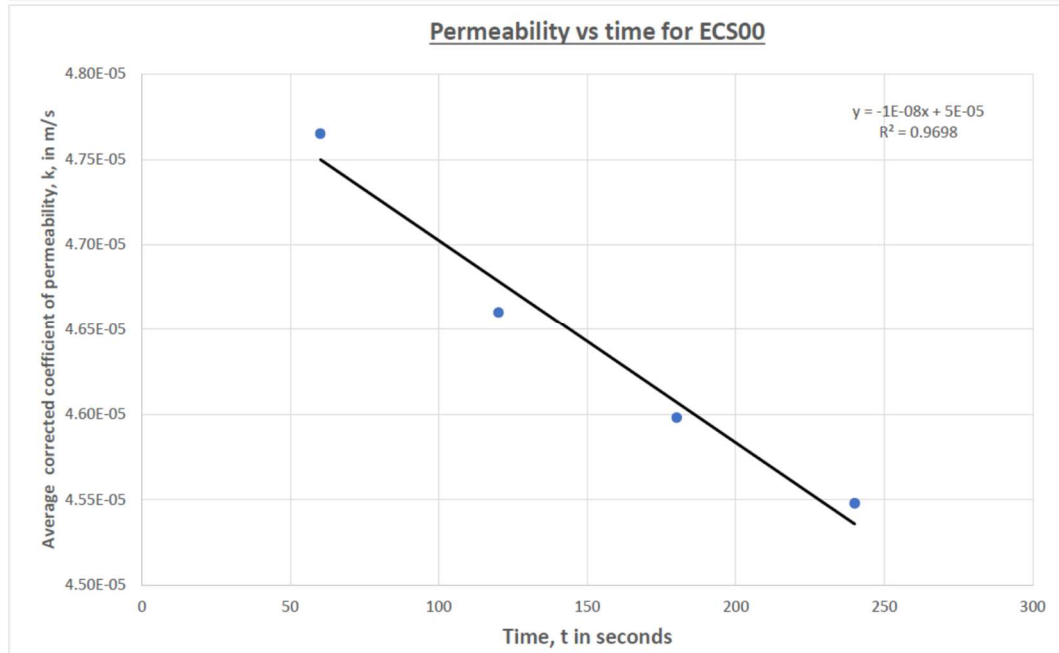
G6: Minimum index density of ECS30

AUT		Minimum Index Density of Soil Samples			
		ASTM D4254-16			
Project Name:	PhD Research	Tested By:	A. Bolarinwa	Date:	3/09/2019
Location:	AUT, City Campus	Checked By:	R. Kalatehjari	Date:	3/09/2019
Sample Name:	Mixed Soil	No. of Moulds:	1		
Sample Number:	ECS-30	Nos of Repeatability.:	3		
Method Used:	Method C				
USCS Soil Classification:		SC			
CALIBRATION OF VOLUME OF MOULD					
			1	2	3
	Mass of Mould, M_1 (g):		5020	5020	5020
	Mass of Mould + Water, M_2 (g):		6020	6020	6020
	Mass of Water (g):		1000	1000	1000
	Temperature of water at Calibration ($^{\circ}\text{C}$):		20	20	20
	Unit Vol. of water at calibrated temp. (mL/g, Table 2, ASTM 4254-16)		1.001800	1.001800	1.001800
	Corrected volume of water in mould (mL or cm^3)		1002	1002	1002
	Average Volume of Water (mL or cm^3)		1002		
	Specific Gravity of Soil Sample, G_s :		2.56		
Determination of Minimum Index Density					
Number of Test Trials:			1	2	3
Mass of Loose Soil + Mould, M_3 (g):			5920	5920	5920
Mass of Loose Soil, m_4 (g):			900	900	900
Minimum density index ($\rho_{\text{dmin},n}$), g/cm^3 :			0.90	0.90	0.90
Average $\rho_{\text{dmin},3}$, (g/cm^3)			0.90		
Average minimum index unit weight (kN/m^3):			8.81		
Average maximum -index void ratio e_{max} :			1.85		

APPENDIX H - Tests datasheets for soil permeability tests

H1: The permeability result of ECS00

Permeability Test Data Sheet (Constant Head)										
Sample No.:		ECS00		Test Date: 19th July 2020.						
USCS Soil Classification:		SP								
Density/Relative Density Calculation:										
Diameter, D, (cm):	10.14	Moisture Content, %:	4.34	W1, g:	2371.16					
Area, A, (cm ²):	80.75	LDR:	0.86	W2, g:	956.09					
Length, L, (cm):	12.16	G _s :	2.60	Net mass of Sample, g:	1415.07					
Volume (cm ³):	981.97	Void ratio, e:	0.80							
ρ (g/cm ³):	1.44									
ρ _{max} (g/cm ³):	1.67									
ρ _{min} (g/cm ³):	1.43									
Rd	0.95									
Permeability Test Records										
Test no.	Manometer Reading		Head	Volume, V _w	t(s)	Temp.	k _θ	η _θ /η ₂₀	k _T	Average k _T
	H1, cm	H2, cm	H, (cm)	mL, cm ³		°C	cm/s		cm/s	cm/s
1	76.50	9.60	66.90	118	60	17	0.004426622	1.077	4.77E-03	4.77E-03
2	76.50	9.50	67.00	118	60	17	0.004420015	1.077	4.76E-03	
3	76.50	9.60	66.90	118	60	17	0.004426622	1.077	4.77E-03	
1	76.50	9.50	67.00	230	120	17	0.004307642	1.077	4.64E-03	4.66E-03
2	77.00	9.60	67.40	230	120	17	0.004282077	1.077	4.61E-03	
3	76.50	9.60	66.90	228	120	16	0.004276567	1.106	4.73E-03	
1	75.70	9.50	66.20	330	180	16	0.004170146	1.106	4.61E-03	4.60E-03
2	75.50	9.50	66.00	325	180	16	0.004119407	1.106	4.56E-03	
3	75.50	9.50	66.00	330	180	16	0.004182783	1.106	4.63E-03	
4	75.00	9.50	65.50	430	240	15	0.004118923	1.106	4.56E-03	4.55E-03
5	74.40	9.50	64.90	430	240	15	0.004157003	1.106	4.60E-03	
6	74.40	9.50	64.90	420	240	15	0.004060328	1.106	4.49E-03	
Formula and Terminologies As Per AS 1289.6.7.1 - 2001 $k_{\theta} = (V_w / At) * (L / H)$ $k_T = k_{\theta} (\eta_{\theta} / \eta_{20})$ Where k_{θ} = coefficient of permeability at test temperature θ , in cm/s V_w = volume of water passing through soil in time $9t$, in mL t = time interval for volume (V_w) measurement, in seconds A = cross-sectional area of specimen, in square centimetres L = thickness of specimen, in centimetres H = hydraulic head in centimetres k_T = coefficient of permeability at 20°C, in cm η_{θ} = dynamic coefficient of viscosity of water at θ °C η_{20} = mean temperature of water during test, in degrees Celsius $LDR = \text{laboratory density ratio}$ $e = (\rho_w \cdot G_s / \rho) - 1$ Where e = void ratio of test soil ρ_w = density of water G_s = specific gravity of soil ρ = measured density of soil sample										



H2: The permeability test of ECS05

Permeability Test Data Sheet (Constant Head)

Sample No.: ECS05

Test Date: 19th July 2020.

USCS Soil Classification: SP

Density/Relative Density Calculation:

Diameter, D, (cm):	10.14	Moisture Content, %:	3.83	W1, g:	2190.25
Area, A, (cm ²):	80.75	LDR:	0.81	W2, g:	891.05
Length, L, (cm):	12.16	G _s :	2.54	Net mass of Sample, g:	1299.20
Volume (cm ³):	981.97	Void ratio, e:	0.92		
ρ (g/cm ³):	1.32				
ρ _{max} (g/cm ³):	1.64				
ρ _{min} (g/cm ³):	1.32				
Rd	0.99				

Permeability Test Records

Test no.	Manometer Reading		Head	Volume, V _w	t(s)	Temp.	k _θ	η _θ /η ₂₀	k _T	Average k _T
	H1, cm	H2, cm	H, (cm)	mL, cm ³		°C	cm/s		cm/s	cm/s
1	98.30	9.50	88.80	142	60	17	0.00401321	1.077	4.32E-03	4.37E-03
2	98.00	9.50	88.50	142	60	16	0.004026814	1.106	4.45E-03	
3	98.00	9.50	88.50	138	60	16	0.003913383	1.106	4.33E-03	
1	97.60	9.50	88.10	265	120	16	0.003774475	1.106	4.17E-03	4.16E-03
2	97.60	9.50	88.10	260	120	16	0.003703258	1.106	4.10E-03	
3	97.50	9.50	88.00	260	120	15	0.003707466	1.135	4.21E-03	
1	96.30	9.50	86.80	360	180	15	0.003469589	1.135	3.94E-03	3.87E-03
2	96.20	9.50	86.70	350	180	15	0.003377102	1.135	3.83E-03	
3	96.00	9.50	86.50	350	180	15	0.003384911	1.135	3.84E-03	
4	95.10	9.50	85.60	440	240	15	0.003225043	1.135	3.66E-03	3.67E-03
5	95.10	9.50	85.60	445	240	15	0.003261691	1.135	3.70E-03	
6	95.20	9.50	85.70	440	240	15	0.003221279	1.135	3.66E-03	

Formula and Terminologies As Per AS 1289.6.7.1 - 2001

$$k_{\theta} = (V_w / At) * (L/H)$$

$$k_{\theta} = k_T(\eta_{\theta}/\eta_{20})$$

Where

k_θ = coefficient of permeability at test temperature θ, in cm/s

V_w = volume of water passing through soil in time 9t, in mL

t = time interval for volume (V_w) measurement, in seconds

A = cross-sectional area of specimen, in square centimetres

L = thickness of specimen, in centimetres

H = hydraulic head in centimetres

k_T = coefficient of permeability at 20°C, in cm

η_θ = dynamic coefficient of viscosity of water at θ°C

η₂₀ = mean temperature of water during test, in degrees Celsius

LDR = laboratory density ratio

$$e = (\rho_w \cdot G_s / \rho) - 1$$

Where

e = void ratio of test soil

ρ_w = density of water

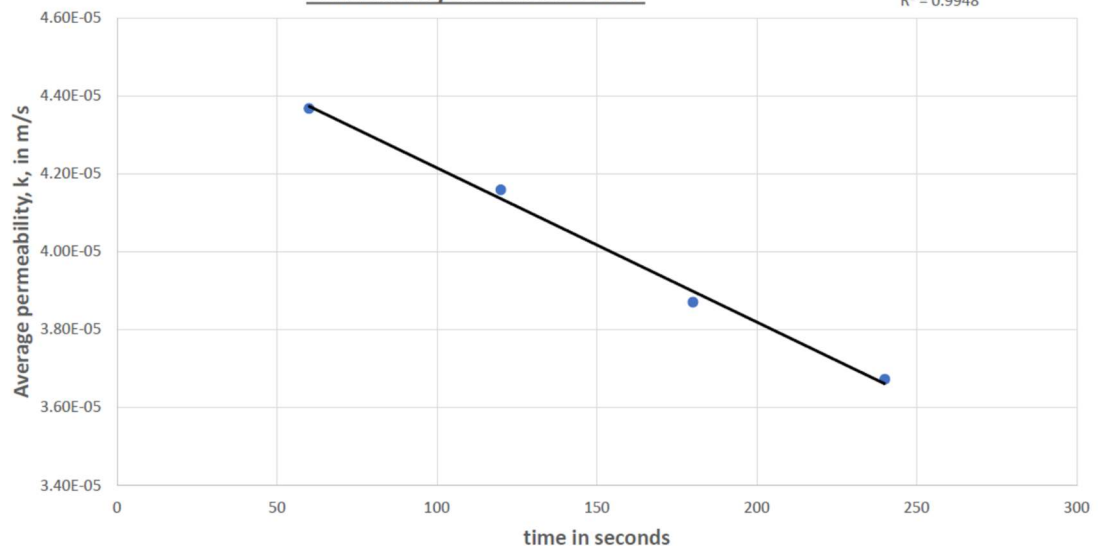
G_s = specific gravity of soil

ρ = measured density of test soil sample

Permeability vs Time for ECS05

$$y = -4E-08x + 5E-05$$

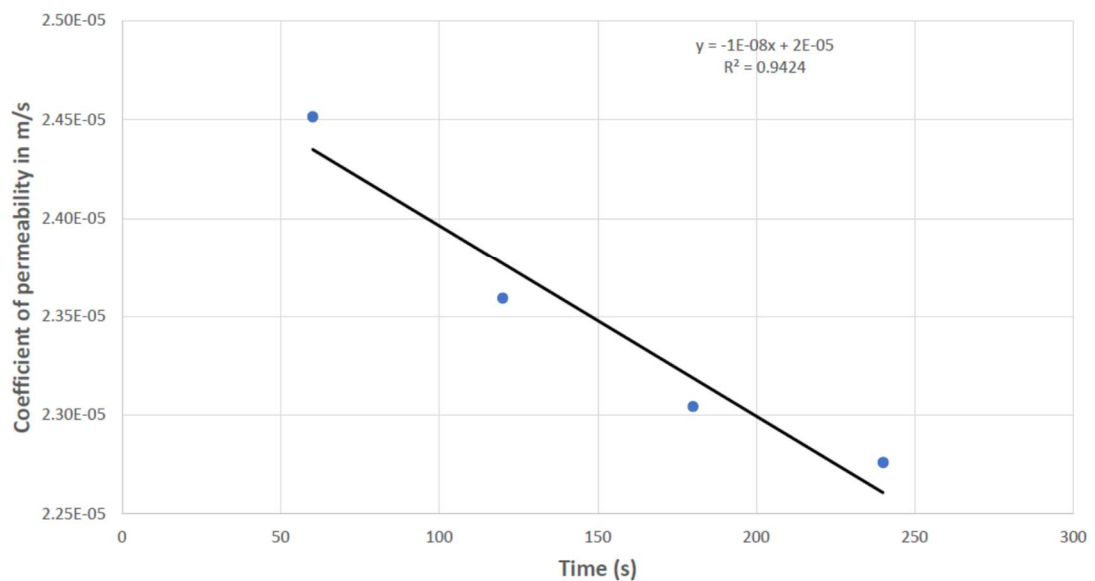
$$R^2 = 0.9948$$



H3: The permeability test of ECS10

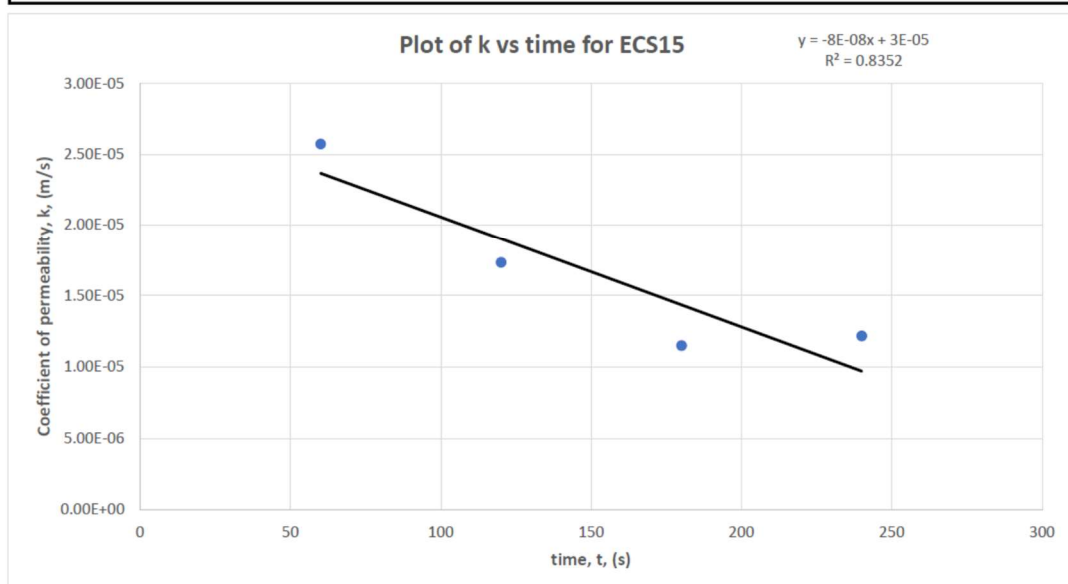
Permeability Test Data Sheet (Constant Head)										
Sample No.:		ECS10		Test Date: 25th July 2020.						
USCS Soil Classification:		SP-SC								
Density/Relative Density Calculation:										
Diameter, D, (cm):	10.14	Moisture Content, %:	4.15	W1, g:	2319.89					
Area, A, (cm ²):	80.75	LDR:	0.80	W2, g:	1091.61					
Length, L, (cm):	12.16	G _s :	2.61	Net mass of Sample, g:	1228.28					
Volume (cm ³):	981.97	Void ratio, e:	1.09							
ρ (g/cm ³):	1.25									
ρ _{max} (g/cm ³):	1.57									
ρ _{min} (g/cm ³):	1.22									
Rd	0.91									
Permeability Test Records										
Test no.	Manometer Reading		Head	Volume, V _w	t(s)	Temp.	k _θ	η _θ /η ₂₀	k _T	Average k _T
	H1, cm	H2, cm	H, (cm)	mL, cm ³		°C	cm/s		cm/s	cm/s
1	97.50	9.10	88.40	76	60	15	0.002157634	1.135	2.45E-03	
2	97.40	9.10	88.30	76	60	15	0.002160078	1.135	2.45E-03	2.45E-03
3	97.30	9.10	88.20	76	60	15	0.002162527	1.135	2.45E-03	
1	97.30	9.10	88.20	146	120	15	0.002077164	1.135	2.36E-03	
2	97.20	9.10	88.10	146	120	15	0.002079522	1.135	2.36E-03	2.36E-03
3	97.20	9.10	88.10	146	120	15	0.002079522	1.135	2.36E-03	
1	97.10	9.10	88.00	214	180	15	0.002034353	1.135	2.31E-03	
2	97.00	9.10	87.90	214	180	15	0.002036668	1.135	2.31E-03	2.30E-03
3	96.90	9.10	87.80	212	180	15	0.002019931	1.135	2.29E-03	
4	96.80	9.10	87.70	280	240	15	0.002003157	1.135	2.27E-03	
5	96.70	9.10	87.60	280	240	15	0.002005444	1.135	2.28E-03	2.28E-03
6	96.60	9.10	87.50	280	240	15	0.002007736	1.135	2.28E-03	
Formula and Terminologies As Per AS 1289.6.7.1 - 2001										
k _θ = (V _w /At) * (L/H)										
k _θ = k _T (η _θ /η ₂₀)										
Where										
k _θ = coefficient of permeability at test temperature θ, in cm/s										
V _w = volume of water passing through soil in time 9t), in mL										
t = time interval for volume (V _w) measurement, in seconds										
A = cross-sectional area of specimen, in square centimetres										
L = thickness of specimen, in centimetres										
H = hydraulic head in centimetres										
k _T = coefficient of permeability at 20°C, in cm										
η _θ = dynamic coefficient of viscosity of water at θ°C										
η ₂₀ = mean temperature of water during test, in degrees Celsius										
LDR = laboratory density ratio										
e = (ρ _w •G _s /ρ) - 1										
Where										
e = void ratio of test soil										
ρ _w = density of water										
G _s = specific gravity of soil										
ρ = measured density of test soil sample										

Coefficient of Permeability (k) vs Time (t) for ECS10



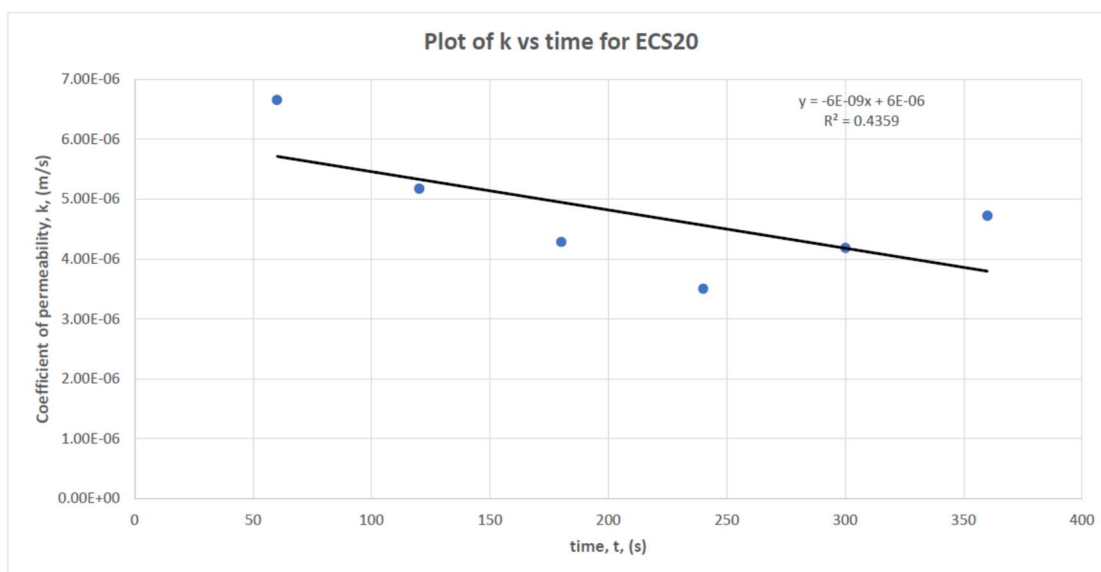
H4: The permeability test of ECS15

Permeability Test Data Sheet (Falling Head)										
Sample No.:		ECS15		Test Date: 1st August 2020.						
USCS Soil Classification:		SC								
Density/Relative Density Calculation:										
Diameter, D, (cm):	10.14	Moisture Content, %:	4.45	W1, g:	2364.22					
Area, A, (cm²):	80.75	LDR:	0.97	W2, g:	1006.34					
Length, L, (cm):	12.16	G _s :	2.53	Net mass of Sample, g:	1357.88					
Volume (cm³):	981.97	Void ratio, e:	0.83							
ρ (g/cm³):	1.38	Standpipe:								
ρ _{max} (g/cm³):	1.43	diameter (cm):	1.01							
ρ _{min} (g/cm³):	1.18	Area (cm²):	0.80							
Rd	0.19									
Permeability Test Records										
Test no.	Manometer Reading		Head H, (cm)	t(s)	Temp. °C	k _θ cm/s	η _θ /η ₂₀	k _T cm/s	Average k _T cm/s	m/s
	H1, cm	H2, cm								
1	10.00	11.50	1.50	15	18	0.00112282	1.051	1.18E-03		
2	15.50	17.00	1.50	15	18	0.000742109	1.051	7.80E-04	8.48E-04	8.48E-06
3	19.60	21.00	1.40	15	18	0.000554275	1.051	5.83E-04		
1	11.20	14.00	2.80	30	18	0.000896346	1.051	9.42E-04		
2	8.20	11.00	2.80	30	18	0.00118001	1.051	1.24E-03	9.84E-04	9.84E-06
3	13.00	15.60	2.60	30	18	0.000732368	1.051	7.70E-04		
1	5.60	11.10	5.50	60	17	0.001374139	1.077	1.48E-03		
2	1.10	7.00	5.90	60	17	0.00371684	1.077	4.00E-03	2.57E-03	2.57E-05
3	3.20	9.00	5.80	60	17	0.002076887	1.077	2.24E-03		
1	2.50	13.60	11.10	120	18	0.001700936	1.051	1.79E-03		
2	2.60	13.90	11.30	120	18	0.001683461	1.051	1.77E-03	1.74E-03	1.74E-05
3	3.00	14.30	11.30	120	18	0.001568246	1.051	1.65E-03		
1	2.20	18.10	15.90	180	18	0.001410907	1.051	1.48E-03		
2	4.20	19.80	15.60	180	18	0.0010381	1.051	1.09E-03	1.15E-03	1.15E-05
3	6.20	21.50	15.30	180	18	0.000832506	1.051	8.75E-04		
1	2.30	22.70	20.40	240	18	0.001149565	1.051	1.21E-03		
2	1.60	22.00	20.40	240	18	0.001316057	1.051	1.38E-03	1.22E-03	1.22E-05
3	3.10	23.20	20.10	240	18	0.001010628	1.051	1.06E-03		
Formula and Terminologies As Per AS 1289.6.7.1 - 2001										
k _θ = (2.3a _s L/At) * log(H2/H1)										
k _θ = kT(η _θ /η ₂₀)										
Where										
k _θ = coefficient of permeability at test temperature θ, in cm/s					LDR = laboratory density ratio					
t = time interval for manometer measurement, in seconds					e = (ρ _w *G _s /ρ) - 1					
A = cross-sectional area of specimen, in square centimetres					Where					
L = thickness of specimen, in centimetres					e = void ratio of test soil					
H = hydraulic head in centimetres					ρ _w = density of water					
k _T = coefficient of permeability at 20°C, in cm					G _s = specific gravity of soil					
η _θ = dynamic coefficient of viscosity of water at θ°C					ρ = measured density of test soil sample					
η ₂₀ = mean temperature of water during test, in degrees Celsius										



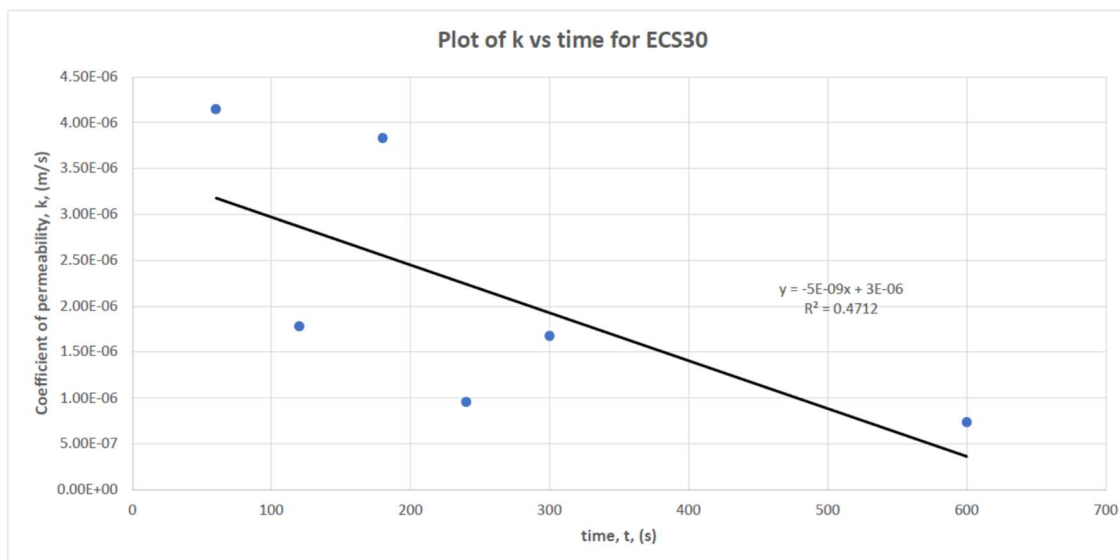
H5: The permeability test of ECS20

Permeability Test Data Sheet (Falling Head)										
Sample No.: ECS20					Test Date: 8th August 2020.					
USCS Soil Classification: SC										
Density/Relative Density Calculation:										
Diameter, D, (cm):		10.14		Moisture Content, %:		5.25		W1, g:		2261.40
Area, A, (cm²):		80.75		LDR:		0.81		W2, g:		717.58
Length, L, (cm):		12.16		G _s :		2.59		Net mass of Sample, g:		1543.82
Volume (cm³):		981.97		Void ratio, e:		0.65				
ρ (g/cm³):		1.57		Standpipe:						
ρ _{max} (g/cm³):		1.95		diameter (cm):		1.01				
ρ _{min} (g/cm³):		1.10		Area (cm²):		0.80				
Rd		0.44								
Permeability Test Records										
Test no.	Manometer Reading		Head	t(s)	Temp.	k _θ	η _θ /η ₂₀	k _T	Average k _T	
	H1, cm	H2, cm	H, (cm)		°C	cm/s		cm/s	cm/s	m/s
1	1.00	1.60	0.60	60	18	0.000943979	1.051	9.92E-04	6.66E-04	6.66E-06
2	4.00	4.60	0.60	60	18	0.000280705	1.051	2.95E-04		
3	1.50	2.10	0.60	60	18	0.000675788	1.051	7.10E-04		
1	2.00	3.30	1.30	120	18	0.000502891	1.051	5.29E-04	5.18E-04	5.18E-06
2	2.00	3.30	1.30	120	18	0.000502891	1.051	5.29E-04		
3	2.00	3.20	1.20	120	18	0.00047199	1.051	4.96E-04		
1	1.80	3.80	2.00	180	18	0.000500248	1.051	5.26E-04	4.29E-04	4.29E-06
2	3.00	5.00	2.00	180	18	0.000341989	1.051	3.59E-04		
3	2.60	4.60	2.00	180	18	0.000381971	1.051	4.01E-04		
1	2.50	5.30	2.80	240	18	0.000377296	1.051	3.97E-04	3.51E-04	3.51E-06
2	2.50	5.30	2.80	240	18	0.000377296	1.051	3.97E-04		
3	4.10	6.70	2.60	240	18	0.000246598	1.051	2.59E-04		
1	1.90	5.50	3.60	300	18	0.000426954	1.051	4.49E-04	4.19E-04	4.19E-06
2	2.90	6.30	3.40	300	18	0.000311647	1.051	3.28E-04		
3	1.70	5.30	3.60	300	18	0.000456753	1.051	4.80E-04		
1	0.50	4.70	4.20	360	18	0.000750059	1.051	7.88E-04	4.73E-04	4.73E-06
2	2.80	6.70	3.90	360	18	0.000292058	1.051	3.07E-04		
3	2.60	6.50	3.90	360	18	0.000306721	1.051	3.22E-04		
Formula and Terminologies As Per AS 1289.6.7.1 - 2001										
k _θ = (2.3a _s L/At) * log(H2/H1)										
k _θ = kT(η _θ /η ₂₀)										
Where										
k _θ = coefficient of permeability at test temperature θ, in cm/s					LDR = laboratory density ratio					
t = time interval for manometer measurement, in seconds					e = (ρ _w *G _s /ρ) - 1					
A = cross-sectional area of specimen, in square centimetres					Where					
L = thickness of specimen, in centimetres					e = void ratio of test soil					
H = hydraulic head in centimetres					ρ _w = density of water					
k _T = coefficient of permeability at 20°C, in cm					G _s = specific gravity of soil					
η _θ = dynamic coefficient of viscosity of water at θ°C					ρ = measured density of test soil sample					
η ₂₀ = mean temperature of water during test, in degrees Celsius										



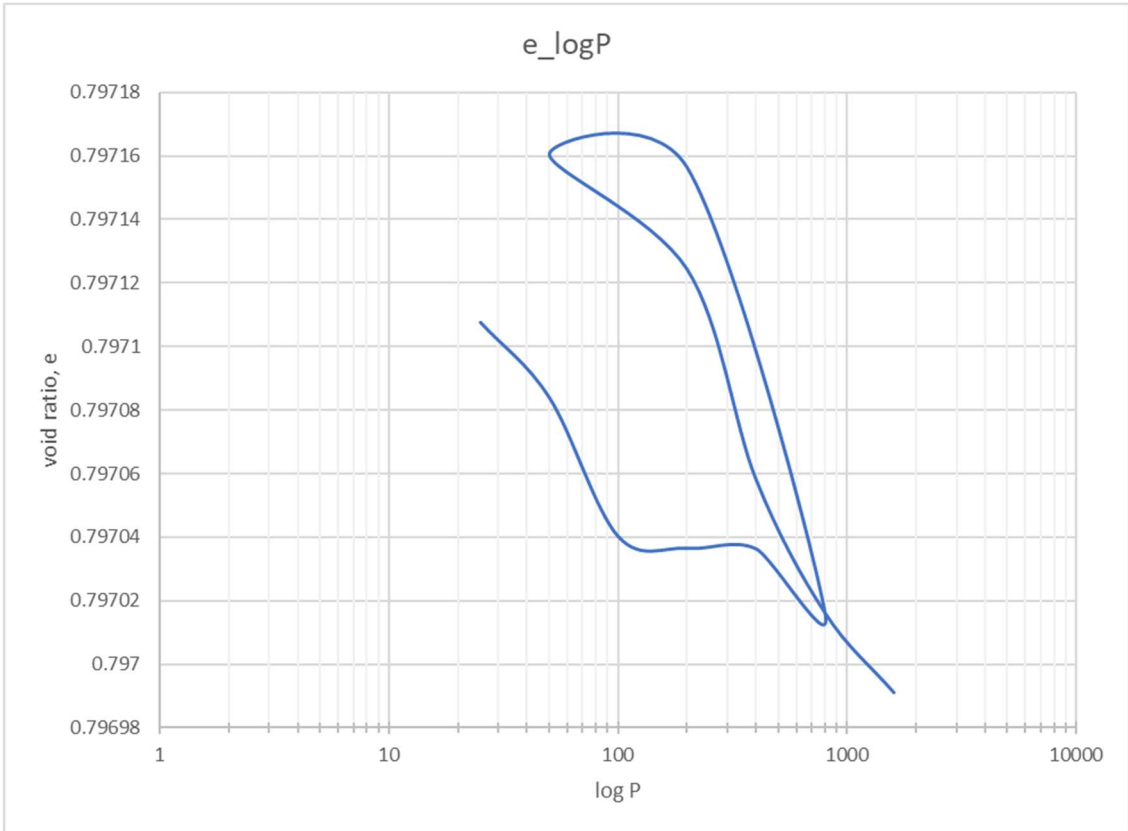
H6: The permeability test of ECS30

Permeability Test Data Sheet (Falling Head)										
Sample No.:		ECS30		Test Date: 1st August 2020.						
USCS Soil Classification:		SC								
Density/Relative Density Calculation:										
Diameter, D, (cm):	10.14		Moisture Content, %:	7.97		W1, g:	2185.22			
Area, A, (cm ²):	80.75		LDR:	0.91		W2, g:	737.55			
Length, L, (cm):	10.12		G _s :	2.56		Net mass of Sample, g:	1447.67			
Volume (cm ³):	817.23		Void ratio, e:	0.45						
ρ (g/cm ³):	1.77		Standpipe:							
ρ _{max} (g/cm ³):	1.94		diameter (cm):	1.01						
ρ _{min} (g/cm ³):	0.90		Area (cm ²):	0.80						
Rd	0.16									
Permeability Test Records										
Test no.	Manometer Reading		Head H, (cm)	t(s)	Temp. °C	k _θ cm/s	η _θ /η ₂₀	k _T cm/s	Average k _T cm/s	
	H1, cm	H2, cm								
1	1.00	1.40	0.40	60	18	0.000562416	1.051	5.91E-04	4.15E-04	4.15E-06
	2 1.70	2.10	0.40	60	18	0.000353205	1.051	3.71E-04		
	3 2.30	2.70	0.40	60	18	0.000268014	1.051	2.82E-04		
	1 2.80	3.70	0.90	120	18	0.000232936	1.051	2.45E-04	1.78E-04	1.78E-06
	2 3.80	4.50	0.70	120	18	0.000141306	1.051	1.49E-04		
	3 4.60	5.40	0.80	120	18	0.000134007	1.051	1.41E-04		
	1 0.60	1.90	1.30	180	17	0.000642237	1.077	6.92E-04	3.83E-04	3.83E-06
	2 2.00	3.10	1.10	180	17	0.000244182	1.077	2.63E-04		
	3 3.25	4.50	1.25	180	17	0.000181315	1.077	1.95E-04		
	1 4.60	6.10	1.50	240	18	0.000117938	1.051	1.24E-04	9.59E-05	9.59E-07
	2 6.30	7.70	1.40	240	18	8.38556E-05	1.051	8.81E-05		
	3 8.00	9.50	1.50	240	18	7.18122E-05	1.051	7.55E-05		
	1 3.10	5.10	2.00	300	18	0.000166428	1.051	1.75E-04	1.68E-04	1.68E-06
	2 2.50	4.50	2.00	300	18	0.000196498	1.051	2.07E-04		
	3 4.60	6.50	1.90	300	18	0.000115583	1.051	1.21E-04		
	1 4.20	8.10	3.90	600	18	0.000109781	1.051	1.15E-04	7.37E-05	7.37E-07
	2 8.30	11.80	3.50	600	18	5.8811E-05	1.051	6.18E-05		
	3 12.00	15.40	3.40	600	18	4.16976E-05	1.051	4.38E-05		
Formula and Terminologies As Per AS 1289.6.7.1 - 2001										
k _θ = (2.3a _p L/At) * log(H2/H1)										
kθ = kT(ηθ/η20)										
Where										
k _θ = coefficient of permeability at test temperature θ, in cm/s					LDR = laboratory density ratio					
t = time interval for manometer measurement, in seconds					e = (ρ _w ·G _s /ρ) - 1					
A = cross-sectional area of specimen, in square centimetres					Where					
L = thickness of specimen, in centimetres					e = void ratio of test soil					
H = hydraulic head in centimetres					ρ _w = density of water					
k _T = coefficient of permeability at 20°C, in cm					G _s = specific gravity of soil					
η _θ = dynamic coefficient of viscosity of water at θ°C					ρ = measured density of test soil sample					
η ₂₀ = mean temperature of water during test, in degrees Celsius										

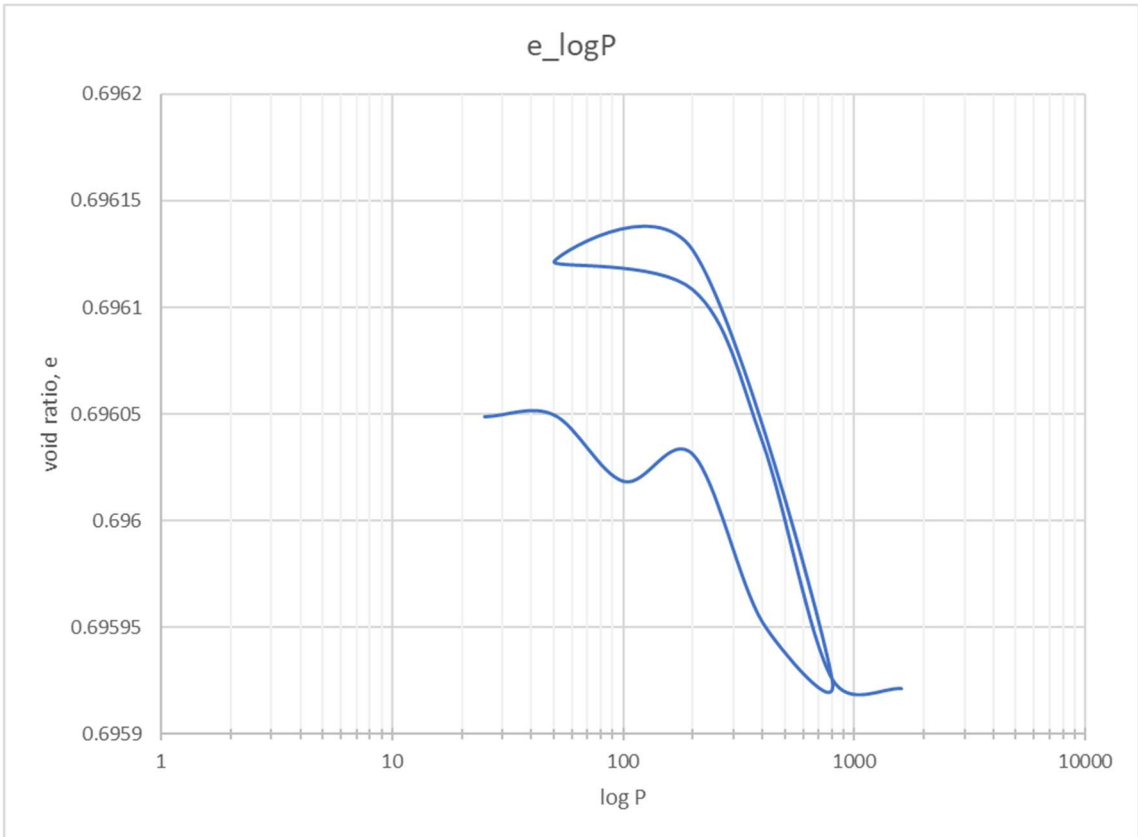


APPENDIX I - Tests results for one-dimensional consolidation oedometer tests

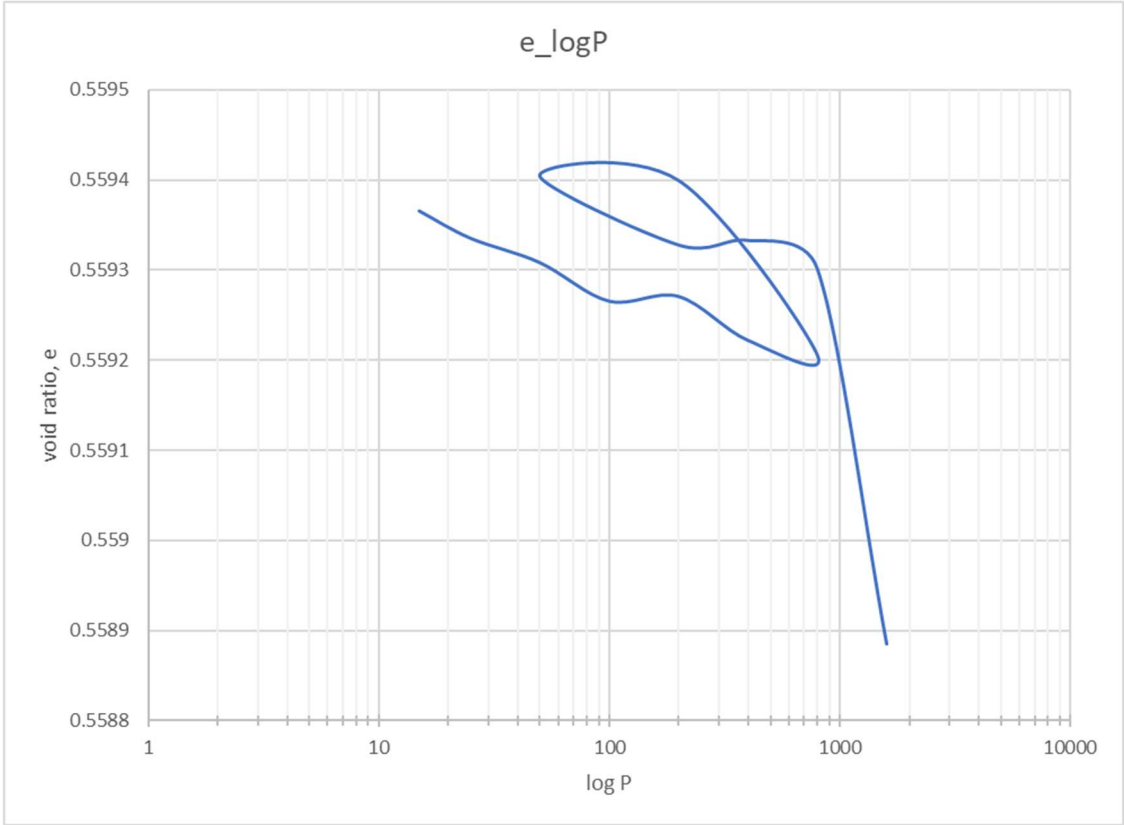
I1: The load-unload loop for ECS00



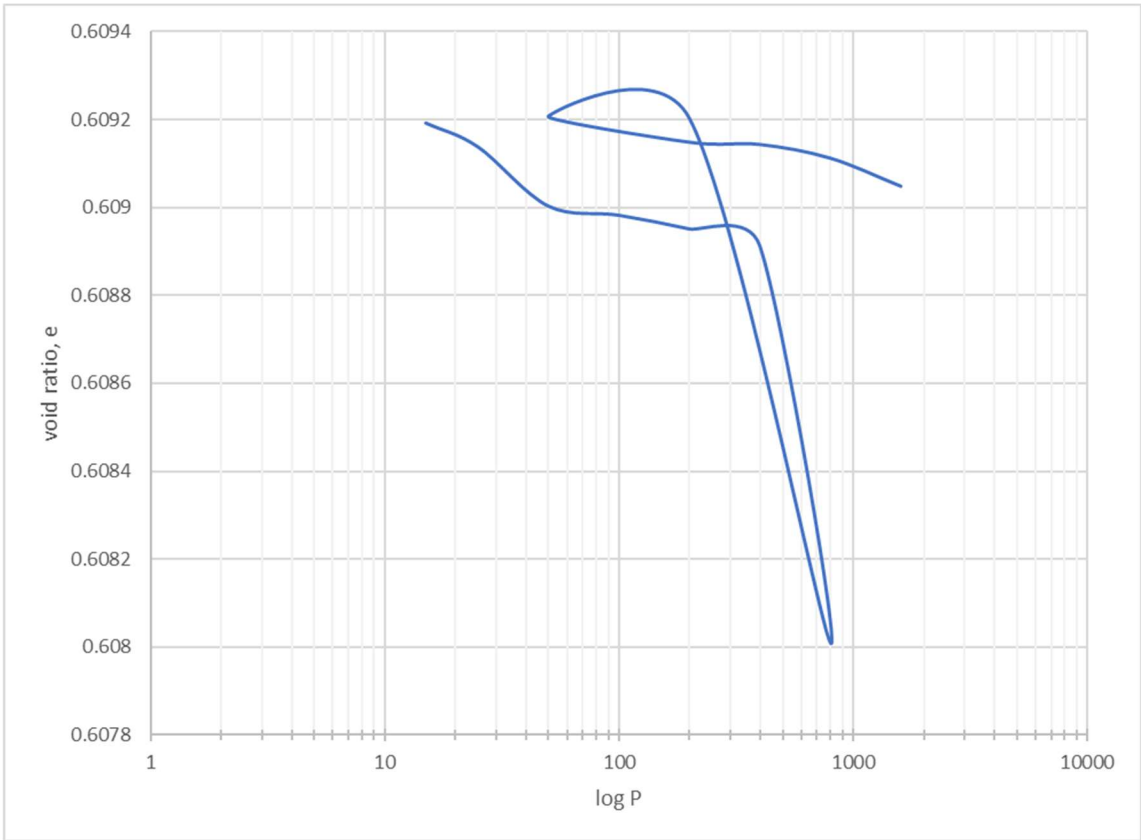
I2: The load-unload loop for ECS10



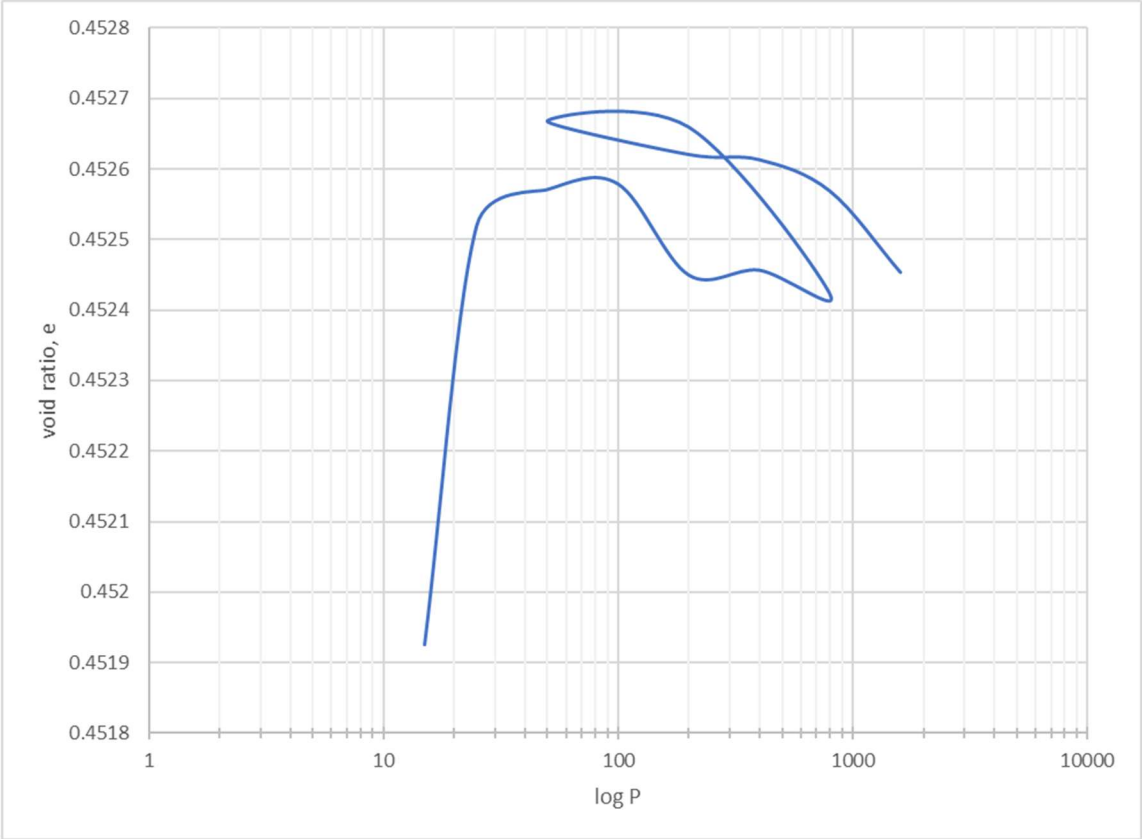
I3: The load-unload loop for ECS15



I4: The load-unload loop for ECS20

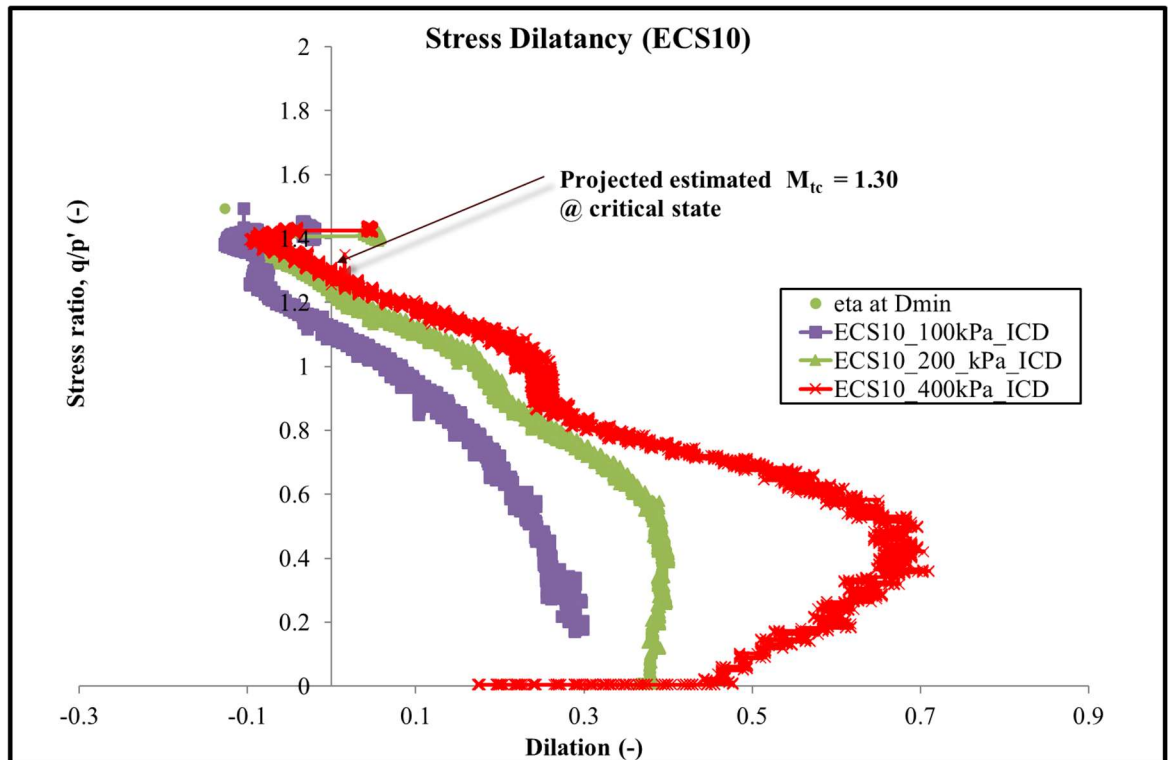


I5: The load-unload loop for ECS30

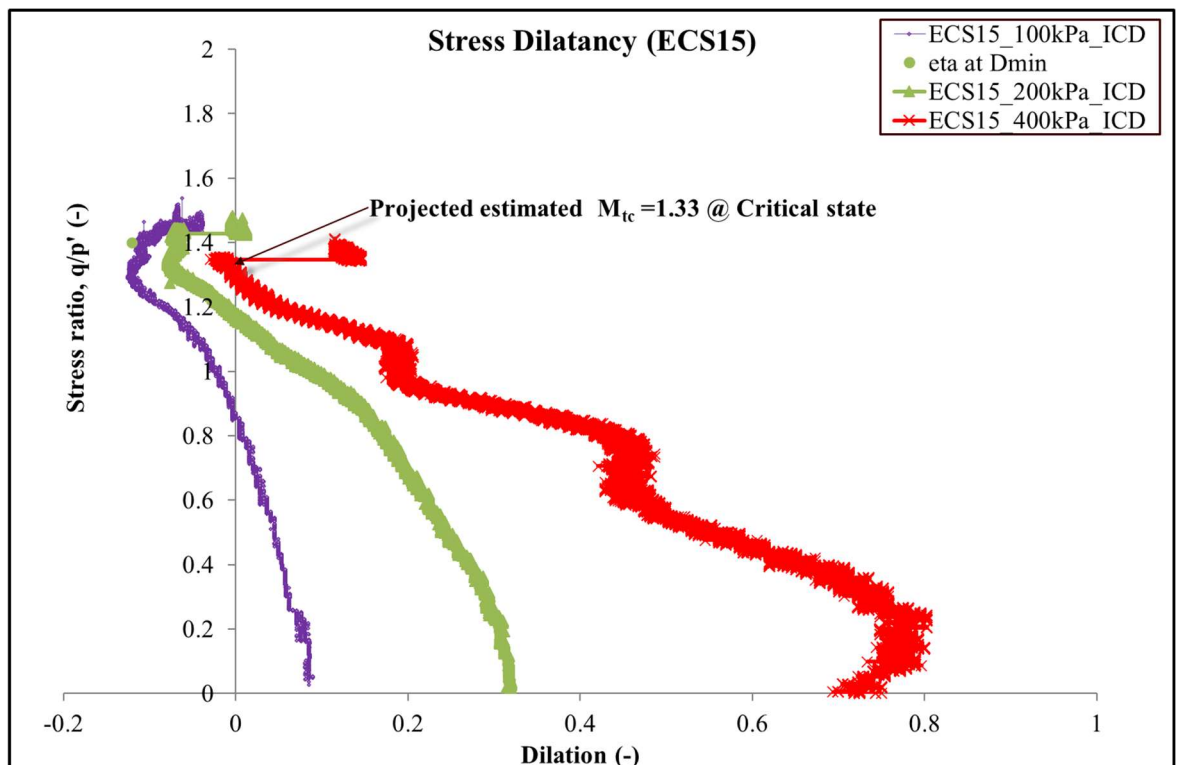


APPENDIX J – The stress – dilatancy relationship measured in sand matrix samples

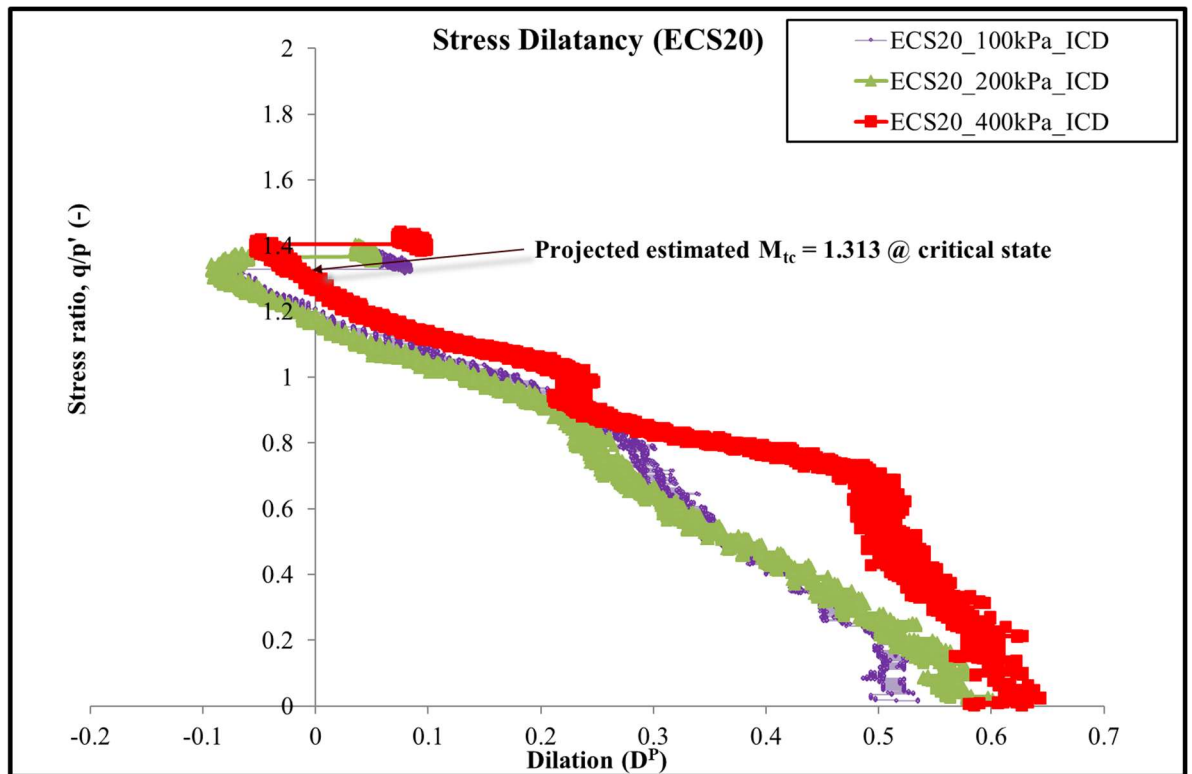
J1: The stress-dilatancy of ECS10



J2: The stress-dilatancy of ECS15



J3: The stress-dilatancy of ECS20



APPENDIX K – Typical undrained FLAC simulation code formatted in notepad

```
;Units: SI: meter-kilogram-second;Date: 19/02/2021
;norsand_undrained_loose.sav
new;
;
def setup
;y_mod = 133.4e6 ; input real value from lab test calibration
_pr = 0.15 ; poisson's ratio
m_g = y_mod / (2.0 * (1.0 + _pr)) ; shear modulus
m_k = y_mod / (3.0 * (1.0 - 2.0 * _pr)) ; maximum elastic bulk modulus
_lambda = 0.07 ; critical state parameter c2 or slope of normal consolidation line lambda in CamClay model
_gamma = 0.64 ; critical state parameter C1
_Mtc = 1.3 ; stress ratio @ critical state calibrated is 1.3 which correspond to critical frictional angle of 30
_N = 0.20 ; volumetric coupling factor
_H = 180 ; Hardening modulus defined as H = H0 + Hy
_chi = 3.5 ; factor dilatancy, default is 2-4.0. It is the parameter retaining minimum dilatancy
_Ir = 90 ; _Ir is ratio of _gref to _pref
_gref = _Ir*100 ; reference elastic shear modulus
_p0 = 500 ; Initial pressure
_psi = 0.2 ; state parameter
_e0 = _psi + _gamma - _lambda*ln(_p0) ; critical state void ratio
_yv = -2e-7 ; y-velocity
_mp0 = -_p0 ; effective confining stress
_xv = 1e-6 ; x-velocity
_ocr = 1.1
end
setup

; Model configuration
config axi gw
grid 1,1
set small
model norsand
prop dens 1.2 csl1 _gamma csl2 _lambda gref _gref poisson _pr
prop rat_crit _Mtc fac_cp _N h0 _H fac_dil _chi sp_ini _psi
prop ocr _ocr

;
; --- fluid part ---
prop poros 0.15
ini ftens -1e20
ini fmod 2e6
set flow off

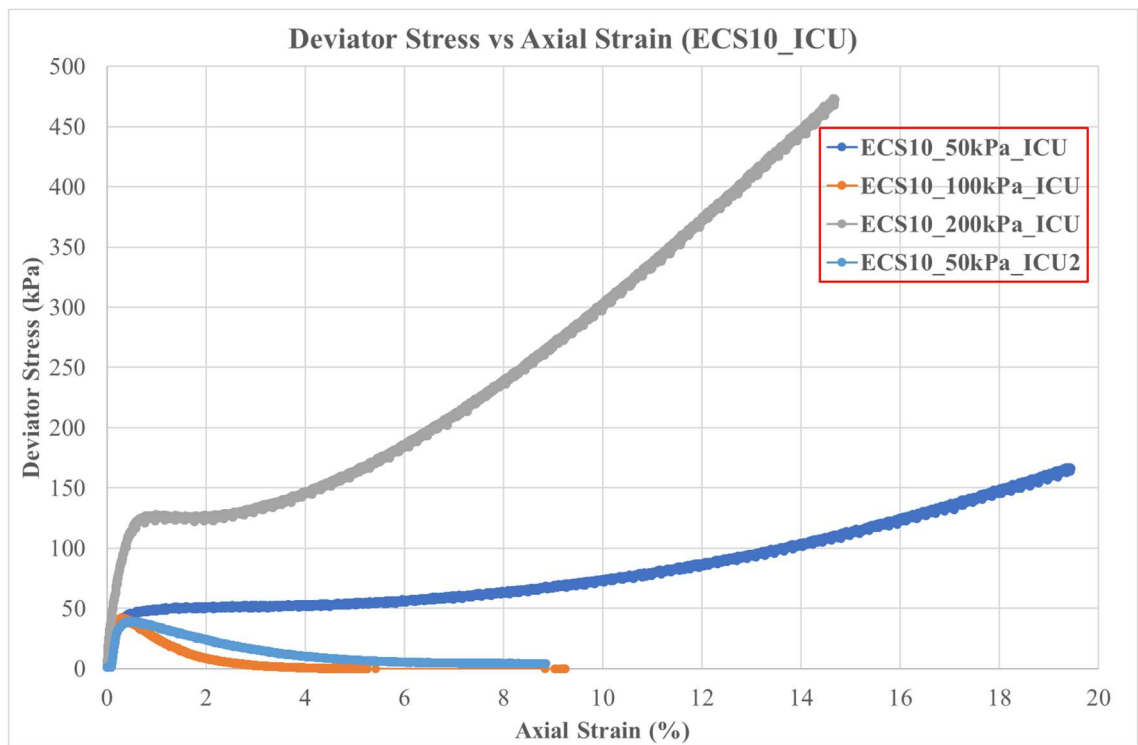
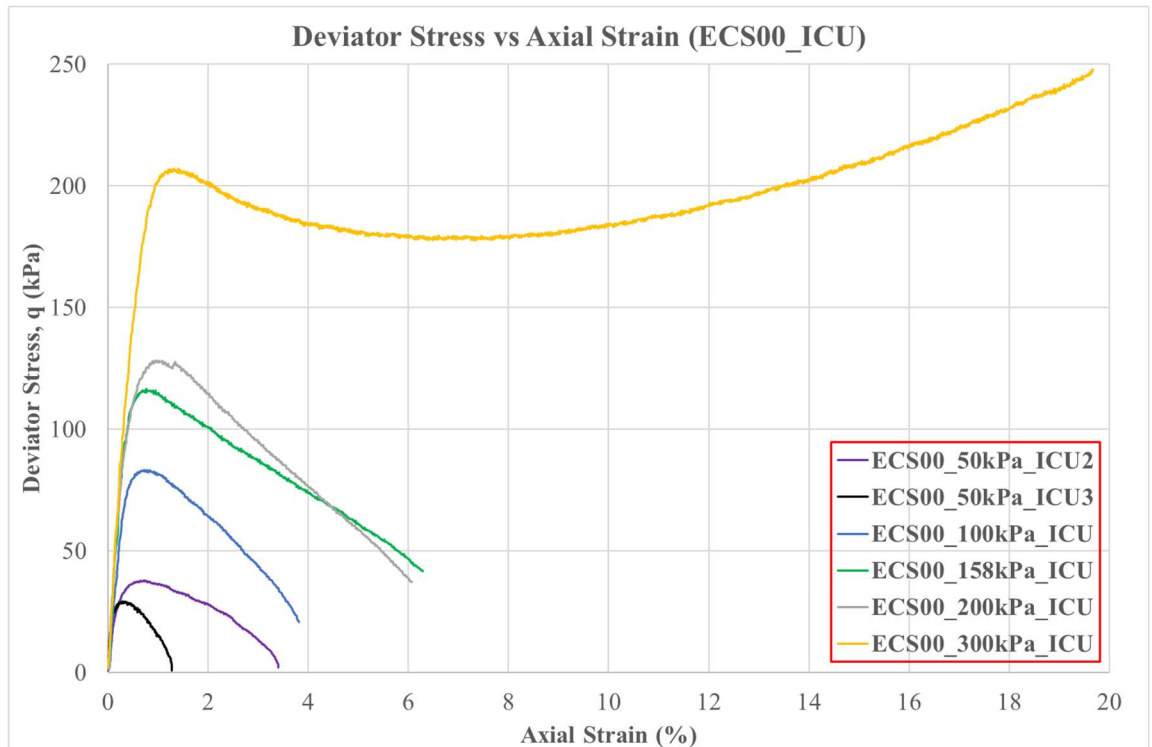
;-----Boundary conditions-----
fix y
ini yvel _yv j 2
ini sxx _mp0 syy _mp0 szz _mp0
apply sxx _mp0 i=2

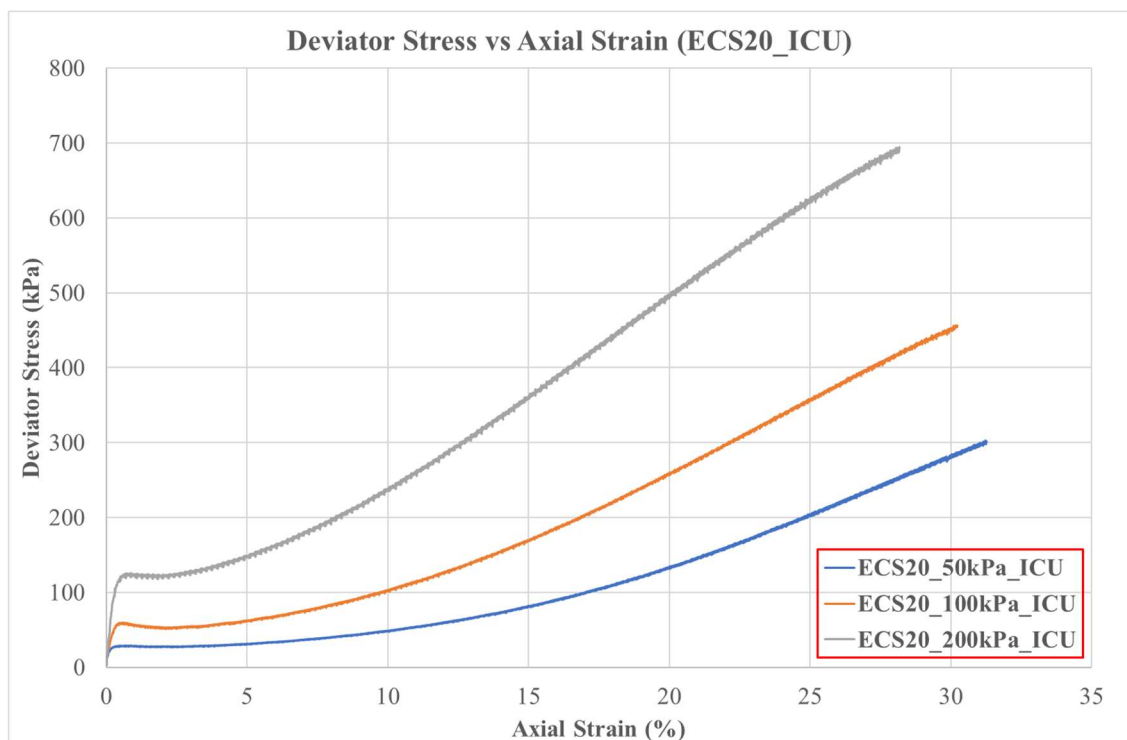
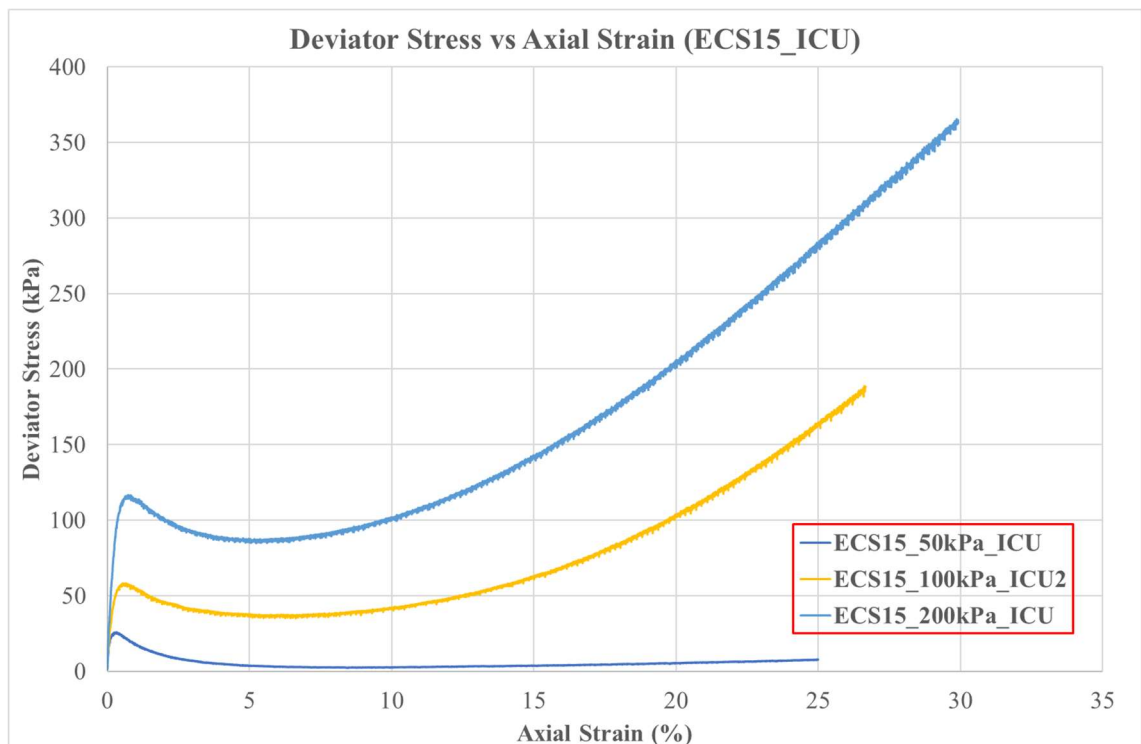
def ini_stress
loop ii (1,izones)
loop jj (1,jzones)
_sxx_0 = esxx(ii,jj)
_syy_0 = esyy(ii,jj)
_szz_0 = eszz(ii,jj)
z_prop(ii,jj,'sxx_ini')=_sxx_0
z_prop(ii,jj,'syy_ini')=_syy_0
z_prop(ii,jj,'szz_ini')=_szz_0
endloop
endloop
;
end
ini_stress
;
define _q1
_q1=sxx(1,1)-syy(1,1)
_p1=-(esxx(1,1)+esyy(1,1)+eszz(1,1))/3
_a1=-ydisp(1,2)*100 ;axial strain(%)
_pi=z_prop(1,1,'str_image')
_sp=z_prop(1,1,'sp_current')
_e=z_prop(1,1,'void_current')
_vsi=vsi(1,1)*100 ;volume strain(%)
_pp=pp(1,1)
end
;histories
hist _q1 ;1
hist _p1 ;2
hist _a1 ;3
hist _pi ;4
hist _sp ;5
hist _e ;6
hist _vsi ;7
hist _pp ;8
;
|

hist nstep 50
step 750000
save TXC_undrained_loose.sav

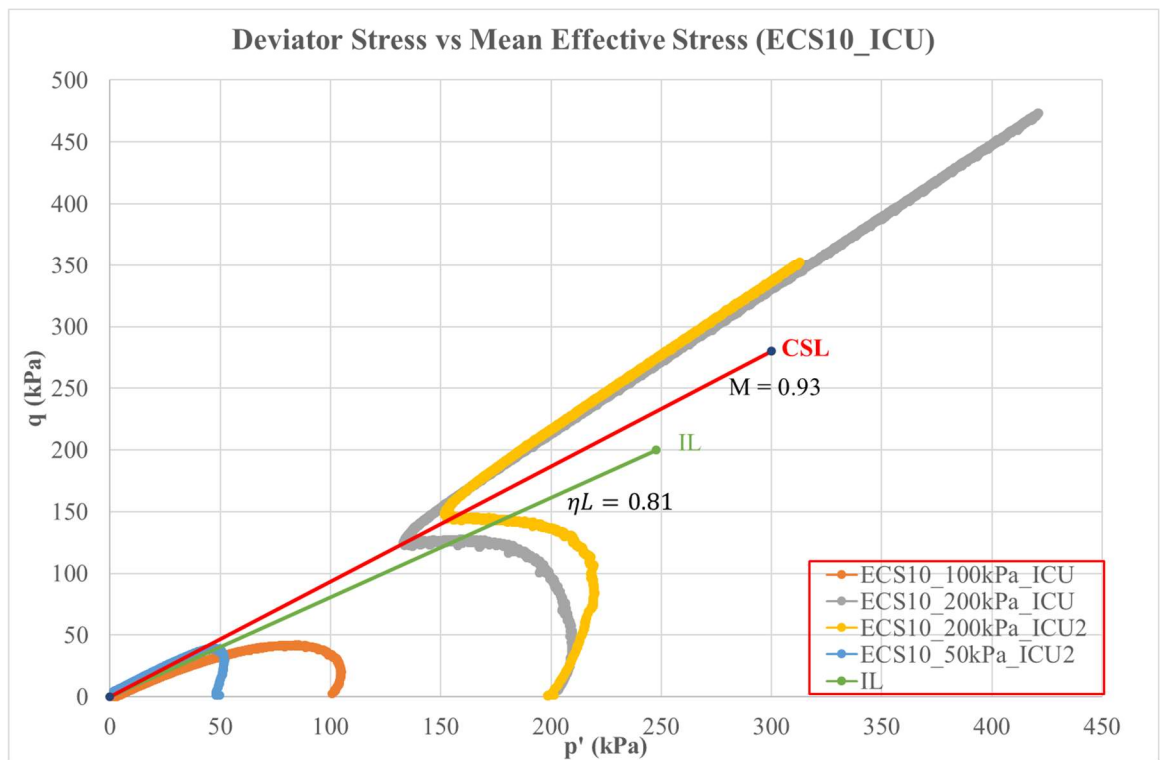
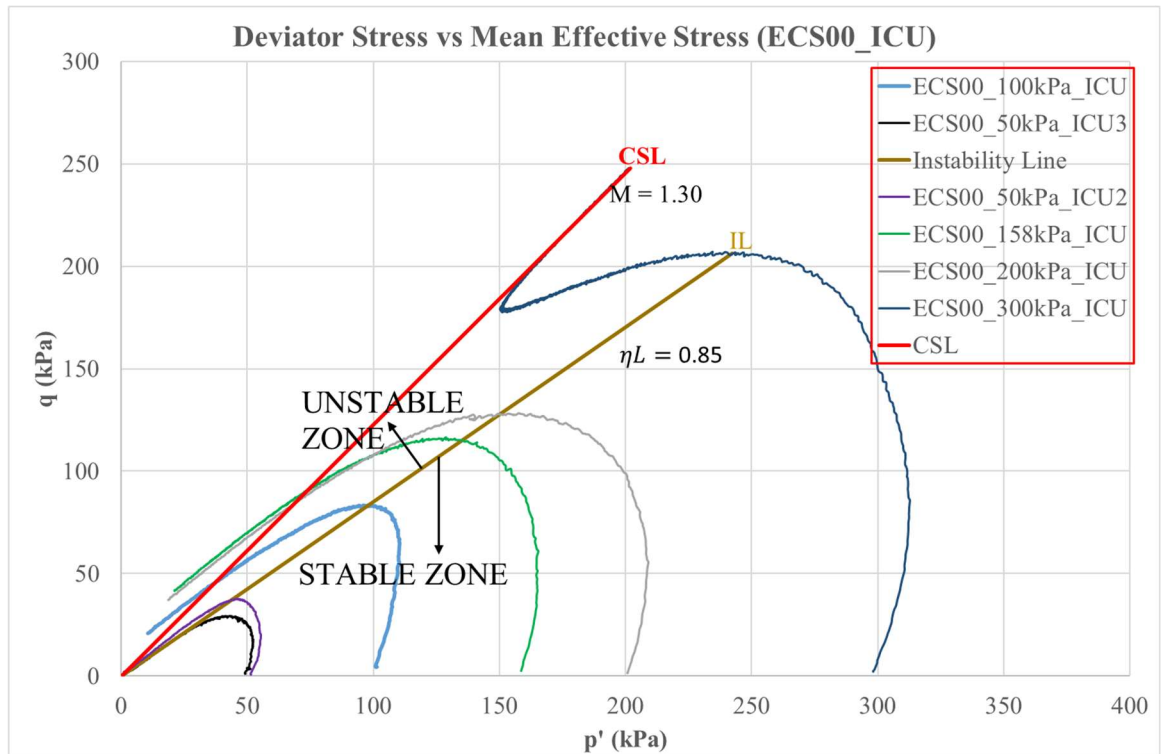
;*** plot commands ***
;plot name: Plot 1
plot hold history 1 line vs 3
;plot name: Plot 2
plot hold history 1 line
;plot name: Plot 4
plot hold history 1 line vs 2
plot hold history 8 line vs 3
```

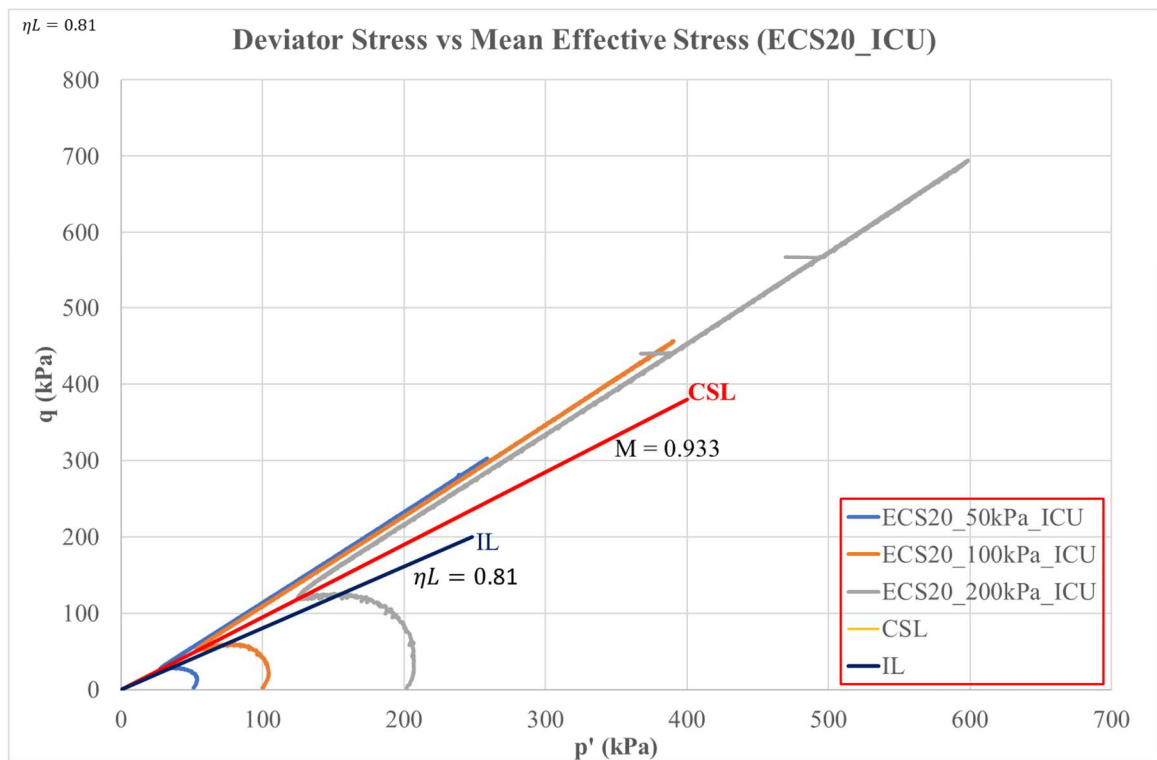
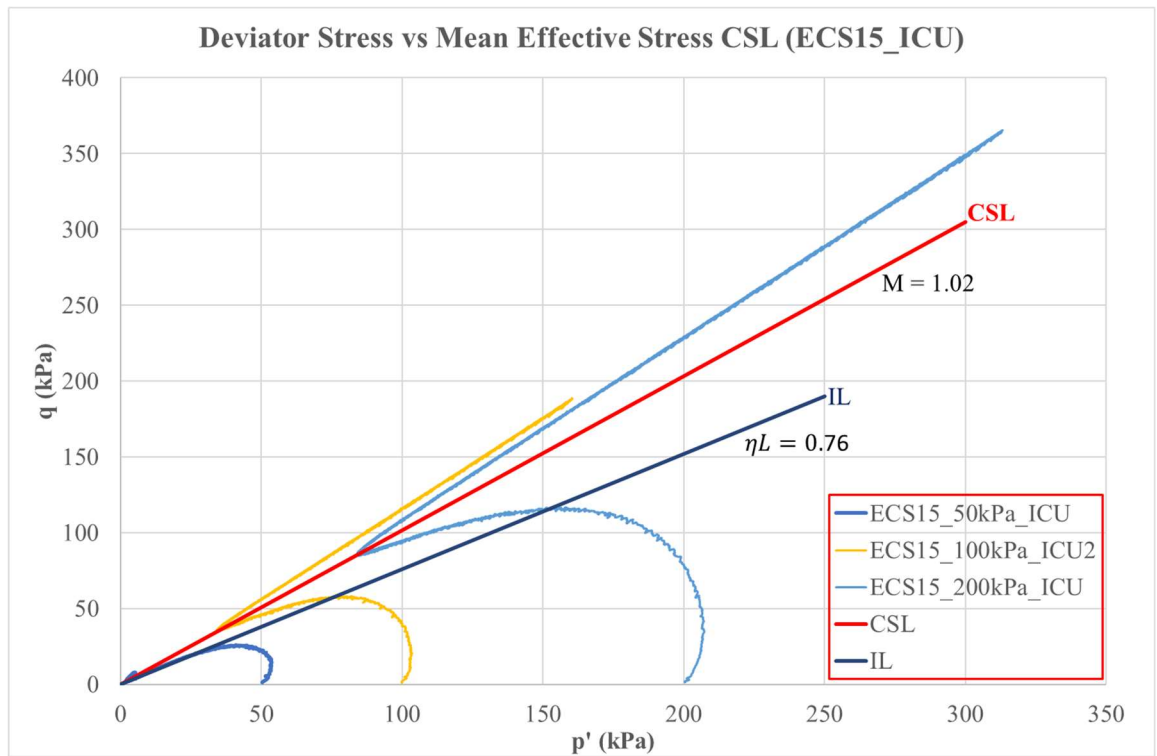

APPENDIX L – Deviatoric stress-strains



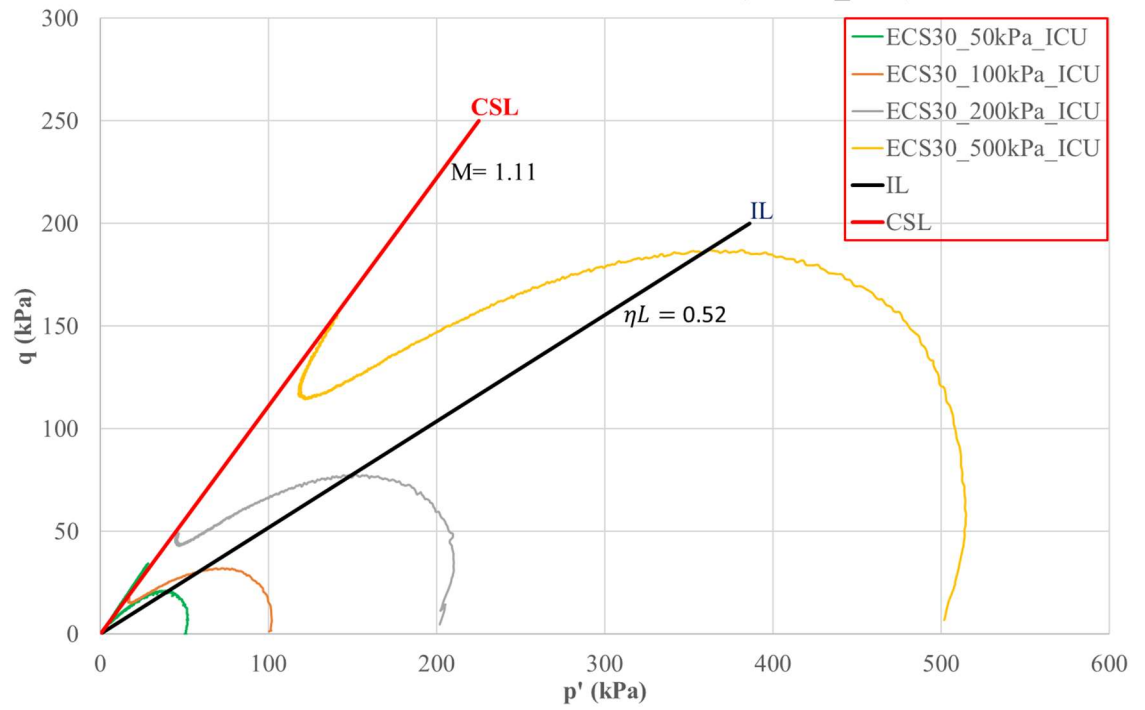


APPENDIX M – Effective stress paths (ESP)





Deviator Stress vs Mean Effective Stress (ECS30_ICU)



APPENDIX N – Evolution of excess pore water pressures (PWP)

